BEILSTEIN JOURNAL OF ORGANIC CHEMISTRY

Peptide–drug conjugates

Edited by Norbert Sewald

Imprint

Beilstein Journal of Organic Chemistry
www.bjoc.org
ISSN 1860-5397
Email: journals-support@beilstein-institut.de

The *Beilstein Journal of Organic Chemistry* is published by the Beilstein-Institut zur Förderung der Chemischen Wissenschaften.

Beilstein-Institut zur Förderung der Chemischen Wissenschaften
Trakehner Straße 7–9
60487 Frankfurt am Main
Germany
www.beilstein-institut.de

BEILSTEIN JOURNAL OF ORGANIC CHEMISTRY

Synthesis and biological evaluation of RGD and isoDGR peptidomimetic-α-amanitin conjugates for tumor-targeting

Lizeth Bodero[‡1], Paula López Rivas[‡2], Barbara Korsak[3], Torsten Hechler[3], Andreas Pahl[3], Christoph Müller[3], Daniela Arosio[4], Luca Pignataro[2], Cesare Gennari[*2] and Umberto Piarulli[*1]

Full Research Paper

Open Access

Address:
[1]Dipartimento di Scienza e Alta Tecnologia, Via Valleggio, 11, 22100, Como, Italy, [2]Dipartimento di Chimica, Università degli Studi di Milano, Via C. Golgi, 19, I-20133, Milan, Italy, [3]Heidelberg Pharma Research GmbH, Schriesheimer Strasse 101, 68526, Ladenburg, Germany and [4]CNR, Istituto di Scienze e Tecnologie Molecolare (ITSM), Via C. Golgi, 19, 20133, Milan, Italy

Email:
Cesare Gennari[*] - cesare.gennari@unimi.it; Umberto Piarulli[*] - umberto.piarulli@uninsubria.it

* Corresponding author ‡ Equal contributors

Keywords:
antitumor agents; cancer; drug delivery; integrins; peptidomimetics

Beilstein J. Org. Chem. **2018,** *14,* 407–415.
doi:10.3762/bjoc.14.29

Received: 30 November 2017
Accepted: 31 January 2018
Published: 14 February 2018

This article is part of the Thematic Series "Peptide–drug conjugates".

Guest Editor: N. Sewald

Abstract

RGD-α-amanitin and isoDGR-α-amanitin conjugates were synthesized by joining integrin ligands to α-amanitin via various linkers and spacers. The conjugates were evaluated for their ability to inhibit biotinylated vitronectin binding to the purified $\alpha_V\beta_3$ receptor, retaining good binding affinity, in the same nanomolar range as the free ligands. The antiproliferative activity of the conjugates was evaluated in three cell lines possessing different levels of $\alpha_V\beta_3$ integrin expression: human glioblastoma U87 ($\alpha_V\beta_3$+), human lung carcinoma A549 ($\alpha_V\beta_3$−) and breast adenocarcinoma MDA-MB-468 ($\alpha_V\beta_3$−). In the U87, in the MDA-MB-468, and partly in the A549 cancer cell lines, the cyclo[DKP-isoDGR]-α-amanitin conjugates bearing the lysosomally cleavable Val-Ala linker were found to be slightly more potent than α-amanitin. Apparently, for all these α-amanitin conjugates there is no correlation between the cytotoxicity and the expression of $\alpha_V\beta_3$ integrin. To determine whether the increased cytotoxicity of the cyclo[DKP-isoDGR]-α-amanitin conjugates is governed by an integrin-mediated binding and internalization process, competition experiments were carried out in which the conjugates were tested with U87 ($\alpha_V\beta_3$+, $\alpha_V\beta_5$+, $\alpha_V\beta_6$−, $\alpha_5\beta_1$+) and MDA-MB-468 ($\alpha_V\beta_3$−, $\alpha_V\beta_5$+, $\alpha_V\beta_6$+, $\alpha_5\beta_1$−) cells in the presence of excess cilengitide, with the aim of blocking integrins on the cell surface. Using the MDA-MB-468 cell line, a fivefold increase of the IC_{50} was observed for the conjugates in the presence of excess cilengitide, which is known to strongly bind not only $\alpha_V\beta_3$, but also $\alpha_V\beta_5$, $\alpha_V\beta_6$, and $\alpha_5\beta_1$. These data indicate that in this case the cyclo[DKP-isoDGR]-α-amanitin conjugates are possibly internalized by a process mediated by integrins different from $\alpha_V\beta_3$ (e.g., $\alpha_V\beta_5$).

Introduction

α-Amanitin is a bicyclic octapeptide toxin belonging to the amatoxin family, found in *Amanita Phalloides* (death cap mushroom), see Figure 1 [1]. Its mechanism of action consists in the inhibition of cellular transcription by an effective blocking of RNA polymerase II, which is present in the nuclei of eukaryotic cells and is responsible for the transcription of DNA to mRNA [1,2]. Despite this strong inhibitory activity, α-amanitin exhibits only a micromolar cytotoxicity and low cellular uptake in most mammalian cells, due to its strong polarity and poor membrane permeability [2]. One notable exception are human hepatocytes, where the transporting protein OATP1B3 internalizes amatoxins resulting in high liver toxicity [2,3].

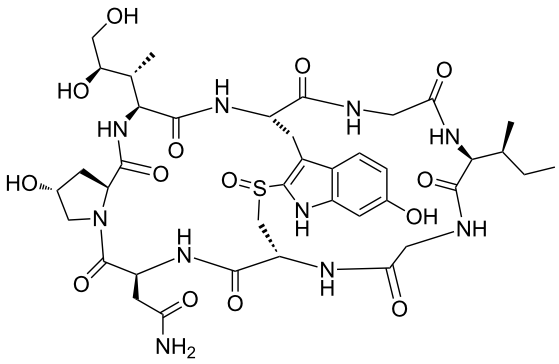

Figure 1: α-Amanitin.

This strong toxicity in the presence of endocytosis mediators allowing cell permeation, aroused interest towards the use of α-amanitin as a payload for targeted cancer therapy. In 1981, Davis and Preston reported the synthesis of the antibody–drug conjugate (ADC) α-amanitin-anti-Thy 1.2 IgG, which was 47-fold more toxic than the unconjugated α-amanitin in the murine T lymphoma S49.1 cell line [4]. In 2012, a new ADC containing α-amanitin and a chimerized anti-EpCAM (epithelial cell-adhesion molecule) monoclonal antibody was prepared by Moldenhauer and co-workers [5]. The cytotoxicity of this conjugate was tested in EpCAM-overexpressing cancer cell lines obtaining IC_{50} values from 2.5×10^{-10} to 2.0×10^{-12} M. Promising results were also observed in mice bearing BxPc-3 pancreatic xenograft tumors, with complete tumor regression in 90% of the cases after two injections of the α-amanitin-anti-EpCAM ADC at a dose of 100 μg/kg with respect to α-amanitin. In these two examples, the internalization of the monoclonal antibody and subsequent release of the toxin leads to the enhancement of α-amanitin activity on the targeted cells.

An alternative approach to the antibody targeted therapy is represented by small molecule–drug conjugates (SMDCs), where the small molecule – usually a peptide or peptidomimetic receptor ligand – avoids the drawbacks of ADCs such as high manufacturing costs, unfavorable pharmacokinetics (low tissue diffusion and low accumulation rate) and possible elicitation of immune response [6]. By conjugation to a specific cell-membrane-receptor ligand, the toxin can be delivered at the tumor site and internalized through receptor-mediated endocytosis. In 2013, Reshetnyak and co-workers conjugated α-amanitin to pHLIP (pH low insertion peptide) via linkers of different hydrophobicities [7]. The results indicated that pHLIP could deliver α-amanitin into cells and induce cell death in 48 h by a pH-mediated direct translocation across the membrane and cleavage of the disulfide linker in the cytoplasm. In another example, Perrin and co-workers conjugated the *N*-propargylasparagine of an amanitin analog to a cycloRGD integrin ligand (cyclo[RGDfK]) using a copper-catalyzed azide–alkyne cycloaddition [8]. The conjugates were tested in the U87 glioblastoma cell line, but only a slight enhancement in toxicity over α-amanitin was observed.

The transmembrane receptor $\alpha_V\beta_3$ integrin is widely expressed on the blood vessels of several human cancers (for example, breast cancer, glioblastoma, pancreatic tumor, prostate carcinoma) but not on the vasculature of healthy tissues [9-11], and therefore constitutes a suitable therapeutic target in the field of SMDCs. Integrin $\alpha_V\beta_3$ recognizes endogenous ligands by the tripeptide arginine-glycine-aspartate [12] (RGD) and also by the related sequence isoaspartate-glycine-arginine (isoDGR) [13-20]. Many synthetic peptides or peptidomimetics containing these sequences have been prepared and show low nanomolar IC_{50} values for integrin $\alpha_V\beta_3$ binding [21-27]. A number of cyclic RGD and isoDGR ligands containing a bifunctional diketopiperazine (DKP) scaffold have been developed by the Gennari and Piarulli groups in the last decade [24-27]. Among them, the cyclo[DKP-RGD] **1** [25] and cyclo[DKP-isoDGR] **3** [26] (Figure 2) showed a binding affinity for the purified receptor $\alpha_V\beta_3$ in the low nanomolar range and a good selectivity for this integrin in comparison with integrin $\alpha_V\beta_5$ (33–34 times, see Table 1).

Furthermore, these ligands were shown to inhibit the FAK (focal adhesion kinase) and Akt (protein kinase B) signaling cascade and the tumor cell infiltration process, performing as true integrin antagonists [27].

Ligands **1** and **3** were also functionalized with an aminomethyl group ($-CH_2NH_2$) as a handle for conjugation to cytotoxic drugs (Figure 2, ligands **2** and **4**) [28-30]. Conjugates of the functionalized ligands **2** and **4** with paclitaxel (PTX) via a 2'-carbamate with a self-immolative spacer and the lysosomally cleavable Val-Ala linker [31] were synthesized (Figure 2, cyclo[DKP-

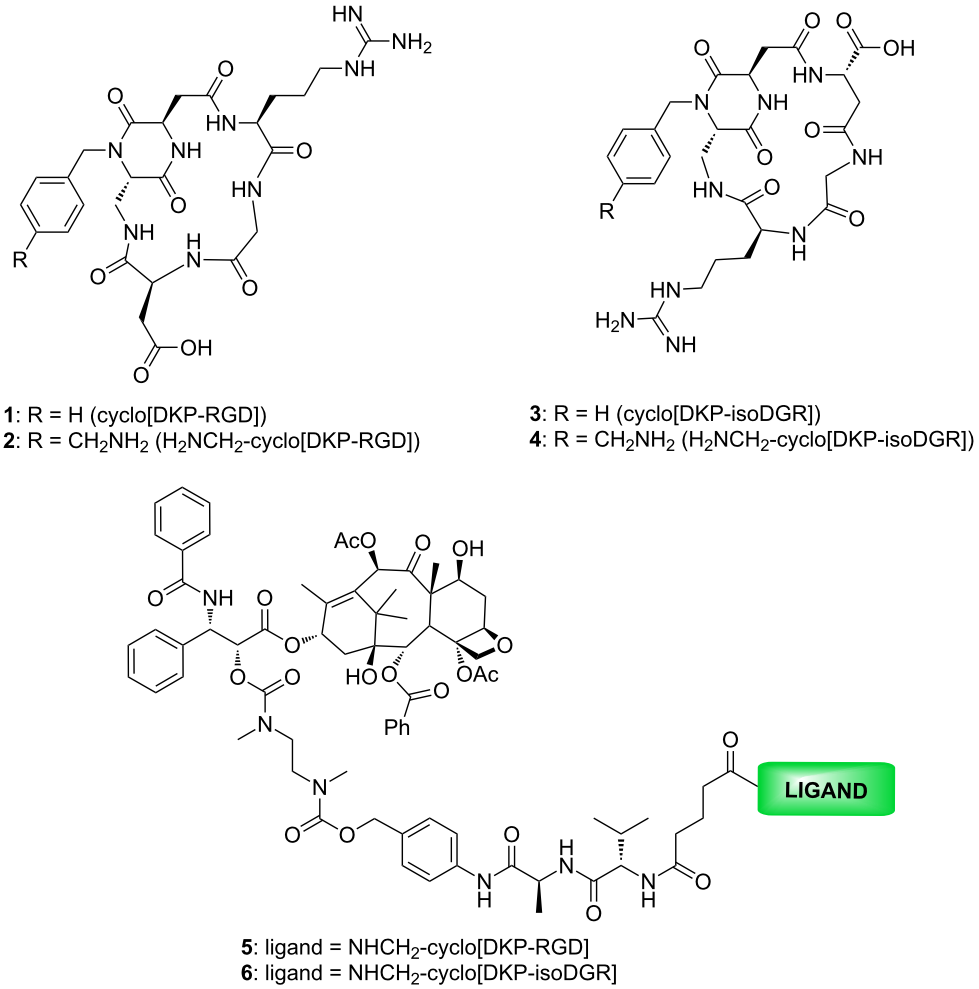

Figure 2: Structure of the ligands cyclo[DKP-RGD] (**1**), NH_2CH_2-cyclo[DKP-RGD] (**2**), cyclo[DKP-isoDGR] (**3**), NH_2CH_2-cyclo[DKP-isoDGR] (**4**) and the related SMDCs cyclo[DKP-RGD]-Val-Ala-PTX (**5**) and cyclo[DKP-isoDGR]-Val-Ala-PTX (**6**).

Table 1: Inhibition of biotinylated vitronectin binding to $\alpha_v\beta_3$ and $\alpha_v\beta_5$ receptors.

ligand	structure (name)	IC_{50} (nM)[a] $\alpha_V\beta_3$	IC_{50} (nM)[a] $\alpha_V\beta_5$
1	cyclo[DKP-RGD]	4.5 ± 1.1	149 ± 25
3	cyclo[DKP-isoDGR]	9.2 ± 1.1	312 ± 21

[a]IC_{50} values were calculated as the concentration of compound required for 50% inhibition of biotinylated vitronectin binding as estimated by GraphPad Prism software. All values are the arithmetic mean ± the standard deviation (SD) of triplicate determinations.

RGD]-Val-Ala-PTX **5** and cyclo[DKP-isoDGR]-Val-Ala-PTX **6**). Their tumor targeting ability was assessed in vitro in anti-proliferative assays comparing an $\alpha_V\beta_3$ positive with an $\alpha_V\beta_3$ negative cell line [29,30]. The cyclo[DKP-isoDGR]-Val-Ala-PTX conjugate **6** displayed a remarkable targeting index (TI = 9.9), especially when compared to the strictly related cyclo[DKP-RGD]-Val-Ala-PTX conjugate **5** (TI = 2.4) [30].

Results and Discussion

In the present paper, we report the synthesis and biological evaluation of two cyclo[DKP-RGD]-α-amanitin and three cyclo[DKP-isoDGR]-α-amanitin conjugates. In these conjugates, the integrin ligands are bound to α-amanitin via a 6'-ether with two different linkers: an "uncleavable" six carbon aliphatic chain (Figure 3, compounds **7** and **8**) and a lysosomally

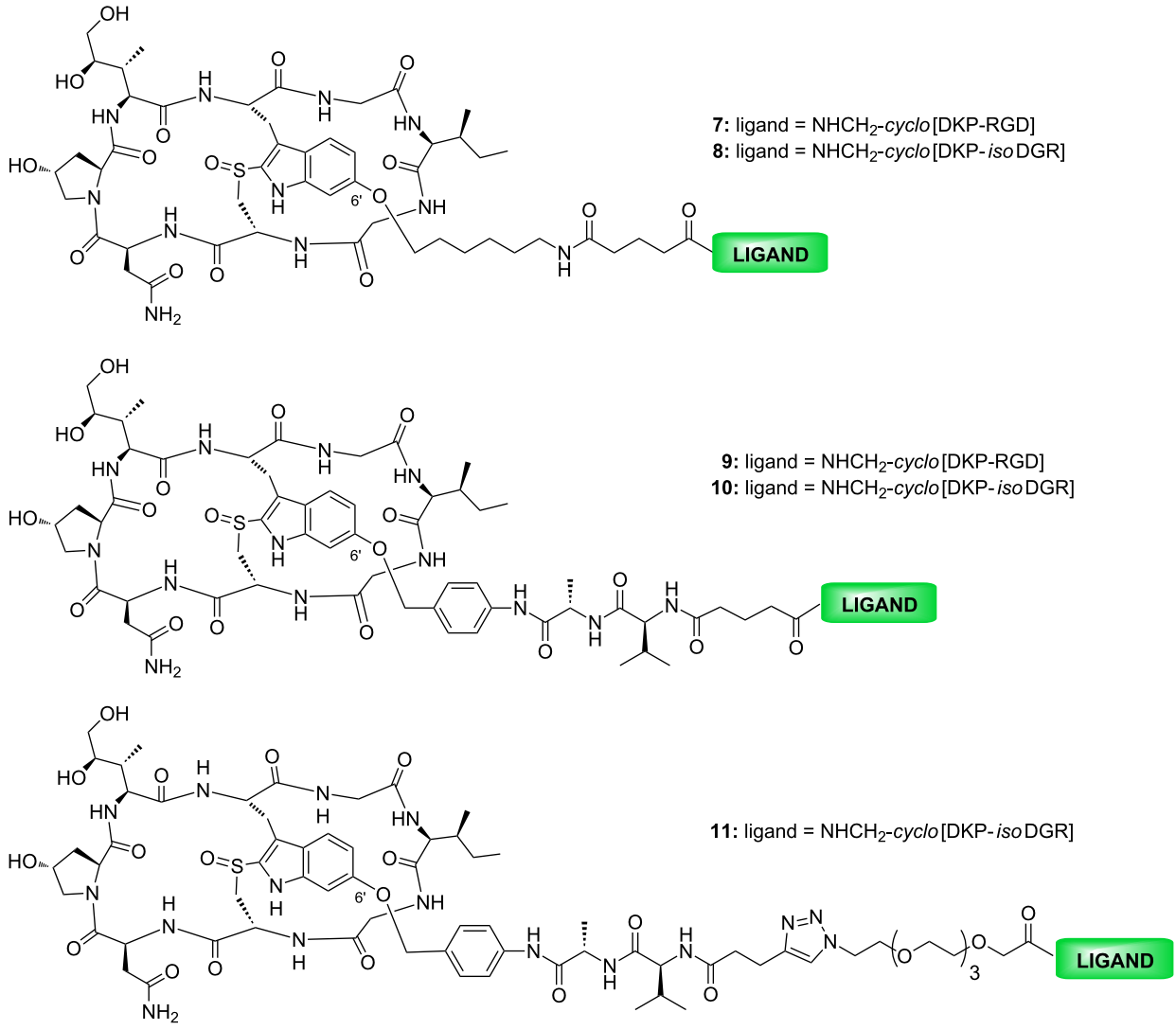

Figure 3: Structure of the α-amanitin conjugates: cyclo[DKP-RGD]-uncleavable-α-amanitin (**7**), cyclo[DKP-isoDGR]-uncleavable-α-amanitin (**8**), cyclo[DKP-RGD]-Val-Ala-α-amanitin (**9**), cyclo[DKP-isoDGR]-Val-Ala-α-amanitin (**10**) and cyclo[DKP-isoDGR]-PEG-4-Val-Ala-α-amanitin (**11**).

cleavable Val-Ala linker bound to a self-immolative spacer (Figure 3, compounds **9**, **10** and **11**). Integrin receptor competitive binding assays and cell proliferation assays with an $\alpha_V\beta_3$ positive (U87) and two $\alpha_V\beta_3$ negative cell lines (A549 and MDA-MB-468) were performed for all the conjugates.

Synthesis

Cyclo[DKP-RGD]-α-amanitin and cyclo[DKP-isoDGR]-α-amanitin conjugates **7**–**11** were synthesized as described in Scheme 1 and Scheme 2, by joining the functionalized ligands H_2NCH_2-cyclo[DKP-RGD] (**2**) [18,29] and H_2NCH_2-cyclo[DKP-isoDGR] (**4**) [30] to α-amanitin via a 6'-ether with various linkers and spacers. Details are reported in Supporting Information File 1.

Integrin receptor competitive binding assays

Conjugates **7**–**11** were evaluated for their ability to inhibit biotinylated vitronectin binding to the purified $\alpha_V\beta_3$ receptor. The calculated half-maximal inhibitory concentrations (IC_{50}) are listed in Table 2. Screening assays were performed by incubating the immobilized integrin receptor with solutions of the cyclo[DKP-RGD]-α-amanitin and cyclo[DKP-isoDGR]-α-amanitin conjugates **7**–**11** at different concentrations (10^{-12} to 10^{-5} M) in the presence of biotinylated vitronectin (1 μg mL^{-1}) and measuring bound vitronectin.

It was found that the cyclo[DKP-RGD]-α-amanitin conjugates **7** and **9** and cyclo[DKP-isoDGR]-α-amanitin conjugates **8**, **10** and **11** retain good binding affinity for $\alpha_V\beta_3$ integrin, in the same

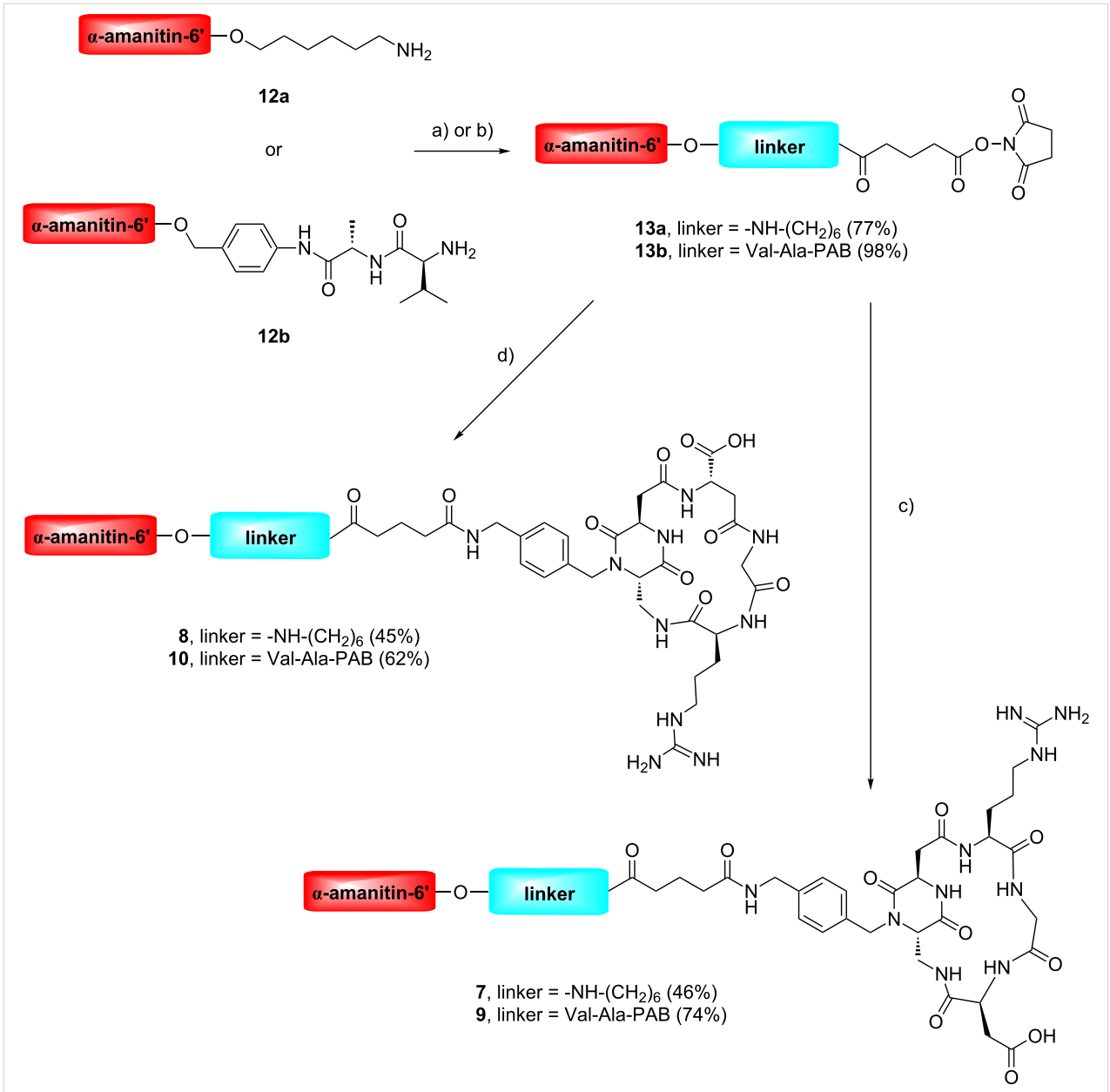

Scheme 1: Synthesis of α-amanitin-cyclo[DKP-RGD] and α-amanitin-cyclo[DKP-isoDGR] conjugates **7**–**10**. Reagents and conditions: a) 1. glutaric anhydride, DMAP, iPr_2NEt, DMF, overnight, 2. DIC, *N*-hydroxysuccinimide, DMF, overnight; b) di-*N*-succinimidyl glutarate, iPr_2NEt, rt, DMF, 6 h; c) H_2NCH_2-cyclo[DKP-RGD] (**2**), PBS/MeCN or PBS/DMF (pH 7.5), overnight; d) H_2NCH_2-cyclo[DKP-isoDGR] (**4**), PBS/DMF (pH 7.5), overnight. DMAP: 4-dimethylaminopyridine; DIC: diisopropylcarbodiimide; PBS: phosphate-buffered saline; PAB: *p*-aminobenzyl.

range as the free ligands (cf. Table 2 with Table 1). These results encouraged us to proceed with cell viability assays in $\alpha_V\beta_3$ positive and $\alpha_V\beta_3$ negative cell lines, to study the ability of the conjugates to selectively target $\alpha_V\beta_3$ expressing tumor cells.

Cell viability assays

The antiproliferative activity of the conjugates was evaluated in three cell lines expressing different levels of $\alpha_V\beta_3$ integrin. U87 cells (human glioblastoma) were selected as $\alpha_V\beta_3$ positive, while A549 cells (human lung carcinoma) and MDA-MB-468 (breast adenocarcinoma) [32] were used as $\alpha_V\beta_3$ negative. The expression of $\alpha_V\beta_3$ integrin on the cell membrane was assessed by flow cytometry (see Supporting Information File 1, Figure S1), and the results were in good agreement with the literature for U87 and A549 [33-35]. In the case of MDA-MB-468, while the presence of the β_3 integrin subunit is still quite controversial in the literature [36-38], our FACS analysis could not detect any $\alpha_V\beta_3$ expression (see Supporting Information File 1).

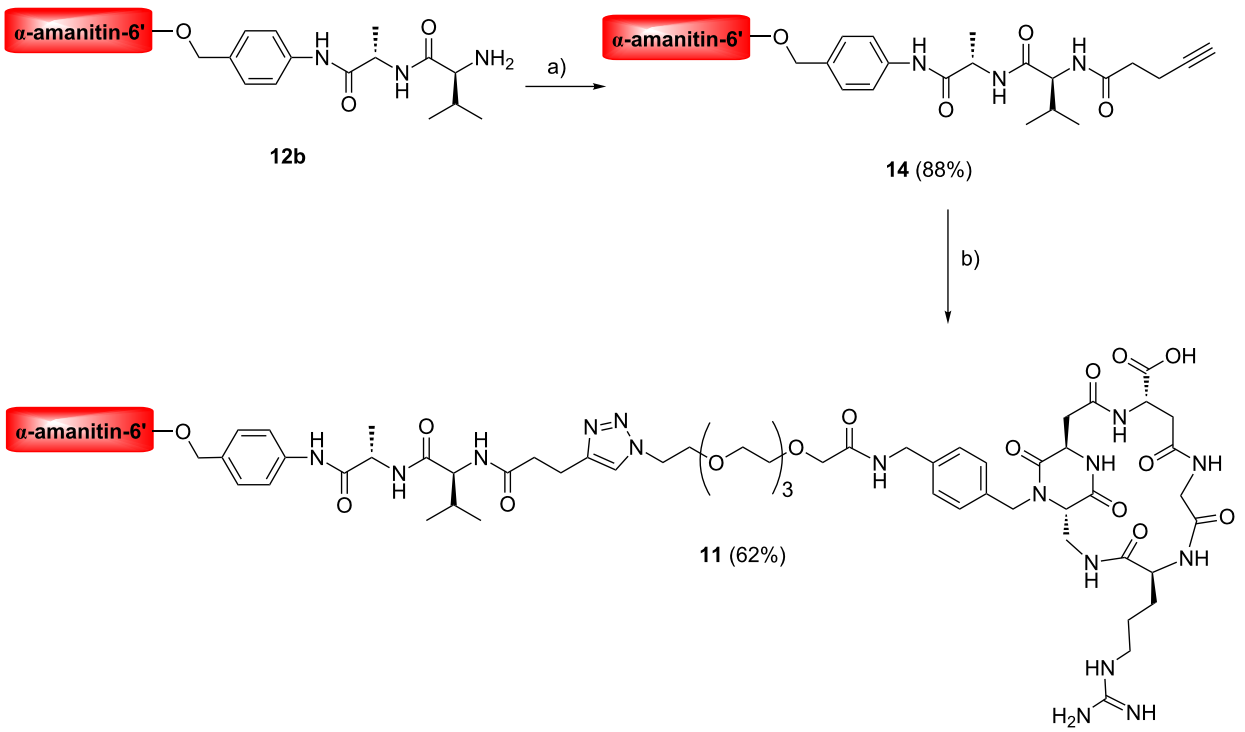

Scheme 2: Synthesis of cyclo[DKP-isoDGR]-PEG-4-Val-Ala-α-amanitin conjugate **11**. Reagents and conditions: a) 4-pentynoic acid *N*-hydroxysuccinimidyl ester, iPr_2NEt, DMF, overnight; b) N_3-PEG-4-cyclo[DKP-isoDGR], sodium ascorbate, $CuSO_4 \cdot 5H_2O$, DMF/water, rt, overnight.

Table 2: Inhibition of biotinylated vitronectin binding to $\alpha_v\beta_3$ receptor.

compound	structure (name)	IC_{50} (nM)[a] $\alpha_V\beta_3$
7	cyclo[DKP-RGD]-uncleavable-α-amanitin	11.6 ± 2.4
8	cyclo[DKP-isoDGR]-uncleavable-α-amanitin	6.8 ± 4.3
9	cyclo[DKP-RGD]-Val-Ala-α-amanitin	14.7 ± 6.6
10	cyclo[DKP-isoDGR]-Val-Ala-α-amanitin	6.4 ± 1.9
11	cyclo[DKP-isoDGR]-PEG-4-Val-Ala-α-amanitin	3.8 ± 0.3

[a]IC_{50} values were calculated as the concentration of compound required for 50% inhibition of biotinylated vitronectin binding as estimated by GraphPad Prism software. All values are the arithmetic mean ± the standard deviation (SD) of triplicate determinations.

The cell lines were treated with different concentrations of the free drug α-amanitin and conjugates **7**–**11** for 96 hours. The cell viability was evaluated with the CellTiterGlo 2.0 assay and the calculated IC_{50} are shown in Table 3.

The cyclo[DKP-isoDGR]-α-amanitin conjugate bearing the lysosomally cleavable Val-Ala linker **10** proved slightly more potent than α-amanitin in the U87 ($\alpha_V\beta_3$+) cell line, as well as in the A549 and MDA-MB-468 ($\alpha_V\beta_3$−) cell lines (2.4–3.1 times, cf. entry 1 with entry 5 in Table 3). The cyclo[DKP-isoDGR]-α-amanitin conjugate bearing the lysosomally cleavable Val-Ala linker and a PEG-4 spacer **11** proved slightly more potent than α-amanitin in both the U87 ($\alpha_V\beta_3$+) and MDA-MB-468 ($\alpha_V\beta_3$−) cell lines (2.1–2.8 times, cf. entry 1 with entry 6 in Table 3), while in A549 cell line ($\alpha_V\beta_3$−) it turned out to be less potent (1.4 times) than the free drug. Cyclo[DKP-RGD]-uncleavable-α-amanitin (**7**), cyclo[DKP-isoDGR]-uncleavable-α-amanitin (**8**) and cyclo[DKP-RGD]-Val-Ala-α-amanitin (**9**) proved less potent than α-amanitin in all cell lines (see Table 3, cf. entry 1 with entries 2–4). In general, one can conclude that the "uncleavable" compounds **7** and **8** are much less cytotoxic than free α-amanitin, while the lysosomally cleavable compounds **9**–**11** show variable results, with RGD compound **9** behaving worse than the free drug but better than the corresponding uncleavable conjugate **7**. The isoDGR motif gives generally better results, with **10** and **11** behaving

Table 3: Evaluation of anti-proliferative activity of α-amanitin and α-amanitin conjugates **7**–**11** in U-87, MDA-MB-468 and A549.

entry	structure (name)	IC_{50} (nM)[a]		
		U87 ($\alpha_V\beta_3$+)	MDA-MB-468 ($\alpha_V\beta_3$−)	A549 ($\alpha_V\beta_3$−)
1	α-amanitin	347 ± 132.5[b]	185 ± 49.6[b]	518 ± 305[b]
2	cyclo[DKP-RGD]-uncleavable-α-amanitin (**7**)	2552 ± 37.6	1111 ± 228.4	n.d.[c]
3	cyclo[DKP-isoDGR]-uncleavable-α-amanitin (**8**)	3355 ± 19.1	2200 ± 96.2	n.d.[c]
4	cyclo[DKP-RGD]-Val-Ala-α-amanitin (**9**)	1446 ± 83.9	202 ± 10.3	2160 ± 23.3
5	cyclo[DKP-isoDGR]-Val-Ala-α-amanitin (**10**)	143 ± 33.8	59 ± 23.4	217 ± 98.3
6	cyclo[DKP-isoDGR]-PEG-4-Val-Ala-α-amanitin (**11**)	165 ± 4.0	66 ± 24.1	720 ± 98.1

[a]IC_{50} values were calculated as the concentration of compound required for 50% inhibition of cell viability. All cell lines were treated with different concentrations of α-amanitin and compounds **7**–**11** for 96 hours. The samples were measured in triplicate. [b]Average values from three independent experiments. [c]n.d.: these data could not be determined.

much better than the corresponding uncleavable conjugate **8** and slightly better than the free drug. Apparently, for all the α-amanitin conjugates there is no direct correlation between the cytotoxicity and the expression of $\alpha_V\beta_3$ integrin [39].

To determine whether the increased cytotoxicity of *cyclo*[DKP-*iso*DGR]-α-amanitin conjugates **10** and **11** is governed by an integrin-mediated binding and internalization process, competition experiments [40] were carried out in which conjugates **10** and **11** were tested on U87 ($\alpha_V\beta_3$+, $\alpha_V\beta_5$+, $\alpha_V\beta_6$−, $\alpha_5\beta_1$+) [34-36] and on MDA-MB-468 ($\alpha_V\beta_3$−, $\alpha_V\beta_5$+, $\alpha_V\beta_6$+, $\alpha_5\beta_1$−) [34-36] cells in the presence of 50-fold excess of cilengitide [23], with the aim of blocking integrins on the cell surface (Table 4, see also Supporting Information File 1, Biological assays). Using the U87 cell line, a modest IC_{50} increase of conjugate **11** from 91 nM (without cilengitide) to 143 nM (with excess cilengitide) was observed (Table 4, entry 2). Using the MDA-MB-468 cell line, a more pronounced IC_{50} increase was observed for both conjugates **10** (from 47 nM without cilengitide to 259 nM with excess cilengitide; Table 4, entry 1) and **11** (from 65 nM without cilengitide to 340 nM with excess cilengitide; Table 4, entry 2). From these results, no correlation emerges between the expression of integrin $\alpha_V\beta_3$ and cytotoxicity. However, it should be noted that these cell lines overexpress other integrins ($\alpha_5\beta_1$ in U87, $\alpha_V\beta_6$ in MDA-MB-468, and $\alpha_V\beta_5$ in both) [34-36]. Thus, the increase of the IC_{50} of conjugates **10** and **11** (up to 5.5 times) may be possibly due to the block of other integrins with excess cilengitide, which is known to efficiently bind not only $\alpha_V\beta_3$ (IC_{50} = 0.6 nM) [23], but also $\alpha_V\beta_5$ (IC_{50} = 8.4 nM) [23], $\alpha_V\beta_6$ (IC_{50} = 82.8 nM) [41], and $\alpha_5\beta_1$ (IC_{50} = 14.9 nM) [23].

Conclusion

In this paper, two cyclo[DKP-RGD]-α-amanitin and three cyclo[DKP-isoDGR]-α-amanitin conjugates were prepared in good yields following a straightforward synthetic route. Conjugates **7**–**11** retain good binding affinities for the purified $\alpha_V\beta_3$ receptor, in the same range as the respective free ligands. Cell proliferation assays were performed with three cell lines possessing different levels of integrin expression: human glioblastoma U87 ($\alpha_V\beta_3$+), human lung carcinoma A549 ($\alpha_V\beta_3$−) and breast adenocarcinoma MDA-MB-468 ($\alpha_V\beta_3$−). With all these cell lines the cyclo[DKP-isoDGR]-α-amanitin conjugate **10** proved slightly more potent than

Table 4: Competition experiments of conjugates **10** and **11** in the presence of a 50-fold excess of cilengitide in U-87 and MDA-MB-468.

entry	compound	IC_{50} (nM)[a]	
		U87 ($\alpha_V\beta_3$+, $\alpha_V\beta_5$+, $\alpha_V\beta_6$−, $\alpha_5\beta_1$+)	MDA-MB-468 ($\alpha_V\beta_3$−, $\alpha_V\beta_5$+, $\alpha_V\beta_6$+, $\alpha_5\beta_1$−)
1	**10**	107 ± 26.8	47 ± 21.1
	10 + 50-fold excess of cilengitide	106 ± 11.6	259 ± 55.2
2	**11**	91 ± 30.6	65 ± 17.6
	11 + 50-fold excess of cilengitide	143 ± 59.3	340 ± 210.3

[a]IC_{50} values were calculated as the concentration of compound required for 50% inhibition of cell viability. Both cell lines were treated with different concentrations of compounds **10** and **11** in the presence of a 50-fold excess of cilengitide during 96 hours. The samples were measured in triplicate.

α-amanitin, whereas conjugate **11** showed enhanced potency compared to the free drug only on U87 and MDA-MB-468 cells.

Apparently, for all these α-amanitin conjugates there is no correlation between the cytotoxicity and the expression of $\alpha_V\beta_3$ integrin. To determine whether the slightly increased cytotoxicity of cyclo[DKP-isoDGR]-α-amanitin conjugates **10** and **11** is governed by an integrin-mediated binding and internalization process, competition experiments were carried out in which conjugates **10** and **11** were tested with U87 ($\alpha_V\beta_3$+, $\alpha_V\beta_5$+, $\alpha_V\beta_6$−, $\alpha_5\beta_1$+) and MDA-MB-468 ($\alpha_V\beta_3$−, $\alpha_V\beta_5$+, $\alpha_V\beta_6$+, $\alpha_5\beta_1$−) cells in the presence of 50-fold excess of cilengitide, with the aim of blocking integrins on the cell surface. Using the U87 cell line, a modest increase of the conjugate **11** IC_{50} was observed in the presence of cilengitide. Employing the MDA-MB-468 cell line, a more pronounced increase of IC_{50} was observed for both conjugates **10** and **11** in the presence of cilengitide. Therefore, it appears that blocking integrins with excess cilengitide, which is known to strongly bind not only $\alpha_V\beta_3$, but also $\alpha_V\beta_5$, $\alpha_V\beta_6$, and $\alpha_5\beta_1$, results in an increase (up to 5.5 times) of the IC_{50} of conjugates **10** and **11** with the MDA-MB-468 cell line. These data suggest that cyclo[DKP-isoDGR]-α-amanitin conjugates **10** and **11** are possibly internalized by a process mediated by integrins different from $\alpha_V\beta_3$ (e.g., $\alpha_V\beta_5$), though the exact nature of this involvement is not clearly defined [42].

Finally, the IC_{50} values of the integrin ligand-α-amanitin conjugates are much worse (cytotoxicity increased three times compared to α-amanitin) than those exhibited by antibody α-amanitin conjugates for which the increase of cytotoxicity is 100–100000 times [5]. Therefore, despite the remarkable progresses that have been realized in recent years, integrin targeting SMDCs are still far from the clinic.

Experimental

Functionalized ligands H_2NCH_2-cyclo[DKP-RGD] (**2**) and H_2NCH_2-cyclo[DKP-isoDGR] (**4**) were prepared according to the literature [28,29]. 6'-Functionalized α-amanitin derivatives **12a** and **12b** were prepared according to references [43,44].

Supporting Information

Supporting Information File 1

Experimental details, characterization data and copies of spectra.
[https://www.beilstein-journals.org/bjoc/content/supplementary/1860-5397-14-29-S1.pdf]

Acknowledgements

We thank the European Commission (Marie Skłodowska-Curie ITN MAGICBULLET 642004) for PhD fellowships (to L.B., P.L.R., B.K.) and financial support.

ORCID® iDs

Lizeth Bodero - https://orcid.org/0000-0003-2552-0064
Paula López Rivas - https://orcid.org/0000-0002-0539-8682
Daniela Arosio - https://orcid.org/0000-0001-5486-3504
Luca Pignataro - https://orcid.org/0000-0002-7200-9720
Cesare Gennari - https://orcid.org/0000-0002-7635-4900
Umberto Piarulli - https://orcid.org/0000-0002-6952-1811

References

1. Wieland, T.; Faulstich, H. *Experientia* **1991,** *47,* 1186–1193. doi:10.1007/BF01918382
2. Anderl, J.; Echner, H.; Faulstich, H. *Beilstein J. Org. Chem.* **2012,** *8,* 2072–2084. doi:10.3762/bjoc.8.233
3. Letschert, K.; Faulstich, H.; Keller, D.; Keppler, D. *Toxicol. Sci.* **2006,** *91,* 140–149. doi:10.1093/toxsci/kfj141
4. Davis, M. T.; Preston, J. F., III. *Science* **1981,** *213,* 1385–1388. doi:10.1126/science.6115471
5. Moldenhauer, G.; Salnikov, A. V.; Lüttgau, S.; Herr, I.; Anderl, J.; Faulstich, H. *J. Natl. Cancer Inst.* **2012,** *104,* 622–634. doi:10.1093/jnci/djs140
6. Krall, N.; Scheuermann, J.; Neri, D. *Angew. Chem., Int. Ed.* **2013,** *52,* 1384–1402. doi:10.1002/anie.201204631
7. Moshnikova, A.; Moshnikova, V.; Andreev, O. A.; Reshetnyak, Y. K. *Biochemistry* **2013,** *52,* 1171–1178. doi:10.1021/bi301647y
8. Zhao, L.; May, J. P.; Blanc, A.; Dietrich, D. J.; Loonchanta, A.; Matinkhoo, K.; Pryyma, A.; Perrin, D. M. *ChemBioChem* **2015,** *16,* 1420–1425. doi:10.1002/cbic.201500226
9. Desgrosellier, J. S.; Cheresh, D. A. *Nat. Rev. Cancer* **2010,** *10,* 9–22. doi:10.1038/nrc2748
10. Danhier, F.; Le Breton, A.; Préat, V. *Mol. Pharmaceutics* **2012,** *9,* 2961–2973. doi:10.1021/mp3002733
11. De Franceschi, N.; Hamidi, H.; Alanko, J.; Sahgal, P.; Ivaska, J. *J. Cell Sci.* **2015,** *128,* 839–852. doi:10.1242/jcs.161653
12. Pierschbacher, M. D.; Ruoslahti, E. *Nature* **1984,** *309,* 30–33. doi:10.1038/309030a0
13. Biochemical studies have shown that a spontaneous post-translational modification, occurring at the Asn-Gly-Arg (NGR) motif of the extracellular matrix protein fibronectin, leads to the *iso*AspGlyArg (isoDGR) sequence.
14. Curnis, F.; Longhi, R.; Crippa, L.; Cattaneo, A.; Dondossola, E.; Bachi, A.; Corti, A. *J. Biol. Chem.* **2006,** *281,* 36466–36476. doi:10.1074/jbc.M604812200
15. Curnis, F.; Sacchi, A.; Gasparri, A.; Longhi, R.; Bachi, A.; Doglioni, C.; Bordignon, C.; Traversari, C.; Rizzardi, G.-P.; Corti, A. *Cancer Res.* **2008,** *68,* 7073–7082. doi:10.1158/0008-5472.CAN-08-1272
16. Corti, A.; Curnis, F. *J. Cell Sci.* **2011,** *124,* 515–522. doi:10.1242/jcs.077172
17. Biochemical, spectroscopic and computational investigations showed that the *iso*DGR sequence can fit into the RGD-binding pocket of $\alpha_V\beta_3$ integrin, establishing the same electrostatic clamp as well as additional polar interactions, see ref. [18-20].

18. Spitaleri, A.; Mari, S.; Curnis, F.; Traversari, C.; Longhi, R.; Bordignon, C.; Corti, A.; Rizzardi, G.-P.; Musco, G. *J. Biol. Chem.* **2008,** *283,* 19757–19768. doi:10.1074/jbc.M710273200
19. Curnis, F.; Cattaneo, A.; Longhi, R.; Sacchi, A.; Gasparri, A. M.; Pastorino, F.; Di Matteo, P.; Traversari, C.; Bachi, A.; Ponzoni, M.; Rizzardi, G.-P.; Corti, A. *J. Biol. Chem.* **2010,** *285,* 9114–9123. doi:10.1074/jbc.M109.044297
20. Ghitti, M.; Spitaleri, A.; Valentinis, B.; Mari, S.; Asperti, C.; Traversari, C.; Rizzardi, G.-P.; Musco, G. *Angew. Chem., Int. Ed.* **2012,** *51,* 7702–7705. doi:10.1002/anie.201202032
21. Gottschalk, K.-E.; Kessler, H. *Angew. Chem., Int. Ed.* **2002,** *41,* 3767–3774. doi:10.1002/1521-3773(20021018)41:20<3767::AID-ANIE3767>3.0.CO;2-T
22. Auzzas, L.; Zanardi, F.; Battistini, L.; Burreddu, P.; Carta, P.; Rassu, G.; Curti, C.; Casiraghi, G. *Curr. Med. Chem.* **2010,** *17,* 1255–1299. doi:10.2174/092986710790936301
23. Kapp, T. G.; Rechenmacher, F.; Neubauer, S.; Maltsev, O. V.; Cavalcanti-Adam, E. A.; Zarka, R.; Reuning, U.; Notni, J.; Wester, H.-J.; Mas-Moruno, C.; Spatz, J.; Geiger, B.; Kessler, H. *Sci. Rep.* **2017,** *7,* No. 39805. doi:10.1038/srep39805
24. da Ressurreição, A. S. M.; Vidu, A.; Civera, M.; Belvisi, L.; Potenza, D.; Manzoni, L.; Ongeri, S.; Gennari, C.; Piarulli, U. *Chem. – Eur. J.* **2009,** *15,* 12184–12188. doi:10.1002/chem.200902398
25. Marchini, M.; Mingozzi, M.; Colombo, R.; Guzzetti, I.; Belvisi, L.; Vasile, F.; Potenza, D.; Piarulli, U.; Arosio, D.; Gennari, C. *Chem. – Eur. J.* **2012,** *18,* 6195–6207. doi:10.1002/chem.201200457
26. Mingozzi, M.; Dal Corso, A.; Marchini, M.; Guzzetti, I.; Civera, M.; Piarulli, U.; Arosio, D.; Belvisi, L.; Potenza, D.; Pignataro, L.; Gennari, C. *Chem. – Eur. J.* **2013,** *19,* 3563–3567. doi:10.1002/chem.201204639
27. Panzeri, S.; Zanella, S.; Arosio, D.; Vahdati, L.; Dal Corso, A.; Pignataro, L.; Paolillo, M.; Schinelli, S.; Belvisi, L.; Gennari, C.; Piarulli, U. *Chem. – Eur. J.* **2015,** *21,* 6265–6271. doi:10.1002/chem.201406567
28. Colombo, R.; Mingozzi, M.; Belvisi, L.; Arosio, D.; Piarulli, U.; Carenini, N.; Perego, P.; Zaffaroni, N.; De Cesare, M.; Castiglioni, V.; Scanziani, E.; Gennari, C. *J. Med. Chem.* **2012,** *55,* 10460–10474. doi:10.1021/jm301058f
29. Dal Corso, A.; Caruso, M.; Belvisi, L.; Arosio, D.; Piarulli, U.; Albanese, C.; Gasparri, F.; Marsiglio, A.; Sola, F.; Troiani, S.; Valsasina, B.; Pignataro, L.; Donati, D.; Gennari, C. *Chem. – Eur. J.* **2015,** *21,* 6921–6929. doi:10.1002/chem.201500158
30. Zanella, S.; Angerani, S.; Pina, A.; López Rivas, P.; Giannini, C.; Panzeri, S.; Arosio, D.; Caruso, M.; Gasparri, F.; Fraietta, I.; Albanese, C.; Marsiglio, A.; Pignataro, L.; Belvisi, L.; Piarulli, U.; Gennari, C. *Chem. – Eur. J.* **2017,** *23,* 7910–7914. doi:10.1002/chem.201701844
31. Dal Corso, A.; Pignataro, L.; Belvisi, L.; Gennari, C. *Curr. Top. Med. Chem.* **2016,** *16,* 314–329. doi:10.2174/1568026615666150701114343
32. Kwon, K. C.; Ko, H. K.; Lee, J.; Lee, E. J.; Kim, K.; Lee, J. *Small* **2016,** *12,* 4241–4253. doi:10.1002/smll.201600917
33. Goodman, S. L.; Grote, H. J.; Wilm, C. *Biol. Open* **2012,** *1,* 329–340. doi:10.1242/bio.2012364
34. Bai, S. Y.; Xu, N.; Chen, C.; Song, Y.-l.; Hu, J.; Bai, C.-x. *Clin. Respir. J.* **2015,** *9,* 457–467. doi:10.1111/crj.12163
35. Currier, N. V.; Ackerman, S. E.; Kintzing, J. R.; Chen, R.; Interrante, M. F.; Steiner, A.; Sato, A. K.; Cochran, J. R. *Mol. Cancer Ther.* **2016,** *15,* 1291–1300. doi:10.1158/1535-7163.MCT-15-0881
36. Meyer, T.; Marshall J. F.; Hart, I. R. *Br. J. Cancer* **1998**, *77*, 530-536. doi:10.1038/bjc.1998.86 For reports on the lack of β3 integrin expression in MDA-MB-468, see also ref. [32,33].
37. Liu, Z.; Yan, Y.; Liu, S.; Wang, F.; Chen, X. *Bioconjugate Chem.* **2009,** *20,* 1016–1025, and ref. [38]. doi:10.1021/bc9000245
38. Lautenschlaeger, T.; Perry, J.; Peereboom, D.; Li, B.; Ibrahim, A.; Huebner, A.; Meng, W.; White, J.; Chakravarti, A. *Radiat. Oncol.* **2013,** *8,* No. 246. doi:10.1186/1748-717X-8-246
39. Sancey, L.; Garanger, E.; Foillard, S.; Schoehn, G.; Hurbin, A.; Albiges-Rizo, C.; Boturyn, D.; Souchier, C.; Grichine, A.; Dumy, P.; Coll, J.-L. *Mol. Ther.* **2009,** *17,* 837–843. doi:10.1038/mt.2009.29
40. Cox, N.; Kintzing, J. R.; Smith, M.; Grant, G. A.; Cochran, J. R. *Angew. Chem., Int. Ed.* **2016,** *55,* 9894–9897. doi:10.1002/anie.201603488 Angew. Chem. 2016, *128*, 10048–10051. doi:10.1002/ange.201603488
41. Civera, M.; Arosio, D.; Bonato, F.; Manzoni, L.; Pignataro, L.; Zanella, S.; Gennari, C.; Piarulli, U.; Belvisi, L. *Cancers* **2017,** *9,* No. 128. doi:10.3390/cancers9100128
42. Memmo, L. M.; McKeown-Longo, P. *J. Cell Sci.* **1998,** *111,* 425–433.
43. Anderl, J.; Mueller, C.; Simon, W. Amatoxin-conjugates with improved linkers. WO Patent WO2012041504, April 5, 2012.
44. Anderl, J.; Hechler, T.; Mueller, C.; Pahl, A. Amatoxin-antibody conjugates. WO Patent WO 2016142049, Sept 15, 2016.

License and Terms

BEILSTEIN JOURNAL OF ORGANIC CHEMISTRY

Synthesis and in vitro biochemical evaluation of oxime bond-linked daunorubicin–GnRH-III conjugates developed for targeted drug delivery

Sabine Schuster[1,2], Beáta Biri-Kovács[1,2], Bálint Szeder[3], Viktor Farkas[4], László Buday[3], Zsuzsanna Szabó[5], Gábor Halmos[5] and Gábor Mező[*1,2]

Full Research Paper

Open Access

Address:
[1]MTA-ELTE Research Group of Peptide Chemistry, Hungarian Academy of Sciences, Eötvös L. University, 1117 Budapest, Hungary, [2]Institute of Chemistry, Eötvös L. University, 1117 Budapest, Hungary, [3]Research Centre for Natural Sciences, Institute of Enzymology, Hungarian Academy of Sciences, 1117 Budapest, Hungary, [4]MTA-ELTE Protein Modelling Research Group, Hungarian Academy of Sciences, Eötvös L. University, 1117 Budapest, Hungary and [5]Department of Biopharmacy, Faculty of Pharmacy, University of Debrecen, 4032 Debrecen, Hungary

Email:
Gábor Mező[*] - gmezo@elte.hu

* Corresponding author

Keywords:
cytostatic effect; daunorubicin; drug-targeting; GnRH derivatives; oxime linkage

Beilstein J. Org. Chem. **2018,** *14,* 756–771.
doi:10.3762/bjoc.14.64

Received: 12 January 2018
Accepted: 15 March 2018
Published: 04 April 2018

This article is part of the Thematic Series "Peptide–drug conjugates".

Guest Editor: N. Sewald

Abstract

Gonadotropin releasing hormone-III (GnRH-III), a native isoform of the human GnRH isolated from sea lamprey, specifically binds to GnRH receptors on cancer cells enabling its application as targeting moieties for anticancer drugs. Recently, we reported on the identification of a novel daunorubicin–GnRH-III conjugate (GnRH-III–[^{4}Lys(Bu), ^{8}Lys(Dau=Aoa)] with efficient in vitro and in vivo antitumor activity. To get a deeper insight into the mechanism of action of our lead compound, the cellular uptake was followed by confocal laser scanning microscopy. Hereby, the drug daunorubicin could be visualized in different subcellular compartments by following the localization of the drug in a time-dependent manner. Colocalization studies were carried out to prove the presence of the drug in lysosomes (early stage) and on its site of action (nuclei after 10 min). Additional flow cytometry studies demonstrated that the cellular uptake of the bioconjugate was inhibited in the presence of the competitive ligand triptorelin indicating a receptor-mediated pathway. For comparative purpose, six novel daunorubicin–GnRH-III bioconjugates have been synthesized and biochemically characterized in which ^{6}Asp was replaced by D-Asp, D-Glu and D-Trp. In addition to the analysis of the in vitro cytostatic effect and cellular uptake, receptor binding studies with ^{125}I-triptorelin as radiotracer and degradation of the GnRH-

III conjugates in the presence of rat liver lysosomal homogenate have been performed. All derivatives showed high binding affinities to GnRH receptors and displayed in vitro cytostatic effects on HT-29 and MCF-7 cancer cells with IC_{50} values in a low micromolar range. Moreover, we found that the release of the active drug metabolite and the cellular uptake of the bioconjugates were strongly affected by the amino acid exchange which in turn had an impact on the antitumor activity of the bioconjugates.

Introduction

Cancer is one of the most serious diseases worldwide and malignant tumors and metastases often lead to high mortality. Chemotherapy is a widely used method to treat cancerous diseases, but the lack of selectivity, drug-specific side-effects and toxicity to healthy tissues result in various complications, which restrict the application of chemotherapeutics. A promising treatment option to overcome these drawbacks can be targeted tumor therapy. This approach is based on the fact that receptors for many regulatory ligands such as peptide hormones are overexpressed on the surface of various cancer cells including gonadotropin-releasing hormone receptors (GnRH-R) [1]. Therefore, these peptides are suitable for specific drug targeting to tumor cells. The native ligand of this receptor is GnRH-I (<EHWSYGLRPG-NH_2, where <E is pyroglutamic acid) which is synthesized and released within the hypothalamus. GnRH stimulates the synthesis and release of the regulatory pituitary glycoprotein luteinizing hormone (LH) and follicle stimulating hormone (FSH) which act on the gonads and regulate the production of the sex steroids androgen and estrogen [2].

In the last decades a large number of synthetic GnRH-I-analogues has been designed with the purpose to interact with the receptor and influence the release of pituitary gonadotropins LH and FSH [1,3-6]. The replacement of ^{6}Gly by D-amino acids in human GnRH-I provides superagonists like the GnRH-I derivatives buserelin [^{6}D-Ser(*t*-Bu), ^{9}Pro-EA], goserelin [^{6}D-Ser(*t*-Bu), ^{10}Azagly-NH_2], leuprolide [^{6}D-Leu, ^{9}Pro-EA] and triporelin [^{6}D-Trp], which are used as pharmaceutical peptides to treat inter alia hormone dependent prostate and/or breast cancer [7].

Since the mid-1980s cytotoxic GnRH-I derivatives were developed and investigated to treat tumor cells [4,5,8,9]. Anthracyclines such as doxorubicin (Dox), daunorubicin (Dau) or epirubicin are frequently used anticancer drugs. Their mode of action is based on a planar ring system which is important for intercalation into DNA [10]. In this way, anthracyclines can affect a broad range of DNA processes leading to an inhibited synthesis of macromolecules such as mRNA and DNA [10,11]. More precisely, anthracyclines act as topoisomerase II toxins inhibiting DNA transcription and replication. They stabilize a DNA topoisomerase-II intermediate in which the DNA strands are separated and a specific tyrosine residue of the topoisomerase II is covalently linked to the DNA by formation of a tyrosine phosphodiester [10-12]. Moreover, anthracyclines provide a beneficial auto-fluorescence allowing the performance of fluorescence based studies like confocal laser scanning microscopy (CLSM) and fluorescence-activated cell sorting (FACS) to investigate the cellular uptake and the subcellular localization of the drug or the drug bioconjugates [13,14]. It is well known from the literature that anthracyclines accumulate in the nucleus, in that manner they also act as DNA stains [14,15].

The first cytotoxic GnRH-I derivative, which was investigated in preclinical and clinical studies, was zoptarelin-doxorubicin also known as AEZS-108 (previously AN-152) [16]. The anthracycline doxorubicin was conjugated to the ε-amino group of GnRH-I-[^{6}D-Lys] by insertion of a glutaric acid linker. The resulting ester bond can be cleaved by carboxylesterases, leading to the release of the cytotoxic agent within the tumor cell. During clinical trials, only mild side effects were observed which are caused by premature drug release [17]. The receptor mediated uptake of zoptarelin has been investigated by blockage of GnRH receptors using an excess of the GnRH-I superagonist triptorelin [14]. In addition, the internalization and the intracellular localization of AN-152 were visualized by CLSM [14]. Despite all these promising findings, zoptarelin-doxorubicin did not achieve its primary endpoint in phase 3 clinical studies on endometrial cancer [18].

A natural isoform of the human GnRH-I, the sea lamprey analogue GnRH-III (<EHWSHDWKPG-NH_2), was identified and characterized by Sower et al. [19]. Due to the significantly lower endocrine effect compared to GnRH-I and the specific binding to GnRH-Rs on cancer cells, GnRH-III might have advantage as a carrier for cytotoxic drugs, especially in case of hormone-independent tumors [20]. Based on these findings, GnRH-III has been used as an efficient homing device for targeted tumor therapy [21,22]. Moreover, it was demonstrated that a modification of the side chain of ^{8}Lys did not hinder the receptor binding or the antiproliferative activity. Furthermore, the absence of the free ε-amino group additionally reduced the endocrine effect [23,24]. Thus, the ^{8}Lys can be utilized as conjugation site for cytotoxic agents like anthracyclines. In the past decade, a variety of different linkage systems has been

carried out including ester or hydrazine bonds, cathepsin-B labile spacers and oxime bonds [21,22,25].

Due to its structural properties, Dau cannot be attached to the homing device by an ester bond like Dox, because of the absence of the primary hydroxy group in position C-14. However, the C-13 carbonyl group of Dox/Dau provides a suitable conjugation site and can be used for the formation of oximes. We have recently reported that Dau was efficiently linked to the ^{8}Lys side-chain by incorporation of an aminooxyacetic acid (Aoa) moiety [21,25]. The formed oxime linkage is more stable under physiological conditions than the ester bond resulting in a longer half-life of the conjugate during circulation. Nevertheless, the drug is released within the cancer cell by lysosomal enzymes, especially by cathepsin B, which leads to various Dau containing metabolites [26]. In case of GnRH-III–[^{8}Lys(Dau=Aoa)] conjugates the smallest Dau metabolite obtained by lysosomal degradation is H-Lys(Dau=Aoa)-OH, which is able to bind to DNA resulting in a cytotoxic effect. A variety of oxime bond containing GnRH-III drug conjugates have been designed in our research group and their in vitro cytotoxic effects on hormone dependent human breast adenocarcinoma cancer cells (MCF-7) and on hormone independent human colon carcinoma cells (HT-29) were analyzed [22,25,27,28]. Thereby, it has been exposed, that an exchange of ^{4}Ser by ^{4}Lys followed by acylation of the ε-amino group with short chain fatty acids (SCFA) improved the cellular uptake and the antitumor activity [29]. Moreover, these GnRH-III bioconjugates displayed an enhanced stability in the presence of gastrointestinal enzymes. The most potent and efficient bioconjugate which has been evaluated in in vitro cytostatic effect measurements on human breast cancer cells (MCF7) and human colon cancer cells (HT-29), is GnRH-III–[^{4}Lys(Bu), ^{8}Lys(Dau=Aoa)] (**K2**). Recent studies demonstrated that the butyrilation of the lysine in position 4 not only leads to an increased in vitro but also to an enhanced in vivo antitumor activity [29,30].

In order to achieve a better understanding of the mechanism of action, the internalization and the intracellular localization, our lead compound **K2** was studied and monitored by CLSM. Furthermore, the cellular uptake of **K2** was evaluated in competition with the GnRH-I superagonist triptorelin by flow cytometry indicating a receptor mediated pathway.

To gain further information about sequence–activity relationship of GnRH-III, we studied the impact of ^{6}Asp on the efficiency of tumor targeting. Since it is known from the literature that an incorporation of D-amino acids (D-Aaa) in position 6 of GnRH-I and II peptides can lead to an improved receptor binding affinity and an enhanced antiproliferative activity without substantial effect on the endocrine activity [31-33], we developed six novel GnRH-III–Dau conjugates in which the ^{6}Asp was replaced by D-Aaa. Here we report on the synthesis of GnRH-III bioconjugates containing D-Asp, D-Glu or D-Trp in position 6 and Ser or Lys(Bu) in position 4. Moreover, the novel GnRH-III–Dau conjugates were compared systematically with our lead compound **K2** in terms of in vitro cytostatic effect, receptor binding affinity, cellular uptake and lysosomal digestion in the presence of rat liver lysosomal homogenate.

Results and Discussion

Synthesis of oxime bond-linked GnRH-III–[^{4}Ser/Lys(Bu), ^{6}Aaa, ^{8}Lys(Dau=Aoa)] bioconjugates

The GnRH-III bioconjugates were prepared as shown in Scheme 1. All peptides were synthesized by standard Fmoc-SPPS using orthogonal lysine protecting groups. Fmoc-Lys(Dde)-OH was incorporated in position 4 and Fmoc-Lys(Mtt)-OH in position 8. After peptide chain elongation the Dde group was removed and ^{4}Lys was butyrylated by using butyric anhydride. Afterwards, the Mtt group was cleaved under mild acidic conditions, followed by Boc-Aoa-OH coupling. After cleavage from the resin with an appropriate TFA–scavenger mixture and purification of the crude compounds by preparative HPLC, the attachment of daunorubicin via oxime

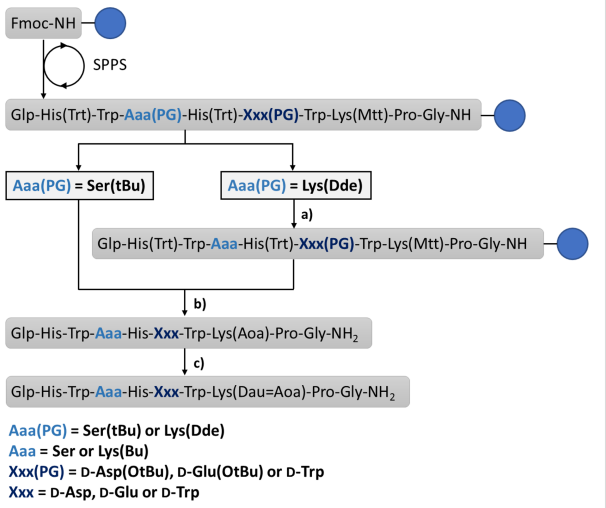

Scheme 1: Syntheses of GnRH-III–[(^{4}Lys(Bu)/^{4}Ser, ^{6}Aaa, ^{8}Lys(Dau=Aoa)] bioconjugates. a) (1) 2% hydrazine in DMF 12 × 5 min; (2) 3 equiv butyric anhydride, 3 equiv DIPEA in DMF, 2 h. b) (1) 2% TFA in DCM, 6 × 5 min; (2) 10% DIPEA in DCM, 3 × 5 min; (3) 3 equiv Boc-Aoa-OH, 3 equiv HOBt, 3 equiv DIC in DMF, 1 h; (4) 95% TFA, 2.5% TIS, 2.5% H_2O, 10 equiv H-Aoa-OH, 2h. c) 1.3 equiv Dau in 0.1 M NH_4OAc buffer (pH 5), overnight. Fmoc: 9-fluorenylmethoxycarbonyl, SPPS: solid-phase peptide synthesis, Dde: 1-(4,4-dimethyl-2,6-dioxocyclohex-1-ylidene)ethyl, Mtt: 4-methyltrityl, Bu: butyryl, Aoa: aminooxyacetyl, Dau: daunorubicin, blue circle: Rink amide MBHA-resin.

linkage was carried out in solution as previously reported [21]. The resulting GnRH-III–Dau conjugates were purified by preparative HPLC, the final products **K1**, **K2** and **1**–**6** were characterized by analytical HPLC and mass spectrometry (Table 1, Supporting Information File 1, Figures S1–S8). The bioconjugates could be obtained in yields up to 27% over all synthesis and purification steps. The lower yields of the D-amino acid containing derivatives, especially in case of D-Trp are related mainly to their decreased solubility compared to the parent compounds. Moreover, the free aminooxy group is highly reactive towards aldehydes and ketones leading to the formation of unwanted side-products [34]. Aminooxy acetylated peptides prone to react with traces of acetone or formaldehyde (e.g., from the softeners of the plastic tubes) not only during the reaction steps (cleavage, ligation) but also under the HPLC purification conditions which has a high impact on the yield [35].

Secondary structure determination by electronic circular dichroism spectroscopy

ECD spectra of GnRH-III–[^{4}Ser/^{4}Lys(Bu), ^{6}D/L-Asp, ^{8}Lys(Dau=Aoa)] (**K1**, **K2**, **1** and **4**) were measured in aqueous solution to study the influence of the exchange of L-Asp to D-Asp in position 6 on the peptide conformation. The D-Trp containing analogs were not soluble under this condition, while we did not expect significant influence of ECD spectra from the exchange of D-Asp to D-Glu. The ECD spectra of all four GnRH-III peptide conjugates reveal two distinct bands: one negative at 200 nm and one positive at 235 nm (Figure 1, Supporting Information File 1, Figures S15 and S16). The negative band is also present in the GnRH-III peptide without the daunorubicin (Dau) part. This indicates that the main conformational preferences are not changed by the conjugation. The shapes of the ECD curves show a highly dynamic peptide structure in water. This is in agreement with the NMR study made by Pappa et al. that presented an extended and more flexible structure of GnRH-III than GnRH-I which has rather more defined U-shape structure [36]. In case of the positive band (235 nm) we can conclude that this is a contribution of the Dau part of the molecules because it has a positive band near 230 nm and in the conjugates this band is shifted to 235 nm. The Dau has also a negative band at 200 nm.

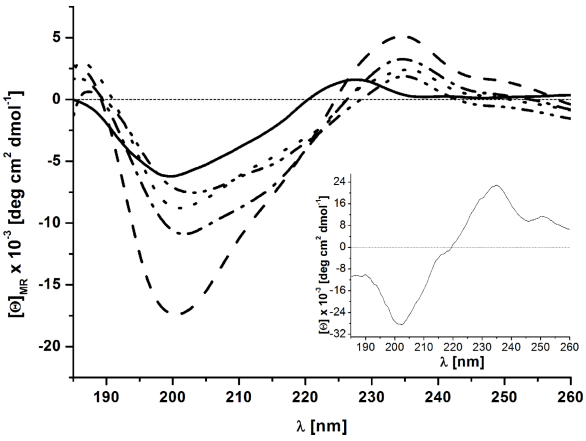

Figure 1: Far-UV ECD spectra of GnRH-III and its drug conjugates in water (GnRH-III solid, **K1** dash, **K2** dot, **1** dash dot, **4** dash dot dot). Insert: far-UV ECD spectra of daunorubicin.

The only difference between the D-Asp derivatives and the original peptides is located near 215 nm. This sign indicates the presence of increased contribution of β-sheet like secondary structure in case of D-Asp derivatives. Because no aggregation could be observed in HPLC or MS measurements, we assume that the presence of the β-hairpin structure is a feasible conception in these cases.

Stability/degradation of the GnRH-III bioconjugates

Drug delivery systems (DDS) are promising therapeutics for tumor therapy providing a selective application to tumor cells

Table 1: Chemical characteristics of Dau–GnRH-III bioconjugates.

Code	[^{8}Lys(Dau=Aoa)]–GnRH-III compound	Purity [%]	RP-HPLC t_R [min][a]	ESIMS MW_{cal}/MW_{exp} [g/mol][b]	Yield [%][c]
K1	[^{6}L-Asp]	>97	27.8	1841.89/1841.66	22
1	[^{6}D-Asp]	>96	28.0	1841.89/1841.60	8
2	[^{6}D-Glu]	>98	29.2	1855.91/1855.70	14
3	[^{6}D-Trp]	>95	32.5	1913.01/1912.80	7
K2	[^{4}Lys(Bu),^{6}L-Asp]	>97	29.3	1953.071952.79	27
4	[^{4}Lys(Bu),^{6}D-Asp]	>98	29.5	1953.07/1952.90	9
5	[^{4}Lys(Bu),^{6}D-Glu]	>96	29.7	1966.93/1966.70	7
6	[^{4}Lys(Bu),^{6}D-Trp]	>97	32.6	2024.03/2023.70	6

[a]Column: Phenomenex Luna C18 column (250 mm × 4.6 mm) with 5 µm silica (100 Å pore size); gradient: 0 min 0% B, 5 min 0% B, 50 min 90% B; eluents: 0.1% TFA in water (A) and 0.1% TFA in acetonitrile/water (80:20, v/v) (B); flow rate: 1 mL/min; detection at 220 nm. [b]Bruker Daltonics Esquire 3000+ ion trap mass spectrometer. [c]Yield over all synthetic and purification steps.

and a reduction of toxic side effects. To ensure these benefits, stability and degradation studies are of great importance during DDS development. In vitro degradation studies in the presence of gastrointestinal enzymes and lysosomal homogenate as well as stability analyses in human serum provide valuable information [37]. On the one hand toxic side effects caused by premature drug release should be avoided, on the other hand an intracellular drug release from the bioconjugates in the targeted cell is mandatory to assure the antitumor activity. Previously, we reported on the stability of the bioconjugates GnRH-III–[^{8}Lys(Dau=Aoa)] (**K1**) and GnRH-III–[^{4}Lys(Ac), ^{8}Lys(Dau=Aoa)] in 90% human serum and in the presence of digestive enzymes trypsin and α-chymotrypsin [26,38]. It was found that both Dau–GnRH-III compounds were stable in human serum and trypsin at 37 °C for at least 24 h. Furthermore, the incorporation of an acetylated lysine instead of the native serine in position 4 decelerated the degradation by α-chymotrypsin which catalyzed the hydrolysis of the peptide bond exclusively between ^{3}Trp and ^{4}Aaa. A similar effect was observed for GnRH-III conjugates in which the ε-amino group of ^{4}Lys was acylated by different SCFAs. It is worth to mention that the main cleavage sites of GnRH peptides by different enzymes are at both sides of serine in position 4 [39,40], that can be prohibited by replacement of Ser with an acylated lysine. Moreover, it has been shown that the stability is increased with the length of the side chain modification [29]. In this manner, the bioconjugate GnRH-III–[^{4}Lys(Bu), ^{8}Lys(Dau=Aoa)] (**K2**) displayed a two-fold higher stability in the presence of α-chymotrypsin than GnRH-III–[^{4}Lys(Ac), ^{8}Lys(Dau=Aoa)] [29,38].

The novel GnRH-III bioconjugates **1**–**6** have been analyzed for their stability/degradation in cell culture medium and in the presence of rat liver lysosomal homogenate. Reaction mixtures were incubated for 24 h at 37 °C, samples were taken at different time points and analyzed by analytical RP-HPLC and LC–MS. The approved bioconjugates **K1** and **K2** were analyzed in the same manner and the achieved results were used for a comparative evaluation of the novel GnRH-III–Dau conjugates.

The stability studies in cell culture medium revealed that all compounds were stable at 37 °C for 24 h which is in accordance with our previous results [29]. During this time, no decomposition of the conjugates was observed, demonstrating that no free drug or small drug containing metabolite was produced in medium during the treatment that might have influence on the in vitro biological assays.

Besides stability under physiological conditions, the release of the drug within cancer cells is of high relevance. In this study the anthracycline daunorubicin was used as anticancer agent. This drug interacts with DNA by intercalation and affects a broad range of DNA processing [11,41]. Orbán et al. recently reported that next to the free drug, also small Dau-containing metabolites revealed an antitumor activity [26,42].

In order to gain insight into the cellular release of the drug, the degradation of the Dau–GnRH-III derivatives **1**–**6, K1** and **K2** was determined in the presence of rat liver lysosomal homogenate at 37 °C. As shown in Figure 2, all GnRH-III–Dau peptides were digested by lysosomal enzymes resulting in various peptide fragments (Supporting Information File 1, Table S1). However, the degradation level and the cleavage sites within the GnRH-III sequence differ considerably depending on the incorporated amino acids, whereby the hydrolyses of the *C*-terminus (H-Gly-NH_2 and H-Pro-Gly-NH_2) occurred first in all eight GnRH-III derivatives. Due to the high chemical and enzymatic stability of the oxime bond, no free Dau was detected by LC–MS. In accordance with our previous results, the digestion of the two peptides containing L-Asp in position 6 (**K1**, **K2**) provided the smallest Dau-containing metabolite (H-Lys(Dau=Aoa)-OH, *m/z* 729.36 $[M + H]^{+}$). This metabolite could already be detected after 1 hour of incubation in case of **K2** and after 2 hours in case of **K1**. The ^{6}D-Asp containing counterparts **1** and **4** exhibited higher lysosomal stabilities preventing the release of H-Lys(Dau=Aoa)-OH. On the contrary, the fragment H-Lys(Dau=Aoa)-OH could be identified in small amount after 24 h digestion of the bioconjugates **2** and **5** (^{6}D-Glu). Surprisingly, in case of the ^{6}D-Trp containing analogues **3**, **6**, the effective metabolite was delivered much faster (after 2 h **6** or 4 h **3**) and in a higher amount (highlighted peaks Figure 2C). Moreover, the detected fragment H-wWK(Dau=Aoa)-OH demonstrated that the D-Trp of conjugate **3** was accepted at the cleavage site of at least one lysosomal protease leading to improved release of the active metabolite. It might be assumed that D-Trp of GnRH-III–[^{4}Lys(Bu), ^{6}D-Tpr, ^{8}Lys(Dau=Aoa)] (**6**) is also accepted at the cleavage site, but due to the prior hydrolysis of the ^{7}Trp-^{8}Lys(Dau=Aoa)-bond an evidential fragment has not been detected. A reason for these diversities might be the subsite specificities of the lysosomal proteases. For instance, lysosomal cysteine proteases also known as cathepsins show a broad substrate specificity [43]. Nearly all human cysteine proteases belong to the group of endopeptidases, whereby cathepsin B is also a carboxydipeptidase and cathepsin X displays carboxymono- and dipeptidase activity [44-46]. On the contrary, cathepsin C functions as an aminodipeptidase and cathepsin H reveals next to its endopeptidase activity also aminomonopeptidase activity [44,46]. Due to the variety of the detected fragments, we suggest that the rat liver homogenate contained a similar mixture of homolog cathepsins. For

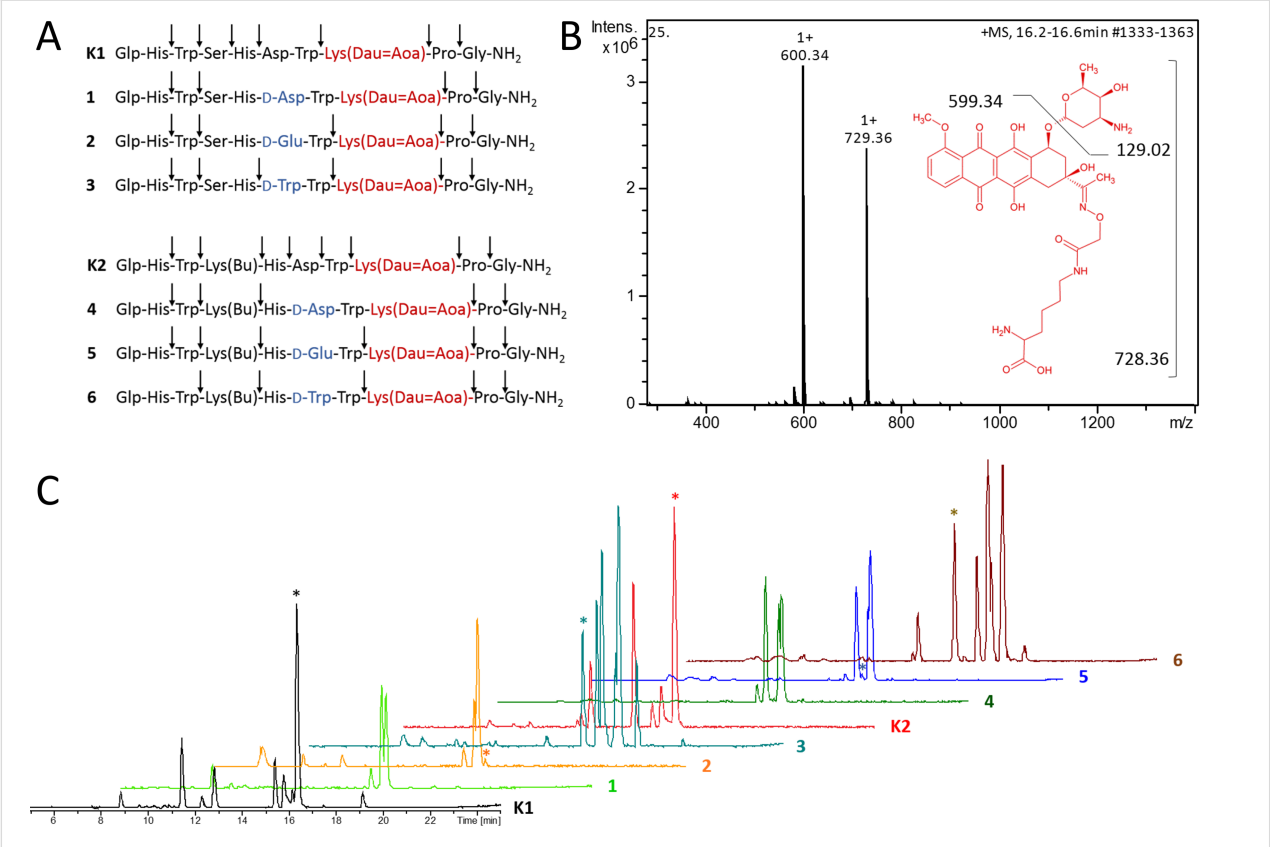

Figure 2: Degradation of the GnRH-III bioconjugates by rat liver lysosomal homogenate. A) Cleavage sites produced by the proteolysis of bioconjugates in the presence of rat liver lysosomal homogenate (full-line arrows). B) Structure of the smallest Dau-containing metabolite and its corresponding mass spectra (analysis of **K1** after 24 h incubation at the retention time 16.2–16.6 min of the LC–MS chromatogram). C) LC–MS chromatogram of the GnRH-III bioconjugates after 24 h of incubation with rat liver lysosomal homogenate at 37 °C (asterisk labeling peak of the smallest Dau-containing metabolite H-K(Dau=Aoa)-OH).

instance, the analyzed fragments of the ^{6}L-Asp derivatives gave clear hints for the presence of endopeptidases, while the digestion of the ^{6}D-Aaa compounds **1**–**3** gave only fragments which evidence the activity of exomono- and/or dipeptidases. Moreover, the obtained results for the bioconjugates that contain ^{4}Lys(Bu) (**K2**, **4**–**6**) instead of serine indicate a proteolytic cleavage by lysosomal endopeptidases, which might be of great importance for the release of the smallest Dau-containing metabolite.

Cytostatic effect of the bioconjugates

Cell lines often function as the first model system of choice to study biological processes or to test the efficiency of drugs or drug conjugates and their cytotoxic effects. Immortal cell lines offer various benefits, for instance they are easy to handle, cost-effective and provide consistent sample and reproducible results [47]. Nevertheless, cell lines also present the disadvantage that after a period of continuous growth, cell characteristics can change and dedifferentiate in culture [47,48]. The serial passaging can cause genotypic and phenotypic variations and the state of confluency can also affect gene expression pattern in some cell lines [47,49]. Due to this, the usage of internal standards during the evaluation of new potential candidates might be necessary to ensure comparability with previous results. The cytostatic effect of the novel GnRH-III bioconjugates was determined on HT-29 human colon cancer and MCF-7 human breast cancer cell lines by alamarBlue® assay. For a better comparison, the well-studied bioconjugates GnRH-III–[^{8}Lys(Dau=Aoa)] (**K1**) and GnRH-III–[^{4}Lys(Bu), ^{8}Lys(Dau=Aoa)] (**K2**) were used as positive controls and internal standards. The corresponding IC_{50} values were calculated by using nonlinear regression (sigmoidal dose response) (Figure 3, Table 2). Unfortunately, the D-Trp containing compounds **3** and **6** started to precipitate in both cell culture media at higher concentrations limiting the concentration down to a maximum of 10 µM. This effect could not be prevented by using DMSO instead of ddH_2O for the preparation of the stock solutions. Unfortunately, the lower concentration range with a maximum of 10 µM was not sufficient to achieve the dose-response. Nevertheless, both D-Trp-containing compounds provided a decreased cell viability at the highest concentration (10 µM) on HT-29 (58% (**3**) and 55% (**6**)) and MCF-7 cells

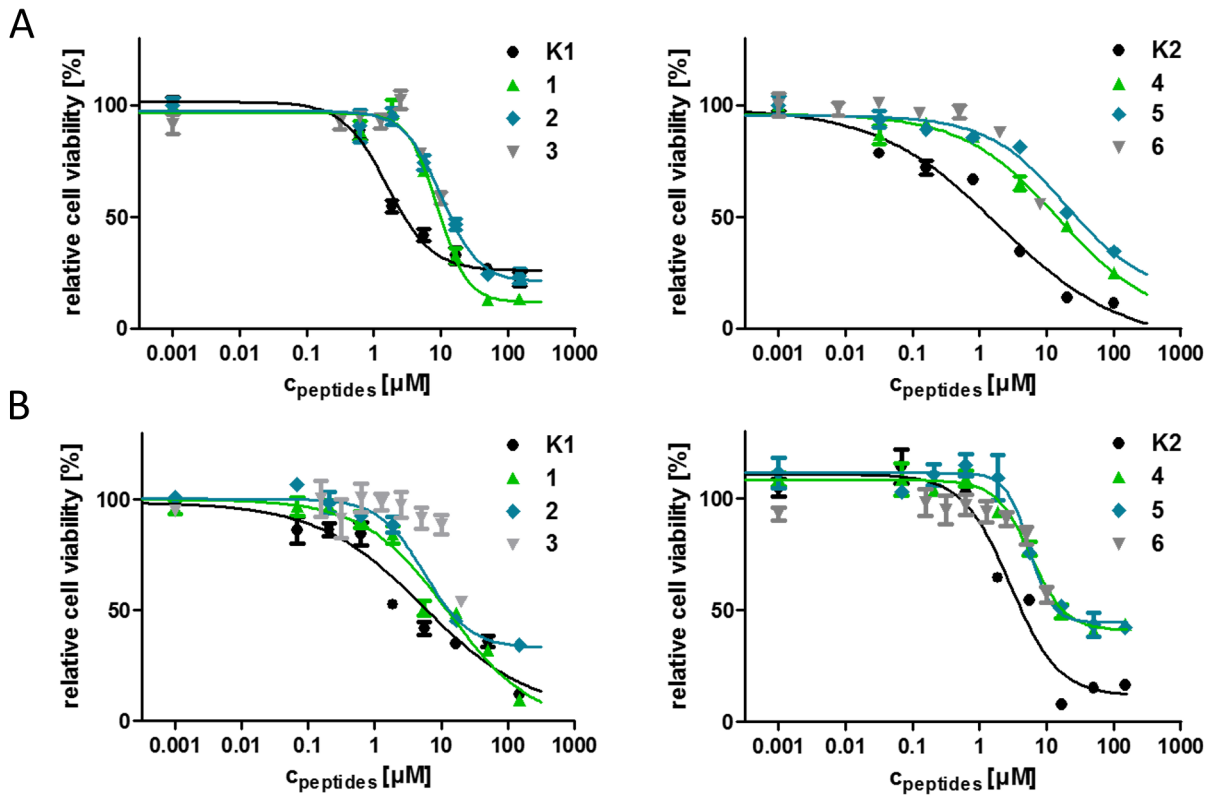

Figure 3: Cytostatic effect of the GnRH-III bioconjugates at different concentrations on A) HT-29 and B) MCF-7 cells after 24 h determined by alamarBlue® cell viability assay. Experiments were carried out by using four replicates with $n = 2$, error bars represent standard deviation. Curves obtained by nonlinear regression (sigmoidal dose response). For IC_{50} values see Table 2.

Table 2: In vitro cytostatic effects of GnRH-III bioconjugates on HT-29 human colon cancer and MCF-7 human breast cancer cell line.

code	[^{8}Lys(Dau=Aoa)]–GnRH-III compound	MCF-7 IC_{50} [μM]	HT-29 IC_{50} [μM]
K1	[^{6}L-Asp]	3.2 ± 0.1	1.5 ± 0.5
1	[^{6}D-Asp]	13.0 ± 0.5	8.9 ± 1.3
2	[^{6}D-Glu]	6.8 ± 1.0	10.1 ± 1.4
3	[^{6}D-Trp]	n.d.[a]	n.d.[a]
K2	[^{4}Lys(Bu),^{6}L-Asp]	2.7 ± 0.1	1.9 ± 0.7
4	[^{4}Lys(Bu),^{6}D-Asp]	6.2 ± 0.2	9.3 ± 1.1
5	[^{4}Lys(Bu),^{6}D-Glu]	7.0 ± 1.2	13.7 ± 2.6
6	[^{4}Lys(Bu),^{6}D-Trp]	n.d.[a]	n.d.[a]

[a]n.d. - no data (compound **3** and **6** precipitated in medium at concentrations higher than 20 μM – no dose response). All values represent mean ± SE.

(69% (**3**) and 53% (**6**)), demonstrating that all measured compounds displayed an in vitro cytotoxic activity. Nevertheless, the replacement of ^{6}Asp by D-Asp, D-Glu or D-Trp led to a decreased cytostatic effect on the estimated cancer cell lines.

Considering the determined IC_{50} values, no relevant differences of the antiproliferative activity between the ^{4}Ser and the corresponding ^{4}Lys(Bu) derivatives could be observed which is not in line with our previous data [29]. This might be a result of the prolonged incubation time which was modified from 6 hours up to 24 hours because of the decreased antitumor activity of the novel compounds and the application of alamarBlue® instead of MTT assay. It can be assumed that the ^{4}Ser bioconjugates require a longer period of treatment to be fully effective. The D-Glu containing GnRH-III derivatives **2** and **4** had slightly higher IC_{50} values on HT-29 cells than the D-Asp

compounds whereby the degradation profile of **2** and **4** displayed an enhanced release of the smallest Dau-containing metabolite indicating that the GnRH-III bioconjugates vary in their affinity for the GnRH-RI and/or their cellular uptake.

Radioligand binding studies

To investigate the binding affinity of the novel compounds to the GnRH-receptor, an in vitro ligand competition assay has been performed on human pituitary and GnRH-R positive human prostate cancer tissues. Hereby, the displacement of radiolabeled triptorelin by the unlabeled bioconjugates **1**, **2**, **4** and **5** was determined. For a better comparison, the bioconjugates **K1** and **K2** were also analyzed and used as reference. The obtained results summarized in Table 3 point out that all bioconjugates replaced [^{125}I]-triptorelin with IC_{50} values in low nanomolar range. With exception of conjugate **5** (7.9 nM and 11.6 nM), all evaluated compounds displayed slightly higher binding affinity on human prostate cancer (3.0–10.4 nM) than on human pituitary tissue (3.9–23.5 nM) being in accordance with our previous observations [29]. The lowest ligand concentration causing 50% inhibition of radioligand binding was obtained for **K2** with 3.9 nM on pituitary and 3.0 nM on prostate cancer tissues which is only slightly higher than the reported values for GnRH-I–[D-Lys^6(Dau=Aoa)] (1.6 nM and 0.9 nM) and GnRH-II–[D-Lys^6(Dau=Aoa)] (4.2 nM and 2.1 nM) [29,50].

Nevertheless, it has to be considered that the determined IC_{50} values are within a narrow, low nanomolar range and do not differ widely. Especially, the binding affinity on prostate cancer tissue deviate only slightly (3.0–11.6 nm) indicating that the incorporation of D-Asp or D-Glu in position 6 did not substantially affect the receptor binding properties of the GnRH-III derivatives. In addition, the selectivity of conjugates **1**, **2**, **4** is a bit higher toward the prostate cancer than the control conjugates **K1** and **K2**. According to our data, the incorporation of Lys(Bu) in position 4 instead of Ser increased the binding affinity but lowered the selectivity of the conjugates.

All investigated GnRH-III derivatives inhibited the binding of radiolabeled triptorelin efficiently by using increasing concentrations (1 pM to 1 μM). It has been reported that the GnRH-I derivatives cetrorelix and buserelin displaced [^{125}I]-triptorelin completely by using the same concentration range, whereas GnRH-unrelated peptides (e.g., somatostatin-14, bombesin) could not inhibit the receptor binding at concentrations up to 1 μM [51,52]. Comparing our results with these findings from literature we can assume that the analyzed GnRH-III–Dau conjugates bind to the GnRH-receptor in a specific manner. However, the binding affinity data of the conjugates cannot explain alone the results of their in vitro antitumor activity.

Cellular uptake of the bioconjugates on MCF-7 human breast and HT-29 human colon cancer cells by flow cytometry

The cellular uptake of the GnRH-III–drug conjugates was studied by flow cytometry on HT-29 and MCF-7 cancer cells (Figure 4). Due to their poor solubility in cell culture medium, the cellular uptake of the D-Trp containing compounds **3** and **6** was not investigated. The other conjugates were utilized in concentrations between 0.15–160 μM. For determination of the cellular uptake exclusively living cells were exploited. Because of the relatively low fluorescence intensity of Dau conjugates, on both cell lines a concentration of at least 2.5 μM was necessary to observe an increased uptake of the bioconjugates. In case of HT-29 cells, the two bioconjugates **K1** and **K2** which were used as internal standards displayed a higher cellular uptake than the new candidates. This became particularly obvious at lower concentrations (2.5 μM and 10 μM). In accordance with our

Table 3: Competitive inhibition of [^{125}I][^{6}D-Trp]-GnRH-I binding to membranes of human pituitary and human prostate cancer specimens by GnRH-III–Dau-conjugates.

		IC_{50} [nM]	
code	[^{8}Lys(Dau=Aoa)]–GnRH-III compound	pituitary	prostate cancer
K1	[^{6}L-Asp]	6.3 ± 0.7	5.2 ± 0.6
1	[^{6}D-Asp]	19.4 ± 2.8	8.9 ± 1.6
2	[^{6}D-Glu]	23.5 ± 2.1	10.4 ± 1.3
3	[^{6}D-Trp]	n.d.[a]	n.d.[a]
K2	[^{4}Lys(Bu),^{6}L-Asp]	3.9 ± 0.7	3.0 ± 1.1
4	[^{4}Lys(Bu),^{6}D-Asp]	6.1 ± 0.1	4.0 ± 1.3
5	[^{4}Lys(Bu),^{6}D-Glu]	7.9 ± 1.1	11.6 ± 2.0
6	[^{4}Lys(Bu),^{6}D-Trp]	n.d.[a]	n.d.[a]

[a]n.d. - no data. All values represent mean ± SE.

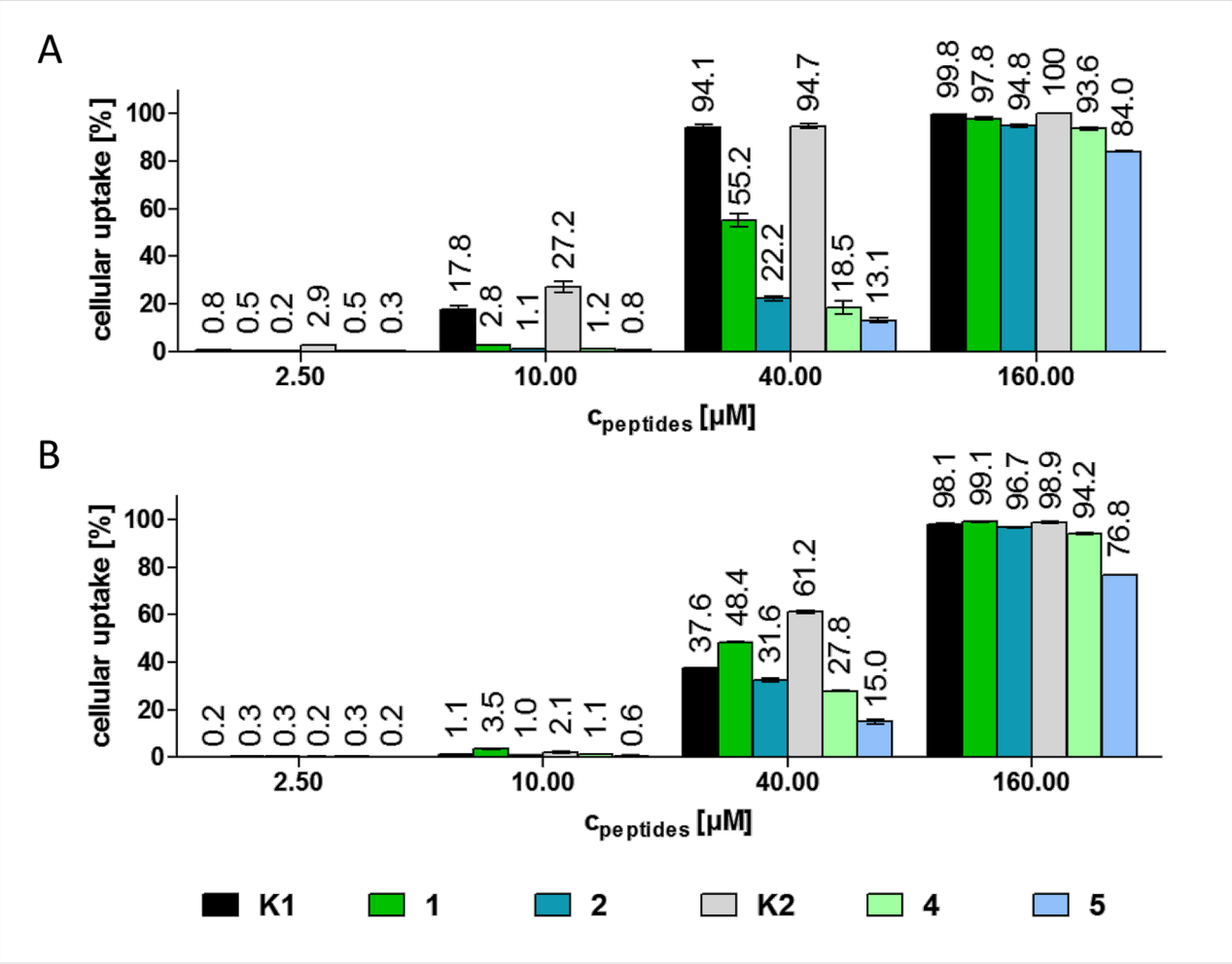

Figure 4: Cellular uptake of the GnRH-III bioconjugates at different concentrations on A) HT-29 and B) MCF-7 cells after 6 h determined by flow cytometry. Experiments were carried out in duplicates; error bars represent standard deviation.

previous data, the cellular uptake of **K2** by HT-29 cells is enhanced in comparison to **K1** [29,38]. Furthermore, the cellular uptake by HT-29 cells at 160 µM concentration was higher than 90% for all bioconjugates except compound **5** (83%). The same effect could be observed on MCF-7 cells, whereby the uptake of bioconjugate **5** was 76%. At 40 µM, **K2** was taken up by MCF-7 cells more effectively (61.2%) than the other compounds. Apart from that, bioconjugate **1** displayed a slightly higher uptake than **K1** at 10 µM and 40 µM concentration. In general, the bioconjugates with ^{6}D-Asp had an improved cellular uptake in comparison with the corresponding ^{6}D-Glu derivatives. Furthermore, in contrast to the control bioconjugates **K1** and **K2** the two compounds with Lys(Bu) in position 4 (**4** and **5**) revealed a declined cellular uptake over the ^{4}Ser counterparts (**1** and **2**) on both cell lines. The differences in the behavior of the new compounds might be a result of the changed conformation of the D-amino acid containing derivatives. Due to the results of the receptor binding studies, we can assume that the binding site of the receptor is not essentially disturbed by the converted conformation, but it might be possible that the receptor internalization is influenced by the structure of the bound ligand.

Considering all these data, we can conclude that the cytostatic effect is not only influenced by the cellular uptake, but also the release of the effective metabolite plays an important role. For instance, the novel bioconjugate **1** provides the highest cellular uptake over the other D-amino acid containing derivatives, but the IC_{50} values are in the same range or even higher than the IC_{50} value of the other compounds **2**, **4** and **5**. It can be assumed that this effect occurred due to the reduced release of the smallest Dau-containing metabolite.

Confocal laser scanning microscopy (CLSM) studies

Next to the quantitative analysis of the cellular uptake by flow cytometry, the cellular uptake and localization of **K1**, **K2**, **1**, **2**, **4** and **5** were studied on MCF-7 cells by CLSM. After 6 h incubation with the GnRH-III–Dau conjugates (c = 10 µM, 40 µM

and 160 µM), MCF-7 cells were fixed and prepared for confocal laser scanning imaging. In order to gain insight into a possible co-localization with nuclei, DAPI-staining was performed. Images are displayed in BestFit mode to improve visualization of low signals and to optimize the image quality. The CLSM observations cannot be considered as quantitative analysis but provide qualitative information about subcellular localization. In case of all investigated compounds and concentrations, the Dau signal could be detected mainly in the nuclei and in small, cytosolic compartments (Figure 5A, Supporting Information File 1, Figures S9–S14) evidencing that the conjugated daunorubicin reaches its site of action.

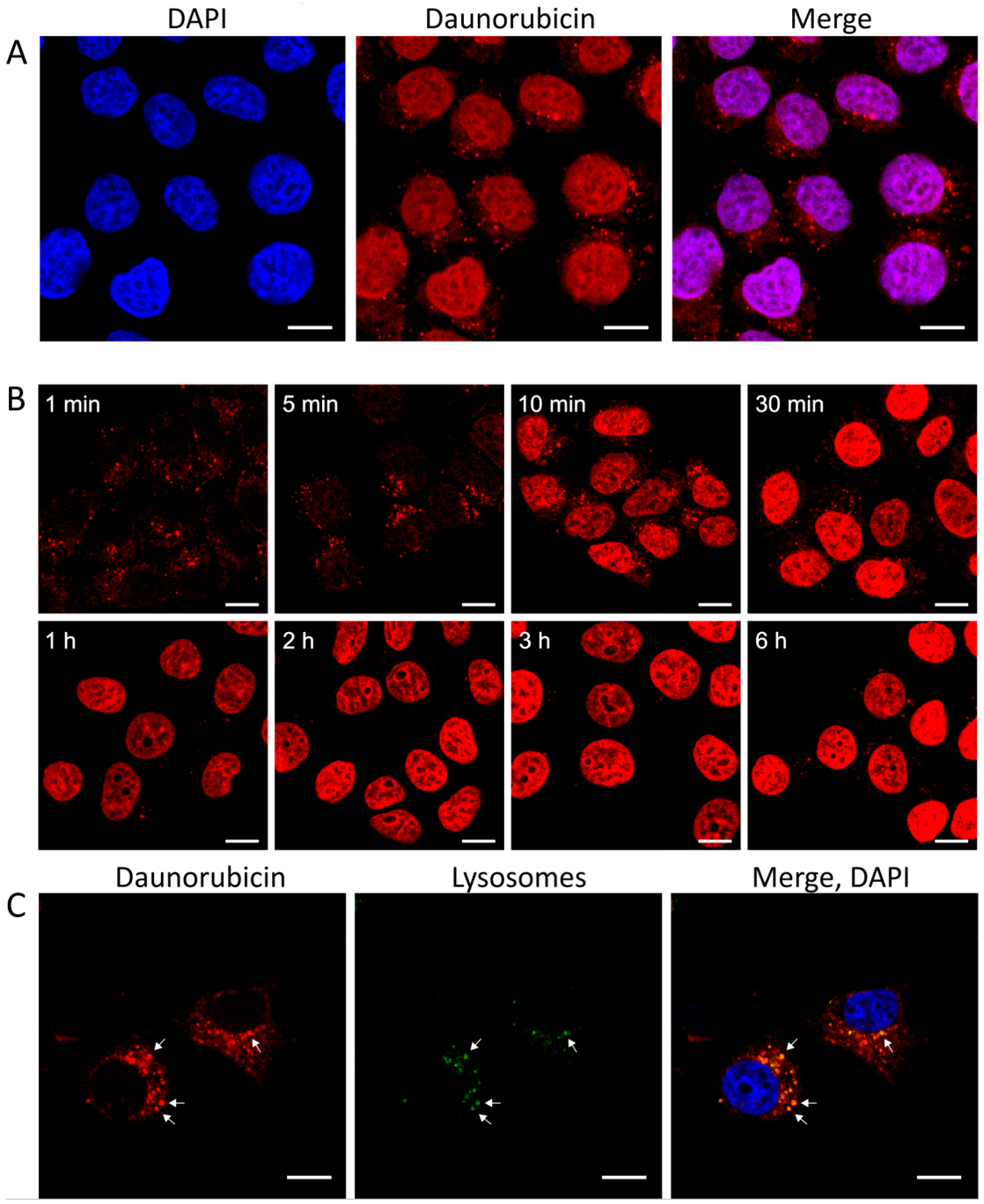

Figure 5: Cellular uptake of bioconjugate **K2** (40 µM) visualized by confocal laser scanning microscopy (CLSM) A) after 6 h incubation, daunorubicin (Dau) accumulates in the nucleus. B) Time dependent localization of bioconjugate **K2** after 1 min, 5 min, 10 min, 30 min, 1 h, 2 h, 3 h and 6 h incubation. C) Co-localization of **K2** (40 µM) with lysosomes (CytoPainter Lysosomal Staining Kit) after 5 min incubation. In the early stages of the cellular uptake the Dau signal is co-localized with the lysosomal staining (scale bars represent 10 µm).

To obtain more detailed information of the cellular mechanism after internalization, we analyzed the subcellular localization of one Dau conjugate at different timepoints by using shorter incubation times (Figure 5B). Due to the results achieved by flow cytometry and cell viability assay **K2** was selected for further investigations. The results indicate that Dau-containing metabolites can be found in high amount in the nuclei after already 10 to 30 minutes, whereas the CLSM images after 1 and 5 minutes display the Dau signal predominantly in small cytosolic vesicles.

We supposed that the smaller cytosolic compartments seen at early timepoints might be lysosomes. To prove this assumption, a lysosomal co-localization study was performed with **K2** on MCF-7 cells. After 5 min incubation, the detected Dau signals corresponded largely with the signal of the lysosomal stain revealing a co-localization with lysosomes (Figure 5C). The remaining vesicles which display only the Dau signal are assumed to be endosomes. Based on these findings it can be concluded that our lead compound **K2** is uptaken through an endocytic pathway.

Receptor blockage by triptorelin

In order to investigate if the bioconjugate **K2** is uptaken in a receptor-mediated manner, a competition assay was performed on MCF-7 human breast cancer cells using an excess of the superagonist triptorelin. This GnRH-R binder was also used to prove the mechanism of action of the Dox–GnRH-I bioconjugate zoptarelin on Hec-1a and Ishikawa endometrial cancer cells [14]. To analyze the effect of triptorelin on the cellular uptake of the GnRH-III bioconjugates, MCF-7 cells were treated collectively with **K2** (fixed concentration of 40 µM) and triptorelin (concentration range of 125–1000 µM). Recently, Gründker et al. reported that triptorelin treatment leads to an increased density of GnRH-I receptors on MCF-7 cells [53]. Hence, our intention was to avoid long term incubation with triptorelin. The results of the CLSM studies indicate that 1–2 hours are sufficient to obtain substantial Dau uptake, therefore cells were treated for 100 min. Afterwards, the cells were analyzed by flow cytometry displaying a reduction of the cellular uptake of **K2** by an increasing triptorelin concentration (Figure 6). These results strongly indicate that the internalization of the Dau–GnRH-III bioconjugates can be blocked by triptorelin suggesting that the cellular uptake occurs in a GnRH-R-mediated manner.

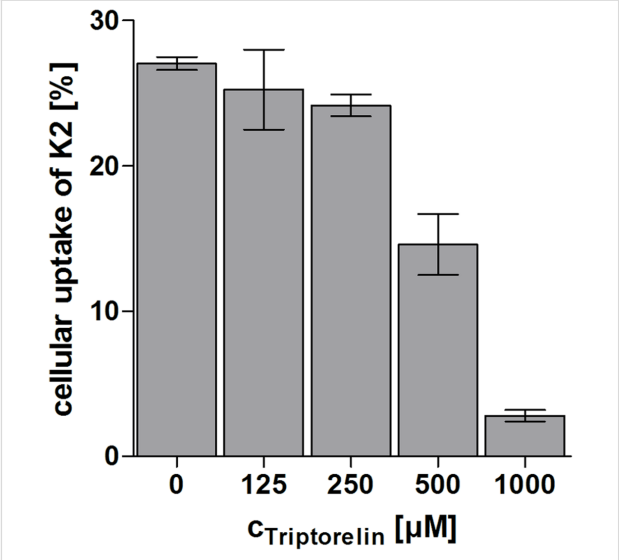

Figure 6: Competitive inhibition of the GnRH-R on MCF-7 cells. Cellular uptake of the GnRH-III bioconjugate **K2** (40 µM) was studied in the presence of superagonist triptorelin (125–1000 µM) by flow cytometry. Cells were treated simultaneously with **K2** and triptorelin for 100 min.

Conclusion

Our studies demonstrate that the cytostatic effect of drug bioconjugates, in our case Dau–GnRH-III derivative conjugates, depend on various cellular events. Thus, the efficiency of DDSs is not only defined by their stability under physiological conditions and the selectivity to cancer cells, but also the cellular uptake of the drug–carrier molecule and the release of the active agent play an important role.

All investigated compounds exhibit cytostatic effects on HT-29 human colon cancer and MCF-7 human breast cancer cells, whereby the well-defined lead compound **K2** remains our most promising drug candidate. The six novel GnRH-III-[^{6}D-Aaa]–Dau conjugates reveal 3–5 times lower antitumor activity than the parent conjugates. Their antitumor effects are influenced by many factors which counteract each other. Therefore, no significant difference in IC_{50} values could be observed. It turned out that the ^{4}Lys(Bu)-containing conjugates **4** and **5** have a higher binding affinity to the GnRH receptors in comparison to the ^{4}Ser-containing ones. Furthermore, the D-Asp derivatives **1** and **4** show slightly improved receptor binding properties than the D-Glu derivatives **2** and **5** which might be the reason for the enhanced cellular uptake of the D-Asp conjugates. However, our lysosomal degradation studies pointed out that the digestion of conjugates **1** and **4** is less effective and results in larger metabolites. These metabolites might have a reduced DNA intercalating potency than the smallest Dau-metabolite (H-Lys(Dau=Aoa)-OH) which could be identified in case of the control peptides **K1** and **K2**. It is worth mentioning that in case of D-Trp containing conjugates a significant amount of H-Lys(Dau=Aoa)-OH metabolite was released, however, other biological study could not be made with them because of their poor solubility in cell culture medium. Due to this observation, the conjugates **3** and **6** might be interesting for further development. Nevertheless, our results provide significant

information about the influence of the cellular uptake and the release of the effective metabolite on the efficiency of the DDS.

Next to these findings, we could systematically specify the receptor-mediated endocytosis pathway for GnRH-III-[^{4}Lys(Bu), ^{8}Lys(Dau=Aoa)] which is also representative for other Dau–GnRH-III bioconjugates. Based on our results, we can assume that the GnRH-III bioconjugates specifically bind the GnRH-Rs on cancer cells and induce in that way their internalization. Moreover, the outcome of the time dependent localization of Dau peptide conjugates or the Dau-containing metabolites can give clear indication for an endocytotic pathway. Furthermore, we could evident the localization of Dau–GnRH-III conjugates in lysosomes by lysosomal staining. All CLSM data attest the intranuclear accumulation of Dau proving the presence of Dau-containing metabolites on its site of action.

In summary, our findings support the development of new therapeutic approaches based on new cytotoxic peptide conjugates targeting GnRH receptors in human cancers.

Experimental

Material

All amino acid derivatives and Rink-Amide MBHA resin were purchased from Iris Biotech GmBH (Marktredwitz, Germany). Boc-aminooxyacetic acid (Boc-Aoa-OH), aminooxyacetic acid, scavengers, coupling agents and cleavage reagents (1-hydroxybenzotriazole hydrate (HOBt), *N,N'*-diisopropylcarbodiimide (DIC), triisopropylsilane (TIS), piperidine, 1,8-diazabicyclo[5.4.0]undec-7-ene (DBU), trifluoroacetic acid (TFA), diisopropylethylamine (DIPEA), acetic anhydride (Ac_2O), methanol (MeOH), *n*-butyric anhydride and solvent for HPLC (acetonitrile (ACN)) were obtained from Sigma-Aldrich Kft (Budapest, Hungary). Daunorubicin hydrochloride was a gift from IVAX (Budapest, Hungary). *N,N*-Dimethylformamide (DMF), dichloromethane (DCM) and diethyl ether (Et_2O) were purchased from Molar Chemicals Kft (Budapest, Hungary). All reagents and solvents were of analytical grade or highest available purity.

Synthesis of oxime bond-linked GnRH-III–[^{4}Ser/^{4}Lys(Bu), ^{6}Aaa, ^{8}Lys(Dau=Aoa)] bioconjugates

The Dau–GnRH-III derivatives were synthesized by solid phase peptide synthesis according to Fmoc/*t*-Bu chemistry on a Rink-Amide MBHA resin (0.73 mmol/g coupling capacity) followed by ligation of Dau (oxime bond) in solution. All peptides were synthesized manually by usage of the following Fmoc-protected amino acid derivatives: Fmoc-Gly-OH, Fmoc-Pro-OH, Fmoc-Lys(Mtt)-OH, Fmoc-Lys(Dde)-OH, Fmoc-Trp-OH, Fmoc-D-Trp-OH, Fmoc-Asp(O*t*-Bu)-OH, Fmoc-D-Asp(O*t*-Bu)-OH, Fmoc-D-Glu(O*t*-Bu)-OH, Fmoc-His(Trt)-OH and Fmoc-Ser(*t*-Bu)-OH. Pyroglutamic acid (Glp or <E) was attached to the peptide chain without any protection. The general protocol for the synthesis started with DMF-washing (4 × 1 min), followed by Fmoc deprotection with 2% piperidine, 2% DBU in DMF (4 times; 2 + 2 + 5 + 10 min). The coupling reaction was performed by using 3 equiv of α-Fmoc-protected amino acid derivative, 3 equiv DIC and 3 equiv HOBt in DMF (60 min). After washing with DMF (3 × 1 min) and DCM (2 × 1 min) the success of the coupling was controlled by ninhydrine test. After assembly of the protected decapeptide the Dde group of ^{4}Lys was removed with 2% hydrazine in DMF (12 × 5 min) and the peptidyl-resin was washed with DMF (5 × 1 min). Afterwards, the ε-NH_2 amino group was butyrylated with 3 equiv butyric anhydride and 3 equiv DIPEA in DMF (2 h). In the next step, ^{8}Lys(Mtt) was deprotected with 2% TFA in DCM (6 × 5 min). Then the resin-bound peptide was neutralized with 10% DIPEA in DCM (3 × 5 min) and Boc-Aoa-OH was coupled for 2 h using DIC, HOBt coupling reagents (3 equiv each to the amino group). The treatment with 95% TFA, 2.5% TIS and 2.5% water (v/v/v) in the presence of 10 equiv free aminooxyacetic acid as "carbonyl capture" reagent (2 h, at room temperature (rt)) resulted in the simultaneous removal of the side chain protecting groups and the cleavage of the peptide from the resin [54]. Peptides were isolated by precipitation with ice-cold Et_2O, centrifuged, washed 3 times, dissolved in water/ACN (0.1% TFA) 4:1 (v/v) and lyophilized. Subsequent to the purification of the crude peptides by RP-HPLC, the solvent was evaporated and Dau was conjugated to the aminooxyacetylated ^{8}Lys. The oxime bond formation was carried out in 0.2 M ammonium acetate buffer (pH 5.0), at a peptide concentration of 10 mg/mL and 1.3 equiv Dau [21]. The reaction mixtures were stirred overnight at rt and then purified by RP-HPLC. The resulting GnRH-III bioconjugates were characterized by analytical RP-HPLC and MS.

RP-HPLC

The crude peptides and the bioconjugates were purified on a KNAUER 2501 HPLC system (H. Knauer, Bad Homburg, Germany) using a preparative Phenomenex Luna C18(2) column (100 Å, 10 µm, 250 mm × 21.2 mm) (Torrance, CA, USA). Linear gradient elution (0 min 20% B; 5 min 20% B; 50 min 80% B) with eluent A (0.1% TFA in water) and eluent B (0.1% TFA in ACN/H_2O (80:20, v/v)) was used at a flow rate of 9.5 mL/min. Peaks were detected at 280 nm.

Analytical RP-HPLC was performed on a KNAUER 2501 HPLC system using a Phenomenex Luna C18 column (100 Å, 5 µm, 250 mm × 4.6 mm) as a stationary phase. Linear gradient elution (0 min 0% B; 5 min 0% B; 50 min 90% B) at a flow rate

of 1 mL/min with eluents described above. Peaks were detected at 220 nm.

Mass spectrometry

Electrospray ionization (ESI) mass spectrometric analyses were carried out on an Esquire 3000+ ion trap mass spectrometer (Bruker Daltonics, Bremen, Germany). Spectra were acquired in the 50–2500 *m*/*z* range. Samples were dissolved in a mixture of ACN/water (1:1, v/v) and 0.1% formic acid.

Liquid chromatography–mass spectrometry (LC–MS) was carried out on the same spectrometer equipped with an Agilent 1100 HPLC system and a diode array detector (Agilent, Waldbronn, Germany). Peptides were separated on a Supelco C18 column (150 mm × 2.1 mm, 3 μm) (Hesperia, CA) using a linear gradient from 2–70% B in 25 min (eluent A: ddH_2O, 0.1% HCOOH; eluent B: 80% ACN, 0.1% HCOOH at a flow rate of 0.2 mL/min). Spectra were recorded in positive ion mode in the 100–2500 *m*/*z* range.

Electronic circular dichroism spectroscopy

Electronic circular dichroism (ECD) spectra were recorded on a Jasco J-810 (Jasco International Co., Ltd., Tokyo, Japan) spectropolarimeter at 25 °C in quartz cells of 0.02 cm path length, under constant nitrogen flush. The instrument was calibrated with 0.06% (w/v) ammonium-D-camphor-10-sulfonate (Katayama Chemical, Japan) in water. The bioconjugates were dissolved in water (c = 340 μM). The spectra show averages of six scans in a wavelength range of 185–260 nm. The results were expressed in terms of mean molar ellipticity (deg cm^2 $dmol^{-1}$) after subtracting the solvent baseline.

Degradation of GnRH-III bioconjugates in rat liver lysosomal homogenate

The rat liver lysosomal homogenate was prepared as previously described [26]. The protein concentration was determined by Qubit Protein Assay Kit according to the manufacturer's protocol (ThermoFisher Scientific, Waltham, MA, USA). The bioconjugates were dissolved in ddH_2O to a concentration of 5 μg/μL. The reaction was carried out in 0.2 M NaOAc buffer (pH 5), with an identical concentration of bioconjugate and rat liver lysosomal homogenate (0.25 μg/μL). The reaction mixtures were incubated at 37 °C and aliquots of 15 μL were taken at 5 min, 1 h, 2 h, 4 h, 8 h and 24 h and quenched with 2 μL of acetic acid. The analysis of the samples was performed by LC–MS.

Cell culture

MCF-7 human breast adenocarcinoma cells were cultured in Dulbecco's Modified Eagle Medium (DMEM, Lonza, Basel, Switzerland), supplemented with 10% (v/v) fetal bovine serum (FBS, Lonza), L-glutamine (2 mM, Lonza), non-essential amino acids (NEAA, Sigma-Aldrich Kft), sodium pyruvate (1 mM, Lonza) and penicillin-streptomycine (Lonza). HT-29 human colon adenocarcinoma cells were cultured in RPMI-1640 (Lonza), supplemented with FBS, L-glutamine and penicillin-streptomycine. Cells were maintained in plastic culture dishes at 37 °C with a humidified atmosphere containing 5% CO_2/95% air.

Stability of GnRH-III bioconjugates in cell culture medium

The GnRH-III bioconjugates were dissolved in water to a concentration of 2.5 mg/mL followed by the dilution with serum-free cell culture medium (final bioconjugate concentration: 0.5 mg/mL). The mixtures were incubated at 37 °C for 24 h and samples of 50 μL were directly monitored by RP-HPLC at time points 0 h, 1 h, 2 h, 6 h and 24 h.

In vitro cytostatic effect studies

Cells were seeded to 96-well plates (Sarstedt, Nümbrecht, Germany, 5 × 10^3 cells/well) one day prior to the treatment in complete cell medium. Cells were treated with bioconjugates in serum-free medium (concentration range 0.07−150 μM, control wells were treated with serum-free medium). After 24 h, cells were washed two times with serum-free medium and were incubated in complete medium for 48 h. Cytostasis detection was performed using alamarBlue reagent® (ThermoFisher Scientific) according to the manufacturer's instructions. Fluorescence was detected using Synergy H4 multi-mode microplate reader (BioTek, Winooski, VT, USA), excitation and emission wavelengths were set to 570 and 620 nm, respectively. Cytostasis was measured using 4 parallels, each experiment was repeated twice. Cytostatic effect (and IC_{50} values) were calculated by using nonlinear regression (sigmoidal dose response) with Origin Pro8 (OriginLab Corp., Northampton, MA, USA.).

Cellular uptake determination by flow cytometry

For determining cellular uptake of the bioconjugates, cells were seeded to 24-well plates (Sarstedt) one day prior to the experiment (10^5 cells/well) in complete cell medium. Treatment with Dau-conjugated peptides was performed in serum-free culture medium for 6 h, concentrations ranging from 0.15–160 μM. In case of the competitive inhibition of the GnRH-Rs, MCF-7 cells were simultaneously treated with triptorelin and **K2** for 100 min, whereby triptorelin was used in a concentration range of 125–1000 μM and **K2** was applied in a fixed concentration of 40 μM. After treatment, cells were washed two times with serum-free medium and one time with HPMI medium (containing 100 mM NaCl, 5.4 mM KCl, 0.4 mM $MgCl_2$, 0.04 mM $CaCl_2$, 10 mM Hepes, 20 mM glucose, 24 mM $NaHCO_3$ and

5 mM Na_2HPO_4 at pH 7.4) and trypsinized for 10 min at 37 °C. Trypsinization was stopped by HPMI medium supplemented with 10% FBS. Detached cells were centrifuged at 216*g* for 5 min at 4 °C and the supernatant was removed. Cells were resuspended in HPMI medium, intracellular fluorescence intensity (that is proportional to the cellular uptake) was monitored by flow cytometer BD LSR II (BD Bioscience, Franklin Lakes, NJ, USA). Data were analyzed by FACSDiVa (BD Bioscience) 5.0 software.

Confocal microscopy imaging

Cells were seeded to cover glass containing (thickness 1, Assistant, Karl Hecht GmbH & Co KG, Sondheim/Rhön Germany) 24-well plates one day prior to the experiment in complete cell medium. Treatment was performed in serum-free medium for the indicated incubation time. Cells were washed two times with phosphate buffered saline (PBS) and fixed by 4% paraformaldehyde for 20 min at 37 °C. After three times washing with PBS, nuclei were stained by 4′,6-diamidine-2-phenylindole dihydrochloride (DAPI, 0.2 μg/mL, dissolved in PBS, Sigma-Aldrich Kft.) for 15 min. After washing, cover glasses were mounted to microscopy slides (VWR International, Debrecen, Hungary) by Mowiol® 4-88 mounting medium (Sigma-Aldrich Kft.). In case of the lysosomal co-localisation study, lysosomes were stained in living cells before treatment with peptide **K2** by CytoPainter Lysosomal Staining Kit - Deep Red Fluorescence (abcam, Cambridge, UK), according to the manufacturer's instructions. Confocal microscopy was carried out using a Zeiss LSM 710 system (Carl Zeiss Microscopy GmbH, Jena, Germany) with a 40× oil objective. Images were processed by software ZEN Lite (Carl Zeiss Microscopy GmbH).

Radioligand binding studies

Radiolabeled triptorelin was used for displacement studies to evaluate the binding affinity of the conjugates **K1**, **K2**, **1**, **2**, **4** and **5** to GnRH-RI on human pituitary and human prostate cancer cells. Tissue samples derived by autopsy from normal human pituitary (anterior lobe) and human prostate cancer cells were obtained from a patient at the time of initial surgical treatment. The collection and the use of these specimens for our studies are approved by the local Institutional Ethics Committee. Membranes for receptor binding studies have been prepared as previously described [29,51,52,55]. Radioiodinated GnRH-I agonist triptorelin was prepared by chloramines-T method and purified by RP-HPLC [29,51,52,56]. This radioligand has been well-characterized and shows high-affinity binding to human and rat pituitaries as well as human breast, prostate, and other cancers [51,52]. The binding affinities of the nonradio-labeled GnRH-III bioconjugates to GnRH-RI were determined by displacement of [^{125}I]-GnRH-I-[^{6}D-Trp] performing an in vitro ligand competition assay as recently reported [29,51,52]. Hereby, membrane homogenates which contain 50–160 mg protein were incubated in duplicate or triplicate with 60–80,000 cpm [^{125}I]-GnRH-I-[^{6}D-Trp] and increasing concentration (1 pM–1 μM) of nonradioactive bioconjugates as competitors in a total volume of 150 mL of binding buffer. After incubation, 125 mL aliquots of suspension were transferred onto the top of 1 mL of ice-cold binding buffer which contained 1.5% bovine serum albumin in siliconized polypropylene microcentrifuge tubes (Sigma-Aldrich Kft.). The tubes were centrifuged at 12,000*g* for 3 min at 4 °C (Beckman J2-21M, Beckman Coulter, Inc., Brea, CA). Supernatants were aspirated and the bottoms of the tubes containing the pellet were cut off and counted in a gamma counter. Protein concentration was determined by the method of Bradford using a Bio-Rad protein assay kit (Bio-Rad Laboratories, USA). The LIGAND-PC computerized curve-fitting program of Munson and Rodbard was used to determine the receptor binding characteristics and IC_{50} values [29,51,52].

Supporting Information

Supporting Information File 1

Characterization data for compounds **1–6**: RP-HPLC chromatograms and ESI–MS spectra; fragments of **1–6** produced by lysosomal rat liver homogenate; cellular uptake of **K1**, **K2**, **1**, **2**, **4**, **5** by CLSM.
[https://www.beilstein-journals.org/bjoc/content/supplementary/1860-5397-14-64-S1.pdf]

Acknowledgements

This project has received funding from the European Union's Horizon 2020 research and innovation program under the Marie Sklodowska-Curie grant agreement No 642004, from the Hungarian National Science Fund (OTKA K104045) and National Research, Development and Innovation Office (NKFIH K119552). The work is also supported by the GINOP-2.3.2-15-2016-00043 (G.H.) project. The project is co-financed by the European Union and the European Regional Development Fund. The authors would like to acknowledge the help of Szilvia Bősze and László Kőhidai in cell culture studies, János Gardi for his help in preparation of radioligand as well as Ildikó Szabó for providing triptorelin reagent.

ORCID® iDs

Sabine Schuster - https://orcid.org/0000-0001-9888-4446
Beáta Biri-Kovács - https://orcid.org/0000-0001-5803-9969
Bálint Szeder - https://orcid.org/0000-0003-3264-3900
Zsuzsanna Szabó - https://orcid.org/0000-0003-4838-4210
Gábor Mező - https://orcid.org/0000-0002-7618-7954

References

1. Mező, G.; Manea, M. *Expert Opin. Drug Delivery* **2010,** *7,* 79–96. doi:10.1517/17425240903418410
2. Kastin, A. J.; Coy, D. H.; Schally, A. V.; Zadina, J. E. *Pharmacol., Biochem. Behav.* **1980,** *13,* 913–914. doi:10.1016/0091-3057(80)90228-2
3. Belchetz, P. E.; Plant, T. M.; Nakai, Y.; Keogh, E. J.; Knobil, E. *Science* **1978,** *202,* 631–633. doi:10.1126/science.100883
4. Nagy, A.; Schally, A. V.; Armatis, P.; Szepeshazi, K.; Halmos, G.; Kovacs, M.; Zarandi, M.; Groot, K.; Miyazaki, M.; Jungwirth, A.; Horvath, J. *Proc. Natl. Acad. Sci. U. S. A.* **1996,** *93,* 7269–7273.
5. Nagy, A.; Schally, A. V. *Biol. Reprod.* **2005,** *73,* 851–859. doi:10.1095/biolreprod.105.043489
6. Ghanghoria, R.; Kesharwani, P.; Tekade, R. K.; Jain, N. K. *J. Controlled Release* **2018,** *269,* 277–301. doi:10.1016/j.jconrel.2016.11.002
7. Mezo, G. *Amino Acids, Pept., Proteins* **2014,** *38,* 203–252. doi:10.1039/9781849737081-00203
8. Bajusz, S.; Janaky, T.; Csernus, V. J.; Bokser, L.; Fekete, M.; Srkalovic, G.; Redding, T. W.; Schally, A. V. *Proc. Natl. Acad. Sci. U. S. A.* **1989,** *86,* 6318–6322.
9. Bajusz, S.; Janaky, T.; Csernus, V. J.; Bokser, L.; Fekete, M.; Srkalovic, G.; Redding, T. W.; Schally, A. V. *Proc. Natl. Acad. Sci. U. S. A.* **1989,** *86,* 6313–6317.
10. Minotti, G.; Menna, P.; Salvatorelli, E.; Cairo, G.; Gianni, L. *Pharmacol. Rev.* **2004,** *56,* 185–229. doi:10.1124/pr.56.2.6
11. Pommier, Y.; Leo, E.; Zhang, H.; Marchand, C. *Chem. Biol.* **2010,** *17,* 421–433. doi:10.1016/j.chembiol.2010.04.012
12. Yang, S. W.; Burgin, A. B.; Huizenga, B. N.; Robertson, C. A.; Yao, K. C.; Nash, H. A. *Proc. Natl. Acad. Sci. U. S. A.* **1996,** *93,* 11534–11539.
13. Coley, H. M.; Amos, W. B.; Twentyman, P. R.; Workman, P. *Br. J. Cancer* **1993,** *67,* 1316–1323. doi:10.1038/bjc.1993.244
14. Westphalen, S.; Kotulla, G.; Kaiser, F.; Krauss, W.; Werning, G.; Elsasser, H. P.; Nagy, A.; Schulz, K. D.; Grundker, C.; Schally, A. V.; Emons, G. *Int. J. Oncol.* **2000,** *17,* 1063–1072. doi:10.3892/ijo.17.5.1063
15. Hannon, M. J. *Chem. Soc. Rev.* **2007,** *36,* 280–295. doi:10.1039/b606046n
16. Engel, J.; Emons, G.; Pinski, J.; Schally, A. V. *Expert Opin. Invest. Drugs* **2012,** *21,* 891–899. doi:10.1517/13543784.2012.685128
17. Emons, G.; Kaufmann, M.; Gorchev, G.; Tsekova, V.; Gründker, C.; Günthert, A. R.; Hanker, L. C.; Velikova, M.; Sindermann, H.; Engel, J.; Schally, A. V. *Gynecol. Oncol.* **2010,** *119,* 457–461. doi:10.1016/j.ygyno.2010.08.003
18. Aeterna Zentaris Announces that ZoptEC Phase 3 Clinical Study of ZoptrexTM Did Not Achieve its Primary Endpoint Æterna Zentaris Investor Center, http://ir.aezsinc.com/press-release/aeternazentaris/aeterna-zentaris-announces-zoptec-phase-3-clinical-study-zoptrex-did (accessed October 21, 2017).
19. Sower, S. A.; Chiang, Y. C.; Lovas, S.; Conlon, J. M. *Endocrinology* **1993,** *132,* 1125–1131.
20. Manea, M.; Mező, G. *Protein Pept. Lett.* **2013,** *20,* 439–449. doi:10.2174/0929866511320040008
21. Szabó, I.; Manea, M.; Orbán, E.; Csámpai, A.; Bősze, S.; Szabó, R.; Tejeda, M.; Gaál, D.; Kapuvári, B.; Przybylski, M.; Hudecz, F.; Mező, G. *Bioconjugate Chem.* **2009,** *20,* 656–665. doi:10.1021/bc800542u
22. Schlage, P.; Mező, G.; Orbán, E.; Bősze, S.; Manea, M. *J. Controlled Release* **2011,** *156,* 170–178. doi:10.1016/j.jconrel.2011.08.005
23. Kovács, M.; Vincze, B.; Horváth, J. E.; Seprődi, J. *Peptides* **2007,** *28,* 821–829. doi:10.1016/j.peptides.2007.01.003
24. Mező, G.; Czajlik, A.; Manea, M.; Jakab, A.; Farkas, V.; Majer, Z.; Vass, E.; Bodor, A.; Kapuvári, B.; Boldizsár, M.; Vincze, B.; Csuka, O.; Kovács, M.; Przybylski, M.; Perczel, A.; Hudecz, F. *Peptides* **2007,** *28,* 806–820. doi:10.1016/j.peptides.2006.12.014
25. Leurs, U.; Mező, G.; Orbán, E.; Öhlschläger, P.; Marquardt, A.; Manea, M. *Pept. Sci.* **2012,** *98,* 1–10. doi:10.1002/bip.21640
26. Orbán, E.; Mező, G.; Schlage, P.; Csík, G.; Kulić, Ž.; Ansorge, P.; Fellinger, E.; Möller, H. M.; Manea, M. *Amino Acids* **2011,** *41,* 469–483. doi:10.1007/s00726-010-0766-1
27. Leurs, U.; Lajkó, E.; Mező, G.; Orbán, E.; Öhlschläger, P.; Marquardt, A.; Kőhidai, L.; Manea, M. *Eur. J. Med. Chem.* **2012,** *52,* 173–183. doi:10.1016/j.ejmech.2012.03.016
28. Hegedüs, R.; Pauschert, A.; Orbán, E.; Szabó, I.; Andreu, D.; Marquardt, A.; Mező, G.; Manea, M. *Pept. Sci.* **2015,** *104,* 167–177. doi:10.1002/bip.22629
29. Hegedüs, R.; Manea, M.; Orbán, E.; Szabó, I.; Kiss, É.; Sipos, É.; Halmos, G.; Mező, G. *Eur. J. Med. Chem.* **2012,** *56,* 155–165. doi:10.1016/j.ejmech.2012.08.014
30. Kapuvári, B.; Hegedüs, R.; Schulcz, Á.; Manea, M.; Tóvári, J.; Gacs, A.; Vincze, B.; Mező, G. *Invest. New Drugs* **2016,** *34,* 416–423. doi:10.1007/s10637-016-0354-7
31. Sealfon, S. C.; Weinstein, H.; Millar, R. P. *Endocr. Rev.* **1997,** *18,* 180–205. doi:10.1210/edrv.18.2.0295
32. Karten, M. J.; Rivier, J. E. *Endocr. Rev.* **1986,** *7,* 44–66. doi:10.1210/edrv-7-1-44
33. López de Maturana, R.; Pawson, A. J.; Lu, Z.-L.; Davidson, L.; Maudsley, S.; Morgan, K.; Langdon, S. P.; Millar, R. P. *Mol. Endocrinol.* **2008,** *22,* 1711–1722. doi:10.1210/me.2006-0537
34. Canne, L. E.; Ferre-D'Amare, A. R.; Burley, S. K.; Kent, S. B. H. *J. Am. Chem. Soc.* **1995,** *117,* 2998–3007. doi:10.1021/ja00116a005
35. Buré, C.; Lelièvre, D.; Delmas, A. *Rapid Commun. Mass Spectrom.* **2000,** *14,* 2158–2164. doi:10.1002/1097-0231(20001215)14:23<2158::AID-RCM147>3.0.CO;2-C
36. Pappa, E. V.; Zompra, A. A.; Diamantopoulou, Z.; Spyranti, Z.; Pairas, G.; Lamari, F. N.; Katsoris, P.; Spyroulias, G. A.; Cordopatis, P. *Biopolymers* **2012,** *98,* 525–534. doi:10.1002/bip.22123
37. Baranczewski, P.; Stańczak, A.; Sundberg, K.; Svensson, R.; Wallin, A.; Jansson, J.; Garberg, P.; Postlind, H. *Pharmacol. Rep.* **2006,** *58,* 453–472.
38. Manea, M.; Leurs, U.; Orbán, E.; Baranyai, Z.; Öhlschläger, P.; Marquardt, A.; Schulcz, Á.; Tejeda, M.; Kapuvári, B.; Tóvári, J.; Mező, G. *Bioconjugate Chem.* **2011,** *22,* 1320–1329. doi:10.1021/bc100547p
39. Walker, G. F.; Ledger, R.; Tucker, I. G. *Int. J. Pharm.* **2001,** *216,* 77–82. doi:10.1016/S0378-5173(01)00571-3
40. Brudel, M.; Kertscher, U.; Berger, H.; Mehlis, B. *J. Chromatogr. A* **1994,** *661,* 55–60. doi:10.1016/0021-9673(94)85177-8
41. Frederick, C. A.; Williams, L. D.; Ughetto, G.; Van der Marel, G. A.; Van Boom, J. H.; Rich, A.; Wang, A. H. J. *Biochemistry* **1990,** *29,* 2538–2549. doi:10.1021/bi00462a016
42. Orbán, E.; Manea, M.; Marquadt, A.; Bánóczi, Z.; Csík, G.; Fellinger, E.; Bősze, S.; Hudecz, F. *Bioconjugate Chem.* **2011,** *22,* 2154–2165. doi:10.1021/bc2004236

43. Impens, F.; Colaert, N.; Helsens, K.; Ghesquière, B.; Timmerman, E.; Bock, P.-J. D.; Chain, B. M.; Vandekerckhove, J.; Gevaert, K. *Mol. Cell. Proteomics* **2010,** *9,* 2327–2333. doi:10.1074/mcp.M110.001271
44. Turk, V.; Turk, B.; Turk, D. *EMBO J.* **2001,** *20,* 4629–4633. doi:10.1093/emboj/20.17.4629
45. Klemenčič, I.; Carmona, A. K.; Cezari, M. H. S.; Juliano, M. A.; Juliano, L.; Guncar, G.; Turk, D.; Križaj, I.; Turk, V.; Turk, B. *Eur. J. Biochem.* **2000,** *267,* 5404–5412. doi:10.1046/j.1432-1327.2000.01592.x
46. Barrett, A.; Woessner, J.; Rawlings, N. Handbook of Proteolytic Enzymes, 2nd Edition. http://store.elsevier.com/Handbook-of-Proteolytic-Enzymes/isbn-9780080984155/ (accessed Oct 26, 2016).
47. Kaur, G.; Dufour, J. M. *Spermatogenesis* **2012,** *2,* 1–5. doi:10.4161/spmg.19885
48. Ruutu, M.; Johansson, B.; Grenman, R.; Syrjänen, K.; Syrjänen, S. *Anticancer Res.* **2004,** *24,* 2627–2631.
49. Lai, J.-Y.; Pittelkow, M. R. *Wound Repair Regen.* **2004,** *12,* 613–617. doi:10.1111/j.1067-1927.2004.12606.x
50. Szabó, I.; Bősze, S.; Orbán, E.; Sipos, É.; Halmos, G.; Kovács, M.; Mező, G. *J. Pept. Sci.* **2015,** *21,* 426–435. doi:10.1002/psc.2775
51. Halmos, G.; J. M. Arencibia, J. M.; Schally, A. V.; Davis, R.; Bostwick, D. G. *J. Urol.* **2000,** *163,* 623–629. doi:10.1016/S0022-5347(05)67947-5
52. Rozsa, B.; Nadji, M.; Schally, A. V.; Dezso, B.; Flasko, T.; Toth, G.; Mile, M.; Block, N. L.; Halmos, G. *Prostate* **2011,** *71,* 445–452. doi:10.1002/pros.21258
53. Gründker, C.; Föst, C.; Fister, S.; Nolte, N.; Günthert, A. R.; Emons, G. *Breast Cancer Res.* **2010,** *12,* R49. doi:10.1186/bcr2606
54. Mezö, G.; Szabó, I.; Kertész, I.; Hegedüs, R.; Orbán, E.; Leurs, U.; Bösze, S.; Halmos, G.; Manea, M. *J. Pept. Sci.* **2011,** *17,* 39–46. doi:10.1002/psc.1294
55. Halmos, G.; Wittliff, J. L.; Schally, A. V. *Cancer Res.* **1995,** *55,* 280–287.
56. Hunter, W. M.; Greenwood, F. C. *Nature* **1962,** *194,* 495–496. doi:10.1038/194495a0

License and Terms

BEILSTEIN JOURNAL OF ORGANIC CHEMISTRY

Development of novel cyclic NGR peptide–daunomycin conjugates with dual targeting property

Andrea Angelo Pierluigi Tripodi[1,2], Szilárd Tóth[3], Kata Nóra Enyedi[1,2], Gitta Schlosser[1,2], Gergely Szakács[3,4] and Gábor Mező[*1,2]

Full Research Paper

Open Access

Address:
[1]Eötvös Loránd University, Faculty of Science, Institute of Chemistry, Pázmány P. stny. 1/A, H-1117 Budapest, Hungary, [2]MTA-ELTE Research Group of Peptide Chemistry, Hungarian Academy of Sciences, Eötvös Loránd University, Pázmány P. stny. 1/A, H-1117 Budapest, Hungary, [3]Institute of Enzimology, Research Center for Natural Sciences, Hungarian Academy of Sciences, Magyar tudósok körútja 2, H-1117 Budapest, Hungary and [4]Institute of Cancer Research, Medical University Vienna, Borschkegasse 8a, A-1090 Vienna, Austria

Email:
Gábor Mező[*] - gmezo@elte.hu

* Corresponding author

Keywords:
antitumor activity; drug release; NGR peptides; oxime-linkage; targeted drug delivery

Beilstein J. Org. Chem. **2018,** *14,* 911–918.
doi:10.3762/bjoc.14.78

Received: 13 January 2018
Accepted: 13 April 2018
Published: 25 April 2018

This article is part of the Thematic Series "Peptide–drug conjugates".

Guest Editor: N. Sewald

Abstract

Cyclic NGR peptides as homing devices are good candidates for the development of drug conjugates for targeted tumor therapy. In our previous study we reported that the Dau=Aoa-GFLGK(c[KNGRE]-GG-)-NH_2 conjugate has a significant antitumor activity against both CD13+ HT-1080 human fibrosarcoma and CD13− but integrin positive HT-29 human colon adenocarcinoma cells. However, it seems that the free ε-amino group of Lys in the cycle is not necessary for the biological activity. Therefore, we developed novel cyclic NGR peptide–daunomycin conjugates in which Lys was replaced by different amino acids (Ala, Leu, Nle, Pro, Ser). The exchange of the Lys residue in the cycle simplified the cyclization step and resulted in a higher yield. The new conjugates showed lower chemostability against deamidation of Asn than the control compound, thus they had lower selectivity to CD13+ cells. However, the cellular uptake and cytotoxic effect of Dau=Aoa-GFLGK(c[NleNGRE]-GG-)-NH_2 was higher in comparison to the control especially on HT-29 cells. Therefore, this conjugate is more suitable for drug targeting with dual targeting property.

Introduction

Targeted chemotherapy is one of the most promising approaches for selective cancer treatment that may decrease the toxic side effects of anticancer drugs. This therapeutic approach is based on the fact that tumor specific receptors are highly expressed on cancer cells/tissues. NGR (Asn-Gly-Arg) motif-containing peptides identified by phage display are suit-

able candidates for selective drug delivery. NGR peptides bind to CD13-receptors on tumor cells and tumor related angiogenic blood vessels [1,2]. CD13 is a transmembrane zinc-dependent metalloprotease that functions in cell proliferation, cell migration and angiogenesis [1,3,4]. However, it is known that the Asn-Gly moiety is subject to Asn deamidation through succinimide formation leading to isoaspartic acid (isoAsp, isoD) and aspartic acid derivatives usually in a ratio of 3:1 after hydrolysis [5-11]. IsoDGR peptides are bound to RGD-integrin receptors with high affinity [12-14]. Due to their function in tumor proliferation, metastasis and angiogenesis, integrin receptors are also promising targets for cancer therapy. Thus, NGR-peptide homing devices may provide dual targeted delivery of anticancer drugs.

According to literature data, one of the most stable and tumor-selective cyclic NGR-peptides is c[KNGRE]-NH_2, in which the α-amino group of the *N*-terminal Lys is coupled to the γ-carboxyl group of the glutamic acid residue (head-to-side chain cycle). In vitro fluorescence microscopy studies of an Oregon Green (OG) labeled c[KNGRE]-NH_2 (OG attached to the side chain of Lys) revealed selective binding to CD13-receptor positive (CD13+) HT-1080 human fibrosarcoma cells and minimal binding to receptor negative (CD13−) MCF-7 human breast adenocarcinoma cells [15]. Moreover, a ^{68}Ga-radiotracer labeled derivative of the cyclic [KNGRE]-NH_2 has been successfully used for tumor diagnostic studies by PET, indicating its specific binding to CD13 receptor expressing tumor tissues [16].

Recently, we reported the synthesis and biochemical characterization of novel cyclic NGR peptides and their corresponding NGR-drug conjugates. Special attention was paid on the chemostability and in vitro biological activity of the compounds [17,18]. Daunomycin (Dau) was used as cytotoxic agent, attached to the NGR-derivatives via oxime linkage. The prepared conjugates revealed substantial in vitro cytostatic/cytotoxic effects. Our results indicated that the conjugates had an antitumor effect against both CD13+ HT-1080 cells and CD13− (but integrin receptor positive) HT-29 human colon cancer cells. Moreover, we showed that the toxicity and the selectivity of the conjugates highly depended on their structure, cellular uptake and propensity to deamidation.

The most active conjugate with dual acting properties was Dau=Aoa-GFLGK(c[KNGRE]-GG-)-NH_2 (**K**, control conjugate in this study). In this conjugate the cyclic NGR peptide was attached through a Gly-Gly dipeptide spacer to the lysine side chain connected to the chatepsin B labile GFLG spacer that allows lysosomal drug release. Dau was conjugated to the GFLG spacer via oxime linkage through an incorporated aminooxyacetyl (Aoa) moiety. The preparation of the conjugate required a sophisticated synthetic route and the use of orthogonal protecting groups (Figure 1A). Previous studies indicated that the free ε-amino group of Lys does not have an impact on the biological activity [15,17]. To prove our assumption, a set of novel cyclic NGR peptide–Dau conjugates were developed in which the Lys was replaced by different amino acids (Ala, Leu, Nle, Pro and Ser). The main goal of the present study was to investigate whether the exchange of the lysine in the cycle has any influence on the chemostability, selectivity and antitumor activity of the conjugates.

Here we report on the synthesis and characterization of the cyclic NGR peptide–Dau bioconjugates including chemostability, lysosomal degradation, cellular uptake studies and in vitro cytostatic/cytotoxic effect.

Results and Discussion

Synthesis of cyclic NGR–Dau conjugates

The NGR cyclic peptides were prepared as shown in Figure 1. All derivatives were synthesized by SPPS on a Rink-Amide MBHA Resin, using Fmoc/*t*-Bu strategy. The anticancer drug daunomycin was conjugated to the Aoa-GFLGK spacer via oxime linkage [17]. This spacer is degraded by lysosomal enzymes ensuring the release of the Dau=Aoa-Gly-OH as the smallest bioactive metabolite in lysosomes [19]. It is well known from our previous studies that not only the free Dau but also Dau containing metabolites like Dau=Aoa-Gly-OH bind to DNA efficiently resulting in antitumor activity. The exchange of the Lys in the cycle simplified the cyclization step and due to the avoidance of the Fmoc cleavage in solution (Figure 1B vs 1A) the compounds could be obtained in higher yields compared to the control (**K**). Isopropylidene protected aminooxyacetyl moiety was used to avoid unwanted reactions with aldehydes or ketones. This protecting group was removed with 1 M methoxylamine in 0.2 M NH_4OAc solution (pH 5.0) prior to the Dau conjugation. The final cyclic NGR peptide–Dau conjugates were characterized by analytical HPLC and mass spectrometry (Table 1, Supporting Information File 1), whereby the purity was over 95% in all cases. In comparison with the control conjugate (**K**) significantly higher overall yield was observed in the case of conjugates **2**, **3** and **4** obtained with a lower yield. The improvement was observed especially in the cyclization step that might be explained by the lack of bulky protecting groups on amino acids used instead of Lys.

Chemostability of cyclic NGR peptide–daunomycin conjugates

The chemostability of cyclic NGR peptide–drug conjugates was studied under the treatment conditions used for the in vitro cytotoxicity experiments. Samples were taken at 0 min, 6 h and

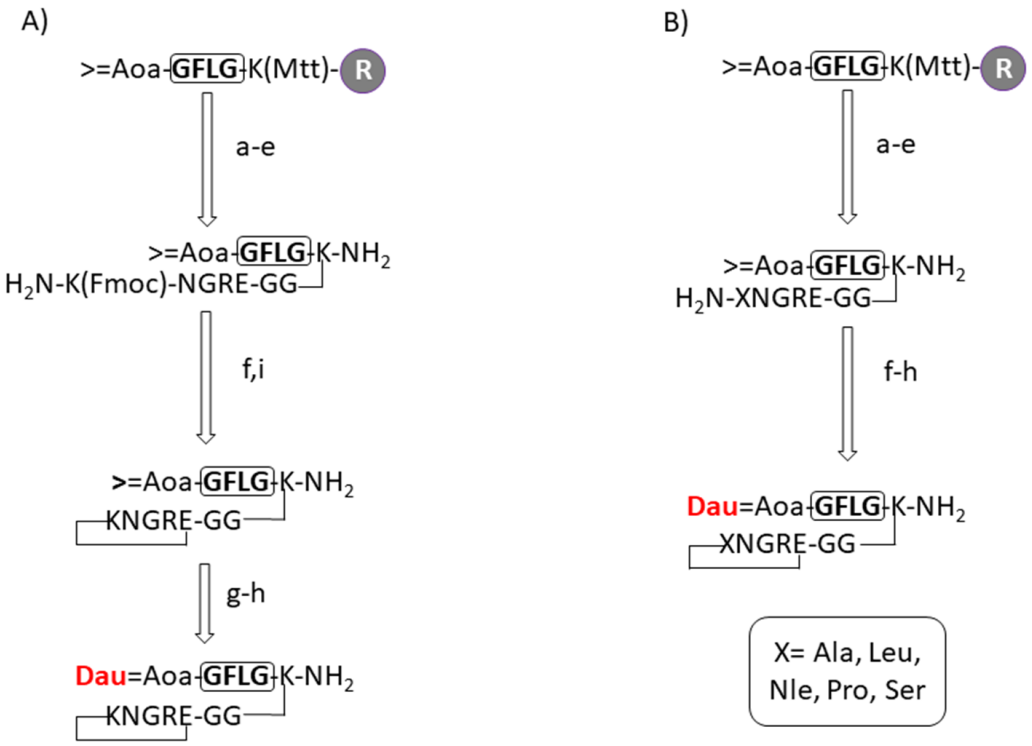

Figure 1: Schematic synthesis of cyclic KNGRE (A) and XNGRE (B) drug conjugates. a) Mtt-cleavage: 2% TFA/DCM; b) Fmoc-Aaa(X)-OH coupling; c) Fmoc-cleavage 2% piperidine/2% DBU/DMF, 0.1 M HOBt; d) cleavage from resin 2.5% TIS/2.5% H_2O/95% TFA (rt, 3 h); e) salt exchange Pyr·HCl 10 equiv/MeOH (1 h); f) cyclization: BOP 3 equiv/HOBt 3 equiv/DIPEA 6 equiv/DMF (c = 0.5 mg/mL, rt, 24 h); g) deprotection of aminooxyacetic acid 0.2 M NH_4OAc solution (pH 5.0)/1 M methoxylamine (rt, 1 h); h) daunomycin conjugation (rt, 24 h) in 0.2 M NH_4OAc solution (pH 5.0); i) Fmoc-cleavage 4% hydrazine/DMF (rt, 2 h).

Table 1: List of the peptide drug-conjugates synthesized.

Code	Compounds	Yield[a] (%)	RP HPLC t_R (min)[b]	ESIMS[c] M(*calc*)/M(*exp*)
1	Dau=Aoa-GFLGK(c[CONH-ANGRE]-GG)-NH_2	2.2	22.2	1725.8/1725.8
2	Dau=Aoa-GFLGK(c[CONH-LNGRE]-GG)-NH_2	7.0	22.4	1767.8/1767.4
3	Dau=Aoa-GFLGK(c[CONH-NIeNGRE]-GG)-NH_2	10.6	22.6	1767.8/1767.2
4	Dau=Aoa-GFLGK(c[CONH-PNGRE]-GG)-NH_2	6.2	17.3	1751.1/1751.4
5	Dau=Aoa-GFLGK(c[CONH-SNGRE]-GG)-NH_2	1.8	20.1	1741.9/1741.7
K	Dau=Aoa-GFLGK(c[CONH-KNGRE]-GG)-NH_2	2.0	23.0	1783.6/1783.0

[a]The overall yield was calculated for the starting amount and capacity of the resin. [b]HPLC: KNAUER 2501; column: Phenomenex Luna C18 (250 mm × 4.6 mm, 5 µm silica, 100 Å pore size; gradient: 0 min 0% B; 5 min 0% B; 50 min 90% B; eluents: A) 0.1% TFA/water, B) 0.1% TFA/MeCN-H_2O (80:20, v/v); flow rate: 1 mL/min; detection: λ = 220 nm. [c]ESIMS: Bruker Daltonics Esquire 3000+ ion trap mass spectrometer; spectra were acquired in the 50–2500 *m/z* range.

72 h. The deamidation rate was evaluated by HPLC–MS. In contrast to the control conjugate (**K**) that showed high stability in our previous study, the new conjugates rearranged in time. The results showed very similar isoAsp/Asp (≈3:1) rates after deamidation of conjugates **1**, **2**, **3**, and **5** calculated from the area under the curve (Table 2, Supporting Information File 1, Figures S1–S5). After 6 h, moderate rearrangement was observed which increased in time. However, 54–58% of the parent cyclic NGR conjugates were still intact after 72 h. Lower stability was observed in the case of the Pro-containing conju-

Table 2: Chemostability of cyclic NGR peptide-Daunomycin conjugates.

Code	AAA in position X of the conjugates	Ratio of Asn-/Asp-/isoAsp-derivatives (DMEM CM, 37 °C)					
		6 h			72 h		
		NGR	DGR	isoDGR	NGR	DGR	isoDGR
1	Ala	96	0	4	58	11	31
2	Leu	93	0	7	54	11	35
3	Nle	93	1	6	58	9	33
4	Pro	73	14	13	19	46	35
5	Ser	93	0	7	56	12	31
K	Lys	100	0	0	100	0	0

gate (**4**) with faster deamidation and higher ratio of DGR. Except deamidation no other decomposition could be observed during this study.

Cytostatic/cytotoxic studies of NGR peptide–Dau conjugates

Similarly to our previous study the antitumor effects of conjugates were examined in vitro on CD13+ HT-1080 human fibrosarcoma and on CD13− HT-29 human colon adenocarcinoma cells. Both cell types are integrin receptor positive [17]. The effect of the new drug conjugates was compared with the toxicity of free Dau and our lead compound Dau=Aoa-GFLGK(c[KNGRE]-GG)-NH_2 (**K**). The bioconjugates enter cancer cells most likely by receptor-mediated endocytosis (at least at lower micromolar concentration) followed by the release of the active metabolite Dau=Aoa-Gly-OH by lysosomal degradation. In contrast, free Dau enters the cells in an unspecific manner which might explain the lower antitumor effect of conjugates in comparison with the free drug. In this experiment we measured the cytostatic effect (6 h treatment and further 66 h incubation after washing out the compounds) and the cytotoxic effect (72 h treatment). The results are summarized in (Table 3). In contrast to **K** that is taken up by HT-1080 cells slightly more efficiently than by HT-29 and therefore shows higher antitumor effect against CD13+ cells, the new conjugates showed higher cytostatic/cytotoxic effects on the CD13− HT-29 colon cancer cells. It seems that the replacement of Lys by the hydrophilic amino acid Ser is not favorite. However, the incorporation of hydrophobic amino acids was well accepted. The conjugate with bulky side chain in this position (Leu) had higher IC_{50} values that might be explained by sterical hindrance. The conjugates with Ala or Nle showed the best antitumor activity on both cell lines. The Nle containing conjugate presented similar activity on HT-1080 and higher activity on HT-29 cells compared to the control conjugate. It is worth mentioning that Nle has a linear hydrocarbon side chain with the same length as Lys, the amino functional group missing. To further characterize the biological activity of the conjugates, their lysosomal degradation and cellular uptake were studied.

In this study our goal was to compare the in vitro antitumor activity of the conjugates. We believe that the measurement of binding affinity on isolated receptors, that was not task of this experiment, could not explain properly the efficacies and selec-

Table 3: In vitro cytostatic/cytotoxic effects of compounds on HT-29 and HT-1080 cells.

Compounds	HT-1080 (6 h) IC_{50} (μM)	HT-29 (6 h) IC_{50} (μM)	HT-1080 (72 h) IC_{50} (μM)	HT-29 (72 h) IC_{50} (μM)
Daunomycin	1.4 ± 0.6	0.3 ± 0.2	0.5 ± 0.2	0.1 ± 0.1
Dau=Aoa-GFLGK(c[KNGRE]-GG)-NH_2 (**K**)	5.7 ± 0.5	8.7 ± 1.2	1.4 ± 0.7	3.0 ± 0.6
Dau=Aoa-GFLGK(c[ANGRE]-GG)-NH_2 (**1**)	8.9 ± 0.8	4.3 ± 0.5	3.6 ± 0.7	3.2 ± 0.8
Dau=Aoa-GFLGK(c[LNGRE]-GG)-NH_2 (**2**)	57.5 ± 6.3	47.0 ± 5.4	20.6 ± 0.4	14.1 ± 0.7
Dau=Aoa-GFLGK(c[NleNGRE]-GG)-NH_2 (**3**)	5.5 ± 0.3	2.2 ± 0.2	2.3 ± 0.6	1.3 ± 0.2
Dau=Aoa-GFLGK(c[PNGRE]-GG)-NH_2 (**4**)	9.4 ± 4.0	14.6 ± 4.7	3.5 ±1.0	3.7 ± 0.8
Dau=Aoa-GFLGK(c[SNGRE]-GG)-NH_2 (**5**)	>100	64.7 ± 4.9	63.7 ± 9.5	39.4 ± 2.9

tivity. The receptor profile of both cell types are very complex. HT-1080 contain different integrins (RGD, collagen, etc) next to CD13 receptor [20]. HT-29 expresses all the known β_1 RGD dependent receptors furthermore $\alpha_v\beta_3$, $\alpha_v\beta_5$, $\alpha_v\beta_6$, $\alpha_v\beta_8$ [21]. Most of the mentioned integrins bind isoDGR peptides with different affinity from nM up to μM concentration that depends on the structure of the peptide [2]. In addition the binding affinity of the different integrins is not consequent to the peptides. Furthermore, there are only a few binding affinity studies for CD13 suggesting several hundred nM IC_{50} values for NGR peptide derivatives [22]. The biological activity of NGR and isoDGR peptides might be influenced also by the density of the different receptors on the tumor cells, which is not so easy to identify in case of such complex receptor profile. Therefore, the resulted amount of isoDGR derivatives might provide similar activity both on CD13+ and CD13− cells.

Lysosomal degradation

Lysosomal degradation studies were carried out as previously described [17]. The results showed that all conjugates decomposed within 6 h (Supporting Information File 1, Figures S6–S10). The main cleavage site of the conjugates could be detected between Gly-Phe within the enzyme labile spacer resulting in the smallest active Dau containing metabolite Dau=Aoa-Gly-OH. No significant difference in degradation speed of the conjugates was observed. Therefore, the replacement of Lys has no influence on the biological activity through the lysosomal degradation.

Cellular uptake

Daunomycin is fluorescent therefore the cellular uptake of Dau containing conjugates can be followed by flow cytometry (Figure 2). The new conjugates were taken up by HT-29 cells in a higher amount than by HT-1080 cells. Conjugates **2**, **3** and **4** showed significantly higher accumulation in HT-29 than in HT-1080 cells compared to the other conjugates. The highest uptake by both cell types was observed in the case of conjugates **3** and **4**. The low cytostatic/cytotoxic effects of conjugate **5** can be explained by the results of cellular uptake study. The Ser-containing conjugate did not enter HT-1080 cells, while a slightly higher cellular uptake was detected in HT-29 cells, although this uptake was still much lower than in the case of the other conjugates.

Conclusion

From this study we can conclude that replacement of Lys in the Dau=Aoa-GFLGK(c[KNGRE]-GG)-NH_2 conjugate by different amino acids provides a more convenient and cost-effective synthetic route resulting in a higher yield, which might be relevant for larger scale synthesis needed for further in vivo studies. We show that the changes decrease the chemostability of the cyclic NGR moiety, resulting in the formation of isoAsp derivatives in higher amount. Among the new cyclic NGR peptide–daunomycin conjugates the most effective compound was Dau=Aoa-GFLGK(c[NleNGRE]-GG)-NH_2, which showed similar activity against HT-1080 CD13+ cells to Dau=Aoa-GFLGK(c[KNGRE]-GG)-NH_2, and a significantly higher antitumor effect against HT-29 CD13− but integrin receptor positive cells. This might be explained by the binding affinity of isoDGR peptides to integrin receptors. However, to confirm this findings further binding studies of cyclic NGR peptide–drug conjugates to different integrin receptors are needed. Taken together, the synthetic and biological results suggest that the Dau=Aoa-GFLGK(c[NleNGRE]-GG)-NH_2 conjugate is more suitable for drug targeting with dual acting propensity than our control lead compound.

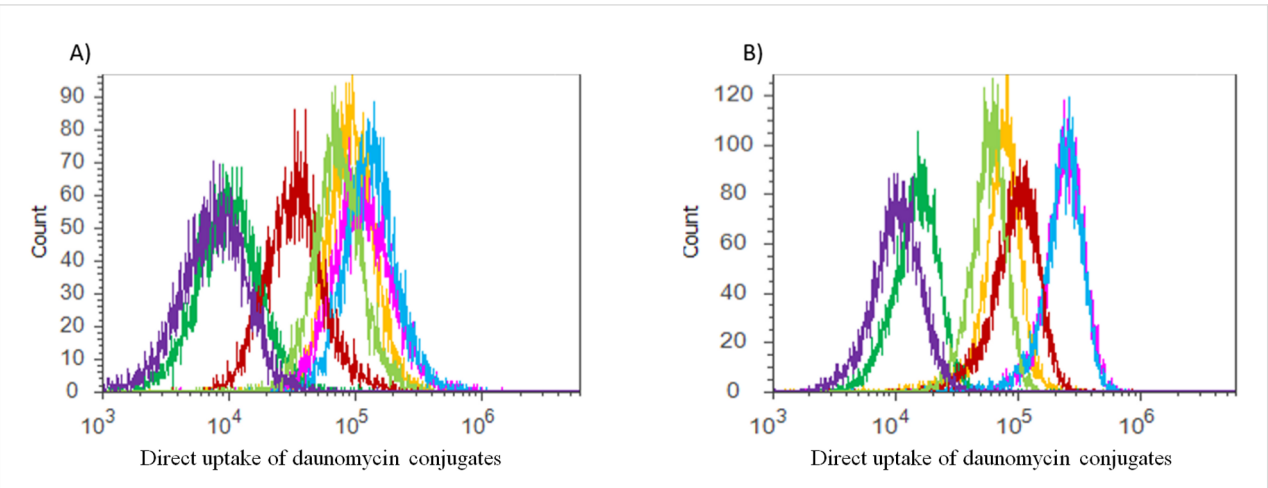

Figure 2: (A) HT1080 and (B) HT-29 cells. Uptake of conjugate **1** (light green); **2** (red); **3** (light blue); **4** (pink); **5** (green); **K** (yellow). Empty control with purple color.

Experimental

Synthesis of the novel peptide–drug conjugates

Linear precursor peptides were prepared on Rink-Amide MBHA resin by SPPS. Standard Fmoc protected amino acids (Iris Biotech GmbH, Marktredwitz, Germany) were used for the synthesis except Fmoc-Lys(Mtt)-OH that was applied for the development of branching in the peptide. The protocol of the SPPS was similarly as described in [17] as follows: (i) DMF washing (4 × 0.5 min), (ii) Fmoc deprotection with 2% DBU, 2% piperidine, 0.1 M HOBt in DMF (4 times; 2 + 2 + 5 + 10 min), (iii) DMF washing (10 × 0.5 min), (iv) coupling of Fmoc-protected amino acid derivative: DIC:HOBt in DMF (4 equiv each) (1 × 60 min), (v) DMF washing (3 × 0.5 min), (vi) DCM washing (2 × 0.5 min), (vii) ninhydrin or isatin test. The cleavage of Mtt protecting group was achieved by using 2% TFA in DCM for 6 × 4 min. The coupling of the isopropylidene protected aminooxyacetic acid [17] to the *N*-terminus of the linker sequence was carried out by using standard protocol DIC/HOBt coupling. The cleavage from the solid support was performed at rt in a solution of 95% TFA, 2.5% triisopropylsilane, and 2.5% water for 3 h. The resin was then filtered and the crude product was precipitated with cold diethyl ether and pellet centrifugated for 5 min at 4000 rpm. After washing (3 times with ether) the remaining pellet was dissolved in water and lyophilized. The lyophilized compound was then purified by RP-HPLC prior to the cyclization.

Cyclization

Prior to the head-to-side chain cyclization a salt exchange needs to be performed using 10 equiv of pyridinium hydrochloride in 5 mL MeOH. After 20 min volatiles were removed under reduced pressure, the remaining oily compound was dissolved in dry DMF at a concentration of 0.5 mg/mL. The pH of the solution was adjusted to pH 8 with DIPEA, then BOP and HOBt (3 equiv each) are added to the mixture. The reaction was followed by analytical HPLC till the complete conversion. At the end DMF was removed and the oily compound was dissolved in acetonitrile–water and purified by RP-HPLC and the collected fractions lyophilized.

Purification

Analogous to the description in [17] RP-HPLC purification was used for the isolation of pure peptides and conjugates. A KNAUER 2501 HPLC system (KNAUER, Bad Homburg, Germany) was applied with a semi-preparative Phenomenex Luna C18 column (250 mm × 21.2 mm) with 10 µm silica (100 Å pore size) (Torrance, CA). Linear gradient elution (0 min 15% B; 5 min 15% B; 55 min 70% B) with eluent A (0.1% TFA in water) and eluent B (0.1% TFA in MeCN–H_2O (80:20, v/v)) was used at a flow rate 9.5 mL/min. Peaks were detected at 220 nm.

Chemostability studies

As described in [17] to check the chemical stability each of the drug conjugates were dissolved in DMSO (2% of the final volume), following the addition of 10% FBS (fetal bovine serum) containing complete cell culture medium (DMEM CM) up to the 1 mg/mL final concentration. Each conjugate was allowed to incubate at 37 °C. Samples were analyzed at experiment time of 0 h, 6 h and 72 h, respectively, and components were purified with Amicon Ultra Centrifugal Filters (cut off 10K Millipore). The membranes were washed with eluent A (HPLC), followed by 3 × 15 min centrifugation at 13000 rpm. The last step is the washing with eluent B (HPLC) 1 × 15 min, followed by lyophilization and concentration of the samples.

In vitro cytostatic effect and cytotoxicity

HT-1080 was maintained in DMEM while HT-29 cells in RPMI (Sigma-Aldrich), respectively, supplemented with 10% FBS, 5 mmol/L glutamine, and 50 units/mL penicillin and streptomycin (Life Technologies). As described in [17] cells were seeded in 5000 cells/well density in 100 µL medium followed by an overnight incubation. The next day 100 µL of serially diluted drugs were added to the cells. For the measurements of cytostatic effect, drug containing medium was gently removed from the plates after 6 h incubation, fresh medium was added to each wells, and the plates were further incubated for additional 66 h (72 h in total). In the case of cytotoxicity measurements, the drug containing medium was on the cells for the full period of the 72 h assay. At 72 h, supernatant was removed from the cells, and viability was assessed by the PrestoBlue® reagent (Life Technologies), which was diluted in PBS to reach the concentration given in the manufacturer's instruction.

Lysosomal degradation

Rat liver lysosomal homogenate was prepared for this experiment. The protein concentration was detected with bicinchoninic acid (Pierce BCA protein assay) following the manufacturer's protocol (ThermoFischer Scientific, Rockford, IL, USA), and it was 17.4 µg/µL. The peptide–drug conjugates were dissolved in deionized water (4 µg/mL concentration). The solutions were further diluted to a concentration of 0.2 µg/µL using 0.2 M of NH_4OAc (pH 5.0). The lysosomal homogenate was diluted with 0.2 M NH_4OAc (pH 5.0) to a concentration of 3.48 µg/µL. The homogenate was then added to the conjugates in a ratio of 1:1 w/w. All the degradation mixtures were kept at 37 °C, samples of 13 µL were taken at 0 h, 6 h and 72 h. Reaction mixtures were quenched by the addition of 2 µL of formic acid. LC–MS analysis was performed at the end on each sample.

Cell uptake

Analogous to the description in [17], prior to the treatment, HT-1080 and HT-29 cells were incubated overnight in cell culture medium (see above) followed by seeding at a 250.000 cells/well density. Peptide–drug conjugates were dissolved in FBS containing cell culture medium and added to the cells at 10 μM final concentration. After 6 h incubation at 37 °C the supernatant was removed, cells were washed with PBS and trypsinised with 0.1% trypsin (Gibco® by Life Technologies) for 10 minutes. Trypsinization was terminated with FBS containing medium, then cells were washed and suspended in serum free medium. For live/dead detection we used Zombie Violet reagent (Biolegend, San Diego CA). Samples were detected and analyzed by using an Attitude® Acoustic Focusing Cytometer (ThermoFischer Scientific).

Supporting Information

Supporting Information File 1

Chemo stability and lysosomal degradation measurements.
[https://www.beilstein-journals.org/bjoc/content/supplementary/1860-5397-14-78-S1.pdf]

Acknowledgements

This project has received funding from the European Union's Horizon 2020 research and innovation program under the Marie Sklodowska-Curie grant agreement No 642004, from the Hungarian National Science Fund (OTKA K104045) and National Research, Development and Innovation Office (NKFIH K119552). GS was supported by the Momentum program of the Hungarian Academy of Sciences. Gitta Schlosser acknowledges the support of the MTA Premium Post-Doctorate Research Program of the Hungarian Academy of Sciences (HAS, MTA).

ORCID® iDs

Andrea Angelo Pierluigi Tripodi - https://orcid.org/0000-0001-9314-4596
Kata Nóra Enyedi - https://orcid.org/0000-0003-3724-5936
Gitta Schlosser - https://orcid.org/0000-0002-7637-7133
Gábor Mező - https://orcid.org/0000-0002-7618-7954

References

1. Curnis, F.; Arrigoni, G.; Sacchi, A.; Fischetti, L.; Arap, W.; Pasqualini, R.; Corti, A. *Cancer Res.* **2002,** *62,* 867–874.
2. Curnis, F.; Cattaneo, A.; Longhi, R.; Sacchi, A.; Gasparri, A. M.; Pastorino, F.; Di Matteo, P.; Traversari, C.; Bachi, A.; Ponzoni, M.; Rizzardi, G.-P.; Corti, A. *J. Biol. Chem.* **2010,** *285,* 9114–9123. doi:10.1074/jbc.M109.044297
3. Rundhaug, J. E. *J. Cell. Mol. Med.* **2005,** *9,* 267–285. doi:10.1111/j.1582-4934.2005.tb00355.x
4. Zou, M.; Zhang, L.; Xie, Y.; Xu, W. *Anti-Cancer Agents Med. Chem.* **2012,** *12,* 239–246. doi:10.2174/187152012800228751
5. Meinwald, Y. C.; Stimson, E. R.; Scheraga, H. A. *Int. J. Pept. Protein Res.* **1986,** *28,* 79–84. doi:10.1111/j.1399-3011.1986.tb03231.x
6. Geiger, T.; Clarke, S. *J. Biol. Chem.* **1987,** *262,* 785–794.
7. Voorter, C. E.; de Haard-Hoekman, W. A.; van den Oetelaar, P. J.; Bloemendal, H.; de Jong, W. W. *J. Biol. Chem.* **1988,** *263,* 19020–19023.
8. Violand, B. N.; Schlittler, M. R.; Toren, P. C.; Siegel, N. R. *J. Protein Chem.* **1990,** *9,* 109–117. doi:10.1007/BF01024992
9. Tyler-Cross, R.; Schirch, V. *J. Biol. Chem.* **1991,** *266,* 22549–22556.
10. Kirikoshi, R.; Manabe, N.; Takahashi, O. *Int. J. Mol. Sci.* **2017,** *18,* No. 429. doi:10.3390/ijms18020429
11. Catak, S.; Monard, G.; Aviyente, V.; Ruiz-López, M. F. *J. Phys. Chem. A* **2008,** *112,* 8752–8761. doi:10.1021/jp8015497
12. Frank, A. O.; Otto, E.; Mas-Moruno, C.; Schiller, H. B.; Marinelli, L.; Cosconati, S.; Bochen, A.; Vossmeyer, D.; Zahn, G.; Stragies, R.; Novellino, E.; Kessler, H. *Angew. Chem., Int. Ed.* **2010,** *49,* 9278–9281. doi:10.1002/anie.201004363
13. Spitaleri, A.; Ghitti, M.; Mari, S.; Alberici, L.; Traversari, C.; Rizzardi, G.; Musco, G. *Angew. Chem., Int. Ed.* **2011,** *50,* 1832–1836. doi:10.1002/anie.201007091
14. Mingozzi, M.; Dal Corso, A.; Marchini, M.; Guzzetti, I.; Civera, M.; Piarulli, U.; Arosio, D.; Belvisi, L.; Potenza, D.; Pignataro, L.; Gennari, C. *Chem. – Eur. J.* **2013,** *19,* 3563–3567. doi:10.1002/chem.201204639
15. Negussie, A. H.; Miller, J. L.; Reddy, G.; Drake, S. K.; Wood, B. J.; Dreher, M. R. *J. Controlled Release* **2010,** *143,* 265–273. doi:10.1016/j.jconrel.2009.12.031
16. Máté, G.; Kertész, I.; Enyedi, K. N.; Mező, G.; Angyal, J.; Vasas, N.; Kis, A.; Szabó, E.; Emri, M.; Biró, T.; Galuska, L.; Trencsényi, G. *Eur. J. Pharm. Sci.* **2015,** *69,* 61–71. doi:10.1016/j.ejps.2015.01.002
17. Enyedi, K. N.; Tóth, S.; Szakács, G.; Mező, G. *PLoS One* **2017,** *12,* e0178632. doi:10.1371/journal.pone.0178632
18. Enyedi, K. N.; Czajlik, A.; Knapp, K.; Láng, A.; Majer, Z.; Lajkó, E.; Kőhidai, L.; Perczel, A.; Mező, G. *J. Med. Chem.* **2015,** *58,* 1806–1817. doi:10.1021/jm501630j
19. Orbán, E.; Mező, G.; Schlage, P.; Csik, G.; Kulić, Ž.; Ansorge, P.; Fellinger, E.; Möller, H. M.; Manea, M. *Amino Acids* **2011,** *41,* 469–483. doi:10.1007/s00726-010-0766-1
20. Wayner, E. A.; Carter, W. G. *J. Cell Biol.* **1987,** *195,* 1873–1884. doi:10.1083/jcb.105.4.1873
21. Kempermann, H.; Wijnands, Y. M.; Roos, E. *Exp. Cell Res.* **1997,** *234,* 156–164. doi:10.1006/excr.1997.3599
22. Ma, W.; Kang, F.; Wang, Z.; Yang, W.; Li, G.; Ma, X.; Li, G.; Chen, K.; Zhang, Y.; Wang, J. *Amino Acids* **2013,** *44,* 1337–1345. doi:10.1007/s00726-013-1469-1

BEILSTEIN JOURNAL OF ORGANIC CHEMISTRY

On the design principles of peptide–drug conjugates for targeted drug delivery to the malignant tumor site

Eirinaios I. Vrettos[1], Gábor Mező[2,3] and Andreas G. Tzakos[*1]

Review

Open Access

Address:
[1]University of Ioannina, Department of Chemistry, Section of Organic Chemistry and Biochemistry, Ioannina, GR-45110, Greece, [2]Eötvös Loránd University, Faculty of Science, Institute of Chemistry, Pázmány P. stny. 1/A, H-1117 Budapest, Hungary and [3]MTA-ELTE Research Group of Peptide Chemistry, Hungarian Academy of Sciences, Eötvös Loránd University, Pázmány P. stny. 1/A, H-1117 Budapest, Hungary

Email:
Andreas G. Tzakos[*] - agtzakos@gmail.com

* Corresponding author

Keywords:
bioconjugates; cancer; drug delivery; PDC; peptide; peptide–drug conjugate; side-products in PDCs

Beilstein J. Org. Chem. **2018,** *14,* 930–954.
doi:10.3762/bjoc.14.80

Received: 29 January 2018
Accepted: 04 April 2018
Published: 26 April 2018

This article is part of the Thematic Series "Peptide–drug conjugates".

Guest Editor: N. Sewald

Abstract

Cancer is the second leading cause of death affecting nearly one in two people, and the appearance of new cases is projected to rise by >70% by 2030. To effectively combat the menace of cancer, a variety of strategies have been exploited. Among them, the development of peptide–drug conjugates (PDCs) is considered as an inextricable part of this armamentarium and is continuously explored as a viable approach to target malignant tumors. The general architecture of PDCs consists of three building blocks: the tumor-homing peptide, the cytotoxic agent and the biodegradable connecting linker. The aim of the current review is to provide a spherical perspective on the basic principles governing PDCs, as also the methodology to construct them. We aim to offer basic and integral knowledge on the rational design towards the construction of PDCs through analyzing each building block, as also to highlight the overall progress of this rapidly growing field. Therefore, we focus on several intriguing examples from the recent literature, including important PDCs that have progressed to phase III clinical trials. Last, we address possible difficulties that may emerge during the synthesis of PDCs, as also report ways to overcome them.

Introduction

Current cancer chemotherapy

Cancer is one of the leading causes of death globally behind the heart and circulatory disorders based on statistics of World Health Organization (WHO) [1]. Among all different types of cancer, the most fatal for males are lung and prostate cancer, while for females are breast cancer, colon & rectum cancer [1]. Notably, more than 12 million cancer cases and 7 million

cancer deaths are estimated to have occurred both in males and females in 2008 worldwide [2]. These numbers have mounted up to 15 million cases and 8.8 million deaths in 2015. These statistics clearly indicate that cancer is not retreating but is creeping up, tending to become the leading cause of mortality. Thus, it can be concluded that the current therapeutic formulations utilized in oncology are not adequately effective against the complexity of cancer, mostly due to the associated collateral toxicity present in healthy tissues. It is estimated that about 30% of the clinical trials on ClinicalTrials.gov are related to cancer, while only 10% of them eventually gain market approval [3], rendering the drug development, especially in this therapeutic direction, costly and inefficient. Specifically, 12 cancer drugs were approved by the FDA in 2017 [4], comprising 26% of the total amount of approvals with respect to other therapeutic areas. These figures suggest that it is of great importance to turn the focus of the global market on targeted therapies. In 2009, the total earnings in the United States, derived from targeted cancer drugs, have reached $10.4 billion, showing an almost 2.2-fold increase since 2005 [5]. However, despite the significant attention that field has gained the past decades, it still remains unfulfilled.

Current treatment processes involve a combination of surgical intervention, radiation and chemotherapy. Drugs used for this purpose are inevitably cytotoxic in order to eliminate cancer cells, but they lack selectivity that could be developed through targeting malignant cells (Figure 1). Due to the uncontrolled peripheral toxicity, anticancer drugs usually kill healthy tissues, resulting in severe effects on the patient's health. One representative example is gemcitabine, which demonstrates higher toxicity for healthy cells, after long-term administration, with respect to cancer cells. This happens since cancer cells evolve more rapidly and develop drug resistance by diminishing expressed nucleoside receptors responsible for the cell uptake of gemcitabine [6].

Additionally, chemotherapy with anticancer agents is often hampered by their poor aqueous solubility, low oral bioavailability and metabolic instability. These drawbacks are linked to the unfavorable ADME (absorption distribution metabolism excretion) that are basically described in the following four consecutive axes: 1) Absorption is directly connected with the transportation process of the drug from the site of administration to the systemic circulation [7]. 2) Distribution refers to the delivery of the drug to the tissues which usually occurs via the bloodstream. Conventional chemotherapeutic drugs (gemcitabine, paclitaxel, doxorubicin, etc.) are not capable to be selectively delivered to the tumor sites and they end up scattered in the whole body. 3) Metabolism is a standard biological strategy for detoxification, breaking down of the administrated drugs, once inserted into the human body. The drugs get decomposed and converted to their metabolites. These metabolites can be pharmacologically inactive, e.g., gemcitabine converted to 2',2'-difluorodeoxyuridine (dFdU) [8] or possess enhanced activity with respect to the parent drug, e.g., temozolomide converted to 5-(3-methyltriazen-1-yl)imidazole-4-carboxamide (MTIC) [9]. 4) Excretion is the final step and is responsible for the removal of the parent drug and/or its metabolites from the human body. Renal excretion is the predominant route of elimination, occurring via urine.

Therefore, most conventional cytotoxic agents applied in chemotherapy lack optimum pharmacokinetic properties

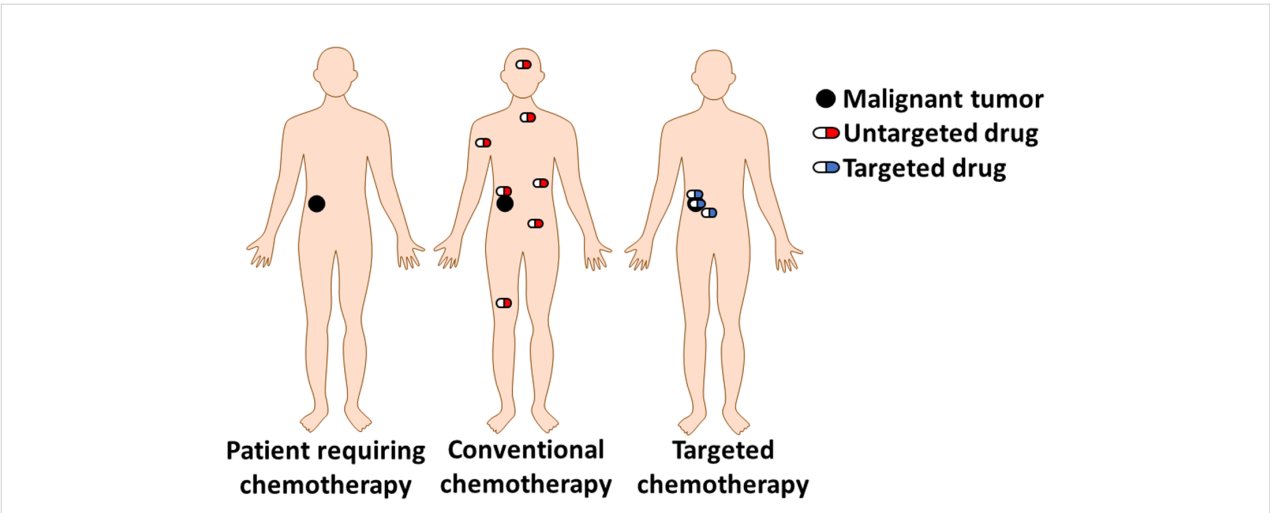

Figure 1: Conventional chemotherapy versus targeted chemotherapy. Black color = Solid malignant tumor; red = conventional untargeted cytotoxic agent; blue = targeted cytotoxic agent.

(ADME) and thus are not very effective to treat malignancies. Moreover, despite the intensive research to construct new cytotoxic drugs, survival rates in most cancers remain low [10] and clinical attrition rates in oncology have been devastating [11]. These data render obvious that the currently developed drugs, as also the continuous attempt to discover new ones, have not provided the expected therapeutic impact in oncology.

It is clear that we do have access to an enormous pool of unspecific cytotoxic agents that can efficiently kill cancer cells. What is currently needed is not to invest so intensively in generating more cytotoxic agents but to re-use and re-cycle available ones and tailor them to be transformed into targeted chemotherapeutics. Along these lines, drug delivery vehicles that can be tailored for different types of cancer and shape personalized therapeutics are continuously gathering attention. Such drug delivery systems are of ultimate importance to effectively surpass these hurdles and eventually improve drug potency.

Charting the malignant tumor microenvironment

In order to selectively deliver cytotoxic drugs to malignant tumor sites, scientists can take advantage and map first the differential microenvironment between cancer and normal cells. The first one to report a fundamental difference between malignant and normal cells was Otto Heinrich Warburg in the early 1900s, who was awarded the Nobel Prize in 1931. He proposed that malignant tumor growth relies on aerobic glycolysis, in contrast to normal cells that generate energy by mitochondrial oxidative phosphorylation. The fact that cells converted pyruvate to lactate, even in the presence of oxygen, rendered his observation puzzling for scientists, who still struggle to elucidate the complete mechanism of action of diseased cells. Following the Warburg effect, ^{18}F-deoxyglucose positron emission tomography (FDG–PET) imaging was developed in order to visualize the phenomenon of increased glucose uptake by cancer cells [12].

Nowadays, it has been demonstrated that malignant cells differ markedly in many metabolic aspects compared to normal cells [13], thus offering the opportunity to target them in various ways. Most cancer tissues exhibit the following characteristics that can be exploited for developing targeted cytotoxic agents:

1. Dysregulation of translation initiation factors and regulators [14].
2. Mutations in epigenetic regulatory genes [15].
3. Overexpression of surface receptors like HER2R [16], folate receptor [17], GnRH receptor [18,19] and amino acid transporters [20].
4. Overwhelming production of stimulus agents and enzymes [21]. For instance, many types of cancer show enhanced levels of reactive oxygen species (ROS) which are reactive molecules and play a crucial role in cell proliferation [22].
5. The slightly acidic pH of the tumor microenvironment [23] (Warburg effect).

These are some noteworthy differences that underlie the discrimination between cancerous and normal cells and are often exploited in order to control the site of the drug release during targeted cancer chemotherapy.

Review

Strategies for targeted delivery of toxic warheads to malignant tumor sites

The main challenge of the drug delivery concept is to transport sufficient amount of the cytotoxic agent to a specific location with minimum adverse side effects. To conquer this, various approaches are being exploited at the moment. These include, but are not limited to: a) utilization of drug delivery vehicles and formulates like nanoparticles [24] and calixarenes or cyclodextrins [25,26], where the cytotoxic drug is loaded and can be released at the malignant tumor site; b) installation of labile chemical groups to the tumor microenvironment (i.e., low pH) able to mask the cytotoxic drug and form a prodrug with enhanced plasma stability and/or cell permeability [27] and in the same time diminished toxicity for normal cells; c) covalent attachment of a drug on a tumor-targeting element (small molecule, peptide or antibody) able to selectively target and permeate cancer cells. The conjugation is being conducted via a rationally designed linker able to release the drug inside the cancer microenvironment [19].

The ideal targeting molecular device would consist of the following modules: a) the cytotoxic agent (drug), b) the transporting - drug delivery vehicle (i.e., lipid, mannan [28-30]), c) the linker tethering the transporting vehicle to the cytotoxic warhead, d) the “programmable” navigating/targeting moiety (i.e., receptor-specific ligand) and e) the “stealth” carrier (i.e., PEG) transfusing enhanced bioavailability. These modules are encoded in Figure 2A with different colors: the transporting vehicle in green color, the drug in blue color, the linker in red color, the navigating/targeting agent in black color and the “stealth” carrier in grey color [31]. The specific color coding will be followed, for simplicity purposes, in all examples of targeting devices that will be presented throughout this review.

Among the most intriguing navigating delivery systems that can combine the transporting vehicle and the navigating/targeting moiety in a single module are the tumor-homing peptides [32].

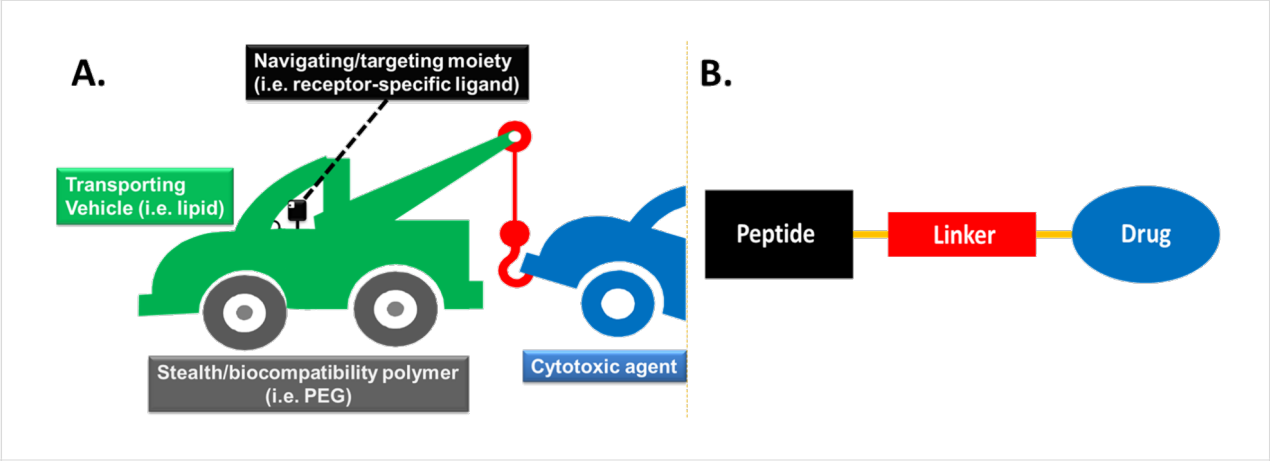

Figure 2: A. General structural architecture of the ideal navigated drug delivery system [31]. B. General structure of a peptide–drug conjugate (PDC).

These peptides are exploited to assemble the peptide–drug conjugates (PDCs) which are considered as prodrugs, due to the covalent coupling of a peptide to a drug via specific linkers. The main building blocks of a simple PDC include a cytotoxic agent (drug), a tumor-homing peptide (navigating/targeting moiety) and a linker between them (Figure 2B).

This class of prodrugs is continuously gaining attention since peptides can be easily produced in large quantities and their purification is simple. Moreover, an array of different tumor-targeting peptides has been discovered [32] for multifarious types of cancer. This bountiful palette can permit the construction of personalized cancer therapeutics upon selecting a tumor-homing peptide that will be most appropriate for the type of cancer needed. In addition, peptide sequences can be selected according to the required physicochemical properties such as solubility, stability and overall charge or the characteristic groups necessary for the conjugation with the therapeutic payload. The overall experimental procedure to synthesize a PDC is usually rapid and facile. Notably, the overall cost to produce a PDC, where an already approved drug can be selected and re-used from a pool of available cytotoxic agents, is much lower compared to the cost of synthesizing a new cytotoxic agent, as it is based on an already applied drug with the addition of a small peptide. Nevertheless, the last years more complex bioconjugates have been synthesized to allow the simultaneous diagnosis and therapy (theranostics) of diseases.

The therapeutic efficacy of a PDC is predominantly associated with the potency of the drug and the targeting efficiency of the assembled conjugate. Thus, PDCs should possess certain features to render them appealing candidates for treatment:

1. The peptide contained in the PDC must bind selectively and with the optimal affinity to a certain receptor, present on the cell surface of the targeted tissues and not within their cytosol or nucleus (i.e., steroid receptors [33]).
2. The selected receptor should be uniquely expressed or overexpressed on cancer cells (usually 3-fold or higher in comparison with normal cells). Additionally, it should be expressed in sufficient levels to pump inside the cell efficacious doses of the drug.
3. The peptide-carrier should be constructed in such way that the conjugation with a drug or/and a fluorophore is feasible. Conjugation usually occurs on lysine, cysteine and glutamic acid [34] via orthogonal coupling or on the free N-terminus of the peptide during solid phase peptide synthesis. Though, the conjugation site should be carefully selected, since perturbations induced in the peptide structural microenvironment may result in the abolishment of its binding affinity/selectivity to the targeted receptor.
4. The linker should be carefully selected to succeed the optimal performance of the PDC. An injudicious selection may cause diminished binding affinity of the peptide to the receptor or/and reduction of the therapeutic window of the drug. Additionally, it should be enzymatically stable during the blood circulation in order to efficiently reach the malignant tumor site and release the payload in its microenvironment, reducing the off-target toxicity.
5. The cytotoxic agent should contain proper functional group that can be linked to the tumor homing peptide (i.e., gemcitabine [19]) or if it is not present it should be rationally installed taking into consideration the final derivative of the cytotoxic agent to retain the original cytotoxic activity. The sections below summarize the basic design principles of peptide–drug conjugates to selectively target the malignant cells.

Selecting the proper tumor-targeting peptide to generate the PDCs

There is an immense variety of peptides (linear or cyclic) that have been exploited as carriers/targeting elements to successfully deliver the cytotoxic warhead to cancer cells [32]. These peptides are cell-specific and bind to certain receptors promoting their internalization. They are usually inserted into the cell via endocytosis and then they are transported to intracellular compartments with higher concentration of enzymes and lower values of pH, where they disassociate from the receptor and afterward from the anticancer agent. The most representative examples of peptides utilized for PDCs are highlighted below.

Linear peptides are included among the rich reservoir of options, finding applications in tumor targeting. They exist in different lengths, structures and with various physicochemical properties.

Attempting to ameliorate certain disadvantages of linear peptides like fast renal clearance or low binding selectivity/affinity due to the unstable structure of the linear peptides, cyclic peptides have been introduced. An immense number of cyclic peptides have been synthesized [35-37] and many of them have displayed superior affinity and selectivity for the receptor than their parent linear counterparts [38]. Cyclic peptides are usually synthesized by reacting the N-terminus with the C-terminus or by exploiting specific functional groups of certain amino acids present in the sequence. A representative example is the sulfhydryl group of cysteine-containing peptides which may cyclize through the formation of intramolecular disulfide bonds [39].

The most commonly used linear peptides and cyclic peptides that can be delivered inside cancer cells via endocytosis and one that smuggles into glioma tissues via transcytosis (angiopep-2) are presented below:

Arginine-glycine-aspartic acid (RGD): A widely applied peptide carrier is the tripeptide arginine-glycine-aspartic acid (RGD) motif, which was first identified by Ruoslahti and Pierschbacher in the early 1980s [40] within fibronectin that mediates cell attachment and was known to target integrin α5β1 [41]. In general, the 'integrin' nomenclature was first used in 1987 to describe a family of receptors, appearing as heterodimers of noncovalently associated α and β subunits, able to link the extracellular matrix (ECM) with the intracellular cytoskeleton to mediate cell adhesion, migration and proliferation [42]. The RGD motif is contained in various proteins like fibrinogen, fibronectin, prothrombin, tenascin and other glycoproteins [43] and is known to be recognized by over 10 integrins, among the over 24 known integrins [44,45], including all αv integrins, α5β1, α8β1 and αIIbβ3 [46].

The fact that carcinogenesis is highly dependent on migration, invasion and angiogenesis renders integrins important anticancer targets. Integrin αvβ3 is an important factor in tumor angiogenesis and metastasis [45], two common characteristics of cancer that discriminates it from other diseases. Notably, integrin αvβ3 (also known as the vitronectin receptor) appears to be the most important among all integrins regarding cell proliferation, invasion and angiogenesis [47]. This integrin is overexpressed on activated endothelial cells, new-born vessels and other tumor cells [48,49], but it is found to be expressed at undetectable levels in most adult epithelial cells, making it a suitable target for anti-angiogenic therapy [50]. Due to its high levels of expression in cancer cells, several peptides containing the RGD motif have been exploited for the formulation of PDCs, with the most representative example to be the peptide CDCRGDCFC [46,51,52].

Gonadotropin-releasing hormone (GnRH): Gonadotropin-releasing hormone (GnRH), also known as luteinizing hormone-releasing hormone (LHRH), is a hormone responsible for the secretion of two gonadotropins: follicle-stimulating hormone (FSH) and luteinizing hormone (LH) from the anterior pituitary gland. GnRH is synthesized and released from GnRH neurons within the hypothalamus and selectively binds to its receptor (GnRH-R), a seven-transmembrane G-protein-coupled receptor. The structure of the GnRH hormone (pGlu-His-Trp-Ser-Tyr-Gly-Leu-Arg-Pro-Gly-NH_2) was first discovered in 1971 by Baba et al. [53]. Besides this form, there is GnRH-II (pGlu-His-Trp-Ser-His-Gly-Trp-Tyr-Pro-Gly-NH_2) discovered in most vertebrates as well as in humans [54]. This peptide acts through a similar receptor (type II GnRH-R), which is expressed in different tissues, including tumor cells. Another natural isoform of GnRH is GnRH-III (pGlu-His-Trp-Ser-His-Asp-Trp-Lys-Pro-Gly-NH_2), which has been isolated from sea lamprey. GnRH-III binds to GnRH-R overexpressed on the cancer cell surface, resulting in an antiproliferative effect but seems to be less potent than the rest GnRH analogs regarding stimulating gonadotropin release at the pituitary level [55].

GnRH peptide analogs constitute an emerging class of tumor homing peptides for malignant tissues expressing the GnRH-R. Their development is based on the fact that specific human cancer cells (mostly ovarian, prostate, lung and breast) uniquely express or overexpress GnRH-R with respect to normal tissues [55-57]. Therefore, covalent attachment of a cytotoxic agent to these peptides provides the possibility to produce potent tumor-targeting PDCs. Various amino acid alterations have been performed with respect to the native hormone [58], while the most

frequently used GnRH analog is D-Lys^6-GnRH-I, which is known to bind selectively to GnRH-R. The substitution of Gly^6 of the native hormone with D-Lys^6 provided an analog with higher binding affinity, stabilized β-bend and resistance to proteolytic cleavage. Moreover, the side chain of lysine contains a free amine group (εNH_2) allowing orthogonal coupling with a cytotoxic warhead [19]. A considerable number of PDCs based on GnRH [59-63] exist and our group has exploited this peptide to construct two PDCs [18,19].

Somatostatin (SST): Somatostatin is a neuropeptide produced by neuroendocrine, inflammatory and immune cells and has an important role in various physiological functions acting as a classical endocrine hormone, a paracrine regulator or a neurotransmitter [64]. Somatostatin appears in two distinct active forms: somatostatin-14 (SST-14) and somatostatin-28 (SST-28). Both SST-14 and SST-28 exhibit biological activity through high-affinity membrane receptors (somatostatin receptor 1–5; SSTR1–5), that are widely distributed throughout the human body in various tissues like the nervous, pituitary, kidney, lung and immune cells [65,66].

SSTRs are overexpressed in various neuroendocrine malignant tumors (NETs) including pancreatic, pituitary, prostate, lung carcinoids, osteosarcoma etc. and other non-NETs including breast, colorectal, ovarian, cervical etc. [67]. Therefore, these receptors can be targeted for selective delivery of efficient concentrations of cytotoxic warheads to the tumor sites. However, native somatostatin gets rapidly hydrolyzed due to enzymatic degradation and therefore, more stable and potent analogs have been developed. These analogs were synthesized by replacing L-amino acids with their D-isomers and reducing the length by keeping only the peptide epitope responsible for the biological activity. The most widely known analogs of somatostatin are cyclic peptides named octreotide (*d*-Phe-*c*[Cys-Phe-*d*-Trp-Lys-Thr-Cys]-Thr-ol), lanreotide (*d*-2Nal-*c*[Cys-Tyr-*d*-Trp-Lys-Val-Cys]-Thr-NH_2) and vapreotide (*d*-Phe-*c*[Cys-Tyr-*d*-Trp-Lys-Val-Cys]-Trp-NH_2), which bind mainly to the subtype 2 receptor (SSTR2) that is known to be the most frequently overexpressed SSTR [68]. There are several examples of PDCs consisting of the aforementioned somatostatin targeting peptides [67,69,70], as also other somatostatin peptide analogs, e.g., pentetreotide (DTPA-*d*-Phe-*c*[Cys-Phe-*d*-Trp-Lys-Thr-Cys]-Thr-ol) [71].

Epidermal growth factor (EGF): Epidermal growth factor receptor (EGFR) is a transmembrane protein belonging to the ErbB family of receptor tyrosine kinases which consists of 4 structurally-related members: EGFR/HER1 (ErbB-1), HER2/neu (ErbB-2), HER3 (ErbB-3) and HER4 (ErbB-4). Cohen and Rita Levi-Montalcini shared the Nobel Prize in Medicine in 1986 for discovering growth factors. EGFR is upregulated in a wide pool of cancer tissues and is able to enter cells usually via clathrin-mediated endocytosis [72]. Many peptides have been discovered to bind the EGFR with high affinity and selectivity through screening phage display libraries and have been used like a viable approach for targeted drug delivery: YHWYGYTPQNVI [73], CMYIEALDKYAC [74], LTVSPWY [75], YWPSVTL [76].

Angiopep-2: A peptide that has recently attracted attention is a 19-mer peptide named angiopep-2 (TFFYGGSRGKRNNFKTEEY), due to its ability to cross the blood-brain barrier (BBB). The BBB is formed by the endothelial cells of the brain, restricting and controlling the exchange of molecules between the central nervous system and the rest body. Angiopep-2 is able to cross the BBB via receptor-mediated transcytosis after binding to the low-density lipoprotein receptor-related protein-1 (LRP-1), which is overexpressed in brain cells [77]. Moreover, the two lysines available in its sequence render angiopep-2 an appealing PDC candidate, with the aim to smuggle therapeutic payloads to brain malignancies [78,79].

Cyclic peptide variants have been developed for the RGD peptide motif, reported above. The most commonly used cyclic peptide is iRGD (CRGDKGPDC), a 9-amino acid cyclic peptide, with tumor tissue penetration activity [80]. iRGD initially binds to αVβ3 and αVβ5 integrins that are overexpressed in tumor endothelial cells. Afterward, a proteolytical cleavage takes place to reveal a cryptic RXXK/R motif located at the C-terminus (CendR motif, C-End Rule), which then binds to neuropilin-1 (NRP-1), activating an endocytic transport pathway responsible for the enhanced transport of anti-cancer drugs into tumors (Figure 3) [80].

In Table 1 are reported the most common peptides (linear and cyclic) utilized in PDCs.

Selecting the proper cytotoxic agent to generate the PDCs

According to the National Cancer Institute (cancer.gov), there are more than 250 FDA-approved anticancer drugs utilized to treat malignancies at the moment. Among this large pool of cytotoxic drugs, an array of them has been utilized as toxic warheads in PDCs and five representative examples are gemcitabine, doxorubicin, daunorubicin, paclitaxel and camptothecin (Figure 4). The main drawback of these original anticancer agents is their uncontrolled toxicity which results in severe side effects. Without the addition of a targeting moiety, they bear low capacity to discriminate cancerous from normal cells. Moreover, the addition of a peptide as a targeting vehicle can enhance the pharmacokinetic and therapeutic window of the

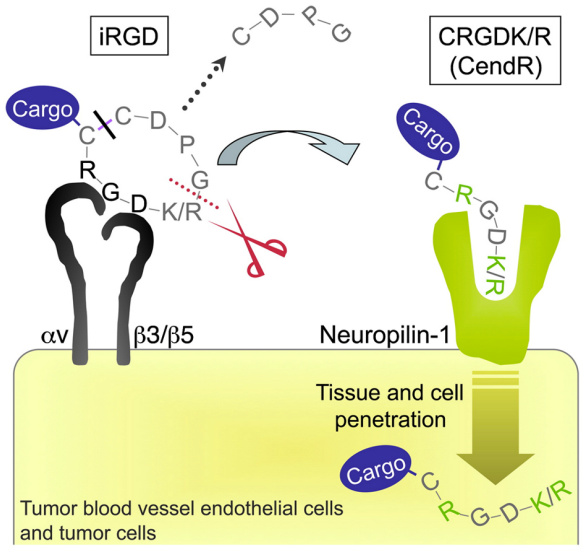

Figure 3: Binding and penetration mechanism of iRGD. The iRGD peptide is accumulated on the surface of αv integrin-expressing endothelial and other cells in malignancies. The RGD motif is responsible for binding to integrins. Afterward, the peptide is cleaved by cell surface-associated protease(s) to eventually expose the cryptic CendR element, RXXK/R, at the C-terminus (red dotted line). The CendR element then interferes with the binding to neuropilin-1, resulting in tissue and cell penetration. The tumor-penetrating peptide can be used to decorate a cargo (a simple chemical moiety or a nanoparticle), but only in the case that the cargo is attached to the N-terminus of the iRGD peptide as the disulfide bond is cleaved before the peptide is internalized (black line). The figure was adopted from reference [81] (© 2009 Elsevier Ltd.).

parent cytotoxic agent. Since different drugs may employ a different mechanistic approach to kill cells, the appropriate drug is selected according to features characterizing the targeted cancerous cells. For instance, daunorubicin and doxorubicin possess similar mechanisms of action [82], whereas gemcitabine [83], camptothecin [84] and paclitaxel [85] function through different mechanisms.

The selected drug must comply with certain design principles in order to serve as an appealing candidate for PDCs. The selected drug must be amenable to the linker chemistry. It must bear an intrinsic functional group for direct conjugation with the peptide/linker (Figure 4) or a functional group able to be derivatized for further conjugation (i.e., click chemistry [86]). In the latter case, the site of derivatization has to be carefully selected so that the biological activity of the drug and the release of the active drug will not be perturbed. In case that the drug binds through recognition of a specific receptor, in silico approaches have to be recruited in order to rationally select the location of the drug that will be chemically modified [18].

Furthermore, it must be sufficiently cytotoxic versus the selected malignant tumor cells in order to eliminate them and consequently promote tumor regression. The selected drug should ideally possess low-nanomolar IC_{50} values for the targeted malignant tumor. A legitimate strategy to overcome a low drug potency problem is by increasing the drug loading of the peptide-carrier. For example, in the PDC ANG1005, 3 drug molecules (paclitaxel) were loaded on a single angiopep-2 peptide which has completed phase II clinical trials [87]. Nevertheless, the concept of higher drug loading is hard to be implemented, in contrast with single drug loading that is usually preferred, mostly due to poor physicochemical properties.

Below we analyze a set of drugs that have been tailored and incorporated in PDCs.

Gemcitabine (Gem): Gemcitabine (dFdC) is a nucleoside analog of deoxycytidine in which the hydrogen atoms on the 2' carbon are replaced by fluorine. It is sold under the brand name Gemzar by Eli Lilly and Company and has been FDA approved for the treatment of various cancers including breast, ovarian, non-small cell lung and pancreatic cancer. The main drawbacks for its use are the high and non-selective toxicity to normal cells, the deactivation through deamination in its inactive metabolite dFdU, the acquired multidrug resistance (MDR) and its high hydrophilicity deterring its prolonged drug release from various vehicles [88], which therefore reduces the effective concentration of gemcitabine. It enters cells through nucleoside transporters hENTs (human equilibrative nucleoside

Table 1: The most common peptides (linear and cyclic) utilized for the formulation of PDCs used in cancer. Letters with bold color stand for D-amino acids.

peptide name	peptide sequence	targeted receptor	reference
RGD	R-G-D	integrin αvβ3	[37,46,51,52]
iRGD	CRGDK/RGPD/EC	integrin αvβ3/αvβ5	[81]
octreotide	**F**-C-F-W-K-T-C-**T**	SSTR2/5	[69]
D-Lys^6-LHRH	Glp-H-W-S-Y-**K**-L-R-P-G	LHRH-R	[18,19,61]
angiopep-2	T-F-F-Y-G-G-S-R-G-K-R-N-N-F-K-T-E-E-Y	LRP-1	[78,79]
GE11	Y-H-W-Y-G-Y-T-P-Q-N-V-I	ErbB1 (EGFR)	[73]

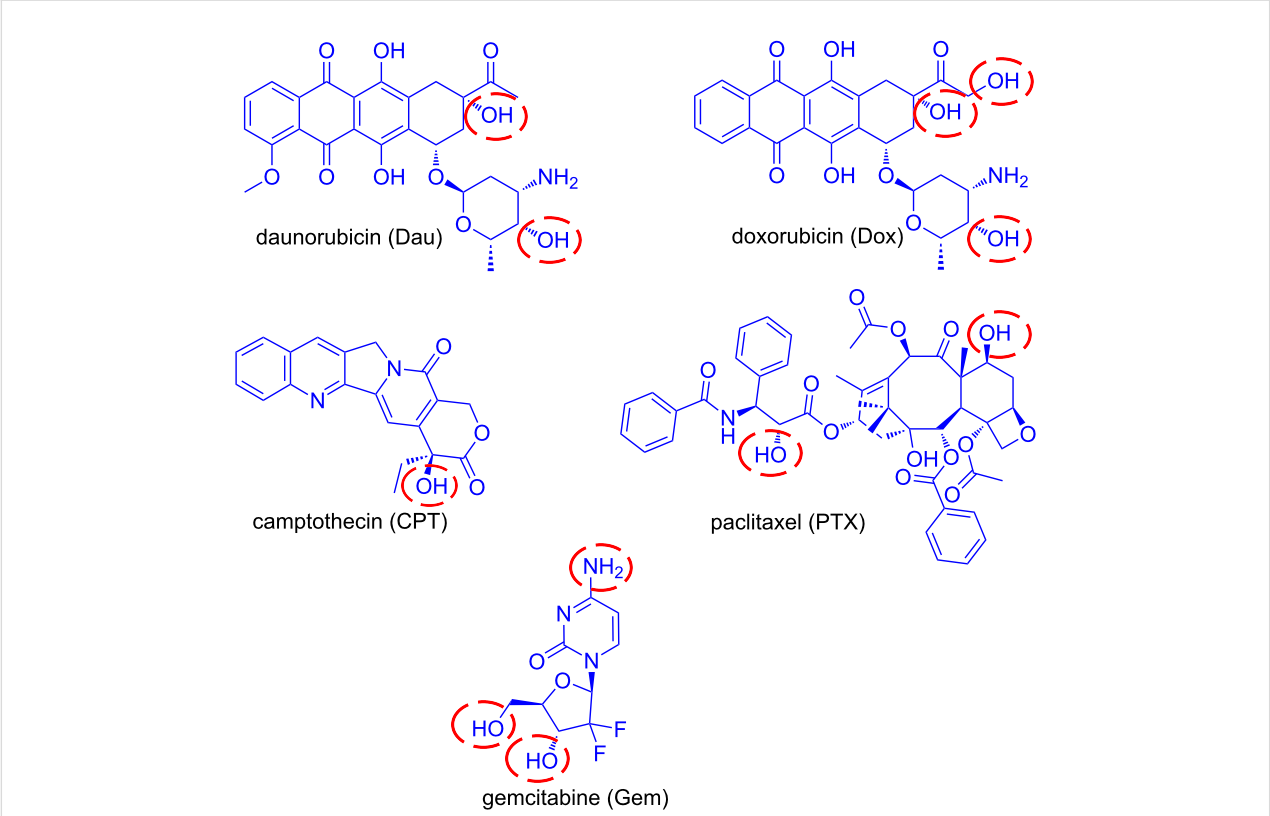

Figure 4: Representative examples of anticancer drugs utilized for the construction of PDCs. The most usual conjugation sites are marked with red cycles.

transporters) and hCNTs (human concentrative nucleoside transporters) and mostly through hENT1 (human equilibrative nucleoside transporter 1) [89,90]. After internalization, gemcitabine is sequentially mono-, di- and tri-phosphorylated by phosphorylating kinases. Gemcitabine diphosphate (dFdCDP) and gemcitabine triphosphate (dFdCTP) are the active metabolites which inhibit processes required for DNA synthesis [91]. The incorporation of dFdCTP into DNA during polymerization, which causes DNA polymerases unable to proceed, is the major mechanism by which gemcitabine causes cell death (masked termination) [83]. Regarding the possible functional sites in gemcitabine that can be used for the construction of PDCs are its primary and secondary alcohols as also the amine (Figure 4).

Paclitaxel (PTX): Paclitaxel (PTX) is a member of the taxane family and one of the most common anticancer agents used against a wide variety of tumors. It is sold under the brand name Taxol by Bristol-Myers Squibb Company and is FDA approved for the treatment of breast cancer, ovarian cancer, non-small cell lung cancer and AIDS-related Kaposi's sarcoma. The main disadvantages in the utilization of paclitaxel are its high hydrophobicity, requiring suitable vehicles to effectively deliver it to tumor tissues, and the development of multidrug resistance due to the P-glycoprotein-mediated efflux [85,92]. Paclitaxel stabilizes microtubules by binding specifically to the beta-tubulin subunit, promoting mitotic halt and consequently cell death [93]. The difference with other known drugs that act on microtubules (vinca alkaloids) is that paclitaxel does not induce the disassembly of microtubules but boosts the polymerization of tubulin [94]. Sites available in PTX for the formation of PDCs are highlighted in Figure 4.

Anthracyclines: Anthracyclines are among the main anticancer drugs that are applied in combinations with other chemotherapeutic agents. They are utilized against a variety of cancers including leukemias, lymphomas, breast, ovarian, bladder and lung. Daunorubicin (Dau) was the first anthracycline discovered that was extracted from *Streptomyces peucetius*, a species of actinobacteria, at the beginning of the 1960s. Shortly after, the isolation of doxorubicin (Dox) from a mutated *Streptomyces* strain was accomplished. Anthracyclines are consisted of a tetracyclin aglycon part and a daunosamine sugar moiety. The difference between Dau and Dox is a hydroxy group substituted at the C-14 carbon atom on Dox providing an extra conjugation site for ester linkage (Figure 6). The mechanism of action of anthracyclines is based on their interca-

lation to DNA inhibiting the macromolecular biosynthesis. Furthermore, they stabilize the topoisomerase II DNA complex preventing the transcription. They may also increase quinone type free radical production, however, this plays a role rather in their cytotoxic side effects. Daunorubicin is mainly used in the treatment of leukemia [95] while doxorubicin in the cure of other types of cancers (breast cancer, bladder cancer, Kaposi's sarcoma) in combination with other anti-cancer agents.

Camptothecin (CPT): Camptothecin is a cytotoxic alkaloid collected from extraction of the bark and stem of the Chinese tree 'Camptotheca acuminata'. It was first isolated and characterized in 1966 by Wall et al. [96,97]. The main mechanism of action involves binding to the reversible complex of topoisomerase I (topo I) and the 3′-phosphate group of the DNA backbone through hydrogen bonding, resulting in accumulation of a persistent ternary complex (the cleavable complex). This stabilized complex prevents the re-ligation step of DNA, catalyzed by topo I, resulting in DNA damage and therefore cell death (apoptosis). CPT is predominantly cytotoxic during the S phase replication of DNA because of the collision of the replication fork with the cleavable complex, converting the single-strand breaks into double-strand breaks and eventually causing cell death [98]. CPT can be conjugated to targeting elements to enhance its efficacy via its primary alcohol marked in Figure 4. Although CPT showed remarkable results during its phase I clinical trials against a variety of solid tumors, its low water-solubility and stability led to the formulation of various new analogs with the same mechanism of action. The two most progressed analogs of CPT are topotecan and irinotecan. Topotecan (hycamtin) has been approved by the FDA for the treatment of ovarian and cervical cancer, as also small cell lung carcinoma. Irinotecan (camptosar) has been approved by the FDA for the treatment of metastatic carcinoma of the colon or rectum, alone or in combination with fluorouracil (5-FU). Camptothecin has been utilized as an anticancer agent in various PDC formulations, such as conjugation with the targeting peptides D-Lys^6-LHRH [99], somatostatin [100] and c(RGDyK) [101].

Linker design for PDCs: Principles and representative examples

Another crucial aspect that should be considered during the design of a PDC is the linker tethering the peptide and the drug. The linker has to be carefully shaped so as not to perturb the binding affinity of the peptide to its receptor and the drug efficacy. An inappropriate linker may impede the release of the drug from the PDC and therefore diminish its overall therapeutic potency. Linkers utilized in PDCs exist in different categories and vary on their length, stability, release mechanism, functional groups, hydrophilicity/hydrophobicity etc.

This linker can be designed to bear an enzyme-hydrolyzable unit (EHU) like a carboxylic ester or an amide bond, cleaved by esterases and amidases, respectively. The most commonly utilized linkers that bear a carboxylic ester bond, as the enzyme-hydrolyzable unit, are succinyl (derived from succinic acid) and glutaryl (derived from glutaric acid). Concerning the utilization of amide bond in the linker as the unit tethering the drug and the peptide, it can be tailored to be cleaved based on the targeted tissue and/or type of cancer where a specific protease is statistically upregulated (i.e., cathepsin B upregulated in various malignancies including lung, brain, prostate and breast [102]). Also, during the design of the PDC specific attention has to be given on the selection of the bonds that will be used in the linker. Specifically, in several currently available PDCs, at least two different bonds are used: one to connect the linker to the peptide and the other to connect the drug to the linker. Such cases have to consider, during the design process, the microenvironment that the assembled PDC is to be located, since different enzymes and/or the tumor microenvironment might trigger the improper release of the drug from the PDC, i.e., to end up with the drug-carrying part of the linker.

Another class of linkers is the stimuli-responsive/degradable linkers, designed to achieve an efficient release of the drug from the bioconjugate in the tumor microenvironment. Such linkers are rationally designed to be cleaved when they sense specific stimuli in the environment of cancerous cells (slightly acidic pH, enhanced levels of reducing agents and/or enzymes) or external stimuli (ultrasound, temperature, irradiation). Specifically, there are certain bonds like imine, oxime, hydrazone, orthoester, acetal, vinyl ether and polyketal [103] that are known to undergo hydrolysis at acidic pH, while being extremely stable during blood circulation. Therefore, acid-labile bonds could be hydrolyzed in the slightly acidic microenvironment and/or in the acidic cellular compartments of cancer cells and consequently release the active drug. Additionally, disulfide linkers are often adopted in PDCs, since they are cleaved by reducing agents like cysteine and glutathione, present in high concentrations in malignant cells.

Linkers bearing enzyme-hydrolyzable units (EHU) responsive to proteases are degradable peptide linkers that have attracted significant interest due to the specificity of certain enzymes and there has been a dramatic escalation over in the past years. The most representative examples in this field are the MMP-2/9 (matrix metalloproteinases) and cathepsin B peptide substrates. MMP-2/9 and cathepsin B are proteolytic enzymes present at elevated levels in cancer cells known to participate in human tumor invasion and metastasis. Cathepsin B is able to recognize specific peptide sequences like Val-Cit (valine-citrulline) [104] and GFLG [105]. On the other hand, GPLGIAGQ [106],

PLGLAG [107] and GPVGLIGK [108] are some common peptide substrates for MMP-2 and MMP-9.

Another rapidly emerging category in PDC linkers that has gained much attention in the last years are the self-immolative or self-destructive spacers/linkers [109,110]. This type of linkers/spacers offers the capability to release the active drug after simultaneous cascade reactions, as shown in Figure 5. *Para*-amino benzyl alcohol (PABC; colored in red) is a representative example that can be connected in the amino group via an amide bond to an enzyme-hydrolyzable unit (EHU; colored in green) and to a tumor-targeting element (i.e. tumor homing peptide; colored in black). The alcohol group at the opposite site can be connected via a carbonate ester/carbamate bond to the cytotoxic agent (colored in blue). The EHU is designed so as to be a substrate for proteases overexpressed in the targeted tumor microenvironment (i.e cathepsin B). Once EHU will be recognized by these enzymes it is cleaved off resulting in the consequent release of the active drug through rapid cascade reactions (Figure 5).

The most representative examples of various types of linkers are summarized in Table 2.

Representative examples of PDCs targeting cancer cells

Integrating the basic design principles in PDCs pinpointed above, a list of representative developed examples is analyzed below, so as to provide a spherical perspective regarding peptide–drug conjugation chemistry.

Currently, there are two PDCs that have been developed utilizing peptides as tumor targeting elements that selectively bind to specific receptors and small molecules as anticancer agents that have reached phase III clinical trials (Table 3) for the treatment of various types of cancer. ClinicalTrials.gov have also announced the initiation of a clinical trial based on various PDCs consisted of two novel peptides selected after phage display that target murine A20 leukemic cells (ClinicalTrials.gov Identifier: NCT02828774). These clinical trials will focus on chronic lymphocytic leukemia (CLL).

Except these two PDCs, there are other types of PDCs that do not consist of peptides as targeting moieties and small molecules as drugs and have reached even up to phase III clinical trials. These PDCs are summarized in Table 4.

Notably, there is only one PDC in the market designated ^{111}In-DTPA-*d*-Phe^{1}-octreotide, which is utilized for diagnostic radiology in somatostatin receptor-positive tumors [118]. It constitutes a complex of ^{111}Indium bound to diethylenetriaminopentaacetic acid (DTPA), which is conjugated to the targeting somatostatin peptide [D-Phe^{1}]-octreotide. Recently, another similar analog, designated ^{111}In-DTPA-*d*-Phe^{-1}-Asp^{0}-*d*-Phe^{1}-octreotide, has been evaluated and presented enhanced tumor accumulation in pancreatic tumor cells and simultaneously lower renal radioactivity [119].

Herein, we will analyze in depth the two PDCs in clinical trials consisted of peptides and small molecules (Table 3), as also

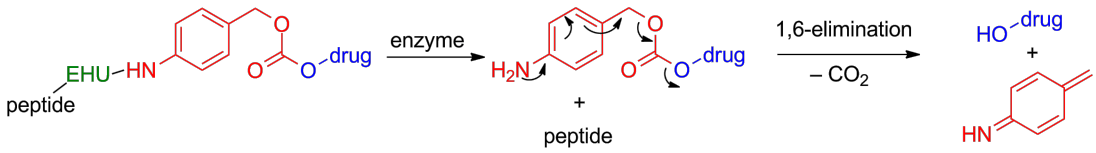

Figure 5: Illustration of the drug release mechanism from the self-immolative spacer PABC conjugated to a tumor homing peptide via an enzyme-hydrolyzable unit. Red color = the self-immolative spacer PABC; blue color = drug; green color = enzyme-hydrolyzable unit (EHU); black color the tumor-homing peptide.

Table 2: Representative examples of biodegradable/responsive linkers utilized for the formulation of PDCs in cancer.

linker	drug release mechanism	reference
succinyl	action of esterases/amidases	[19]
glutaryl	action of esterases/amidases	[67]
PABC	1,6-elimination	[109,110]
oxime bond	hydrolysis in acidic pH	[111]
peptide GFLG	action of cathepsin B	[105]
peptide PLGLAG	action of MMP-2/9	[107]

Table 3: Peptide–drug conjugates consisting of peptides and small molecules that have been used in clinical trials.

peptide	cytotoxic agent	linker	drug release mechanism	name	target	CCT[a]	reference
D-Lys^6-LHRH	Dox (SM)[b]	glutaryl	esterases/amidases	AEZS-108	LHRH-R	phase III	[112]
angiopep-2	PTX (SM)	succinyl	esterases/amidases	ANG1005	LRP-1	phase II	[79]

[a]CCT= current clinical trials; [b]SM= small molecule.

Table 4: Various other types of peptide–drug conjugates in clinical trials.

peptide	cytotoxic agent	linker	drug release mechanism	target	name	CCT[a]	reference
CNGRCG	hTNFα (Protein)	–	amidases	CD13 receptor	NGR015	phase III	[113]
polyglutamic acid	PTX (SM)[b]	–	esterases	–	CT2103	phase III	[114]
LHRH	CLIP71[c] (lytic peptide)	–	amidases	LHRH-R	EP-100	phase I	[115]
DRDDS (spacer)	DAVBLH[d] (SM)[b]	2-mercapto-ethanol	glutathione	folate receptor	EC145	phase III	[116]
D-γ-E-γ-E-γ-E-E (masking moiety)	12ADT[e]-Asp	–	PSMA	PSMA	G-202	phase II	[117]

[a]CCT = current clinical trials; [b]SM = small molecule; [c]CLIP71 = KFAKFAKKFAKFAKKFAK; [d]DAVBLH = desacetyl vinblastine hydrazide; [e]12ADT = 8-*O*-(12-aminododecanoyl)-8-*O*-debutanoyl thapsigargin.

various other similar PDC formulations existed in the current literature that have been evaluated in preclinical models.

First, two widely-known peptide–drug conjugates named AN-152 (AEZS-108) and AN-207 will be analyzed. These conjugates contain the luteinizing hormone-releasing hormone (LHRH) as the peptide-targeting module and doxorubicin (DOX) or its daunosamine-modified derivative 2-pyrrolino-DOX as the cytotoxic agent, respectively (Figure 6). Specifically, Andrew V. Schally and his group first synthesized the corresponding analogs [120] where they covalently coupled the two drugs to the epsilon-amino group of the D-Lys side chain of the peptide D-Lys^6-LHRH.

Notably, both conjugates fully preserved the cytotoxic activity of the parent drugs, DOX or 2-pyrrolino-DOX, respectively, in vitro and also retained the high binding affinity of their peptide carrier to receptors for LHRH on rat pituitary [120]. The two conjugates were subjected to stability tests and they showed slow drug release in human serum in contrast with nude mice that carboxylesterase enzymes are about 10 times higher [121]. Consequently, the two analogs were heavily evaluated in in

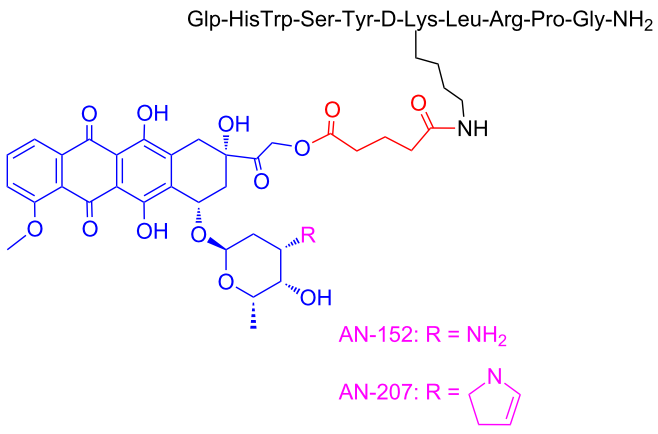

Figure 6: Structures of the PDCs named AN-152 and AN-207.

vivo models in nude mice bearing various types of cancer. Mice bearing OV-1063 (LHRH receptor positive) or UCI-107 (LHRH receptor negative) human epithelial ovarian cancers were treated with AN-152 or DOX with systematic intraperitoneal administration. The growth of UCI-107 cells was not inhibited by AN-152 but systemic administration of AN-152 in OV-1063 cells proved that AN-152 is less toxic but inhibits tumor growth better than equimolar doses of DOX [122]. These results were confirmed in nude mice bearing other ovarian human cancers (ES-2), where AN-207 caused up to 59.5% inhibition in tumor growth [123]. Also, AN-207 and AN-152 were tested in female BDF mice bearing estrogen independent MXT mouse mammary cancers, presenting stronger tumor inhibitory effects than their respective cytotoxic radicals up to 93%, while equimolar quantities of their respective radicals were more toxic [124]. Moreover, PDC AN-207 was significantly more potent, regarding the growth inhibition of hormone-dependent Dunning R-3327-H prostate cancers in rats, reaching up to 50% of the initial tumor volume in comparison with 2-pyrrolino-DOX. Shortly afterward, they tested the two conjugates in membranes of human breast cancer cells: MCF-7 hormone-dependent and MDA-MB-231 hormone- independent [125]. They proved that the specific analogs retained the high binding affinity of the D-Lys^6-LHRH carrier to the relevant receptors. Both conjugates displayed IC_{50} values in the low nanomolar concentration range for MCF-7 (13.7 ± 1.09 nM for AN-152 and 6.08 ± 0.5 nM for AN-207) and MDA-MB-231 (5.60 ± 1.24 nM for AN-152 and 1.89 ± 0.4 nM for AN-207) cells. AN-152 was tested regarding the inhibition of tumor growth of subcutaneously (sc) implanted androgen-dependent LNCaP and MDA-PCa-2b and androgen-independent C4-2 prostate cancers, xenografted into nude mice. The results demonstrated the stronger inhibition of AN-152 on the tumor with respect to the free DOX [126]. Similarly, in vivo experiments were conducted regarding AN-207 in nude mice bearing xenografts of MDA-PCa-2b prostate cancer cells, showing identical results like AN-152 [127]. Gründker et. al. evaluated the antitumor effects of AN-152 in vivo in human LHRH-R-positive HEC-1B endometrial and NIH:OVCAR-3 ovarian cancers, and in the LHRH-R-negative SK-OV-3 ovarian cancer cell line via intravenous injections [128]. The tumor volumes of HEC-1B and NIH:OVCAR-3 cancers were reduced significantly even after 1 week of treatment with AN-152 while presenting no toxic side effects. Treatment with DOX arrested tumor growth but did not reduce tumor volume. The growth of SK-OV-3 cancers was not affected by AN-152. Based on the presented results, it can be concluded that these two analogs possess higher antitumor activity but less toxicity with respect to the parent drugs DOX and 2-pyrrolino-DOX and can be used versus a wide variety of ovarian, prostate, endometrial and breast tumors.

Notably, after the extensive evaluation of analog AN-152 in preclinical models, starting from 2006 it has been tested in phase I and phase II studies (AN-152 was renamed to AEZS-108 for the clinical trials) of LHRH-R positive recurrent endometrial and ovarian cancers. The phase I/II study in castration-resistant prostate cancer (CRPC) and chemotherapy refractory bladder cancer also showed promising results. Due to the promising results from phase II trials in endometrial cancer, a multinational phase III clinical study is underway [112].

It is important to note that despite the fact that analog AN-207 presented a better biological profile, evident in all the preclinical models, its further development fell short due to chemical and plasma instability.

According to ClinicalTrials.gov, during phase I analog AEZS-108 was tested in 17 women with epithelial cancer of the ovary, endometrium or breast and for which standard treatment could not be used or was no longer effective. The results showed promising tolerance from the patients with fewer side effects than the commonly applied drugs. Moreover, AEZS-108 was evaluated in phase I clinical trial on patients with castration- and taxane-resistant prostate cancer and the results proved that AEZS-108 possesses a sufficient safety profile and efficacy. It succeeded in lowering the PSA levels in some patients with prostate cancer and it became evident that the internalization of AEZS-108 in prostate cancer circulating tumor cells (CTCs) may be a viable pharmacodynamic marker [129].

These promising results led to phase II clinical trials to patients with castration- and taxane-resistant prostate cancer and their disease showed progression after taxane-based chemotherapy. AEZS-108 showed significant activity in these patients who were pretreated with taxanes and maintained an acceptable safety profile [130].

Last, phase II clinical trials were conducted in collaboration with the German Gynecological Oncology Group (AGO) and 3 other centers from Bulgaria on 43 women. The patients had platinum-resistant advanced ovarian cancer, FIGO (Fédération Internationale de Gynécologie et d'Obstétrique) III or IV or recurrent endometrial cancer (EC) and LHRH receptor-positive tumor status. The treatment with AEZS-108 had significant activity and low toxicity in these women [131,132].

Based on the fact that the previously described analog AN-207 showed superior in vitro and in vivo results compared to AN-152 but lacked stability, Andrew V. Schally and his group turned their focus on its building block 2-pyrrolino-DOX and tried to construct new PDCs using other peptides. Therefore, they synthesized a new analog, designated AN-238, consisting

of the octapeptide RC-121 linked through the α-amino group of its N-terminal D-Phe moiety and a glutaric acid spacer to the 14-OH group of 2-pyrrolino-DOX (Figure 7). The octapeptide RC-121 was utilized due to its high binding affinity to the somatostatin receptor (SST-R) [133].

The anti-cancer activity was first evaluated in various rat/human cancer lines xenografted into nude mice with breast human tumors (MDA-MB-238, MCF-7, MX-1) and prostate rat/human tumors (Dunning AT-1, PC-3). All cell lines showed a great response to the treatment with AN-238 with high inhibition of the tumor, while 5 of 10 mice with MX-1 tumor were totally cured [61]. The cytotoxic profile of this analog was similarly evaluated in additional cancer cell lines xenografted into nude mice including prostate, renal, mammary, ovarian, gastric, colorectal and pancreatic [134]. Various types of renal, colorectal, pancreatic and gastric cancers showed a major response to the treatment with more than 70% inhibition while all the other types showed a good response to the treatment with an average of 60% inhibition. AN-238 was also evaluated in U87-MG brain cancer cells with good response, inducing 82% growth inhibition of subcutaneous tumors [134]. Therefore, AN-238 has been proved to be a promising candidate for a large number of tumors, being able to suppress the growth of these tumors and their metastases. Last, Engel et. al. showed that AN-238 inhibits tumor growth in human experimental endometrial carcinomas which express SST receptors, regardless of the expression levels of multidrug resistance protein MDR-1 [135]. The analog AN-238 is still pending for clinical trials.

An interesting example of a PDC able to cross the blood-brain barrier (BBB), is ANG1005 [136], composed of three molecules of paclitaxel linked by a cleavable succinyl ester linkage to the angiopep-2 peptide (Figure 8).

BBB is formed by the brain capillary endothelium with very low permeability as it excludes about 100% of the large molecules and about 98% of the small molecules attempting to pass to the brain [137]. Being mandatory to surpass the BBB in order to deliver pharmaceuticals to the brain, scientists have struggled to discover either novel small molecules able to cross it through various mechanisms [138] or novel techniques able to disrupt its dense structure like ultrasound-mediated drug delivery [139,140]. The design principles on the synthesis of the specific conjugate, ANG1005, were the following: the peptide angiopep-2 is able to cross the BBB via receptor-mediated transcytosis after binding to LRP-1 and consequently it is often used as drug delivery vehicle, while paclitaxel bears cytotoxicity against glioblastoma. It has been shown that the brain uptake of ANG1005 was 4.5-fold higher compared to paclitaxel and the cytotoxicity remained higher in all cancer cell lines tested (glioblastoma U87 MG, U118, U251; lung carcinoma A549, NCI-H460, Calu-3; ovarian carcinoma SK-OV-3). It has been also proved that human tumor xenografts were inhibited more with ANG1005 than paclitaxel. Finally, mice with intracerebral implantation of U87 MG glioblastoma cells or NCI-H460 lung carcinoma cells exhibited increased survival rates after ANG1005 administration.

Because of these promising results, ANG1005 progressed to phase I clinical trials in 2007 in 63 patients with recurrent or progressive malignant glioma. It was found that ANG1005 delivers paclitaxel across the BBB and achieves therapeutic concentrations in the tumor site. It became evident that this PDC possessed similar toxicity to paclitaxel as also enhanced activity in recurrent glioma [141]. Phase II clinical trials were then initiated on patients with recurrent high-grade glioma and on breast cancer patients with recurrent brain metastases. The results have not been published yet but it has already been stated that very promising results were collected and phase III clinical trials will start shortly. Based on the overall progress of ANG1005, other similar molecules have been synthesized and studied in preclinical models [142].

The group of Prof. G. Mező has achieved a great progression in the field of PDCs the last years working mostly on GnRH-III (Glp-His-Trp-Ser-His-Asp-Trp-Lys-Pro-Gly-NH_2), which was

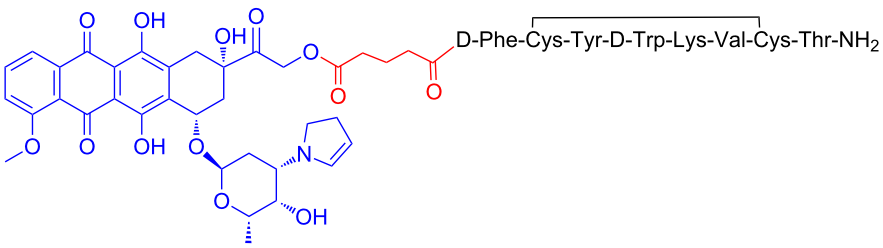

Figure 7: Structure of the PDC named AN-238.

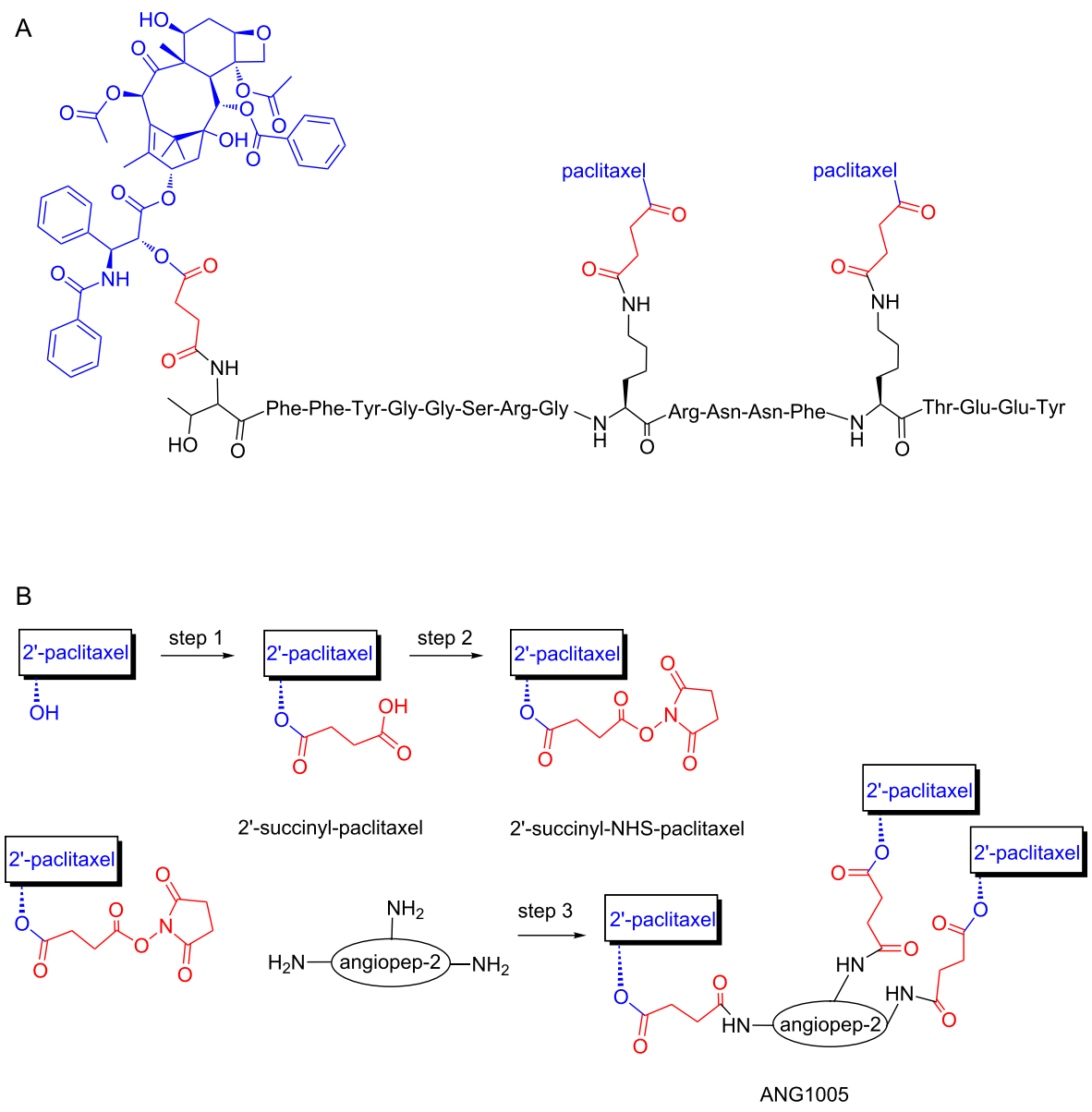

Figure 8: Chemical structure and synthetic scheme for the PDC ANG1005. (A) ANG1005 is composed of three molecules of paclitaxel linked by a cleavable succinyl ester linkage to the angiopep-2 peptide. (B) Schematic representation of ANG1005 synthesis steps. Paclitaxel was first reacted with succinic anhydride and then activated with *N*-hydroxysuccinimide to form 2′-succinyl-NHS-paclitaxel in two steps. In the conjugation step (step 3), amines of the angiopep-2 peptide react with 2′-succinyl-NHS-paclitaxel. The scheme was modified according to *Br. J. Pharmacol.* **2008,** *155,* 185–197 [136].

exploited as a tumor homing device for drug targeting 10 years ago [111]. The aim of this was to apply a peptide hormone with lower endocrine effect than GnRH-I that might be useful especially for hormone-independent tumors like colon cancer [143]. In addition, GnRH-III has Lys at position 8 of the sequence providing a conjugation site without inducing perturbation in the receptor recognition. In the first conjugates, daunorubicin (Dau) was attached to the lysine side chain via oxime linkage through an aminooxyacetyl (Aoa) moiety (Glp-His-Trp-Ser-His-Asp-Trp-Lys(Dau=Aoa)-Pro-Gly-NH_2). The oxime bond, developed between the aminooxyacetyl function and the carbonyl group of C-13 on Dau is stable under physiological conditions and prevents the early drug release in contrast to the ester bond (Figure 9).

Thus, no free drug release can be detected from such type of conjugates before reaching their targets. However, oxime bond is also stable in lysosomes where the conjugates decomposed after receptor-mediated endocytosis. Among the fragments arose during lysosomal degradation, H-Lys(Dau=Aoa)-OH was

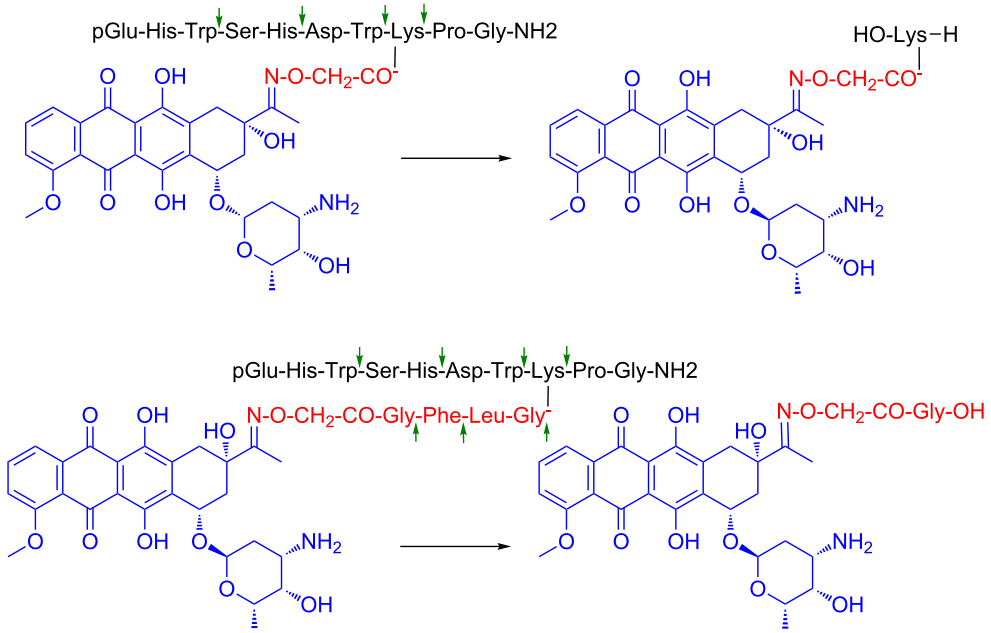

Figure 9: Structure of oxime linked Dau–GnRH-III conjugate with or without cathepsin B labile spacer and their metabolite released in lysosomal homogenate [144].

observed as the smallest Dau containing metabolite [144]. Therefore, the DNA binding propensity of this metabolite was also examined and it was found that although it is efficient it presented lower binding capacity with respect to the parent drug.

The in vitro antitumor activity of the above-mentioned conjugate was studied on MCF-7 human breast and HT-29 human colon adenocarcinoma cells [144]. The IC_{50} values showed two orders of magnitude lower effect compared to the free Dau. Thus, a systematic comparative study of various anthracycline-GnRH conjugates was conducted in order to conduct their complete evaluation as potential targeted cancer chemotherapeutics. The influence of different: (i) anthracycline drugs, (ii) linkers among the tumor-homing peptide moiety and the drug, and (iii) tumor-homing peptides (e.g., GnRH-III and D-Lys^6-GnRH-I) was examined regarding their in vitro cellular uptake, drug release and cytostatic effect [145]. Doxorubicin (Dox) was coupled to both GnRH-III and D-Lys^6-GnRH-I through a glutaric acid linker via ester bond. AN-152, the GnRH-I based PDC (see above), served as a control. No significant differences in cellular uptake and cytostatic effect were observed between the two PDCs. Recently, it was also indicated that the cellular uptake of carboxyfluorescein-labeled GnRH-I, GnRH-II and GnRH-III conjugates might be influenced not only by the targeting moiety, but also by the type of cancer cells [146]. However, no significant differences could be observed regarding the cellular uptake of the three GnRH conjugates by MCF-7 and HT-29 cells. It is worth mentioning that the highest water solubility was detected for the GnRH-III conjugate. The ester bond can be cleaved by esterases not only in cancer cells, but also in human plasma during blood circulation. The early drug release in the bloodstream may cause unwanted side effects. Furthermore, O–N acyl shift was detected both during the synthesis and the storage of ester-linked doxorubicin conjugate, resulting to an inactive compound where the tumor-homing peptide acylated the amine of the daunosamine sugar moiety. This was found through the mass spectrometric (MS) fragmentation profile of the PDC [146].

In a different PDC, Dau was linked to GnRH-III through a hydrazone bond or by incorporation of a self-immolative spacer [145]. The hydrazone linkage was formed similarly to the oxime bond on C-13 atom of Dau but it allows the effective drug release under slightly acidic conditions in lysosomes. The *p*-aminobenzylalcohol-based self-immolative spacer, combined with the dipeptide Lys-Phe (cathepsin-B lysosomal enzyme cleavable spacer), was connected to the amino functional group of daunosamine moiety. The last construct also provided the free drug release. Both conjugates illustrated similar cytostatic effects and cellular uptake as the conjugates with ester bonds. All these conjugates showed IC_{50} values in the range of

0.2–0.5 μM on MCF-7 cells while 1–3 μM on HT-29 cells. The free Dau or Dox had higher in vitro cytostatic effect than the conjugates, especially on HT-29 cells. Nevertheless, the synthesis of these conjugates was not so efficient and their chemical, biological and long-term shelf-stability of these PDCs were not so sufficient for drug development.

In another construct, daunorubicin and doxorubicin were attached to the ε-amino group of Lys of GnRH-III through oxime linkage [111,145]. The conjugation of the drug and the aminooxyacetylated tumor homing peptide was almost quantitative under slightly acidic conditions. Interestingly, the conjugate with Dox illustrated much lower antitumor effect than the Dau conjugate. The oxime-linked Dau-GnRH-III conjugate (non-cleavable linker) had one order of magnitude lower antitumor activity than the conjugates with the cleavable linkers. The cellular uptake of the oxime-linked conjugates was lower, too, but this effect might come from the different fluorescent properties of the free Dau and the peptide/metabolite-linked Dau. Because of the high synthetic yield and stability of oxime-linked conjugates, it can be suggested that such conjugates might be good candidates for the development of targeted tumor therapeutics. Therefore, efforts were made to develop further conjugates with higher antitumor activity.

To achieve higher antitumor activity, the sequence of the peptide GnRH-III was modified. Previous studies indicated that only a few changes are acceptable without significant loss of the anti-proliferative effect of the hormone peptide. Interestingly, Ser at position 4 could be replaced by Lys or acetylated Lys [147]. It is worth mentioning that the Ser in GnRH agonist and antagonist analogs are rarely modified [148]. The incorporation of Lys or Lys(Ac) in position 4 of GnRH-III increased the antitumor activity of the conjugate GnRH-III(Dau=Aoa). However, in the case of [^{4}Lys]-GnRH-III(Dau=Aoa) enzyme stability of the conjugate was decreased while [^{4}Lys(Ac)]-GnRH-III(Dau=Aoa) showed higher stability [149]. When the acetyl group was exchanged to other short-chain fatty acids (SCFAs) the enzyme stability was enhanced by the length of hydrocarbon chain of SCFAs [150]. According to the cellular uptake and cytostatic *in vitro* studies, the optimal compound was the butyric acid containing [^{4}Lys(Bu)]-GnRH-III(Dau=Aoa) conjugate that almost reached the in vitro biological effects of the conjugates with a cleavable linker. This conjugate showed significant tumor growth inhibition in vivo, not only on subcutaneous implanted but also on orthotopically developed HT-29 colon cancer-bearing mice [151]. The PDC in the applied dose (15 mg Dau content/kg body weight) showed similar or higher antitumor activity than the free Dau at a maximal tolerated dose (MTD) without significant toxic side effects on organs. In contrast to the conjugate, Dau presented toxicity on the liver causing worse condition and higher mortality during the treatment.

In addition, the incorporation of Lys at position 4 provided a new conjugation site. Therefore, Dau or methotrexate (MTX) were attached to the ε-amino group of ^{4}Lys resulting in conjugates with two identical ([^{4}Lys(Dau=Aoa), ^{8}Lys(Dau=Aoa)]-GnRH-III), or different drug molecules ([^{4}Lys(MTX), ^{8}Lys(Dau=Aoa)]-GnRH-III) [152,153]. Some improvement in the cytostatic effect could be detected compared with the conjugates containing only one drug molecule, but they were not better than the conjugate with butyric acid. This observation led to retain the Lys(Bu) at position 4 and the two Dau molecules were attached to the amino groups of an additional Lys through the enzyme labile GFLG spacer coupled to ^{8}Lys (Figure 10).

The resulted PDC presented a reduced aqueous solubility, thus an oligoethylene glycol linker was inserted between the spacer and the tumor-homing peptide [154]. This PDC showed the best in vitro cytostatic effects among the oxime-linked Dau-containing conjugates, but the improvement of the synthetic process to lead to higher amounts of this PDC is required to proceed for in vivo studies. Thus, it can be concluded that oxime linked Dau–homing peptide conjugates could be good candidates for targeted tumor therapy.

Furthermore, the tumor homing peptide D-Lys^6-GnRH-I has been exploited by our group to selectively deliver the anticancer agent gemcitabine to the tumor site. We, therefore, designed and synthesized four different bioconjugates consisting of D-Lys^6-GnRH-I and the anticancer agent gemcitabine (named GSG, GSG_2, 3G, $3G_2$) through different conjugation sites (the primary and secondary alcohol groups of gemcitabine) and using linkers of different lengths (succinyl and glutaryl) as shown in Figure 11.

In order to evaluate whether the tethering of the cytotoxic agent to the D-Lys^6-GnRH-I peptide induces any perturbation on the local microenvironment of the peptide that is responsible for receptor recognition, we utilized ^{1}H ^{1}H 2D-TOCSY NMR [19]. Upon superimposing the relevant spectra of the different PDCs on the relevant spectrum of the native hormone we found that these PDCs didn't alter the microenvironment of D-Lys^6-GnRH-I allowing to suggest that they will not influence the binding affinity of the targeting peptide unit of these PDC to the GnRH-R. This was further validated since the new conjugates were found to possess higher binding affinity with respect to the parent peptide, with IC50 ranging even up to 1.9 nM for the conjugate 3G. The conjugates were evaluated regarding their antiproliferative effect on prostate cancer cells (DU145 and

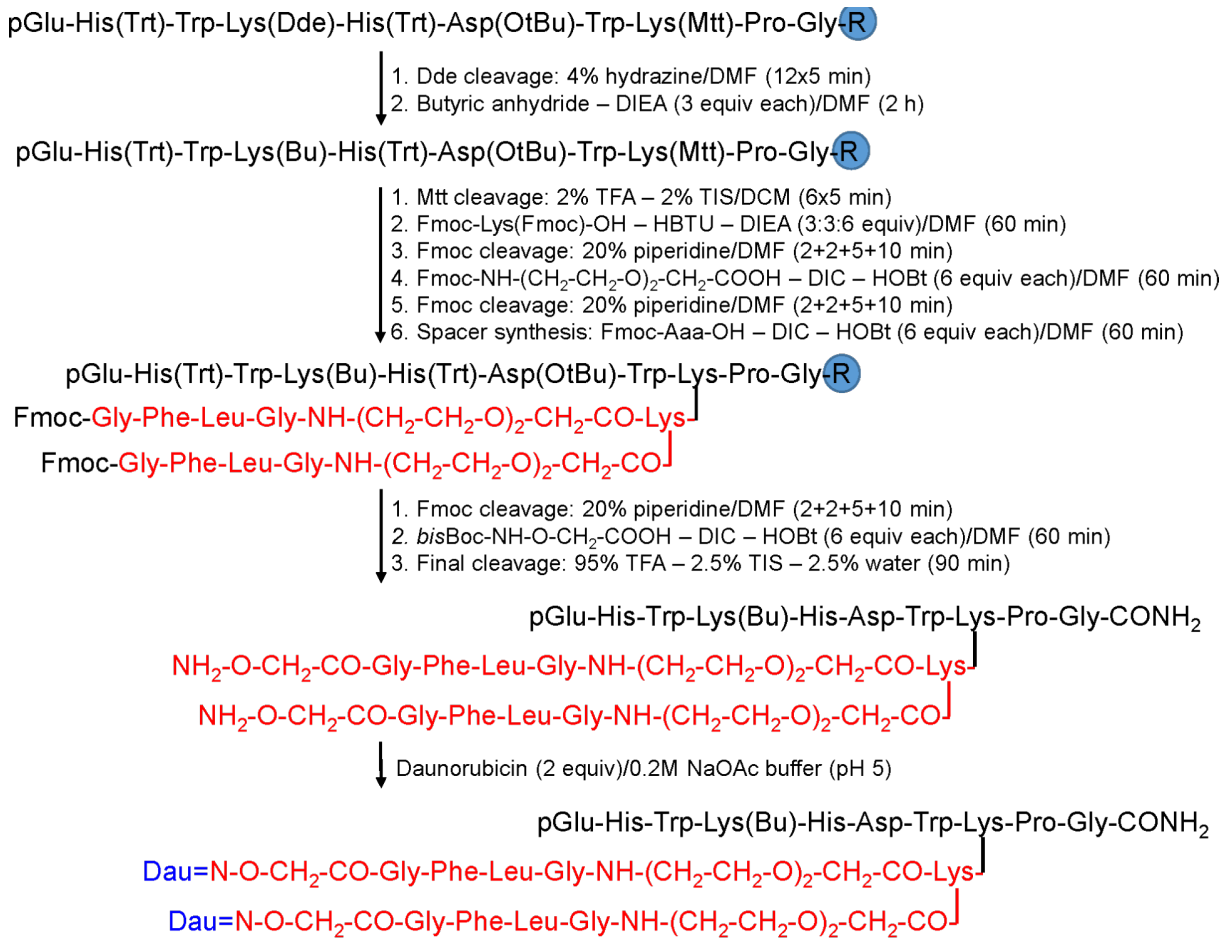

Figure 10: Synthesis of the most effective GnRH-III–Dau conjugate with two drug molecules [153].

PC-3) and the PDC GSG showed IC50 values similar to gemcitabine GSG that possessed the highest antiproliferative effect was utilized for further pharmacokinetic studies in mice. These pinpointed that GSG is able to release a high amount of gemcitabine (averaging 500 ng/mL) for a period of over ≈250 min, while administered free gemcitabine was consumed in less than 100 min. At the same time, the levels of the inactive metabolite of gemcitabine (dFdU) were maintained at very low levels for the GSG conjugate in contrast to the direct administration of free gemcitabine. Finally, when injected into mice with xenografted tumors, GSG inhibited the tumor growth more effectively than gemcitabine when using equimolar quantities. Therefore, GSG could pave the way for the construction of other similar bioconjugates in order to effectively enhance the concentration of the cytotoxic drug in the tumor cells and inhibit their uncontrolled growth.

OuWe have also designed and synthesized a PDC containing the cytotoxic agent sunitinib and the D-Lys^6-GnRH peptide-targeting-unit tethered through a succinyl linker [7]. Sunitinib is a small orally administrated drug that inhibits the phosphorylation of several receptor tyrosine kinases (RTKs). It was approved by the FDA in 2006 for the treatment of renal cell carcinoma (RCC) and imatinib-resistant gastrointestinal stromal tumor (GIST). Though, sunitinib has proved to cause severe side effects like cardiac and coronary microvascular dysfunction [155]. Therefore, these data rendered sunitinib as an appealing candidate for targeted therapy using a PDC.

Native sunitinib (Figure 12A) does lack functional groups that could be exploited for conjugation to the peptide-targeting unit, thus, a novel analog had to be constructed (SAN1, Figure 12B). This was constructed based on in silico studies and modifying properly the drug scaffold so as not to perturb the drug binding to the targeted receptors. In silico, in vitro and pharmacokinetic evaluation of the synthesized SAN1 were conducted and compared with native sunitinib. The results indicated that SAN1 exhibited similar properties and thus could serve as an alterna-

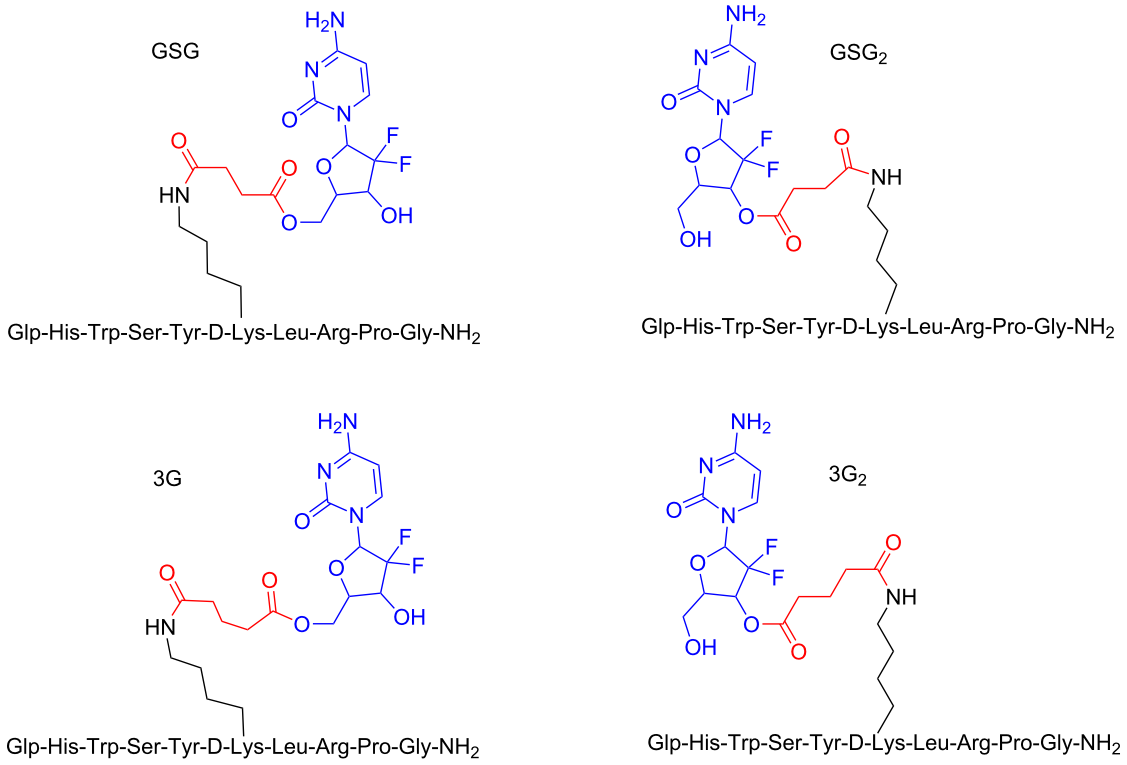

Figure 11: Structures of the four different PDCs of D-Lys^6-GnRH-I and gemcitabine (GSG, GSG_2, 3G, $3G_2$) [19].

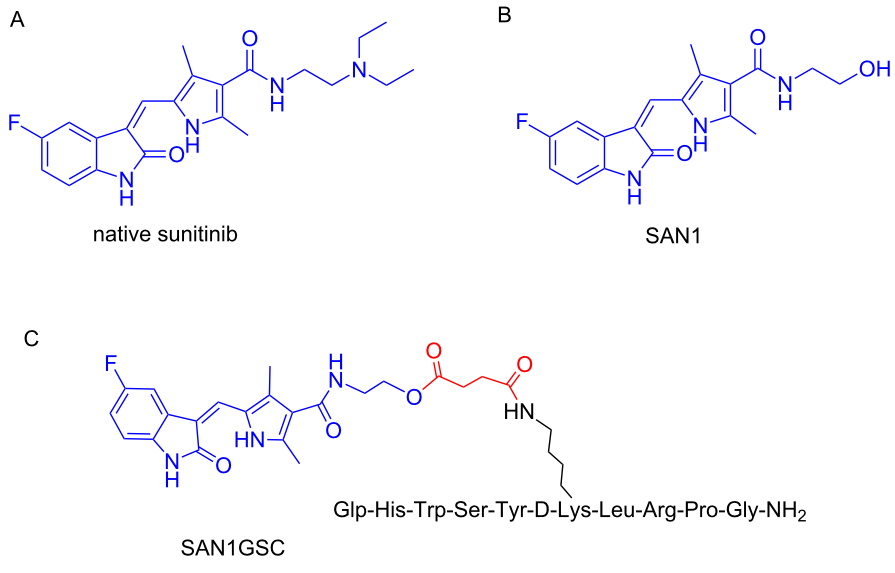

Figure 12: Structures of (A) native sunitinib; (B) SAN1 analog of sunitinib and (C) assembled PDC named SAN1GSC [18].

tive to the parent drug for the formulation of the final PDC. Additionally, SAN1 was further explored in in vivo models: mice xenografted with a castration-resistant CaP (CRPC) cell line were subjected to treatment based on SAN1 and sunitinib. Mice were dosed daily via intraperitoneal injection and the results unveiled the potency of SAN1, which showed to inhibit the

tumor growth in a similar way like native sunitinib. In the installed hydroxy group in the core of SAN1, a succinyl linker was conjugated that was then connected to the free amine group of Lys^8 of D-Lys^6-GnRH to form the PDC named SAN1GSC (Figure 12C).

SAN1GSC was evaluated in vitro and then in vivo, in mice xenografted with the CRPC model, showing similar bioactivity as SAN1. The most promising results arose from the measured concentration of SAN1 in the blood circulation and in the tumor site. The levels of free SAN1 released from SAN1GSC were 4 times higher inside the malignant cells with respect to SAN1 levels from the unconjugated SAN1. It is worth mentioning that in the frame of our construct, cardiotoxic and hematotoxic effects in treated mice were minimal and elevations of blood pressure that contribute to cardiac dysfunction were absent [18].

Problems and solutions during synthesis of PDCs

Although the synthesis of PDCs is usually a rapid and facile procedure, various synthetic problems may arise. The most common ones appear during peptide synthesis and might refer to low aqueous solubility and/or difficulty to synthesize. Insolubility issues can be overcome by altering the C-/N-terminus and/or substituting specific residues. Difficulties in the synthesis can be handled by decreasing the number of hydrophobic residues and/or shortening the sequence. Similar synthetic problems have been encountered during peptide synthesis the last decades and have been fully addressed.

During the conjugation of 5'-*O*-gemcitabine hemisuccinate to the D-Lys^6-GnRH peptide towards the synthesis of the PDC GSG (presented in Figure 10) we recently unveiled the formation of a previously unnoticed side product in addition to the desired product [156]. Specifically, we found that when guanidinium salts are utilized in peptide coupling conditions, a uronium derivative can be installed on specific amino acid scaffolds, beside to the formation of the expected amide bonds. This side product was persistent even after HPLC purification and was also apparent in the recorded mass spectrum of GSG as a second peak, besides the expected product, bearing the mass of the expected PDC plus 100 amu, leading to the reduction of the overall yield below 10%. Specifically, the guanidinium/uronium coupling reagent (HATU) was utilized for the formation of the amide bond between D-Lys^6 of the peptide carrier and the carboxylic acid of the succinate linker connected to gemcitabine to synthesize the PDC GSG (Figure 13). We hypothesized that the side product was originated from the coupling reagent (HATU) and after conducting template reactions with every amino acid present in the sequence of D-Lys^6-GnRH with Fmoc-Ser(*t*-Bu)-OH in the presence of HATU or HBTU and DIPEA, it became evident that the aminium moiety of HATU/HBTU could be installed either on the amino ($–NH_2$) group of Lys or on the phenol (–OH) group of Tyr [156].

Our findings were further verified by reacting other tumor-homing peptides like D-Lys^6-GnRH and Fmoc-HER2-BP1 (LTVSPWY, a heptapeptide known for its activity against erbB2) with HATU/DIPEA and characterizing the final products by ESIMS and ^{1}H NMR spectroscopy where the same aminium side product was also recorded. Interestingly, when the dipeptide Fmoc-Cys-Tyr-NH_2 was reacted with HATU, we found that the side product could be installed both on the phenol group of Tyr as also on the sulfhydryl group of Cys. Therefore, we tested these reaction conditions on the peptide $C1B5_{141–151}$ subdomain peptide (RCVRSVPSLCG) of protein kinase C (PKC) γ isozymes, which possess 2 cysteines (but no tyrosine or lysine or free N-terminus amine) and bears anticancer properties [157]. Again, a side product with two aminium moieties on the two cysteines was formed and characterized with ESIMS. This observation was also applied to a simple phenol where again a side product was recorded pinpointing the broad impact of our findings beyond traditional peptide chemistry. We thus revealed the formation of a previously unnoticed side product during the synthesis of PDCs, derived from guanidinium/uronium peptide coupling reagents that occurs on phenols, primary amines and sulfhydryl groups (Figure 14).

Along these lines, we suggested a mechanism that this side-product formation is taking place, directly after the formation of the amide bond that occurs from structure (II) to structure (III), as shown in Figure 15.

We discovered that the side product, which is difficult to be separated from the expected PDC and therefore results in reduced synthetic yield, could be avoided by using 1 equiv of HATU/HBTU, instead of the classical and established protocols using 1.5 equiv [156]. Taking into account that uronium/guanidinium coupling reagents are among the most expensive ones, using the specified conditions (equimolar quantity) may also reduce the total cost of the synthesis.

Conclusion

Currently used chemotherapeutics are in their majority highly toxic, causing severe side effects. Thus, with the aim to enhance their narrow therapeutic index, a wide variety of strategies have been explored. Selective drug delivery via special carriers represents a viable approach to deal with tumors with higher efficacy while using lower doses of the anticancer agent. Specifically, peptide–drug conjugates (PDCs) operate as potent drug delivery carriers and thus have attracted considerable attention over the last decades. The simplicity, versatility and

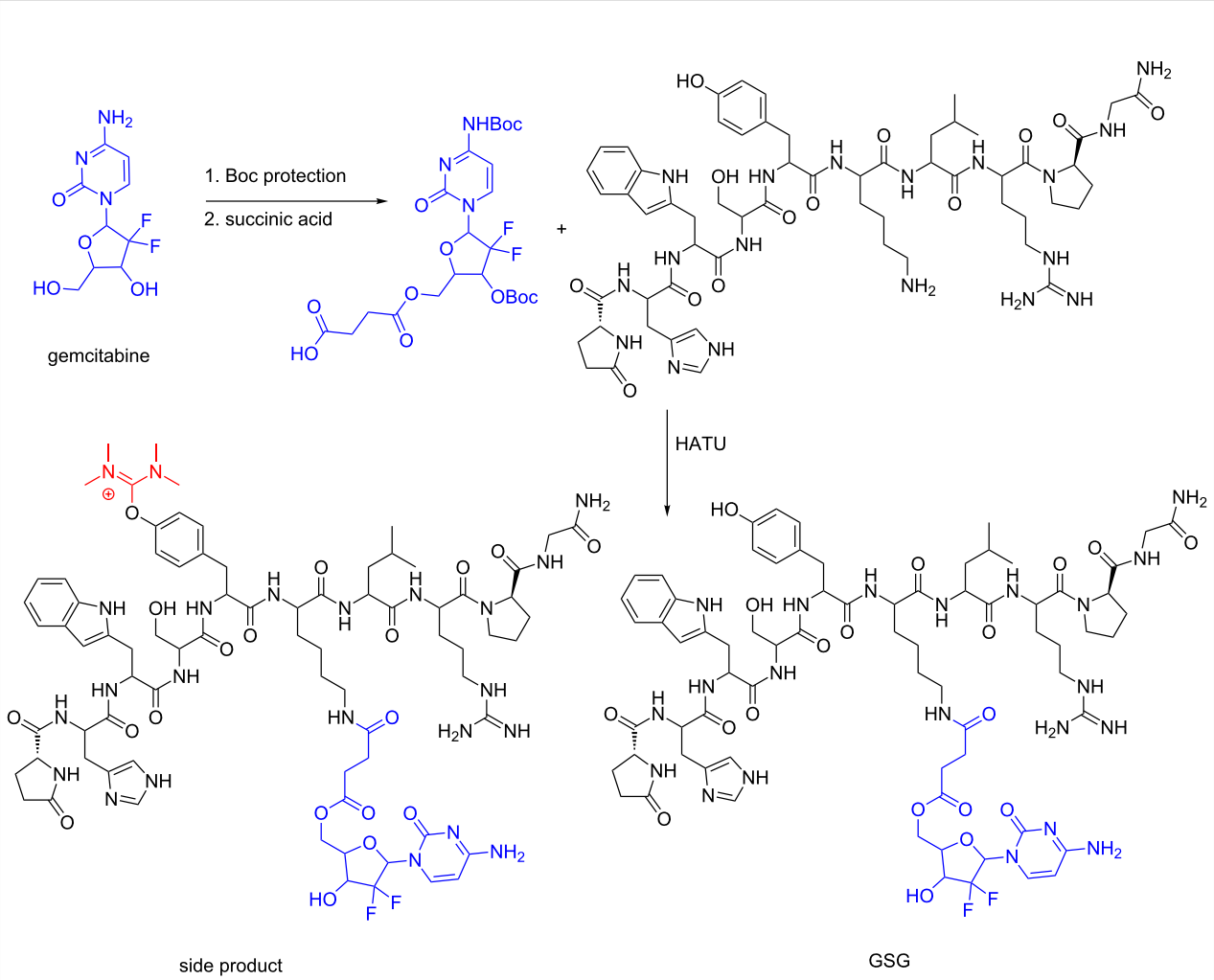

Figure 13: Synthetic scheme for the formation of GSG and the unexpected side product [156].

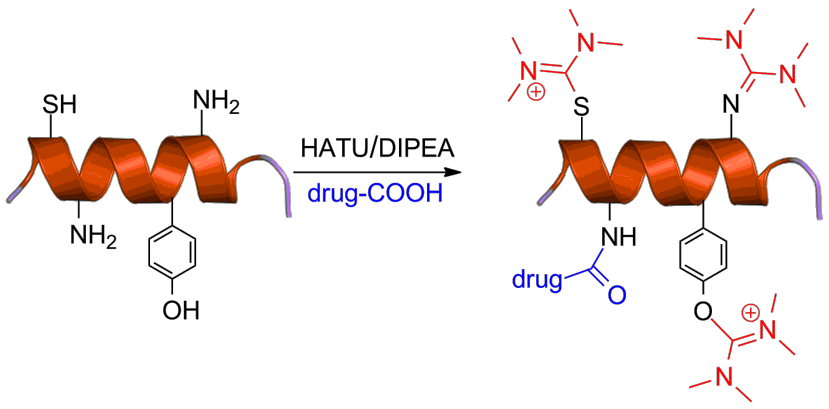

Figure 14: Illustration of uncharted guanidinium peptide coupling reagent side reactions during PDCs synthesis [156].

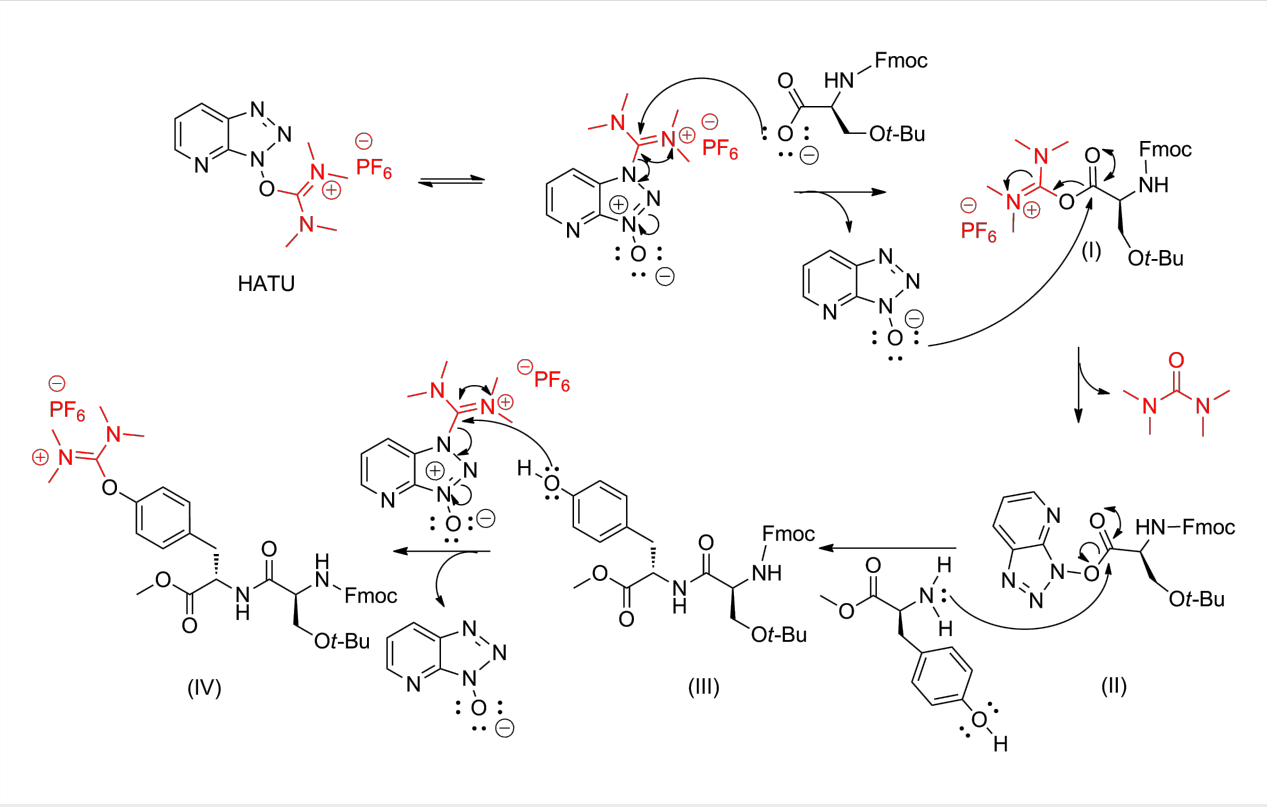

Figure 15: Putative mechanism for the formation of the uronium side product [156].

the relatively low cost for the construction of PDCs have rendered them appealing candidates. In the present review, basic and integral knowledge has been accumulated towards the PDCs design through examining every module required to assemble the fully decorated PDC: the peptide, the cytotoxic agent and the linker. We highlighted the overall progress of this field through selective analysis of noteworthy examples in the literature, as also possible synthetic problems that may arise and their solutions. Based on the fact that several PDCs have been selected for clinical trials and presented tumor inhibition with minimum side effects, this field needs to be further refined and explored. Through this review, we made efforts to provide an influential impetus for the construction of new peptide–drug conjugates, which could eventually transform undesired toxic drugs to highly potent formulations for the effective treatment of cancer.

Acknowledgements

This work was co-financed by the European Union (European Social Fund ESF) and Greek national funds through the Operational Program "Education and Lifelong Learning" of the National Strategic Reference Framework (NSRF) - Research Funding Program: ARISTEIA II [grant number: 5199]. The authors would also like to thank National Research, Development and Innovation Office (NKFIH K119552), Hungary.

ORCID® iDs

Eirinaios I. Vrettos - https://orcid.org/0000-0002-4801-1900
Gábor Mező - https://orcid.org/0000-0002-7618-7954

References

1. Organization, W. H.. *The global burden of disease,* 2004 update ed.; World Health Organization: Geneva, 2008.
2. Jemal, A.; Bray, F.; Center, M. M.; Ferlay, J.; Ward, E.; Forman, D. *Ca-Cancer J. Clin.* **2011,** *61,* 69–90. doi:10.3322/caac.20107
3. Yan, L.; Rosen, N.; Arteaga, C. *Chin. J. Cancer* **2011,** *30,* 1–4. doi:10.5732/cjc.010.10553
4. Mullard, A. *Nat. Rev. Drug Discovery* **2018,** *17,* 81–85. doi:10.1038/nrd.2018.4
5. Aggarwal, S. *Nat. Rev. Drug Discovery* **2010,** *9,* 427–428. doi:10.1038/nrd3186
6. Szakács, G.; Paterson, J. K.; Ludwig, J. A.; Booth-Genthe, C.; Gottesman, M. M. *Nat. Rev. Drug Discovery* **2006,** *5,* 219–234. doi:10.1038/nrd1984
7. Undevia, S. D.; Gomez-Abuin, G.; Ratain, M. J. *Nat. Rev. Cancer* **2005,** *5,* 447–458. doi:10.1038/nrc1629
8. de Sousa Cavalcante, L.; Monteiro, G. *Eur. J. Pharmacol.* **2014,** *741,* 8–16. doi:10.1016/j.ejphar.2014.07.041
9. Bocci, G.; Kerbel, R. S. *Nat. Rev. Clin. Oncol.* **2016,** *13,* 659–673. doi:10.1038/nrclinonc.2016.64
10. Ferlay, J.; Steliarova-Foucher, E.; Lortet-Tieulent, J.; Rosso, S.; Coebergh, J. W. W.; Comber, H.; Forman, D.; Bray, F. *Eur. J. Cancer* **2013,** *49,* 1374–1403. doi:10.1016/j.ejca.2012.12.027

11. Kola, I.; Landis, J. *Nat. Rev. Drug Discovery* **2004,** *3,* 711–716. doi:10.1038/nrd1470
12. Vander Heiden, M. G. *Nat. Rev. Drug Discovery* **2011,** *10,* 671–684. doi:10.1038/nrd3504
13. Galluzzi, L.; Kepp, O.; Vander Heiden, M. G.; Kroemer, G. *Nat. Rev. Drug Discovery* **2013,** *12,* 829–846. doi:10.1038/nrd4145
14. Bhat, M.; Robichaud, N.; Hulea, L.; Sonenberg, N.; Pelletier, J.; Topisirovic, I. *Nat. Rev. Drug Discovery* **2015,** *14,* 261–278. doi:10.1038/nrd4505
15. Pfister, S. X.; Ashworth, A. *Nat. Rev. Drug Discovery* **2017,** *16,* 241–263. doi:10.1038/nrd.2016.256
16. Tai, W.; Mahato, R.; Cheng, K. *J. Controlled Release* **2010,** *146,* 264–275. doi:10.1016/j.jconrel.2010.04.009
17. Zwicke, G. L.; Mansoori, G. A.; Jeffery, C. J. *Nano Rev.* **2012,** *3,* No. 18496. doi:10.3402/nano.v3i0.18496
18. Argyros, O.; Karampelas, T.; Asvos, X.; Varela, A.; Sayyad, N.; Papakyriakou, A.; Davos, C. H.; Tzakos, A. G.; Fokas, D.; Tamvakopoulos, C. *Cancer Res.* **2016,** *76,* 1181–1192. doi:10.1158/0008-5472.CAN-15-2138
19. Karampelas, T.; Argyros, O.; Sayyad, N.; Spyridaki, K.; Pappas, C.; Morgan, K.; Kolios, G.; Millar, R. P.; Liapakis, G.; Tzakos, A. G.; Fokas, D.; Tamvakopoulos, C. *Bioconjugate Chem.* **2014,** *25,* 813–823. doi:10.1021/bc500081g
20. Kellici, T. F.; Chatziathanasiadou, M. V.; Lee, M.-S.; Sayyad, N.; Geromichalou, E. G.; Vrettos, E. I.; Tsiailanis, A. D.; Chi, S.-W.; Geromichalos, G. D.; Mavromoustakos, T.; Tzakos, A. G. *Org. Biomol. Chem.* **2017,** *15,* 7956–7976. doi:10.1039/C7OB02045G
21. DeBerardinis, R. J.; Chandel, N. S. *Sci. Adv.* **2016,** *2,* e1600200. doi:10.1126/sciadv.1600200
22. Trachootham, D.; Alexandre, J.; Huang, P. *Nat. Rev. Drug Discovery* **2009,** *8,* 579–591. doi:10.1038/nrd2803
23. Kato, Y.; Ozawa, S.; Miyamoto, C.; Maehata, Y.; Suzuki, A.; Maeda, T.; Baba, Y. *Cancer Cell Int.* **2013,** *13,* 89. doi:10.1186/1475-2867-13-89
24. Singh, R.; Lillard, J. W., Jr. *Exp. Mol. Pathol.* **2009,** *86,* 215–223. doi:10.1016/j.yexmp.2008.12.004
25. Karakurt, S.; Kellici, T. F.; Mavromoustakos, T.; Tzakos, A. G.; Yilmaz, M. *Curr. Org. Chem.* **2016,** *20,* 1043–1057. doi:10.2174/1385272820666151211192249
26. Kellici, T. F.; Chatziathanasiadou, M. V.; Diamantis, D.; Chatzikonstantinou, A. V.; Andreadelis, I.; Christodoulou, E.; Valsami, G.; Mavromoustakos, T.; Tzakos, A. G. *Int. J. Pharm.* **2016,** *511,* 303–311. doi:10.1016/j.ijpharm.2016.07.008
27. Tsume, Y.; Incecayir, T.; Song, X.; Hilfinger, J. M.; Amidon, G. L. *Eur. J. Pharm. Biopharm.* **2014,** *86,* 514–523. doi:10.1016/j.ejpb.2013.12.009
28. Apostolopoulos, V.; Pietersz, G. A.; Tsibanis, A.; Tsikkinis, A.; Drakaki, H.; Loveland, B. E.; Piddlesden, S. J.; Plebanski, M.; Pouniotis, D. S.; Alexis, M. N.; McKenzie, I. F.; Vassilaros, S. *Breast Cancer Res.* **2006,** *8,* R27. doi:10.1186/bcr1505
29. Tang, C. K.; Lodding, J.; Minigo, G.; Pouniotis, D. S.; Plebanski, M.; Scholzen, A.; McKenzie, I. F. C.; Pietersz, G. A.; Apostolopoulos, V. *Immunology* **2007,** *120,* 325–335. doi:10.1111/j.1365-2567.2006.02506.x
30. Apostolopoulos, V.; McKenzie, I. F.; Pietersz, G. A. *Immunol. Cell Biol.* **1996,** *74,* 457–464. doi:10.1038/icb.1996.76
31. Tzakos, A. G.; Briasoulis, E.; Thalhammer, T.; Jager, W.; Apostolopoulos, V. *J. Drug Delivery* **2013,** No. 918304. doi:10.1155/2013/918304
32. Kapoor, P.; Singh, H.; Gautam, A.; Chaudhary, K.; Kumar, R.; Raghava, G. P. S. *PLoS One* **2012,** *7,* e35187. doi:10.1371/journal.pone.0035187
33. Carson-Jurica, M. A.; Schrader, W. T.; O'Malley, B. W. *Endocr. Rev.* **1990,** *11,* 201–220. doi:10.1210/edrv-11-2-201
34. Su, H.; Koo, J. M.; Cui, H. *J. Controlled Release* **2015,** *219,* 383–395. doi:10.1016/j.jconrel.2015.09.056
35. Apostolopoulos, V.; Deraos, G.; Matsoukas, M.-T.; Day, S.; Stojanovska, L.; Tselios, T.; Androutsou, M.-E.; Matsoukas, J. *Bioorg. Med. Chem.* **2017,** *25,* 528–538. doi:10.1016/j.bmc.2016.11.029
36. Lourbopoulos, A.; Deraos, G.; Matsoukas, M.-T.; Touloumi, O.; Giannakopoulou, A.; Kalbacher, H.; Grigoriadis, N.; Apostolopoulos, V.; Matsoukas, J. *Bioorg. Med. Chem.* **2017,** *25,* 4163–4174. doi:10.1016/j.bmc.2017.06.005
37. Hou, J.; Diao, Y.; Li, W.; Yang, Z.; Zhang, L.; Chen, Z.; Wu, Y. *Int. J. Pharm.* **2016,** *505,* 329–340. doi:10.1016/j.ijpharm.2016.04.017
38. Fung, S.; Hruby, V. J. *Curr. Opin. Chem. Biol.* **2005,** *9,* 352–358. doi:10.1016/j.cbpa.2005.06.010
39. Johnson, M.; Liu, M.; Struble, E.; Hettiarachchi, K. *J. Pharm. Biomed. Anal.* **2015,** *109,* 112–120. doi:10.1016/j.jpba.2015.01.009
40. Pierschbacher, M. D.; Ruoslahti, E. *Nature* **1984,** *309,* 30–33. doi:10.1038/309030a0
41. Kapp, T. G.; Rechenmacher, F.; Neubauer, S.; Maltsev, O. V.; Cavalcanti-Adam, E. A.; Zarka, R.; Reuning, U.; Notni, J.; Wester, H.-J.; Mas-Moruno, C.; Spatz, J.; Geiger, B.; Kessler, H. *Sci. Rep.* **2017,** *7,* No. 39805. doi:10.1038/srep39805
42. Schwartz, M. A.; Schaller, M. D.; Ginsberg, M. H. *Annu. Rev. Cell Dev. Biol.* **1995,** *11,* 549–599. doi:10.1146/annurev.cb.11.110195.003001
43. Plow, E. F.; Haas, T. A.; Zhang, L.; Loftus, J.; Smith, J. W. *J. Biol. Chem.* **2000,** *275,* 21785–21788. doi:10.1074/jbc.R000003200
44. Gilad, Y.; Firer, M.; Gellerman, G. *Biomedicines* **2016,** *4,* No. 11. doi:10.3390/biomedicines4020011
45. Cox, D.; Brennan, M.; Moran, N. *Nat. Rev. Drug Discovery* **2010,** *9,* 804–820. doi:10.1038/nrd3266
46. Chen, K.; Chen, X. *Theranostics* **2011,** *1,* 189–200. doi:10.7150/thno/v01p0189
47. Kumar, C. C. *Curr. Drug Targets* **2003,** *4,* 123–131. doi:10.2174/1389450033346830
48. Ganguly, K. K.; Pal, S.; Moulik, S.; Chatterjee, A. *Cell Adhes. Migr.* **2013,** *7,* 251–261. doi:10.4161/cam.23840
49. Liu, Z.; Wang, F.; Chen, X. *Drug Dev. Res.* **2008,** *69,* 329–339. doi:10.1002/ddr.20265
50. Cai, W.; Chen, X. *Anti-Cancer Agents Med. Chem.* **2006,** *6,* 407–428. doi:10.2174/187152006778226530
51. Burkhart, D. J.; Kalet, B. T.; Coleman, M. P.; Post, G. C.; Koch, T. H. *Mol. Cancer Ther.* **2004,** *3,* 1593–1604.
52. Gilad, Y.; Noy, E.; Senderowitz, H.; Albeck, A.; Firer, M. A.; Gellerman, G. *Pept. Sci.* **2016,** *106,* 160–171. doi:10.1002/bip.22800
53. Baba, Y.; Matsuo, H.; Schally, A. V. *Biochem. Biophys. Res. Commun.* **1971,** *44,* 459–463. doi:10.1016/0006-291X(71)90623-1
54. Marelli, M. M.; Moretti, R. M.; Januszkiewicz-Caulier, J.; Motta, M.; Limonta, P. *Curr. Cancer Drug Targets* **2006,** *6,* 257–269. doi:10.2174/156800906776842966
55. Limonta, P.; Marelli, M. M.; Mai, S.; Motta, M.; Martini, L.; Moretti, R. M. *Endocr. Rev.* **2012,** *33,* 784–811. doi:10.1210/er.2012-1014

56. Chen, A.; Kaganovsky, E.; Rahimipour, S.; Ben-Aroya, N.; Okon, E.; Koch, Y. *Cancer Res.* **2002,** *62,* 1036–1044.
57. Cheung, L. W. T.; Yung, S.; Chan, T.-M.; Leung, P. C. K.; Wong, A. S. T. *Mol. Ther.* **2013,** *21,* 78–90. doi:10.1038/mt.2012.187
58. Padula, A. M. *Anim. Reprod. Sci.* **2005,** *88,* 115–126. doi:10.1016/j.anireprosci.2005.05.005
59. Zhu, S.; Wang, Q.; Jiang, J.; Luo, Y.; Sun, Z. *Sci. Rep.* **2016,** *6,* No. 33894. doi:10.1038/srep33894
60. Dharap, S. S.; Wang, Y.; Chandna, P.; Khandare, J. J.; Qiu, B.; Gunaseelan, S.; Sinko, P. J.; Stein, S.; Farmanfarmaian, A.; Minko, T. *Proc. Natl. Acad. Sci. U. S. A.* **2005,** *102,* 12962–12967. doi:10.1073/pnas.0504274102
61. Schally, A. V.; Nagy, A. *Eur. J. Endocrinol.* **1999,** *141,* 1–14. doi:10.1530/eje.0.1410001
62. Laimou, D.; Katsila, T.; Matsoukas, J.; Schally, A.; Gkountelias, K.; Liapakis, G.; Tamvakopoulos, C.; Tselios, T. *Eur. J. Med. Chem.* **2012,** *58,* 237–247. doi:10.1016/j.ejmech.2012.09.043
63. Katsila, T.; Balafas, E.; Liapakis, G.; Limonta, P.; Marelli, M. M.; Gkountelias, K.; Tselios, T.; Kostomitsopoulos, N.; Matsoukas, J.; Tamvakopoulos, C. *J. Pharmacol. Exp. Ther.* **2011,** *336,* 613–623. doi:10.1124/jpet.110.174375
64. Martinez, V. Chapter 180 - Somatostatin A2. In *Handbook of Biologically Active Peptides,* 2nd ed.; Kastin Abba, J., Ed.; Academic Press: Boston, 2013; pp 1320–1329. doi:10.1016/B978-0-12-385095-9.00180-9
65. Keskin, O.; Yalcin, S. *OncoTargets Ther.* **2013,** *6,* 471–483. doi:10.2147/OTT.S39987
66. Lahlou, H.; Guillermet, J.; Hortala, M.; Vernejoul, F.; Pyronnet, S.; Bousquet, C.; Susini, C. *Ann. N. Y. Acad. Sci.* **2004,** *1014,* 121–131. doi:10.1196/annals.1294.012
67. Sun, L.-C.; Coy, D. H. *Curr. Drug Delivery* **2011,** *8,* 2–10. doi:10.2174/156720111793663633
68. Modlin, I. M.; Pavel, M.; Kidd, M.; Gustafsson, B. I. *Aliment. Pharmacol. Ther.* **2010,** *31,* 169–188. doi:10.1111/j.1365-2036.2009.04174.x
69. Lelle, M.; Kaloyanova, S.; Freidel, C.; Theodoropoulou, M.; Musheev, M.; Niehrs, C.; Stalla, G.; Peneva, K. *Mol. Pharmaceutics* **2015,** *12,* 4290–4300. doi:10.1021/acs.molpharmaceut.5b00487
70. Sun, L.-C.; Mackey, L. V.; Luo, J.; Fuselier, J. A.; Coy, D. H. *Clin. Med.: Oncol.* **2008,** *2,* 491–499. doi:10.4137/CMO.S970
71. Fuselier, J. A.; Sun, L.; Woltering, S. N.; Murphy, W. A.; Vasilevich, N.; Coy, D. H. *Bioorg. Med. Chem. Lett.* **2003,** *13,* 799–803. doi:10.1016/S0960-894X(03)00016-7
72. Grandal, M. V.; Madshus, I. H. *J. Cell. Mol. Med.* **2008,** *12,* 1527–1534. doi:10.1111/j.1582-4934.2008.00298.x
73. Li, Z.; Zhao, R.; Wu, X.; Sun, Y.; Yao, M.; Li, J.; Xu, Y.; Gu, J. *FASEB J.* **2005,** *19,* 1978–1985. doi:10.1096/fj.05-4058com
74. Ai, S.; Jia, T.; Ai, W.; Duan, J.; Liu, Y.; Chen, J.; Liu, X.; Yang, F.; Tian, Y.; Huang, Z. *Br. J. Pharmacol.* **2013,** *168,* 1719–1735. doi:10.1111/bph.12055
75. Orbán, E.; Manea, M.; Marquadt, A.; Bánóczi, Z.; Csık, G.; Fellinger, E.; Bősze, S.; Hudecz, F. *Bioconjugate Chem.* **2011,** *22,* 2154–2165. doi:10.1021/bc2004236
76. Wang, X.-F.; Birringer, M.; Dong, L. F.; Veprek, P.; Low, P.; Swettenham, E.; Stantic, M.; Yuan, L.-H.; Zobalova, R.; Wu, K.; Ledvina, M.; Ralph, S. J.; Neuzil, J. *Cancer Res.* **2007,** *67,* 3337–3344. doi:10.1158/0008-5472.CAN-06-2480
77. Bertrand, Y.; Currie, J.-C.; Demeule, M.; Régina, A.; Ché, C.; Abulrob, A.; Fatehi, D.; Sartelet, H.; Gabathuler, R.; Castaigne, J.-P.; Stanimirovic, D.; Béliveau, R. *J. Cell. Mol. Med.* **2010,** *14,* 2827–2839. doi:10.1111/j.1582-4934.2009.00930.x
78. Li, Y.; Zheng, X.; Gong, M.; Zhang, J. *Oncotarget* **2016,** *7,* 79401–79407. doi:10.18632/oncotarget.12708
79. Li, F.; Tang, S.-C. *Genes Dis.* **2017,** *4,* 1–3. doi:10.1016/j.gendis.2017.01.004
80. Teesalu, T.; Sugahara, K. N.; Ruoslahti, E. *Front. Oncol.* **2013,** *3,* 216. doi:10.3389/fonc.2013.00216
81. Sugahara, K. N.; Teesalu, T.; Karmali, P. P.; Kotamraju, V. R.; Agemy, L.; Girard, O. M.; Hanahan, D.; Mattrey, R. F.; Ruoslahti, E. *Cancer Cell* **2009,** *16,* 510–520. doi:10.1016/j.ccr.2009.10.013
82. Aubel-Sadron, G.; Londos-Gagliardi, D. *Biochimie* **1984,** *66,* 333–352. doi:10.1016/0300-9084(84)90018-X
83. Plunkett, W.; Huang, P.; Xu, Y. Z.; Heinemann, V.; Grunewald, R.; Gandhi, V. *Semin. Oncol.* **1995,** *22* (4, Suppl. 11), 3–10.
84. Liu, L. F.; Desai, S. D.; Li, T.-K.; Mao, Y.; Sun, M.; Sim, S.-P. *Ann. N. Y. Acad. Sci.* **2000,** *922,* 1–10. doi:10.1111/j.1749-6632.2000.tb07020.x
85. Barbuti, A.; Chen, Z.-S. *Cancers* **2015,** *7,* 0897.
86. Li, H.; Aneja, R.; Chaiken, I. *Molecules* **2013,** *18,* 9797–9817. doi:10.3390/molecules18089797
87. Füreder, L. M.; Berghoff, A. S.; Gatterbauer, B.; Dieckmann, K.; Widhalm, G.; Hainfellner, J. A.; Birner, P.; Bartsch, R.; Zielinski, C. C.; Preusser, M. *Neuro-Oncology* **2016,** *18* (Suppl. 4), iv16–iv17. doi:10.1093/neuonc/now188.054
88. Chitkara, D.; Mittal, A.; Behrman, S. W.; Kumar, N.; Mahato, R. I. *Bioconjugate Chem.* **2013,** *24,* 1161–1173. doi:10.1021/bc400032x
89. Garcia-Manteiga, J.; Molina-Arcas, M.; Casado, F. J.; Mazo, A.; Pastor-Anglada, M. *Clin. Cancer Res.* **2003,** *9,* 5000–5008.
90. Santini, D.; Schiavon, G.; Vincenzi, B.; Cass, C. E.; Vasile, E.; Manazza, A. D.; Catalano, V.; Baldi, G. G.; Lai, R.; Rizzo, S.; Giacobino, A.; Chiusa, L.; Caraglia, M.; Russo, A.; Mackey, J.; Falcone, A.; Tonini, G. *Curr. Cancer Drug Targets* **2011,** *11,* 123–129. doi:10.2174/156800911793743600
91. Huang, P.; Chubb, S.; Hertel, L. W.; Grindey, G. B.; Plunkett, W. *Cancer Res.* **1991,** *51,* 6110–6117.
92. Vargas, J. R.; Stanzl, E. G.; Teng, N. N. H.; Wender, P. A. *Mol. Pharmaceutics* **2014,** *11,* 2553–2565. doi:10.1021/mp500161z
93. Xiao, H.; Verdier-Pinard, P.; Fernandez-Fuentes, N.; Burd, B.; Angeletti, R.; Fiser, A.; Horwitz, S. B.; Orr, G. A. *Proc. Natl. Acad. Sci. U. S. A.* **2006,** *103,* 10166–10173. doi:10.1073/pnas.0603704103
94. Burkhart, C. A.; Berman, J. W.; Swindell, C. S.; Horwitz, S. B. *Cancer Res.* **1994,** *54,* 5779–5782.
95. Murphy, T.; Yee, K. W. L. *Expert Opin. Pharmacother.* **2017,** *18,* 1765–1780. doi:10.1080/14656566.2017.1391216
96. Wall, M. E.; Wani, M. C. *J. Ethnopharmacol.* **1996,** *51,* 239–254. doi:10.1016/0378-8741(95)01367-9
97. Wall, M. E.; Wani, M. C.; Cook, C. E.; Palmer, K. H.; McPhail, A. T.; Sim, G. A. *J. Am. Chem. Soc.* **1966,** *88,* 3888–3890. doi:10.1021/ja00968a057
98. Znojek, P.; Willmore, E.; Curtin, N. J. *Br. J. Cancer* **2014,** *111,* 1319–1326. doi:10.1038/bjc.2014.378
99. Dharap, S. S.; Qiu, B.; Williams, G. C.; Sinko, P.; Stein, S.; Minko, T. *J. Controlled Release* **2003,** *91,* 61–73. doi:10.1016/S0168-3659(03)00209-8
100. Sun, L.; Fuselier, J. A.; Coy, D. H. *Drug Delivery* **2004,** *11,* 231–238. doi:10.1080/10717540490446125

101. Lee, M. H.; Kim, J. Y.; Han, J. H.; Bhuniya, S.; Sessler, J. L.; Kang, C.; Kim, J. S. *J. Am. Chem. Soc.* **2012,** *134,* 12668–12674. doi:10.1021/ja303998y
102. Gondi, C. S.; Rao, J. S. *Expert Opin. Ther. Targets* **2013,** *17,* 281–291. doi:10.1517/14728222.2013.740461
103. Chang, M.; Zhang, F.; Wei, T.; Zuo, T.; Guan, Y.; Lin, G.; Shao, W. *J. Drug Targeting* **2016,** *24,* 475–491. doi:10.3109/1061186X.2015.1108324
104. Szlachcic, A.; Zakrzewska, M.; Lobocki, M.; Jakimowicz, P.; Otlewski, J. *Drug Des., Dev. Ther.* **2016,** *10,* 2547–2560. doi:10.2147/DDDT.S105896
105. Naqvi, S. A. R.; Matzow, T.; Finucane, C.; Nagra, S. A.; Ishfaq, M. M.; Mather, S. J.; Sosabowski, J. *Cancer Biother. Radiopharm.* **2010,** *25,* 89–95. doi:10.1089/cbr.2009.0666
106. Zhu, L.; Wang, T.; Perche, F.; Taigind, A.; Torchilin, V. P. *Proc. Natl. Acad. Sci. U. S. A.* **2013,** *110,* 17047–17052. doi:10.1073/pnas.1304987110
107. van Duijnhoven, S. M. J.; Robillard, M. S.; Nicolay, K.; Grüll, H. *J. Nucl. Med.* **2011,** *52,* 279–286. doi:10.2967/jnumed.110.082503
108. Zhang, X.; Wang, X.; Zhong, W.; Ren, X.; Sha, X.; Fang, X. *Int. J. Nanomed.* **2016,** *11,* 1643–1661. doi:10.2147/IJN.S101030
109. Zhang, X.; Li, X.; You, Q.; Zhang, X. *Eur. J. Med. Chem.* **2017,** *139,* 542–563. doi:10.1016/j.ejmech.2017.08.010
110. Vhora, I.; Patil, S.; Bhatt, P.; Misra, A. Chapter One - Protein– and Peptide–Drug Conjugates: An Emerging Drug Delivery Technology. In *Advances in Protein Chemistry and Structural Biology,;* Donev, R., Ed.; Academic Press, 2015; Vol. 98, pp 1–55.
111. Szabó, I.; Manea, M.; Orbán, E.; Csámpai, A.; Bősze, S.; Szabó, R.; Tejeda, M.; Gaál, D.; Kapuvári, B.; Przybylski, M.; Hudecz, F.; Mező, G. *Bioconjugate Chem.* **2009,** *20,* 656–665. doi:10.1021/bc800542u
112. Engel, J. B.; Tinneberg, H.-R.; Rick, F. G.; Berkes, E.; Schally, A. V. *Curr. Drug Targets* **2016,** *17,* 488–494. doi:10.2174/1389450117051603030154717
113. Gaafar, R. M.; Favaretto, A. G.; Gregorc, V.; Grossi, F.; Jassem, J.; Polychronis, A.; Bidoli, P.; Tiseo, M.; O'Brien, M. E. R.; Shah, R.; Taylor, P.; Novello, S.; Muzio, A.; Bearz, A.; Badurak, P.; Greillier, L.; Lambiase, A.; Bordignon, C. *J. Clin. Oncol.* **2015,** *33,* 7501.
114. Langer, C. J.; O'Byrne, K. J.; Socinski, M. A.; Mikhailov, S. M.; Leśniewski-Kmak, K.; Smakal, M.; Ciuleanu, T. E.; Orlov, S. V.; Dediu, M.; Heigener, D.; Eisenfeld, A. J.; Sandalic, L.; Oldham, F. B.; Singer, J. W.; Ross, H. J. *J. Thorac. Oncol.* **2008,** *3,* 623–630. doi:10.1097/JTO.0b013e3181753b4b
115. Curtis, K. K.; Sarantopoulos, J.; Northfelt, D. W.; Weiss, G. J.; Barnhart, K. M.; Whisnant, J. K.; Leuschner, C.; Alila, H.; Borad, M. J.; Ramanathan, R. K. *Cancer Chemother. Pharmacol.* **2014,** *73,* 931–941. doi:10.1007/s00280-014-2424-x
116. Graybill, W. S.; Coleman, R. L. *Future Oncol.* **2014,** *10,* 541–548. doi:10.2217/fon.14.8
117. Mahalingam, D.; Wilding, G.; Denmeade, S.; Sarantopoulas, J.; Cosgrove, D.; Cetnar, J.; Azad, N.; Bruce, J.; Kurman, M.; Allgood, V. E.; Carducci, M. *Br. J. Cancer* **2016,** *114,* 986–994. doi:10.1038/bjc.2016.72
118. Bakker, W. H.; Albert, R.; Bruns, C.; Breeman, W. A. P.; Hofland, L. J.; Marbach, P.; Pless, J.; Pralet, D.; Stolz, B.; Koper, J. W.; Lamberts, S. W. J.; Visser, T. J.; Krenning, E. P. *Life Sci.* **1991,** *49,* 1583–1591. doi:10.1016/0024-3205(91)90052-D
119. Oshima, N.; Akizawa, H.; Kitaura, H.; Kawashima, H.; Zhao, S.; Zhao, Y.; Nishijima, K.-i.; Kitamura, Y.; Arano, Y.; Kuge, Y.; Ohkura, K. *Nucl. Med. Biol.* **2017,** *54,* 18–26. doi:10.1016/j.nucmedbio.2017.07.002
120. Nagy, A.; Schally, A. V.; Armatis, P.; Szepeshazi, K.; Halmos, G.; Kovacs, M.; Zarandi, M.; Groot, K.; Miyazaki, M.; Jungwirth, A.; Horvath, J. *Proc. Natl. Acad. Sci. U. S. A.* **1996,** *93,* 7269–7273. doi:10.1073/pnas.93.14.7269
121. Nagy, A.; Plonowski, A.; Schally, A. V. *Proc. Natl. Acad. Sci. U. S. A.* **2000,** *97,* 829–834. doi:10.1073/pnas.97.2.829
122. Miyazaki, M.; Nagy, A.; Schally, A. V.; Lamharzi, N.; Halmos, G.; Szepeshazi, K.; Groot, K.; Armatis, P. *J. Natl. Cancer Inst.* **1997,** *89,* 1803–1809. doi:10.1093/jnci/89.23.1803
123. Arencibia, J. M.; Bajo, A. M.; Schally, A. V.; Krupa, M.; Chatzistamou, I.; Nagy, A. *Anti-Cancer Drugs* **2002,** *13,* 949–956. doi:10.1097/00001813-200210000-00007
124. Szepeshazi, K.; Schally, A. V.; Nagy, A.; Halmos, G.; Groot, K. *Anti-Cancer Drugs* **1997,** *8,* 974–987. doi:10.1097/00001813-199711000-00009
125. Halmos, G.; Nagy, A.; Lamharzi, N.; Schally, A. V. *Cancer Lett.* **1999,** *136,* 129–136. doi:10.1016/S0304-3835(98)00316-4
126. Letsch, M.; Schally, A. V.; Szepeshazi, K.; Halmos, G.; Nagy, A. *Clin. Cancer Res.* **2003,** *9,* 4505–4513.
127. Plonowski, A.; Schally, A. V.; Nagy, A.; Groot, K.; Krupa, M.; Navone, N. M.; Logothetis, C. *Cancer Lett.* **2002,** *176,* 57–63. doi:10.1016/S0304-3835(01)00734-0
128. Gründker, C.; Völker, P.; Griesinger, F.; Ramaswamy, A.; Nagy, A.; Schally, A. V.; Emons, G. *Am. J. Obstet. Gynecol.* **2002,** *187,* 528–537. doi:10.1067/mob.2002.124278
129. Liu, S. V.; Tsao-Wei, D. D.; Xiong, S.; Groshen, S.; Dorff, T. B.; Quinn, D. I.; Tai, Y.-C.; Engel, J.; Hawes, D.; Schally, A. V.; Pinski, J. K. *Clin. Cancer Res.* **2014,** *20,* 6277–6283. doi:10.1158/1078-0432.CCR-14-0489
130. Yu, S. S.; Athreya, K.; Liu, S. V.; Schally, A. V.; Tsao-Wei, D.; Groshen, S.; Quinn, D. I.; Dorff, T. B.; Xiong, S.; Engel, J.; Pinski, J. *Clin. Genitourin. Cancer* **2017,** *15,* 742–749. doi:10.1016/j.clgc.2017.06.002
131. Emons, G.; Gorchev, G.; Harter, P.; Wimberger, P.; Stähle, A.; Hanker, L.; Hilpert, F.; Beckmann, M. W.; Dall, P.; Gründker, C.; Sindermann, H.; Sehouli, J. *Int. J. Gynecol. Cancer* **2014,** *24,* 260–265. doi:10.1097/IGC.0000000000000044
132. Engel, J.; Emons, G.; Pinski, J.; Schally, A. V. *Expert Opin. Invest. Drugs* **2012,** *21,* 891–899. doi:10.1517/13543784.2012.685128
133. Cai, R. Z.; Szoke, B.; Lu, R.; Fu, D.; Redding, T. W.; Schally, A. V. *Proc. Natl. Acad. Sci. U. S. A.* **1986,** *83,* 1896–1900. doi:10.1073/pnas.83.6.1896
134. Schally, A. V.; Nagy, A. *Trends Endocrinol. Metab.* **2004,** *15,* 300–310. doi:10.1016/j.tem.2004.07.002
135. Engel, J. B.; Schally, A. V.; Halmos, G.; Baker, B.; Nagy, A.; Keller, G. *Cancer* **2005,** *104,* 1312–1321. doi:10.1002/cncr.21327
136. Régina, A.; Demeule, M.; Ché, C.; Lavallée, I.; Poirier, J.; Gabathuler, R.; Béliveau, R.; Castaigne, J.-P. *Br. J. Pharmacol.* **2008,** *155,* 185–197. doi:10.1038/bjp.2008.260
137. Pardridge, W. M. *NeuroRx* **2005,** *2,* 3–14. doi:10.1602/neurorx.2.1.3
138. Banks, W. A. *BMC Neurol.* **2009,** *9* (Suppl. 1), S3. doi:10.1186/1471-2377-9-S1-S3
139. Etame, A. B.; Diaz, R. J.; Smith, C. A.; Mainprize, T. G.; Hynynen, K.; Rutka, J. T. *Neurosurg. Focus* **2012,** *32,* E3. doi:10.3171/2011.10.FOCUS11252

140. Thanou, M.; Gedroyc, W. *J. Drug Delivery* **2013,** No. 616197. doi:10.1155/2013/616197
141. Drappatz, J.; Brenner, A.; Wong, E. T.; Eichler, A.; Schiff, D.; Groves, M. D.; Mikkelsen, T.; Rosenfeld, S.; Sarantopoulos, J.; Meyers, C. A.; Fielding, R. M.; Elian, K.; Wang, X.; Lawrence, B.; Shing, M.; Kelsey, S.; Castaigne, J. P.; Wen, P. Y. *Clin. Cancer Res.* **2013,** *19,* 1567–1576. doi:10.1158/1078-0432.CCR-12-2481
142. Ché, C.; Yang, G.; Thiot, C.; Lacoste, M.-C.; Currie, J.-C.; Demeule, M.; Régina, A.; Béliveau, R.; Castaigne, J.-P. *J. Med. Chem.* **2010,** *53,* 2814–2824. doi:10.1021/jm9016637
143. Manea, M.; Mezo, G. *Protein Pept. Lett.* **2013,** *20,* 439–449. doi:10.2174/092986613805290381
144. Orbán, E.; Mező, G.; Schlage, P.; Csík, G.; Kulić, Ž.; Ansorge, P.; Fellinger, E.; Möller, H. M.; Manea, M. *Amino Acids* **2011,** *41,* 469–483. doi:10.1007/s00726-010-0766-1
145. Schlage, P.; Mező, G.; Orbán, E.; Bősze, S.; Manea, M. *J. Controlled Release* **2011,** *156,* 170–178. doi:10.1016/j.jconrel.2011.08.005
146. Murányi, J.; Gyulavári, P.; Varga, A.; Bökönyi, G.; Tanai, H.; Vántus, T.; Pap, D.; Ludányi, K.; Mező, G.; Kéri, G. *J. Pept. Sci.* **2016,** *22,* 552–560. doi:10.1002/psc.2904
147. Mezö, I.; Lovas, S.; Pályi, I.; Vincze, B.; Kálnay, A.; Turi, G.; Vadász, Z.; Seprödi, J.; Idei, M.; Tóth, G.; Gulyás, É.; Ötvös, F.; Mák, M.; Horváth, J. E.; Teplán, I.; Murphy, R. F. *J. Med. Chem.* **1997,** *40,* 3353–3358. doi:10.1021/jm9700981
148. Mezo, G. Peptide and protein based pharmaceuticals. *Amino Acids, Peptides and Proteins;* The Royal Society of Chemistry: 2014; Vol. 38, pp 203–252.
149. Manea, M.; Leurs, U.; Orbán, E.; Baranyai, Z.; Öhlschläger, P.; Marquardt, Á.; Schulcz, A.; Tejeda, M.; Kapuvári, B.; Tóvári, J.; Mező, G. *Bioconjugate Chem.* **2011,** *22,* 1320–1329. doi:10.1021/bc100547p
150. Hegedüs, R.; Manea, M.; Orbán, E.; Szabó, I.; Kiss, É.; Sipos, É.; Halmos, G.; Mező, G. *Eur. J. Med. Chem.* **2012,** *56,* 155–165. doi:10.1016/j.ejmech.2012.08.014
151. Kapuvári, B.; Hegedüs, R.; Schulcz, Á.; Manea, M.; Tóvári, J.; Gacs, A.; Vincze, B.; Mező, G. *Invest. New Drugs* **2016,** *34,* 416–423. doi:10.1007/s10637-016-0354-7
152. Leurs, U.; Mező, G.; Orbán, E.; Öhlschläger, P.; Marquardt, A.; Manea, M. *Pept. Sci.* **2012,** *98,* 1–10. doi:10.1002/bip.21640
153. Leurs, U.; Lajkó, E.; Mező, G.; Orbán, E.; Öhlschläger, P.; Marquardt, A.; Kőhidai, L.; Manea, M. *Eur. J. Med. Chem.* **2012,** *52,* 173–183. doi:10.1016/j.ejmech.2012.03.016
154. Hegedüs, R.; Pauschert, A.; Orbán, E.; Szabó, I.; Andreu, D.; Marquardt, A.; Mező, G.; Manea, M. *Pept. Sci.* **2015,** *104,* 167–177. doi:10.1002/bip.22629
155. Chintalgattu, V.; Rees, M. L.; Culver, J. C.; Goel, A.; Jiffar, T.; Zhang, J.; Dunner, K., Jr.; Pati, S.; Bankson, J. A.; Pasqualini, R.; Arap, W.; Bryan, N. S.; Taegtmeyer, H.; Langley, R. R.; Yao, H.; Kupferman, M. E.; Entman, M. L.; Dickinson, M. E.; Khakoo, A. Y. *Sci. Transl. Med.* **2013,** *5,* 187ra69. doi:10.1126/scitranslmed.3005066
156. Vrettos, E. I.; Sayyad, N.; Mavrogiannaki, E. M.; Stylos, E.; Kostagianni, A. D.; Papas, S.; Mavromoustakos, T.; Theodorou, V.; Tzakos, A. G. *RSC Adv.* **2017,** *7,* 50519–50526. doi:10.1039/C7RA06655D
157. Ishiguro, S.; Kawabata, A.; Zulbaran-Rojas, A.; Monson, K.; Uppalapati, D.; Ohta, N.; Inui, M.; Pappas, C. G.; Tzakos, A. G.; Tamura, M. *Biochem. Biophys. Res. Commun.* **2018,** *495,* 962–968. doi:10.1016/j.bbrc.2017.11.102

License and Terms

BEILSTEIN JOURNAL OF ORGANIC CHEMISTRY

Novel unit B cryptophycin analogues as payloads for targeted therapy

Eduard Figueras, Adina Borbély, Mohamed Ismail, Marcel Frese and Norbert Sewald*

Full Research Paper

Open Access

Address:
Department of Chemistry, Organic and Bioorganic Chemistry, Bielefeld University, Universitätsstraße 25, 33615 Bielefeld, Germany

Email:
Norbert Sewald* - Norbert.sewald@uni-bielefeld.de

* Corresponding author

Keywords:
cryptophycin; cytotoxic agents; novel payloads; tubulin inhibitors; tumour targeting

Beilstein J. Org. Chem. **2018,** *14,* 1281–1286.
doi:10.3762/bjoc.14.109

Received: 16 February 2018
Accepted: 02 May 2018
Published: 01 June 2018

This article is part of the Thematic Series "Peptide–drug conjugates".

Associate Editor: A. Kirschning

Abstract

Cryptophycins are naturally occurring cytotoxins with great potential for chemotherapy. Since targeted therapy provides new perspectives for treatment of cancer, new potent analogues of cytotoxic agents containing functional groups for conjugation to homing devices are required. We describe the design, synthesis and biological evaluation of three new unit B cryptophycin analogues. The *O*-methyl group of the unit B D-tyrosine analogue was replaced by an *O*-(allyloxyethyl) moiety, an *O*-(hydroxyethyl) group, or an *O*-(((azidoethoxy)ethoxy)ethoxyethyl) substituent. While the former two maintain cytotoxicity in the subnanomolar range, the attachment of the triethylene glycol spacer with a terminal azide results in a complete loss of activity. Docking studies of the novel cryptophycin analogues to β-tubulin provided a rationale for the observed cytotoxicities.

Introduction

Cryptophycins are natural occurring cyclic depsipeptides that were first isolated from cyanobacteria Nostoc sp. ATCC 53789 in 1990 [1]. Cryptophycins target tubulin, in particular the peptide site of the vinca domain. They block microtubule formation, inhibiting their assembly and, hence, are antimitotic agents [2,3]. Their high cytotoxicity prompted manifold studies that were initially focussed on the total synthesis and structure–activity relationships [4-20]. This work resulted in the identification of cryptophycin-52, a highly biologically active analogue of cryptophycin-1 (Figure 1).

Eli Lilly took cryptophycin-52 into clinical trials. Although almost half of the patients obtained a benefit from the treatment, neurotoxic side effects forced the termination of the clinical trials [21-23]. In order to overcome the side effects of cryptophycin-52 and to better understand the fundamental structure for biological activity, numerous structure–activity relationship studies have been carried out [24-35]. However, like cryptophycin-52, the new analogues were not selective against cancer cells making them not better than its parent.

In recent years the targeted delivery of cytotoxic agents has emerged as a highly promising method to tackle selectivity issues [36-40]. Cryptophycin-52 and many analogues lack an addressable group to conjugate the toxin to a homing device. For this reason, new analogues containing functional groups

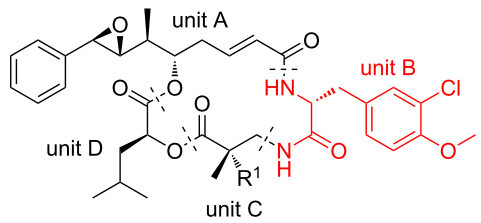

Figure 1: Cryptophycin-1 (**1**) and -52 (**2**).

that would allow the conjugation of a homing device were developed [41-46]. Some of these functionalized analogues have been recently used for the preparation of antibody–drug conjugates (ADCs) and peptide–drug conjugates (PDCs) [46-51]. Nevertheless, there is still a strong need of novel cryptophycin analogues with maintained activity containing a suitable functional group that would allow the conjugation to the homing device. Cryptophycin-1 contains a methoxy group in the aromatic ring of the unit B, which is a chlorinated derivative of D-tyrosine. Different chains for unit B have been investigated, albeit the elongation of the methoxy group is still unknown. Therefore, in the current study, we embarked on the synthesis of novel cryptophycin analogues containing different substituents at the phenolic hydroxy group of the unit B. We intended to investigate whether the high biological activity of the parent compound is retained and thus, construction of ADCs and PDCs would be feasible. This preparation could be done using traceless cleavable linkers that are sensitive to the distinct physiology of the tumour with enhanced level and activity of specific enzymes. The connection between the payload and the linker is of crucial importance since its stability can dramatically change the release and thus, the activity of the compound. For this reason, the included functional groups were designed with the consideration to provide appropriate stability and activity to the future conjugate.

Results and Discussion

Design and synthesis

Previous docking studies have postulated that the methyl group of unit B is not involved in the cryptophycin–tubulin interaction [52]. Moreover, its absence did not produce a dramatic loss of activity [24].

Based on this, we designed cryptophycin analogues modified in the unit B. Instead of the *O*-methyl group that is present in the natural cryptophycin, we attached a hydroxyethyl group or a triethylene glycol chain terminated with an alcohol or azide, respectively. These functional groups would allow the conjugation of the novel cryptophycin analogues across an appropriate linker to an antibody or peptide. Either a virtually uncleavable triazole (introduced by CuAAC) or scissile ester, carbonate, or carbamate moieties were taken into account.

The synthesis of the modified unit B (Scheme 1) started with the preparation of the two different spacers that were later connected to the phenol. Starting from triethylene glycol (**3**) or

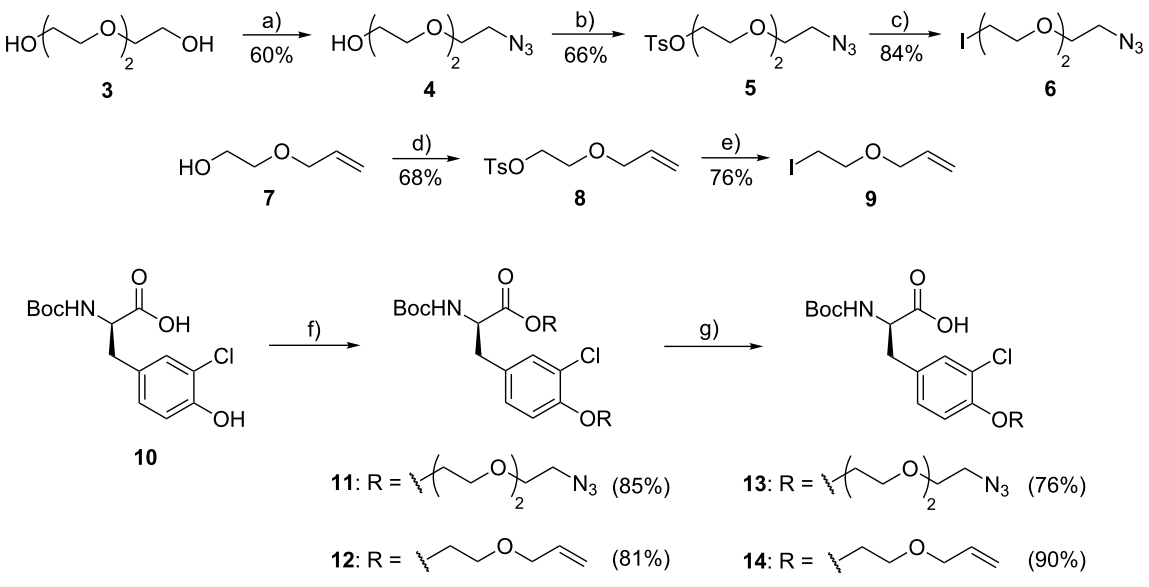

Scheme 1: Synthesis of modified unit B (**13** and **14**). Reagents and conditions: (a) 1) TsCl, DMAP, Et_3N, CH_2Cl_2, rt, 4 h; 2) NaN_3, DMF, 70 °C, overnight; (b) TsCl, Et_3N, CH_2Cl_2, rt, overnight; (c) NaI, acetone, reflux, overnight; (d) TsCl, Et_3N, CH_2Cl_2, rt, overnight; (e) NaI, acetone, reflux, overnight; (f) **6** or **9**, K_2CO_3, DMF, 50 °C, overnight; (g) LiOH, H_2O/MeOH/THF 1:1:1, rt, 2 h.

2-allyloxyethanol (**7**) tosylations and nucleophilic displacements by azide or iodide substitution provided **6** and **9** in good yields. O-Alkylation of Boc-protected 3-chlorinated D-tyrosine **10** with **6** or **9** gave **11** and **12**, again in satisfactory yields (81–85%). Saponification of the ester moiety in **11** and **12** that was formed concomitantly with the O-alkylation in the previous reaction provided Boc-protected modified units B **13** and **14** in 76 and 90% yield, respectively.

The synthesis of units C–D and A succeeded as previously described in the literature; unit A (**15**) and C–D (**16**) were connected by Yamaguchi esterification to give **17** (Scheme 2) [45]. Then, Fmoc was cleaved from the N-terminus of unit C–D–A (**17**) using piperidine and the resulting crude amine was coupled to the corresponding modified unit B (**13** or **14**), affording the according linear cryptophycins **18** and **19** in acceptable yields (51–59%). Compounds **18** and **19** were treated with trifluoroacetic acid for simultaneous Boc and *t*-Bu removal, which also cleaved the dioxolane ring. Subsequently, macrolactamization was performed under pseudo-high-dilution conditions to afford **20** and **21** as described previously [16]. Then the diol was transformed into the epoxide following a three-step one-pot reaction as extensively used in the synthesis of cryptophycin analogues [46]. Cryptophycin analogues **22** and

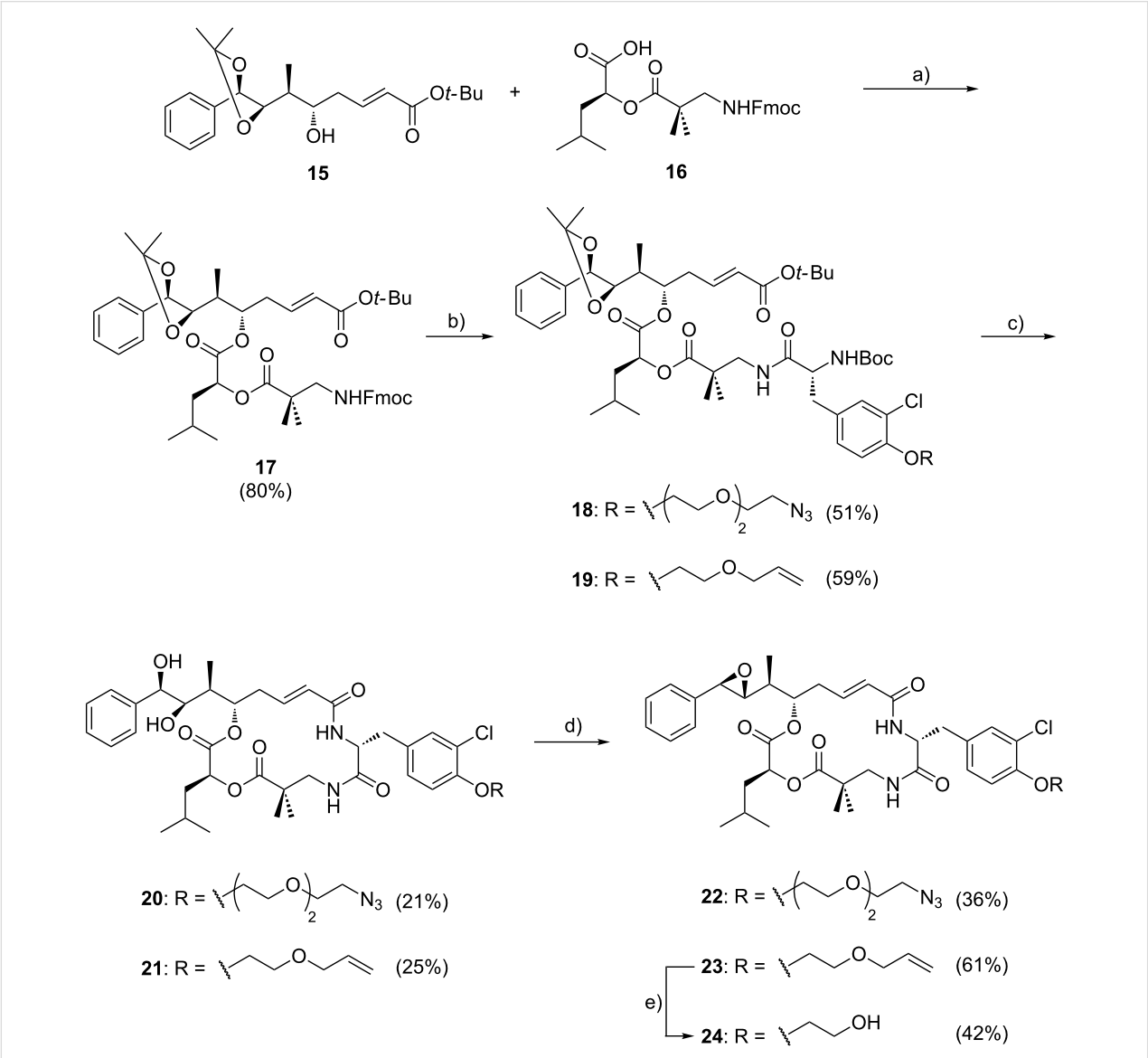

Scheme 2: Synthesis of cryptophycin analogues **22**, **23** and **24**. Reagents and conditions: (a) 4-DMAP, 2,4,6-trichlorobenzoyl chloride, Et_3N, THF, 0 °C, 3 h; (b) 1) piperidine, DMF, rt, 2 h; 2) **13** or **14**, HOAt, EDC·HCl, Et_3N, CH_2Cl_2, 0 °C → rt, overnight; (c) 1) TFA/CH_2Cl_2/H_2O, rt, 2 h; 2) HATU, HOAt, DIPEA, DMF, rt, slow addition + 2 h; (d) 1) $(CH_3O)_3CH$, PPTS, CH_2Cl_2, rt, 2 h; 2) AcBr, CH_2Cl_2, rt, 4 h; 3) K_2CO_3, DME/ethylene glycol (2:1 v/v), rt, 5 min; (e) $Pd(PPh_3)_4$, phenylsilane, CH_2Cl_2, rt, 7 h.

23 were obtained in good purity after column chromatography. The allyl ether in **23** was cleaved using $Pd(PPh_3)_4$ as Pd(0) source and phenylsilane as scavenger to obtain the cryptophycin analogue **24** in good purity.

Biological evaluation

The biological activity of the modified unit B analogues was determined in a cell viability assay using the human cervix carcinoma cell line KB-3-1 (Table 1). The cryptophycin analogue **22** showed a dramatic loss of activity compared to cryptophycin-52 (**2**), while analogues **23** and **24** showed a reduced cytotoxicity although their IC_{50} values are still in the low nanomolar range. The observed dramatic loss of activity of analogue **22** could be due to its poor internalization or the modification could alter the interaction with tubulin. In order to get an extensive knowledge of the novel analogues, we embarked in docking and modelling studies, herein reported, and internalization studies are ongoing in our research group.

Table 1: Cytotoxicity of cryptophycin-52 and its unit B analogues.

compd	unit B	IC_{50} KB-3-1 (nM)
2	CH_2Ph(*m*-Cl,*p*-OMe)	0.015
22	CH_2Ph(*m*-Cl,*p*-$(OCH_2CH_2)_3N_3$)	195000
23	CH_2Ph(*m*-Cl,*p*-$OCH_2CH_2OCH_2CHCH_2$)	0.748
24	CH_2Ph(*m*-Cl,*p*-OCH_2CH_2OH)	0.184

Docking and modelling of cryptophycin derivatives

There is no X-ray analysis of cryptophycin–tubulin complexes available to provide information on the binding site. Based on biochemical evidence, binding close to the vinca-alkaloid binding site of β-tubulin, the so called "peptide-site", has been proposed [2,52,53]. We performed a docking study to explain the different affinities of the newly synthesized derivatives. The parent compound **2** scored highest with respect to β-tubulin binding (Table 2). Three hydrogen bonds were detected to key residues in the peptide binding pocket of the vinca domain (Lys176, Val177 and Tyr210). Other than previously reported [52], the methoxy group of subunit B forms a hydrogen bond with Lys176 (Figure 2). Another binding mode of **2** with high binding affinity and hydrogen bond formation did not involve any interaction of subunit B, yet it was oriented towards the GDP binding site that might influence GTP hydrolysis.

Table 2: Binding energies for the different cryptophycin analogues.

compd	binding energy (kJ/mol)	max. binding energy (kJ/mol)	min. binding energy (kJ/mol)
2	36.17	36.17	17.21
22	22.61	22.61	5.44
23	32.20	32.20	10.38
24	32.70	32.70	11.72

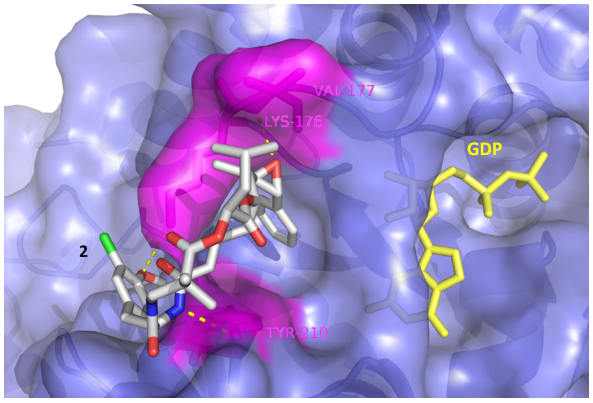

Figure 2: Binding mode of **2**, showing the interaction to the vinca domain peptide binding pocket (blue). Hydrogen bonds are shown as yellow dots with the interacting amino acid residues in magenta.

Compound **22** with the triethylene glycol-based substituent prevents correct binding, the binding energy was decreased and mainly nonspecific interactions outside the binding pocket were observed (Figure 3). This was not the case for the other derivatives **23** and **24** (Figure 4).

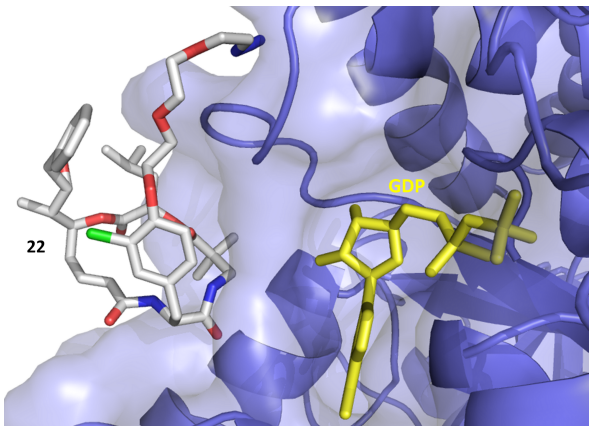

Figure 3: Docking of **22** to the vinca domain of β-tubulin. Surface and backbone of β-tubulin are shown in blue, GDP in yellow. No hydrogen bond formation was detected. The orientation of the azidoethoxyethoxyethyl substituent prevents the inhibitor from the correct interaction with the protein. The epoxide and benzyl group of subunit A are pointing away from the binding pocket.

Besides hydrogen bond formation and binding affinity of inhibitors **2**, **23** and **24**, π-interactions and hydrophobic contacts with the binding pocket of the vinca domain were detected

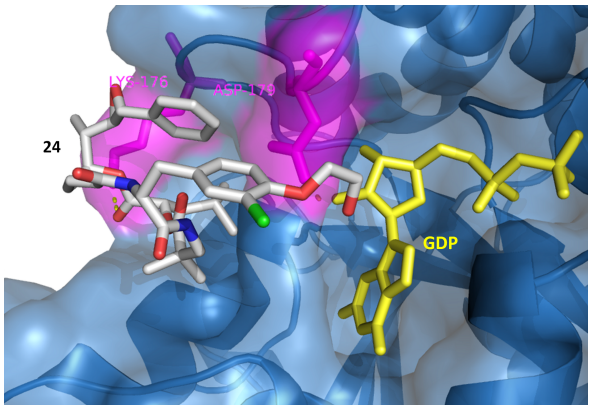

Figure 4: Docking of **24** to β-tubulin. Surface and backbone of β-tubulin are shown in blue, GDP in yellow. H-bonding (yellow dots) was detected with Lys176 and Asp179 in magenta. The benzyl group and the epoxide of subunit A are directed towards the peptide binding pocket, while the hydroxyethyl group is positioned towards the GDP binding pocket forming an H-bond with Asp179.

that would in turn increase the affinity of the inhibitor and its effect on the protein (Supporting Information File 1, Table S1).

Conclusion

In summary, three new cryptophycin analogues with a modified unit B have been designed and successfully synthesized. The novel analogues were less active than cryptophycin-52 in the KB-3-1 cell line. Analogue **22** showed a dramatic loss of activity whereas analogues **23** and **24** showed a reduced activity but were still very cytotoxic.

Supporting Information

Supporting Information File 1

Experimental part and analytical data.
[https://www.beilstein-journals.org/bjoc/content/supplementary/1860-5397-14-109-S1.pdf]

Acknowledgements

This project has received funding from the European Union's Horizon 2020 research and innovation programme under the Marie Skłodowska-Curie grant agreement No 642004. The authors like to acknowledge M. Wißbrock, A. Nieß and C. Michalek for technical support.

ORCID® iDs

Eduard Figueras - https://orcid.org/0000-0002-1853-9974
Adina Borbély - https://orcid.org/0000-0002-5506-6555
Norbert Sewald - https://orcid.org/0000-0002-0309-2655

References

1. Schwartz, R. E.; Hirsch, C. F.; Sesin, D. F.; Flor, J. E.; Chartrain, M.; Fromtling, R. E.; Harris, G. H.; Salvatore, M. J.; Liesch, J. M.; Yudin, K. *J. Ind. Microbiol.* **1990,** *5,* 113–123. doi:10.1007/BF01573860
2. Bai, R.; Schwartz, R. E.; Kepler, J. A.; Pettit, G. R.; Hamel, E. *Cancer Res.* **1996,** *56,* 4398–4406.
3. Smith, C. D.; Zhang, X. *J. Biol. Chem.* **1996,** *271,* 6192–6198. doi:10.1074/jbc.271.11.6192
4. Barrow, R. A.; Hemscheidt, T.; Liang, J.; Paik, S.; Moore, R. E.; Tius, M. A. *J. Am. Chem. Soc.* **1995,** *117,* 2479–2490. doi:10.1021/ja00114a011
5. Kobayashi, M.; Wang, W.; Ohyabu, N.; Kurosu, M.; Kitagawa, I. *Chem. Pharm. Bull.* **1995,** *43,* 1598–1600. doi:10.1248/cpb.43.1598
6. de Muys, J.-M.; Rej, R.; Nguyen, D.; Go, B.; Fortin, S.; Lavallée, J.-F. *Bioorg. Med. Chem. Lett.* **1996,** *6,* 1111–1116. doi:10.1016/0960-894X(96)00182-5
7. Rej, R.; Nguyen, D.; Go, B.; Fortin, S.; Lavallée, J.-F. *J. Org. Chem.* **1996,** *61,* 6289–6295. doi:10.1021/jo960816b
8. Gardinier, K. M.; Leahy, J. W. *J. Org. Chem.* **1997,** *62,* 7098–7099. doi:10.1021/jo971645t
9. Norman, B. H.; Hemscheidt, T.; Schultz, R. M.; Andis, S. L. *J. Org. Chem.* **1998,** *63,* 5288–5294. doi:10.1021/jo980536r
10. Georg, G. I.; Ali, S. M.; Stella, V. J.; Waugh, W. N.; Himmes, R. H. *Bioorg. Med. Chem. Lett.* **1998,** *8,* 1959–1962. doi:10.1016/S0960-894X(98)00356-4
11. Ghosh, A. K.; Bischoff, A. *Org. Lett.* **2000,** *2,* 1573–1575. doi:10.1021/ol000058i
12. Eggen, M.; Mossman, C. J.; Buck, S. B.; Nair, S. K.; Bhat, L.; Ali, S. M.; Reiff, E. A.; Boge, T. C.; Georg, G. I. *J. Org. Chem.* **2000,** *65,* 7792–7799. doi:10.1021/jo000767+
13. Murakami, N.; Wang, W.; Ohyabu, N.; Ito, T.; Tamura, S.; Aoki, S.; Kobayashi, M.; Kitagawa, I. *Tetrahedron* **2000,** *56,* 9121–9128. doi:10.1016/S0040-4020(00)00766-3
14. Murakami, N.; Tamura, S.; Wang, W.; Takagi, T.; Kobayashi, M. *Tetrahedron* **2001,** *57,* 4323–4336. doi:10.1016/S0040-4020(01)00339-8
15. Ghosh, A. K.; Swanson, L. *J. Org. Chem.* **2003,** *68,* 9823–9826. doi:10.1021/jo035077v
16. Mast, C. A.; Eißler, S.; Stončius, A.; Stammler, H.-G.; Neumann, B.; Sewald, N. *Chem. – Eur. J.* **2005,** *11,* 4667–4677. doi:10.1002/chem.200500282
17. Danner, P.; Bauer, M.; Phukan, P.; Maier, M. E. *Eur. J. Org. Chem.* **2005,** 317–325. doi:10.1002/ejoc.200400558
18. Eißler, S.; Neumann, B.; Stammler, H.-G.; Sewald, N. *Synlett* **2008,** 273–277. doi:10.1055/s-2007-1000868
19. Sammet, B.; Radzey, H.; Neumann, B.; Stammler, H.-G.; Sewald, N. *Synlett* **2009,** 417–420. doi:10.1055/s-0028-1087541
20. Sammet, B.; Brax, M.; Sewald, N. *Beilstein J. Org. Chem.* **2011,** *7,* 243–245. doi:10.3762/bjoc.7.32
21. Sessa, C.; Weigang-Köhler, K.; Pagani, O.; Greim, G.; Mor, O.; De Pas, T.; Burgess, M.; Weimer, I.; Johnson, R. *Eur. J. Cancer* **2002,** *38,* 2388–2396. doi:10.1016/S0959-8049(02)00489-6
22. Stevenson, J. P.; Sun, W.; Gallagher, M.; Johnson, R.; Vaughn, D.; Schuchter, L.; Algazy, K.; Hahn, S.; Enas, N.; Ellis, D.; Thornton, D.; O'Dwyer, P. J. *Clin. Cancer Res.* **2002,** *8,* 2524–2529.
23. D'Agostino, G.; Del Campo, J.; Mellado, B.; Izquierdo, M. A.; Minarik, T.; Cirri, L.; Marini, L.; Perez-Gracia, J. L.; Scambia, G. *Int. J. Gynecol. Cancer* **2006,** *16,* 71–76. doi:10.1111/j.1525-1438.2006.00276.x

24. Patel, V. F.; Andis, S. L.; Kennedy, J. H.; Ray, J. E.; Schultz, R. M. *J. Med. Chem.* **1999,** *42,* 2588–2603. doi:10.1021/jm980706s
25. Varie, D. L.; Shih, C.; Hay, D. A.; Andis, S. L.; Corbett, T. H.; Gossett, L. S.; Janisse, S. K.; Martinelli, M. J.; Moher, E. D.; Schultz, R. M.; Toth, J. E. *Bioorg. Med. Chem. Lett.* **1999,** *9,* 369–374. doi:10.1016/S0960-894X(98)00748-3
26. Shih, C.; Gossett, L. S.; Gruber, J. M.; Sue Grossman, C.; Andis, S. L.; Schultz, R. M.; Worzalla, J. F.; Corbett, T. H.; Metz, J. T. *Bioorg. Med. Chem. Lett.* **1999,** *9,* 69–74. doi:10.1016/S0960-894X(98)00682-9
27. Vidya, R.; Eggen, M. J.; Georg, G. I.; Himes, R. H. *Bioorg. Med. Chem. Lett.* **2003,** *13,* 757–760. doi:10.1016/S0960-894X(02)01023-5
28. Buck, S. B.; Huff, J. K.; Himes, R. H.; Georg, G. I. *J. Med. Chem.* **2004,** *47,* 696–702. doi:10.1021/jm030278c
29. Buck, S. B.; Huff, J. K.; Himes, R. H.; Georg, G. I. *J. Med. Chem.* **2004,** *47,* 3697–3699. doi:10.1021/jm030555f
30. Eißler, S.; Bogner, T.; Nahrwold, M.; Sewald, N. *Chem. – Eur. J.* **2009,** *15,* 11273–11287. doi:10.1002/chem.200901750
31. Liu, W. L.; Zhang, J. C.; Jiang, F. Q.; Fu, L. *Arch. Pharm.* **2009,** *342,* 577–583. doi:10.1002/ardp.200900067
32. Nahrwold, M.; Bogner, T.; Eissler, S.; Verma, S.; Sewald, N. *Org. Lett.* **2010,** *12,* 1064–1067. doi:10.1021/ol1000473
33. Weiß, C.; Bogner, T.; Sammet, B.; Sewald, N. *Beilstein J. Org. Chem.* **2012,** *8,* 2060–2066. doi:10.3762/bjoc.8.231
34. Kumar, A.; Kumar, M.; Sharma, S.; Guru, S. K.; Bhushan, S.; Shah, B. A. *Eur. J. Med. Chem.* **2015,** *93,* 55–63. doi:10.1016/j.ejmech.2014.11.068
35. Weiss, C.; Figueras, E.; Borbely, A. N.; Sewald, N. *J. Pept. Sci.* **2017,** *23,* 514–531. doi:10.1002/psc.3015
36. Chari, R. V. J.; Miller, M. L.; Widdison, W. C. *Angew. Chem., Int. Ed.* **2014,** *53,* 3796–3827. doi:10.1002/anie.201307628
37. Srinivasarao, M.; Low, P. S. *Chem. Rev.* **2017,** *117,* 12133–12164. doi:10.1021/acs.chemrev.7b00013
38. Krall, N.; Scheuermann, J.; Neri, D. *Angew. Chem., Int. Ed.* **2013,** *52,* 1384–1402. doi:10.1002/anie.201204631
39. Dal Corso, A.; Pignataro, L.; Belvisi, L.; Gennari, C. *Curr. Top. Med. Chem.* **2016,** *16,* 314–329. doi:10.2174/1568026615666150701114343
40. Le Joncour, V.; Laakkonen, P. *Bioorg. Med. Chem.* **2018,** *26,* 2797–2806. doi:10.1016/j.bmc.2017.08.052
41. Al-awar, R. S.; Ray, J. E.; Schultz, R. M.; Andis, S. L.; Kennedy, J. H.; Moore, R. E.; Liang, J.; Golakoti, T.; Subbaraju, G. V.; Corbett, T. H. *J. Med. Chem.* **2003,** *46,* 2985–3007. doi:10.1021/jm0203884
42. Al-Awar, R. S.; Corbett, T. H.; Ray, J. E.; Polin, L.; Kennedy, J. H.; Wagner, M. M.; Williams, D. C. *Mol. Cancer Ther.* **2004,** *3,* 1061–1067.
43. Kotoku, N.; Kato, T.; Narumi, F.; Ohtani, E.; Kamada, S.; Aoki, S.; Okada, N.; Nakagawa, S.; Kobayashi, M. *Bioorg. Med. Chem.* **2006,** *14,* 7446–7457. doi:10.1016/j.bmc.2006.07.019
44. Sammet, B.; Bogner, T.; Nahrwold, M.; Weiss, C.; Sewald, N. *J. Org. Chem.* **2010,** *75,* 6953–6960. doi:10.1021/jo101563s
45. Weiss, C.; Sammet, B.; Sewald, N. *Nat. Prod. Rep.* **2013,** *30,* 924–940. doi:10.1039/c3np70022d
46. Nahrwold, M.; Weiß, C.; Bogner, T.; Mertink, F.; Conradi, J.; Sammet, B.; Palmisano, R.; Royo Gracia, S.; Preuße, T.; Sewald, N. *J. Med. Chem.* **2013,** *56,* 1853–1864. doi:10.1021/jm301346z
47. Bouchard, H.; Brun, M.-P.; Commerçon, A.; Zhang, J. Novel conjugates, preparation thereof, and therapeutic use thereof. WO Patent WO2011/001052, Jan 6, 2011.
48. Verma, V. A.; Pillow, T. H.; Depalatis, L.; Li, G.; Phillips, G. L.; Polson, A. G.; Raab, H. E.; Spencer, S.; Zheng, B. *Bioorg. Med. Chem. Lett.* **2015,** *25,* 864–868. doi:10.1016/j.bmcl.2014.12.070
49. Steinkuhler, M. C.; Gallinari, M. P.; Osswald, B.; Sewald, N.; Ritzefeld, M.; Frese, M.; Figueras, E.; Pethö, L. Cryptophycin-based antibody-drug conjugates with novel self-immolative linkers. WO Patent WO2016/146638 A1, Sept 22, 2016.
50. Bigot, A.; Bouchard, H.; Brun, M.-P.; Clerc, F.; Zhang, J. Novel cryptophycin compounds and conjugates, their preparation and their therapeutic use. WO Patent WO2017/076998 A1, May 11, 2017.
51. Chen, H.; Lin, Z.; Arnst, K. E.; Miller, D. D.; Li, W. *Molecules* **2017,** *22,* No. 1281. doi:10.3390/molecules22081281
52. Mitra, A.; Sept, D. *Biochemistry* **2004,** *43,* 13955–13962. doi:10.1021/bi0487387
53. Bai, R.; Pettit, G. R.; Hamel, E. *Biochem. Pharmacol.* **1990,** *39,* 1941–1949. doi:10.1016/0006-2952(90)90613-P

License and Terms

BEILSTEIN JOURNAL OF ORGANIC CHEMISTRY

Design and biological characterization of novel cell-penetrating peptides preferentially targeting cell nuclei and subnuclear regions

Anja Gronewold, Mareike Horn and Ines Neundorf*

Full Research Paper

Open Access

Address:
Department of Chemistry, Biochemistry, University of Cologne, Zuelpicher Str. 47a, 50674 Cologne, Germany

Email:
Ines Neundorf* - ines.neundorf@uni-koeln.de

* Corresponding author

Keywords:
anticancer drugs; cell nuclei; cell-penetrating peptides; nucleoli; subcellular targeting

Beilstein J. Org. Chem. **2018,** *14,* 1378–1388.
doi:10.3762/bjoc.14.116

Received: 15 January 2018
Accepted: 16 May 2018
Published: 07 June 2018

This article is part of the Thematic Series "Peptide–drug conjugates".

Guest Editor: N. Sewald

Abstract

Within this study, we report about the design and biological characterization of novel cell-penetrating peptides (CPPs) with selective suborganelle-targeting properties. The nuclear localization sequence N50, as well as the nucleoli-targeting sequence NrTP, respectively, were fused to a shortened version of the cell-penetrating peptide sC18. We examined cellular uptake, subcellular fate and cytotoxicity of these novel peptides, N50-sC18* and NrTP-sC18*, and found that they are nontoxic up to a concentration of 50 or 100 μM depending on the cell lines used. Moreover, detailed cellular uptake studies revealed that both peptides enter cells via energy-independent uptake, although endocytotic processes cannot completely excluded. However, initial drug delivery studies demonstrated the high versatility of these new peptides as efficient transport vectors targeting specifically nuclei and nucleoli. In future, they could be further explored as parts of newly created peptide–drug conjugates.

Introduction

Various drugs act on targets that are located within the nucleus, the control center of the eukaryotic cell. A lipid bilayer membrane, which is perforated with nuclear pore complex structures through which the transfer of molecules is regulated, separates the nucleus from the cytosol. Macromolecules, like proteins, gain access to the nucleus by recognition of their nuclear localization sequences (NLS) by NLS-receptors, and following energy-dependent uptake processes. Several such natural occurring protein-derived NLS have been already identified and described [1]. Moreover, peptides that specifically target to subnuclear sites, e.g., nucleoli, have been characterized [2,3]. The nucleolus is formed at discrete chromosomal loci and its major role is the generation of ribosomal key components and assembly of the ribosomes [4]. Selective inhibition of the ribosomal machinery has been shown to be an effective anticancer therapeutic strategy [5]. That is why selective drug transport to

the nucleoli has emerged a potent new strategy in anticancer drug development [6,7].

Based on these homing domains, a substantial number of sequences have been designed for addressing and delivering anticancer drugs to the nuclei and its subnuclear regions. Although several drugs might be delivered successfully inside a cell, they often fail since they are not able to reach their subcellular target. In order to circumvent adverse side effects, there is a need to develop suitable delivery vectors for the safe transport of drugs to the nucleus. Such nuclear-targeting sequences have already proven to be successful delivery tools. According to their often basic nature, they are also able to traverse the cellular membrane [8]. Based on this, these peptides have been added to the growing family of cell-penetrating peptides (CPPs). CPPs are able to overcome the cellular membrane and to enhance the intracellular uptake of CPP-modified molecules [9]. Usually, these peptides are relatively short (≤30 amino acids (aa)) and display an amphipathic or basic character. During the last 25–30 years, many different CPPs have been described and used for manifold applications like the delivery of nucleic acids, proteins, peptides, nanoparticles, small organic drugs, and others [10]. CPP conjugates can be generated by covalent conjugation between cargo and CPP or by forming non-covalent complexes. Notably, the mechanism of cell entry is still not fully understood, and can only hardly, if in any case, be predicted [9]. In fact, whereas one of the main mechanisms is endocytosis, there exist also CPPs that translocate through cellular membranes by direct penetration. The latter is described for those cases, where only small cargos are attached to the CPP [11]. We have designed a cell-penetrating peptide sequence, namely sC18, which we efficiently used in previous studies as drug transporter [12-17]. sC18 is composed of the last 16 *C*-terminal aa of the cationic antimicrobial peptide CAP18 [18]. When it comes in contact with lipid membranes, it forms a helical structure, probably supporting membrane interaction [19]. However, the main uptake mechanism that was observed followed endocytotic processes, although we have seen that sC18 is also able to enter cells directly to some extent, which is among others depending on the cell lines used [20].

For a further exploration and development of peptide–drug conjugates, peptide sequences that specifically accumulate at intracellular target sites are needed. CPPs have been already described as beneficial tools in the creation of anticancer drugs [21]. Within this study, we aimed to design novel efficient cell-penetrating peptides that preferentially locate within cell nuclei and subnuclear regions. For this, we generated peptide chimera consisting of a shortened version of the recently described sC18 peptide and a nuclear- or nucleolar-targeting sequence. These novel peptides proved to be very efficiently taken up by cancer cells and to accumulate within their target destinations. Beside a careful characterization concerning their uptake behavior, we used these peptides in an initial study for the delivery of the anticancer drug doxorubicin.

Results and Discussion

Peptide synthesis and analysis of the secondary structure

We chose two different nuclear-targeting sequences, on the one hand the N50 peptide, which was derived from the NF-κB/p50 subunit. N50 binds the adaptor protein importin-α at the nuclear envelope and triggers the uptake of the transcription factor NF-κB [22,23]. As second sequence we chose the NrTP sequence, which is a designed peptide coming from the rattlesnake toxin, called crotamine [3]. For both peptides, preferential accumulation within the nuclei has been already described. Moreover, for NrTP a subnuclear localization within the nucleoli has been reported. We designed peptide chimera by attaching these nuclear targeting sequences at the *N*-terminus of a shortened version of the sC18 peptide, namely sC18*, lacking the four *C*-terminal amino acids of sC18. Recently, we could show that sC18* was still able to enter cells, although with lower efficiency than sC18 itself [19,20]. However, to keep the final peptide sequence as short as possible, we used this minimalistic version. As control peptides, we additionally prepared the nuclear targeting sequences, as well as sC18* alone. All peptides were readily synthesized via Fmoc/*t*-Bu solid-phase peptide synthesis, purified, and analyzed by LC–MS methods as previously described [19,20]. Moreover, 5(6)-carboxyfluorescein (CF)-labeled versions were generated (Table 1).

As shown in Table 1 and Figures S1–S4 (Supporting Information File 1), all peptides could be successfully synthesized in high purities.

First, we performed a structural analysis by diluting all peptides to a concentration of 20 μM in phosphate buffer (pH 7.0), with or without the presence of the secondary structure inducing solvent trifluoroethanol (TFE) [24].

As can be depicted from Figure 1, all peptides exhibited a random coil structure in phosphate buffer without TFE. In the presence of TFE, the peptides N50 and NrTP also exhibited a random coil structure, whereas N50-sC18* and NrTP-sC18* formed α-helices. This was also confirmed by the calculated R-values, which were 0.83 for N50-sC18* and 0.70 for NrTP-sC18* [25]. In agreement with our recent studies sC18* exhibited an α-helical character in TFE solution (data not shown) [19]. Thus, the helical character of the novel fusion peptides likely results from the sC18* part. Furthermore, N50-sC18* and NrTP-sC18* formed α-helices that showed amphipathic

Table 1: Names, sequences, molecular weights and net charges of the peptides that were investigated in this study. All peptides were obtained in >99% purity.

Name	Sequence[a]	MW_{calcd} [Da]	MW_{exp} [Da]	Net charge
sC18*	GLRKRLRKFRNK	1570.96	1571.36	+8
N50	VQRKRQKLMP	1282.61	1282.76	+5
N50-sC18*	VQRKRQKLMPGLRKRLRKFRNK	2836.51	2837.20	+12
NrTP	YKQCHKKGGKKGSG	1504.76	1505.03	+6
NrTP-sC18*	YKQCHKKGGKKGSGGLRKRLRKFRNK	3058.67	3059.31	+13

[a]All peptides are *C*-terminally amidated. For internalization studies, also 5(6)-carboxyfluorescein-labeled peptides were synthesized.

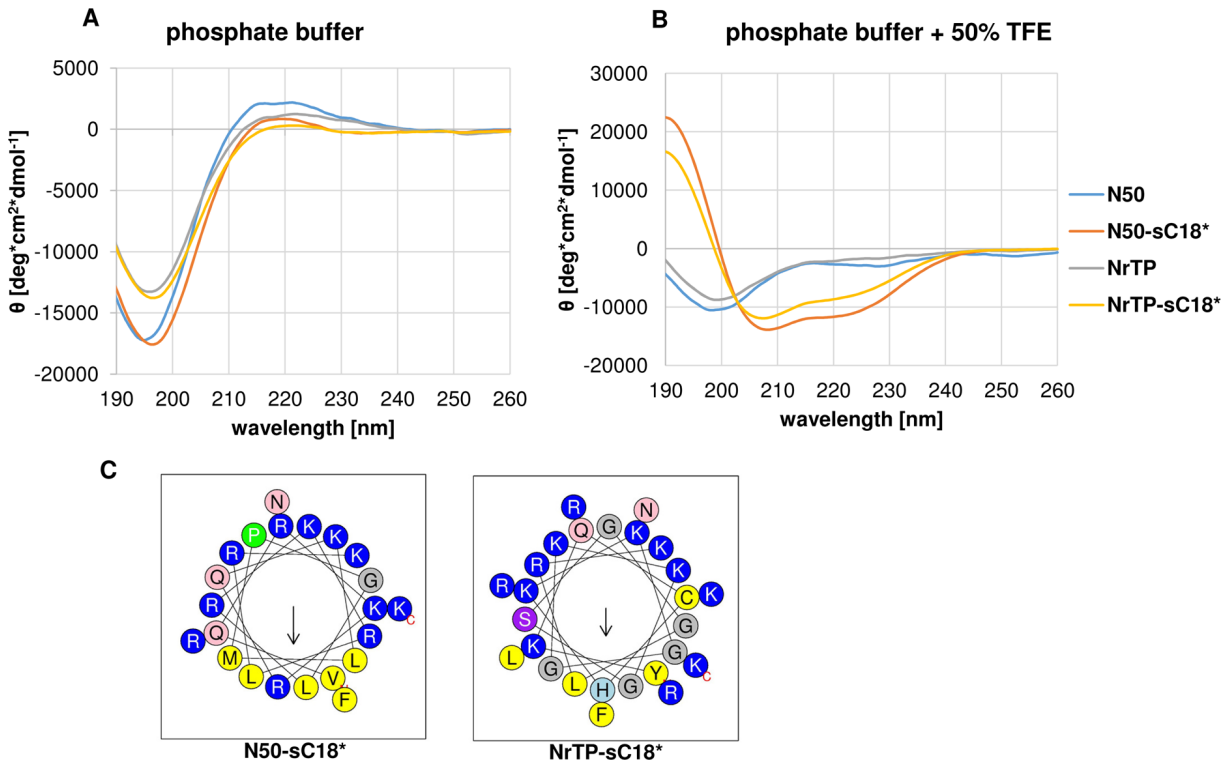

Figure 1: Circular dichroism spectra of the novel peptides solved in 10 mM phosphate buffer (pH 7) (A), or phosphate buffer with the addition of TFE (50%) (B). Peptide concentration was 20 µM. (C) Helical wheel projections of the peptides N50-sC18* and NrTP-sC18*, respectively [26].

character with a clear hydrophilic and hydrophobic face (Figure 1C). This property might support the interaction with the plasma membrane.

Cytotoxic profile of novel CPPs

In the next step, the cytotoxicity profiles of the novel peptide chimera were investigated. Therefore, we chose two different cancer cell lines, namely breast cancer MCF-7 and cervix carcinoma HeLa cells, which were exposed for 24 h to various concentrations of the peptides sC18*, N50, N50-sC18*, NrTP and NrTP-sC18* (Figure 2).

We observed no toxic effects of the peptides when incubated with MCF-7 cells up to a concentration of 100 µM. Also after treating HeLa cells with the peptides up to a concentration of 50 µM, no significant toxicity could be observed for sC18*, N50, N50-sC18* and NrTP. Besides N50, all other peptide sequences did lower the amount of viable cells to an amount of around 80% at higher concentrations. For sC18* the results are in very good agreement to our former studies, in which we also examined the toxicity in other cell lines, like human epithelial kidney cells (HEK-293) and human colorectal adenocarcinoma cells (HCT-15) [19,20]. Notably, NrTP-sC18* seemed to affect

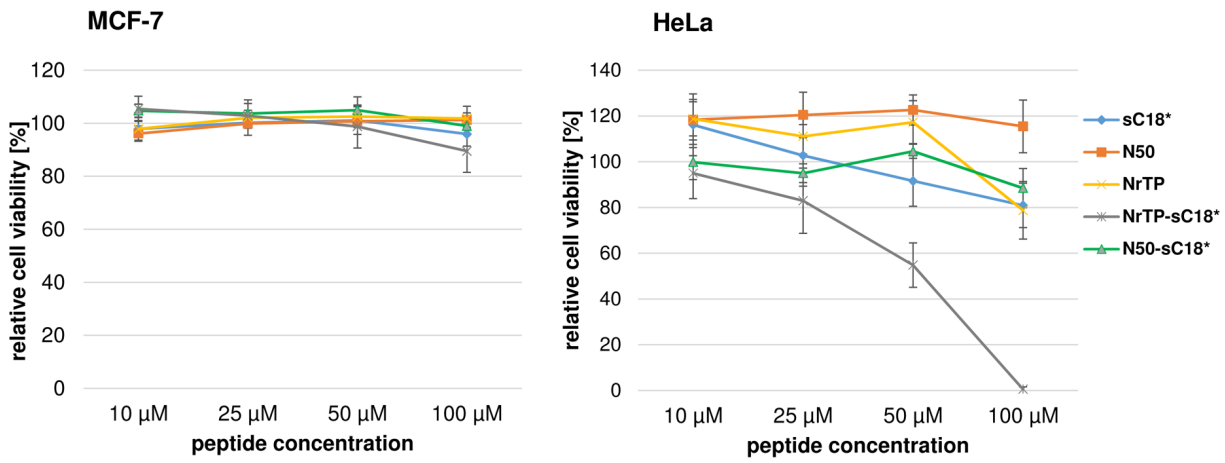

Figure 2: Cytotoxicity profiles of the peptides in MCF-7 and HeLa cells. Cells were incubated for 24 h with different concentrations of peptide solutions. Untreated cells served as negative control, cells treated with 70% ethanol as positive control. Values from the positive control were subtracted from all data, and the untreated cells were set to 100%; assays were performed with n = 3 in triplicate.

cell viability at a concentration of 50 µM, and at higher concentrations, all cells were dead. To get a more detailed picture, we additionally determined the IC_{50} value of this peptide, NrTP-sC18*, when in presence of HeLa cells. An IC_{50} value of about 53.72 ± 4.79 µM was calculated after incubating the cells with various concentrations from 1 to 100 µM (Figure S5, Supporting Information File 1), demonstrating its high toxic effects in this cell line. Probably NrTP-sC18* interacts with distinct intracellular targets, but this has to be elucidated in further studies. However, all following uptake experiments were conducted at peptide concentrations between 1 and 10 µM, where no significant effect on cell viability was observed in both cell lines.

Cellular uptake studies

Next, we analyzed the intracellular fate of the new peptide variants using confocal fluorescence microscopy. Thus, MCF-7 and HeLa cells were incubated with 10 µM peptide solutions at 37 °C and inspected after 30 min (Figure 3).

Surprisingly, both new peptide variants, N50-sC18* and NrTP-sC18*, entered the cells extremely efficiently compared to sC18* alone. For sC18*, only small dots were detectable, which were probably representing vesicles, since an endocytotic uptake pathway for this CPP and its longer version sC18 was already demonstrated [13,18,19]. In addition, the nuclear locali-

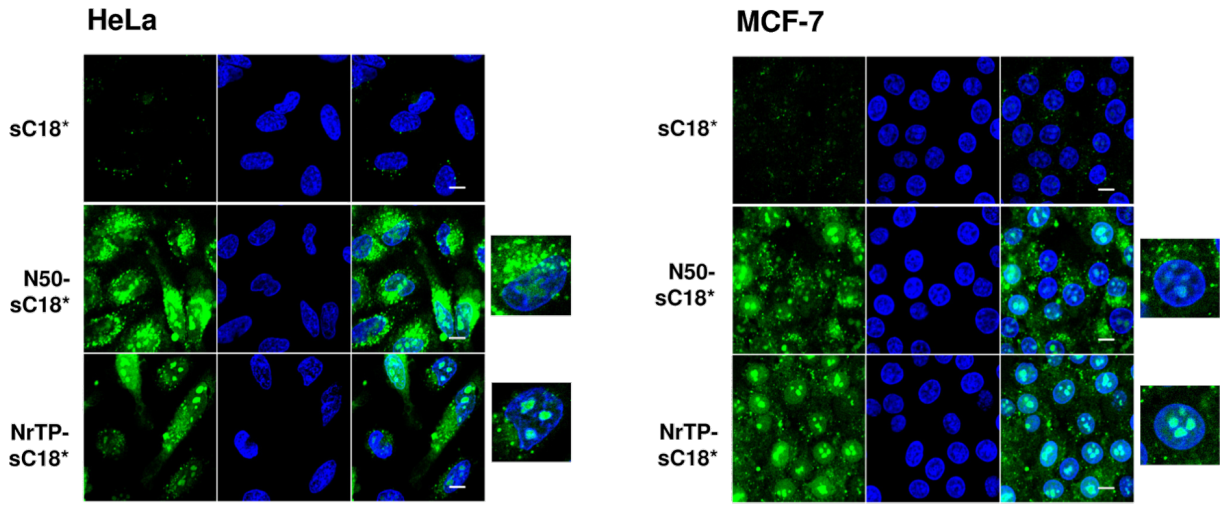

Figure 3: Cellular uptake in HeLa and MCF-7 cells. Cells were incubated for 30 min with 10 µM of CF-labeled peptide solutions. Green: CF-labeled peptide; blue: Hoechst 33342 nuclear stain; scale bar is 10 µm.

zation sequence N50 alone was not noticeable present within both cell lines at the tested concentration (Figure S6, Supporting Information File 1), not even after a longer incubation period of two hours (data not shown). For NrTP alone, a slight fluorescent signal was visible in the nucleoli of MCF-7 cells (Figure S6, Supporting Information File 1). Notably, N50-sC18* was distributed within the whole cell cytosol, and accumulated particularly around the nucleus. In addition to that, a large fraction was also centered within the nuclei and nucleoli. For the fusion peptide NrTP-sC18* a strong accumulation within the nucleoli of both cell lines was visible. Thus, former results about the preferential localization within the nucleolar region of the peptide NrTP alone could be confirmed also for NrTP-sC18* [3].

We then quantified the cellular uptake by using flow cytometry. As expected, the novel peptides N50-sC18* and NrTP-sC18* were characterized by an extremely high uptake compared to the CPP sC18*, as well as the nuclei targeting sequences alone (Figure 4).

Rádis-Baptista et al. recently reported about the effective uptake of rhodamine B-labeled NrTP in different tumor cell lines [3,27]. Within their studies, the authors used higher concentrations, longer incubation times and other cell lines, what could probably explain the different results obtained in our study. In fact, it is very likely that working with increased concentrations of the NrTP sequence could probably improve the cell-penetrating capability of this peptide. Also for the N50 sequence alone, the internalization ability in several different cell lines was already determined [28]. In this case, the uptake turned out to be very low, what is in agreement with our results. The observed enhanced cellular uptake of the novel chimeric peptides might be due to an increased amount of positive charges caused by the presence of more lysine and arginine residues within the sequences. These effects were already described by other

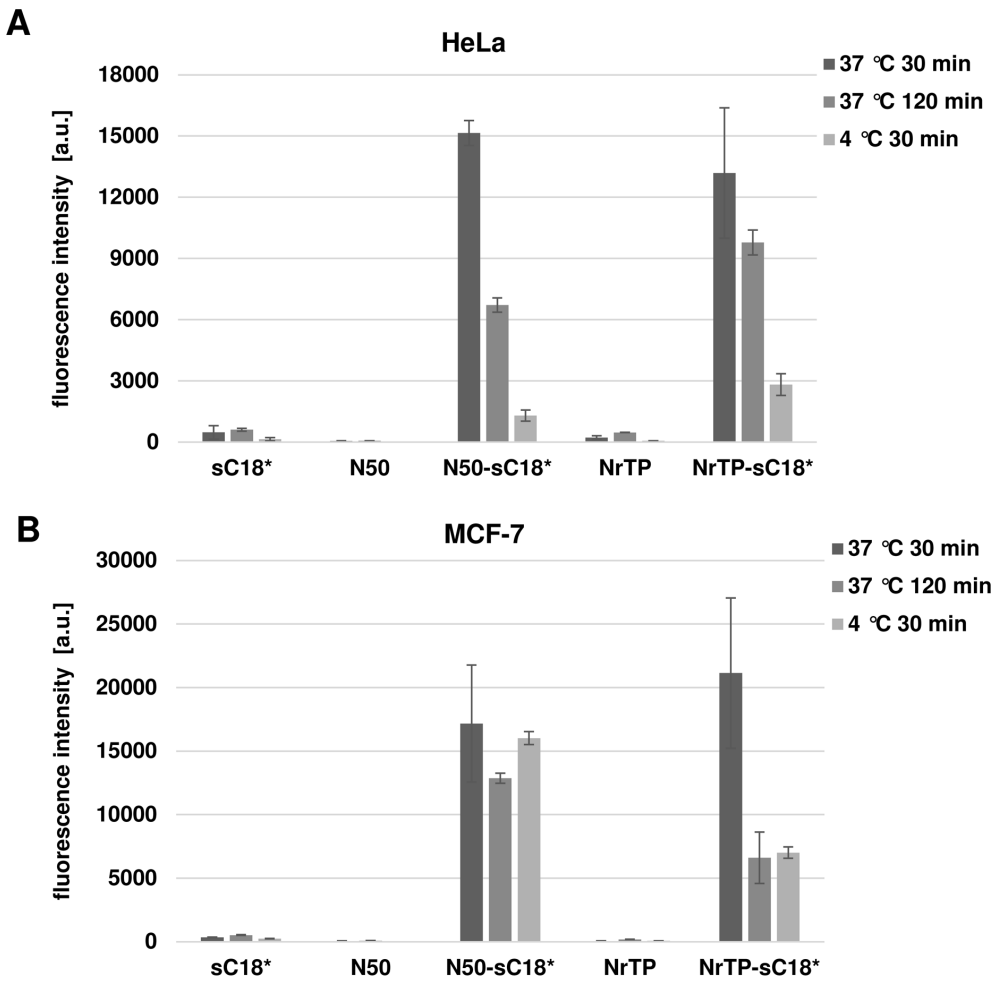

Figure 4: Cellular uptake in MCF-7 and HeLa cells was quantified by flow cytometry. Cells were incubated with 10 μM peptide solutions for 30 min at 37 °C.

groups working with highly cationic CPPs [29-32]. Moreover, the formation of amphipathic α-helices is often one major factor for efficient peptide/lipid interaction, initiating the following internalization process [33]. We have observed that CPP attachment to the nuclei-targeting sequences promotes the formation of such favored secondary structures (e.g., α-helices). Hence, this could be one important key factor for the detected efficient cellular uptake.

Furthermore, we observed that still after 2 hours of incubation with the peptides, strong green signals were visible (Figure 5). In contrast to the pictures taken after 30 min, it seemed that the peptides also formed aggregated structures within the cytosol, beside the fraction that is still localizing in the nuclei. Qian et al. recently discussed such structures as a result of peptide/lipid aggregation [34]. However, since only the fluorescence of the fluorophore can be detected, it can of course not be ruled out that degradation of the peptides has been already started. Quantifying the amount of the novel peptides after 120 min demonstrated further that the uptake was lower compared to 30 min, but still very high compared to sC18* alone (Figure 4).

Anyway, as the internalization with 10 µM of the peptides was quite high and the accumulation, especially for N50-sC18* was not precisely detectable in HeLa cells caused by an intense green signal in the whole cell, we performed experiments using a lower peptide concentration of 1 µM. Next to this, also the shorter peptides, namely sC18*, N50 and NrTP alone were tested at these concentrations for 30 and 120 min. Hereby, no uptake at all was detected (data not shown). In contrast, both fusion peptides were able to efficiently internalize into HeLa cells (Figure S7, Supporting Information File 1). Obviously, the uptake was less compared to that one at a concentration of 10 µM. N50-sC18* was diffusely distributed within the cytosol and the nuclei of HeLa cells, and after 120 min it mainly accumulated within the nuclei. In contrast to this, the uptake of 1 µM of NrTP-sC18* indicated that the peptide accumulates in endosomes after cellular uptake. Interestingly, at this concentration, the peptide was neither detectable in the nuclei nor in the nucleoli. Probably the concentration of NrTP-sC18* was not high enough to escape from the vesicles and to reach the nuclei. This might indicate that a certain concentration threshold is indispensable for efficient internalization, a phenomenon that was already discussed for other CPPs [29,35].

Considering all these observations, it was presumed that the chimeric peptides enter the cells concentration-dependent by direct penetration or by endocytosis, followed by an endosomal release, which could already be shown for other sC18 derived CPP variants [20].

To get an idea about the involvement of endocytotic processes during peptide internalization, uptake studies at 4 °C were performed (Figure 4 and Figure 6). Hereby, energy-dependent pathways are usually suppressed and direct peptide translocation can be observed [36]. After treating MCF-7 and HeLa cells for 30 min with the peptides at 4 °C, both fusion peptides were distributed within the cytoplasm and also accumulated in the

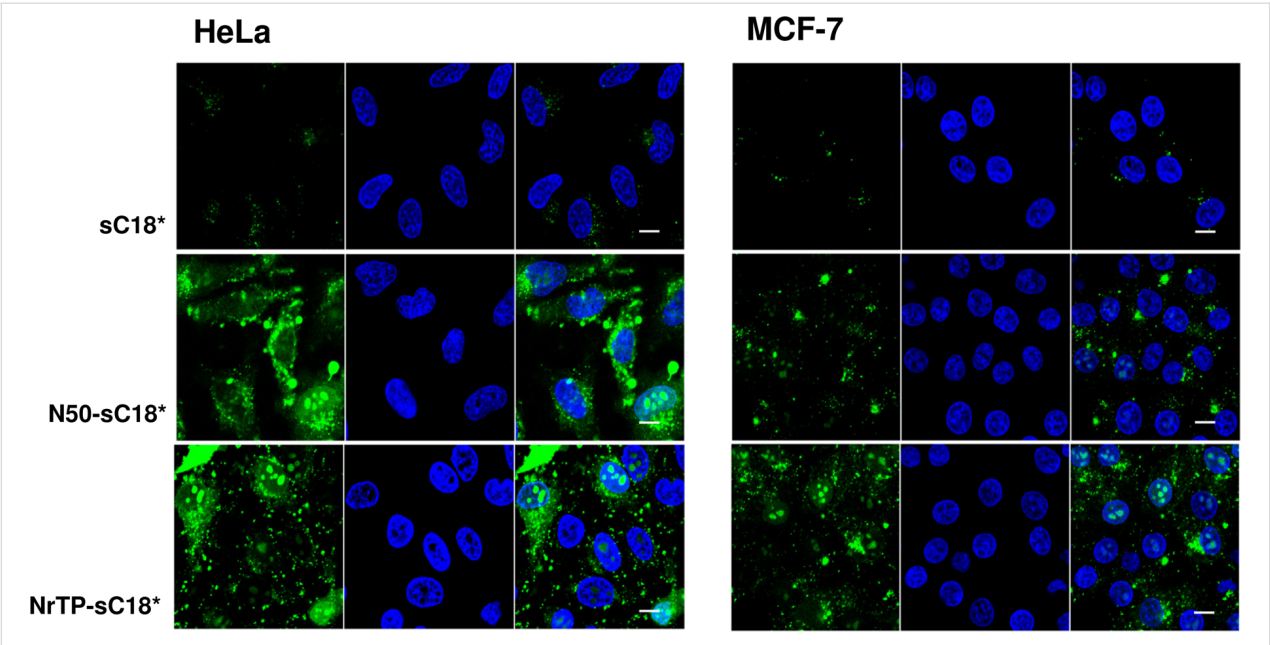

Figure 5: Distribution pattern of the peptides in HeLa and MCF-7 cells when incubating 10 µM CF-labeled peptide solutions for 120 min at 37 °C. Green: CF-labeled peptide; blue: Hoechst 33342 nuclear stain; scale bar is 10 µm.

cell nuclei and nucleoli. This observation supported the idea of cellular entry via direct penetration when using a concentration of 10 µM. In MCF-7 cells, NrTP-sC18* was also evenly distributed throughout the whole cell, including strong accumulation in the nuclei. Notably, N50-sC18* was mainly detectable within the nuclei. Thus, the fusion peptides might indeed enter the cells via direct translocation, although also energy-dependent uptake pathways cannot be ruled out, especially when lower concentrations are applied. However, for both peptides N50-sC18* and NrTP-sC18*, we could prove that they potently address the nuclei/nucleoli. Moreover, as can be depicted from Figure 4, the peptides were taken up to a significant less extent in both cell lines, when cells were incubated at 4 °C. This points again to an involvement of energy-dependent uptake pathways. Notably, the uptake was not completely reduced, indicating the involvement of direct entry processes that may play a role during cellular uptake.

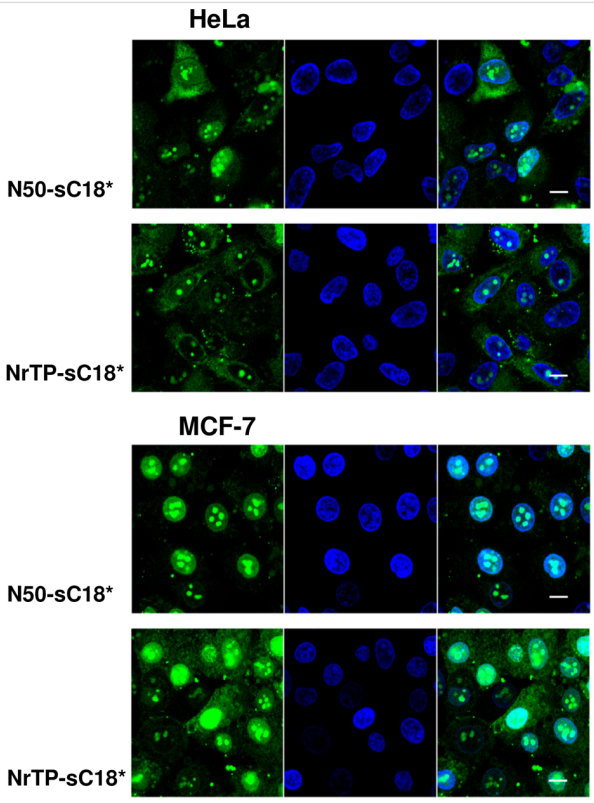

Figure 6: Cellular uptake in HeLa and MCF-7 cells when incubating the cells at 4 °C for 30 min with the CF-labeled chimeric peptides (10 µM). Green: CF-labeled peptide; blue: Hoechst 33342 nuclear stain; scale bar is 10 µm.

Use of novel peptides as cargo delivery systems

In the last experiment, we investigated if the peptides could be used to enhance the efficacy of an anticancer drug. Therefore, HeLa and MCF-7 cells were exposed to the chemotherapeutic drug doxorubicin (DOX) that is already clinically applied in cancer therapy [37]. Doxorubicin interacts with DNA by intercalation and thereby inhibits the macromolecular biosynthesis [38]. Instead of covalent conjugation of the drug, we aimed to investigate the effect of the fusion peptides on drug delivery and efficacy within co-administration. Indeed, the covalent binding of doxorubicin to different CPPs was already reported and the induction of cell death in various cell lines has been observed [39,40]. However, the non-covalent approach of co-administration is often favored owing to the ease of preparation and a higher capacity of drug that can be administered. Such a combination therapy of DOX and a tumor-penetrating peptide has been recently investigated in vivo using clinically relevant tumor models [41].

Doxorubicin is known to be fluorescent [42] and this property was used to test if the peptides were able to enhance the intracellular uptake of the drug. Therefore, solutions out of DOX and the sequences N50-sC18* and NrTP-sC18* were incubated with HeLa and MCF-7 cells, respectively, and observed for red fluorescence afterwards (Figure 7A and 7B).

Minor red fluorescence could be detected in the negative control (DOX only), indicating that the chemotherapeutic drug was also able to translocate in the cells by itself at the used concentration of 10 µg/mL. Apart from that, it is visible that DOX fluorescence is increased when co-administered with the novel peptides (Figure 7A and 7B). Since this effect was more intense in MCF-7 cells, these cells were used for a following cytotoxicity assay. Herein, the drug alone (1 µg/mL) or in presence of 10 µM solutions of the peptides sC18*, N50-sC18* and NrTP-sC18*, respectively, were incubated for 48 h with MCF-7 cells. As can be depicted from Figure 7C, treatment with doxorubicin alone reduced the amount of viable cells to about 60%. The peptides alone were not toxic at a concentration of 10 µM, which was already demonstrated (Figure 2). In contrast, when co-incubating N50-sC18* and NrTP-sC18* with DOX, the toxic effect of the drug could be significantly improved. After co-treatment with NrTP-sC18*, the number of viable cells was decreased to 40% and for N50-sC18* to 30%, although no significant difference in activity of both peptides could be determined. Notably, the peptides NrTP-sC18* and N50-sC18* are more efficient than the sC18* sequence alone. While the presence of sC18* could not enhance the efficacy of DOX, the combination of sC18* with the nuclear targeting sequences N50 and NrTP led to an improved drug uptake, and very likely to an increased accumulation of the drug within the nuclei.

Conclusion

In summary, we presented herein the design and activity of novel CPPs, namely N50-sC18* and NrTP-sC18*. Their low

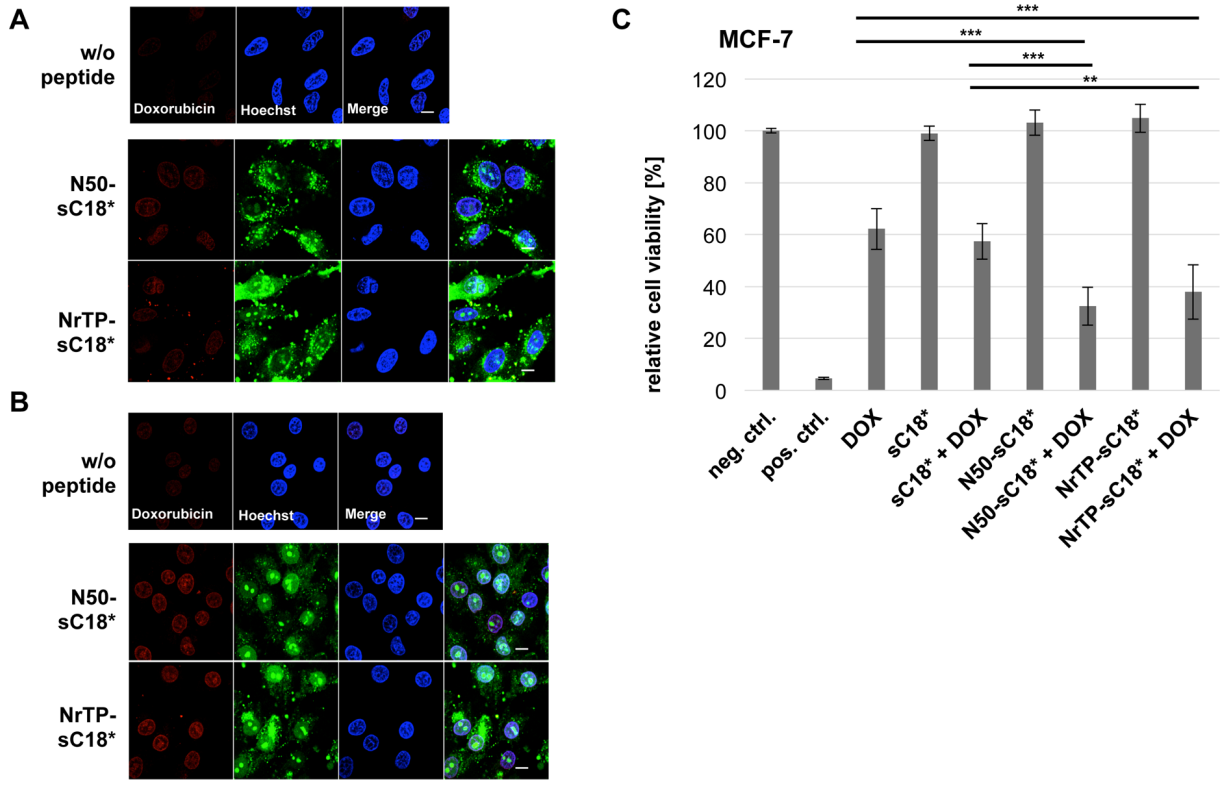

Figure 7: Uptake and delivery of DOX into HeLa and MCF-7 cells. Fluorescence microscopic images after 30 min incubation in HeLa (A) and MCF-7 (B) cells with 10 µM CF-labeled peptides N50-sC18* or NrTP-sC18* co-incubated with 10 µg/mL doxorubicin at 37 °C, respectively. Cells treated with DOX alone served as negative control; Green: CF-labeled peptide; blue: Hoechst 33342 nuclear stain; red: doxorubicin; scale bar is 10 µm. (C) Cells were incubated for 48 h with DOX (1 µg/mL), or solutions out of peptides (10 µM) and DOX (1 µg/mL), or peptide solutions (10 µM) alone. Untreated cells served as negative control, cells treated for 10 min with 70% ethanol as positive control. Experiments were conducted in triplicate with $n = 2$.

cytotoxicity in combination with their high internalization efficiency and target selectivity make these novel peptides promising new transport shuttles. Having shown the great potency of CPP in anticancer drug research, these peptides could be used in future for the development of further innovative and highly effective peptide–drug conjugates.

Experimental

Materials

All N_α-Fmoc protected amino acids (aa) were purchased from IRIS Biotech (Marktredwitz, Germany). Other chemicals and consumables including 1-[bis(dimethylamino)methylene]-1*H*-1,2,3-triazolo[4,5-*b*]pyridinium 3-oxide hexafluorophosphate (HATU), *N*,*N*-diisopropylethylamine (DIPEA), acetonitrile (ACN), and trifluoroacetic acid (TFA), dimethylformamide (DMF), *N*-methylpyrrolidine (NMP), Oxyma, *N*,*N*'-diisopropylcarbodiimide (DIC), doxorubicin (DOX) and 5(6)-carboxyfluorescein (CF) were derived from Fluka (Taufkirchen, Germany), Merck (Darmstadt, Germany), Sarstedt (Nümbrecht, Germany), Sigma-Aldrich (Taufkirchen, Germany) and VWR (Darmstadt, Germany).

Peptide synthesis

All peptides were synthesized using a combination of standard Fmoc/*t*-Bu solid-phase peptide synthesis (SPPS) on a Syro I peptide synthesizer (MultiSynTech, Bochum, Germany) and manual coupling protocols according to previous works [17,19,20]. Peptides were generated on a Rink amide resin (loading 0.48 mmol/g) yielding *C*-terminally amidated molecules.

All syntheses were performed in open polypropylene reactor vessels (2 mL syringes) stocked with a fritted filter disc. All aa were dissolved in DMF except from phenylalanine that was dissolved in NMP. Amino acids were coupled in 8-fold excess and every coupling step was performed twice using Oxyma/DIC as activating reagent. Every coupling step proceeded for 40 min. After complete synthesis, the samples were washed with CH_2Cl_2, MeOH and Et_2O and the resin beads were dried in the Speedvac.

5(6)-Carboxyfluorescein (CF) was coupled with 3 equiv HATU and DIPEA in DMF for 2 h at rt as described previously [20].

CF-polymers were cleaved by treatment with 20% piperidine for 45 min. The successful coupling was verified by a Kaiser test [43].

To cleave the peptides from the resin, a mixture of triisopropylsilane (TIS), H_2O and concentrated trifluoroacetic acid (TFA) (1:1:38 v/v/v) was added for 3 h. Afterwards, the peptides were precipitated in ice cold diethyl ether, washed and lyophilized from water/*tert*-butanol (3:1 v/v). Then, peptides were analyzed by RP-HPLC/ESI-MS on a Kinetex C18 column (100 × 4.6 mm; 2.6 µm/100 Å) using linear gradients of 10–60% B in A (A = 0.1% FA or TFA in water; B = 0.1% FA or TFA in acetonitrile) over 20 min and a flow rate of 0.6 mL·min^{-1}. Further purification of the peptides was achieved by preparative HPLC on RP18 Phenomenex column (Jupiter Proteo, 250 × 15 mm, 4 µm/90 Å) using linear gradients of 10–60% B in A (A = 0.1% TFA in water; B = 0.1% TFA in acetonitrile) over 45 min and a flow rate of 6 mL·min^{-1}. All peptides were obtained with purities >99%.

CD spectroscopy

All peptides were analyzed in 10 mM potassium phosphate buffer (pH 7.0) with or without the addition of TFE (1:1 dilution) using a peptide concentration of 20 µM. Peptides were measured in a 0.1 cm quartz cuvette with a sensitivity of 100 mdeg in the range from 260 to 180 nm in 0.5 nm intervals. The scanning mode was continuous and a scanning speed of 50 nm/min was chosen. The results of pure buffer were subtracted from the spectra of the peptides. The ratio between the molar ellipticity at 222 nm and 207 nm was used to confirm an α-helical structure of peptides [25].

Cell culturing

All cell lines were grown in sterile culture dishes in a CO_2 incubator (5% CO_2) at 37 °C. HeLa and MCF-7 were grown in RPMI-1640 medium containing 10% fetal bovine serum (FBS) and 4 mM L-Gln. HeLa and MCF-7 cells were not used above the 40th passage.

For seeding a defined number of cells, they were removed with trypsin/EDTA solution and a hemocytometer was used for cell counting.

Cell viability assay

A total volume of 200 µL of cells (HeLa 40’000, MCF-7 50’000 cells per well) were seeded in 96-well plates and grown to 70–80% confluency. Afterwards, they were incubated with peptide or doxorubicin solutions (diluted in serum-free medium) in a total volume of 100 µL. In the wells that served as positive and negative controls, the medium was replaced by fresh medium without FBS. The plates were incubated for 24 h or 48 h at 37 °C. Afterwards, the positive control was treated with 100 µL of 70% EtOH for 10 min, and then all cells were washed with PBS. Cells were covered with 100 µL of a 10% resazurin solution in medium without FBS and incubated for 1–2 h at 37 °C. Afterwards, fluorescence was quantified by using a Tecan infinite M200 plate reader (excitation: 550 nm, emission: 595 nm).

To achieve comparably results, the positive control was subtracted from all data and the negative control was set to 100%, so that the results of the peptide-treated cells represent relative cell viability values in %. Experiments were done in triplicate.

Microscopy

For microscopic analyses, a confocal laser scanning system (Nikon D-Eclipse C1) with an inverted microscope (Nikon Eclipse Ti) was used. Pictures were taken with a 60× oil immersion objective (N.A. 1.4, Plan APO VC; Nikon) using the software EZ-C1 3.91 from Nikon.

Cells were seeded in 350 µL medium in an 8-well ibidi plate (HeLa 45,000, MCF-7 70,000 cells per well) and were grown to 70–80% confluency. Then, the medium was removed and the cells were treated with the peptides and substances in various concentrations for the requested time. Cells were incubated at 4 °C or 37 °C and 10 min prior to the end of incubation 0.6 µL of Hoechst stain (bisbenzimide H33342, 1 mg/mL in H_2O, sterile filtered) was added to each well to stain the cell nuclei. After removing the solutions, cells were quenched with 200 µL of 150 µM trypan blue solution (in acetate buffer) for 30 s. The stain was removed and the cells were washed twice with medium. After adding 300 µL of fresh medium, pictures were taken using a fluorescence confocal microscope. Images were edited in Image J 1.43m.

Flow cytometry

Cells were seeded in 24-well plates (HeLa 170,000, MCF-7 200,000 cells per well) and grown to 70–80% confluency. Then, cells were treated with 400 µL of peptide solutions dissolved in serum-free medium for the appropriate time at 4 °C or 37 °C. Afterwards, the cells were washed twice with PBS and detached with Trypsin-EDTA 1× in PBS without phenol red for 3–5 min followed by adding 800 µL of indicator-free medium. Cells were resuspended and 200 µL of the suspension were transferred to a 96-well plate for measuring the fluorescence in the Guava® easyCyte flow cytometer (Merck). In each sample, 10,000 cells were measured and each experiment was done in triplicate. Cells treated with medium only served as negative control and their fluorescent signal was subtracted from all other samples in each set of experiment.

Supporting Information

Supporting Information File 1

Additional information.
[https://www.beilstein-journals.org/bjoc/content/supplementary/1860-5397-14-116-S1.pdf]

Acknowledgements

A. Gronewold acknowledges financial support by the Jürgen-Manchot Stiftung. Financing by the European Union within the MSCA-ITN-2014-ETN MAGICBULLET (grant agreement number 642004) is kindly acknowledged by I.N.

ORCID® iDs

Ines Neundorf - https://orcid.org/0000-0001-6450-3991

References

1. Sakhrani, N. M.; Padh, H. *Drug Des., Dev. Ther.* **2013,** *7,* 585. doi:10.2147/DDDT.S45614
2. Martin, R. M.; Ter-Avetisyan, G.; Herce, H. D.; Ludwig, A. K.; Lättig-Tünnemann, G.; Cardoso, M. C. *Nucleus (Philadelphia, PA, U. S.)* **2015,** *6,* 314. doi:10.1080/19491034.2015.1079680
3. Rádis-Baptista, G.; de la Torre, B. G.; Andreu, D. *J. Med. Chem.* **2008,** *51,* 7041. doi:10.1021/jm8009475
4. Hein, N.; Hannan, K. M.; George, A. J.; Sanij, E.; Hannan, R. D. *Trends Mol. Med.* **2013,** *19,* 643. doi:10.1016/j.molmed.2013.07.005
5. Orsolic, I.; Jurada, D.; Pullen, N.; Oren, M.; Eliopoulos, A. G.; Volarevic, S. *Semin. Cancer Biol.* **2016,** *37-38,* 36. doi:10.1016/j.semcancer.2015.12.004
6. Burger, K.; Mühl, B.; Harasim, T.; Rohrmoser, M.; Malamoussi, A.; Orban, M.; Kellner, M.; Gruber-Eber, A.; Kremmer, E.; Hölzel, M.; Eick, D. *J. Biol. Chem.* **2010,** *285,* 12416. doi:10.1074/jbc.M109.074211
7. Quin, J. E.; Devlin, J. R.; Cameron, D.; Hannan, K. M.; Pearson, R. B.; Hannan, R. D. *Biochim. Biophys. Acta* **2014,** *1842,* 802. doi:10.1016/j.bbadis.2013.12.009
8. Cerrato, C. P.; Künnapuu, K.; Langel, U. *Expert Opin. Drug Delivery* **2017,** *14,* 245. doi:10.1080/17425247.2016.1213237
9. Kalafatovic, D.; Giralt, E. *Molecules* **2017,** *22,* 1929. doi:10.3390/molecules22111929
10. Reissmann, S. *J. Pept. Sci.* **2014,** *20,* 760. doi:10.1002/psc.2672
11. Kauffman, W. B.; Fuselier, T.; He, J.; Wimley, W. C. *Trends Biochem. Sci.* **2015,** *40,* 749. doi:10.1016/j.tibs.2015.10.004
12. Geldmacher, Y.; Splith, K.; Kitanovic, I.; Alborzinia, H.; Can, S.; Rubbiani, R.; Nazif, M. A.; Wefelmeier, P.; Prokop, A.; Ott, I.; Wölfl, S.; Neundorf, I.; Sheldrick, W. S. *J. Biol. Inorg. Chem.* **2012,** *17,* 631. doi:10.1007/s00775-012-0883-2
13. Hoyer, J.; Schatzschneider, U.; Schulz-Siegmund, M.; Neundorf, I. *Beilstein J. Org. Chem.* **2012,** *8,* 1788. doi:10.3762/bjoc.8.204
14. Hu, W.; Splith, K.; Neundorf, I.; Merz, K.; Schatzschneider, U. *J. Biol. Inorg. Chem.* **2012,** *17,* 175. doi:10.1007/s00775-011-0840-5
15. Richter, S.; Bouvet, V.; Wuest, M.; Bergmann, R.; Steinbach, J.; Pietzsch, J.; Neundorf, I.; Wuest, F. *Nucl. Med. Biol.* **2012,** *39,* 1202. doi:10.1016/j.nucmedbio.2012.06.003
16. Splith, K.; Bergmann, R.; Pietzsch, J.; Neundorf, I. *ChemMedChem* **2012,** *7,* 57. doi:10.1002/cmdc.201100401
17. Kuhlmann, N.; Chollet, C.; Baldus, L.; Neundorf, I.; Lammers, M. *ChemMedChem* **2017,** *12,* 1703. doi:10.1002/cmdc.201700414
18. Neundorf, I.; Rennert, R.; Hoyer, J.; Schramm, F.; Löbner, K.; Kitanovic, I.; Wölfl, S. *Pharmaceuticals* **2009,** *2,* 49. doi:10.3390/ph2020049
19. Horn, M.; Reichart, F.; Natividad-Tietz, S.; Diaz, D.; Neundorf, I. *Chem. Commun.* **2016,** *52,* 2261. doi:10.1039/C5CC08938G
20. Gronewold, A.; Horn, M.; Randelović, I.; Tóvári, J.; Muñoz Vázquez, S.; Schomäcker, K.; Neundorf, I. *ChemMedChem* **2017,** *12,* 42. doi:10.1002/cmdc.201600498
21. Feni, L.; Neundorf, I. *Adv. Exp. Med. Biol.* **2017,** *1030,* 279. doi:10.1007/978-3-319-66095-0_13
22. Hoesel, B.; Schmid, J. A. *Mol. Cancer* **2013,** *12,* No. 86. doi:10.1186/1476-4598-12-86
23. Zienkiewicz, J.; Armitage, A.; Hawiger, J. *J. Am. Heart Assoc.* **2013,** *2,* e000386. doi:10.1161/JAHA.113.000386
24. Roccatano, D.; Colombo, G.; Fioroni, M.; Mark, A. E. *Proc. Natl. Acad. Sci. U. S. A.* **2002,** *99,* 12179. doi:10.1073/pnas.182199699
25. Manning, M. C.; Woody, R. W. *Biopolymers* **1991,** *31,* 569. doi:10.1002/bip.360310511
26. Gautier, R.; Douguet, D.; Antonny, B.; Drin, G. *Bioinformatics* **2008,** *24,* 2101. doi:10.1093/bioinformatics/btn392
27. Rádis-Baptista, G.; de la Torre, B. G.; Andreu, D. *Chem. Biol. Drug Des.* **2012,** *79,* 907. doi:10.1111/j.1747-0285.2012.01377.x
28. Scherer, W. F.; Syverton, J. T.; Gey, G. O. *J. Exp. Med.* **1953,** *97,* 695. doi:10.1084/jem.97.5.695
29. Futaki, S.; Nakase, I. *Acc. Chem. Res.* **2017,** *50,* 2449. doi:10.1021/acs.accounts.7b00221
30. Murayama, T.; Masuda, T.; Afonin, S.; Kawano, K.; Takatani-Nakase, T.; Ida, H.; Takahashi, Y.; Fukuma, T.; Ulrich, A. S.; Futaki, S. *Angew. Chem., Int. Ed.* **2017,** *56,* 7644. doi:10.1002/anie.201703578
31. Kosuge, M.; Takeuchi, T.; Nakase, I.; Jones, A. T.; Futaki, S. *Bioconjugate Chem.* **2008,** *19,* 656. doi:10.1021/bc700289w
32. Maniti, O.; Piao, H.-R.; Ayala-Sanmartin, J. *Int. J. Biochem. Cell Biol.* **2014,** *50,* 73. doi:10.1016/j.biocel.2014.02.017
33. Koren, E.; Torchilin, V. P. *Trends Mol. Med.* **2012,** *18,* 385. doi:10.1016/j.molmed.2012.04.012
34. Qian, Z.; Martyna, A.; Hard, R. L.; Wang, J.; Appiah-Kubi, G.; Coss, C.; Phelps, M. A.; Rossman, J. S.; Pei, D. *Biochemistry* **2016,** *55,* 2601. doi:10.1021/acs.biochem.6b00226
35. Madani, F.; Lindberg, S.; Langel, Ü.; Futaki, S.; Gräslund, A. *J. Biophys.* **2011,** No. 414729. doi:10.1155/2011/414729
36. Gestin, M.; Dowaidar, M.; Langel, Ü. *Adv. Exp. Med. Biol.* **2017,** *1030,* 255. doi:10.1007/978-3-319-66095-0_11
37. http://www.cytrx.com/aldoxorubicin.
38. Yang, F.; Teves, S. S.; Kemp, C. J.; Henikoff, S. *Biochim. Biophys. Acta* **2014,** *1845,* 84. doi:10.1016/j.bbcan.2013.12.002
39. Aroui, S.; Brahim, S.; Hamelin, J.; De Waard, M.; Bréard, J.; Kenani, A. *Apoptosis* **2009,** *14,* No. 1352. doi:10.1007/s10495-009-0397-8
40. Liang, J. F.; Yang, V. C. *Bioorg. Med. Chem. Lett.* **2005,** *15,* 5071. doi:10.1016/j.bmcl.2005.07.087
41. Sugahara, K. N.; Teesalu, T.; Karmali, P. P.; Kotamraju, V. R.; Agemy, L.; Greenwald, D. R.; Ruoslahti, E. *Science* **2010,** *328,* 1031. doi:10.1126/science.1183057

42. Bhattacharya, A.; Seshadri, M.; Oven, S. D.; Tóth, K.; Vaughan, M. M.; Rustum, Y. M. *Clin. Cancer Res.* **2008,** *14,* 3926. doi:10.1158/1078-0432.CCR-08-0212
43. Kaiser, E.; Colescott, R. L.; Bossinger, C. D.; Cook, P. I. *Anal. Biochem.* **1970,** *34,* 595. doi:10.1016/0003-2697(70)90146-6

License and Terms

BEILSTEIN JOURNAL OF ORGANIC CHEMISTRY

Drug targeting to decrease cardiotoxicity – determination of the cytotoxic effect of GnRH-based conjugates containing doxorubicin, daunorubicin and methotrexate on human cardiomyocytes and endothelial cells

Livia Polgár[1,2], Eszter Lajkó[2], Pál Soós[1], Orsolya Láng[2], Marilena Manea[3], Béla Merkely[1], Gábor Mező[‡4,5] and László Kőhidai[*,‡2]

Full Research Paper

Open Access

Address:
[1]Heart and Vascular Center, Semmelweis University, Városmajor u. 68., Budapest, 1122, Hungary, [2]Chemotaxis Research Group, Department of Genetics, Cell- and Immunobiology, Semmelweis University, Nagyvárad tér 4., Budapest, 1089, Hungary, [3]University of Konstanz, Department of Chemistry and Zukunftskolleg, Universitätsstrasse 10, 78467 Konstanz, Germany, [4]Eötvös Loránd University, Faculty of Science, Institute of Chemistry, Pázmány P. stny 1/A Budapest, 1117, Hungary and [5]MTA-ELTE Research Group of Peptide Chemistry, Pázmány P. stny 1/A, Hungarian Academy of Science, Budapest, 1117, Hungary

Email:
László Kőhidai[*] - kohlasz2@gmail.com

* Corresponding author ‡ Equal contributors

Keywords:
cardiotoxicity; drug targeting; GnRH-conjugates; HCM; HUVEC; impedimetry

Beilstein J. Org. Chem. **2018,** *14,* 1583–1594.
doi:10.3762/bjoc.14.136

Received: 30 January 2018
Accepted: 08 June 2018
Published: 28 June 2018

This article is part of the Thematic Series "Peptide–drug conjugates".

Guest Editor: N. Sewald

Abstract

Background: Cardiomyopathy induced by the chemotherapeutic agents doxorubicin and daunorubicin is a major limiting factor for their application in cancer therapy. Chemotactic drug targeting potentially increases the tumor selectivity of drugs and decreases their cardiotoxicity. Increased expression of gonadotropin-releasing hormone (GnRH) receptors on the surface of tumor cells has been reported. Thus, the attachment of the aforementioned chemotherapeutic drugs to GnRH-based peptides may result in compounds with increased therapeutic efficacy. The objective of the present study was to examine the cytotoxic effect of anticancer drug–GnRH-conjugates against two essential cardiovascular cell types, such as cardiomyocytes and endothelial cells. Sixteen different previously developed GnRH-conjugates containing doxorubicin, daunorubicin and methotrexate were investigated in this study. Their cytotoxicity was determined on primary human cardiac myocytes (HCM) and human umbilical vein endothelial cells (HUVEC) using the xCELLigence SP system, which measures impedance changes caused by adhering cells on golden electrode arrays placed at the bottom of the wells. Slopes of impedance–time curves were calculated and for the quantitative determination of cytotoxicity, the difference to the control was analysed.

Results: Doxorubicin and daunorubicin exhibited a cytotoxic effect on both cell types, at the highest concentrations tested. Doxorubicin-based conjugates (AN-152, GnRH-III(Dox-*O*-glut), GnRH-III(Dox-glut-GFLG) and GnRH-III(Dox=Aoa-GFLG) showed the same cytotoxic effect on cardiomyocytes. Among the daunorubicin-based conjugates, [^{4}Lys(Ac)]-GnRH-III(Dau=Aoa), GnRH-III(Dau=Aoa-YRRL), {GnRH-III(Dau=Aoa-YRRL-C)}$_2$ and {[^{4}*N*-MeSer]-GnRH-III(Dau-C)}$_2$ had a significant but decreased cytotoxic effect, while the other conjugates – GnRH-III(Dau=Aoa), GnRH-III(Dau=Aoa-K(Dau=Aoa)), [^{4}Lys(Dau=Aoa)]-GnRH-III(Dau=Aoa), GnRH-III(Dau=Aoa-GFLG), {GnRH-III(Dau-C)}$_2$ and [^{4}*N*-MeSer]-GnRH-III(Dau=Aoa) – exerted no cytotoxic effect on cardiomyocytes. Mixed conjugates containing methotrexate and daunorubicin – GnRH-III(Mtx-K(Dau=Aoa)) and [^{4}Lys(Mtx)]-GnRH-III(Dau=Aoa) – showed no cytotoxic effect on cardiomyocytes, as well.

Conclusion: Based on these results, anticancer drug–GnRH-based conjugates with no cytotoxic effect on cardiomyocytes were identified. In the future, these compounds could provide a more targeted antitumor therapy with no cardiotoxic adverse effects. Moreover, impedimetric cytotoxicity analysis could be a valuable technique to determine the effect of drugs on cardiomyocytes.

Introduction

Gonadotropin-releasing hormone (GnRH) is a peptide hormone secreted by the hypothalamus, which stimulates the release of follicle-stimulating hormone (FSH) and luteinizing hormone (LH) from the pituitary. Thus, it represents the first step in the hypothalamus-pituitary-gonadal axis, which plays an important role in reproduction [1]. It has been reported that gonadotropin-releasing hormone receptors (GnRH-Rs) are highly expressed on the surface of tumor cells, especially in gynaecological malignant tumors (breast, ovarian and endometrial cancers) [2]. GnRH and its analogues (both agonists and antagonists) are used for the treatment of different types of cancer [3]. They can inhibit the tumor growth in a direct way, through the GnRH-Rs on tumor cells or by an indirect way, through the influence of hormone secretion by the pituitary [4]. GnRH-III (Glp-His-Trp-Ser-His-Trp-Lys-Pro-Gly-NH_2, where Glp is pyroglutamic acid) is a naturally occurring isoform of GnRH, which was first isolated from sea lamprey [5]. GnRH-III has been shown to exert an effective antitumor activity against a number of tumor types [6-8]. However, it exerted a significantly lower endocrine effect in mammals than the human GnRH (GnRH-I: Glp-His-Trp-Ser-Tyr-Gly-Leu-Arg-Pro-Gly-NH_2) and other GnRH analogues [9]. This low hormonal effect might provide an advantage in the treatment of hormone-independent tumors [10].

Targeted drug delivery is a technique of high interest, by which cytotoxic drugs are attached to specific molecules (homing devices) with the aim of increasing the accumulation of the drug in the specific target cells. Consequently, this leads to a more efficient antitumor effect and to the reduction of potential adverse side effects. Small peptides that recognize target receptors on tumor cells might be suitable targeting moieties for this purpose. Hormone peptides, in particular, GnRH and somatostatin derivatives that possess antiproliferative effect on their own, are among the best candidates as homing peptides [10]. A.V. Schally and his co-workers developed the first GnRH derivative–drug conjugates for targeted tumor therapy. One of these compounds Zoptarelin doxorubicin (developmental code names AEZS-108, AN-152) Glp-His-Trp-Ser-Tyr-*D*-Lys(Dox-*O*-glut)-Leu-Arg-Pro-Gly-NH_2 (where glut is glutaric acid) [11] reached phase III clinical trial, which was discontinued for all indications under development in May 2017 [12]. GnRH-III-based conjugates have been investigated in our laboratory as promising candidates for targeted drug delivery with positive results in human tumor cell lines, both related (e.g., MCF-7) and unrelated (e.g., HT-29, MonoMac6) to the reproductive system [13-15].

Doxorubicin, daunorubicin and methotrexate are clinically used chemotherapeutic agents, with applications in a variety of malignant tumorous diseases [16,17]. Doxorubicin and daunorubicin belong to the anthracycline family and act by damaging the DNA of the cancer cells. Methotrexate is an antimetabolite that inhibits the folate metabolism of tumor cells. All three drugs have a great number of adverse effects; doxorubicin and daunorubicin are especially known for their cardiotoxicity, leading to cardiomyopathy and heart failure [18,19]. These side effects can limit the applicability of these chemotherapeutic drugs. The conjugation of doxorubicin and daunorubicin to a GnRH-III-based targeting peptide could lead to decreased cardiotoxic effect through the more specific drug targeting.

Drug delivery systems containing doxorubicin, daunorubicin and methotrexate attached to various GnRH-III derivatives were previously designed, synthesized and characterized for their antitumor effects in our laboratories [14,15,20-25]. Several approaches including sequence modification of GnRH-III [20], incorporation of enzymatic cleavable oligopeptide spacers (e.g., GFLG, YRRL) [15,21], dimerization of the targeting GnRH-III unit [22], attachment of drugs through different linkages (e.g., ester, amide or oxime bond) [14,23], and multiplication of drugs [24,25] were pursued in order to achieve an increased antitumor effect.

The main objective of the study reported here was to evaluate the in vitro cardiotoxic effects (as undesired side effects) of sixteen GnRH-III-based conjugates containing doxorubicin, daunorubicin and methotrexate on two essential target cells of cardiovascular diseases: vascular endothelial cells and cardiomyocytes. The rate of cytotoxicity (antitumor effect) vs cardiotoxicity (toxic effects on cardiomyocytes and vascular endothelium) is an important factor for efficient drug development for targeted tumor therapy with minimized side effects. The technique used in this work – impedimetry – is a dedicated one for real-time monitoring of cells to distinguish short-term (0–2 hours) and long-term (0–72 hours) effects elicited by the drug or carrier–drug conjugates. The basic theory of impedimetry is that proliferation/viability of cells is well detectable by monitoring of the electric impedance (*Z*) in an AC environment, due to the electric insulator character of intact surface membranes composed of the phospholipid bilayer. Application of cytotoxic compounds results in disturbed electrophysical integrity (decreasing value of impedance) of surface membranes as a signal of cell death. While cell physiological responses of short-term exposures result in characteristic changes of cell morphology (e.g., spreading), long-term effects characteristically influence in particular the proliferation of cells, and therefore the cytotoxic effects. The presented dimensionless values of delta slope (DS) measure the difference between the slope of the curve corresponding to the treatment and that of the control curve in impedimetric recordings, the negative signs refer to the relative values to the identical control.

In the following, the long-term effects of GnRH-III-based conjugates are presented in detail (see Figure 3b–g and Figure 4b–g), whereas the data on short-term effects are presented in Supporting Information File 2. As mentioned above, the modified cytotoxic/cardiotoxic moiety of antitumor drugs in GnRH conjugates is focused in the present work.

Results

Synthesis of GnRH derivative–drug conjugates

In this study, the cardiotoxic effect of 15 GnRH-III–drug conjugates [14,15,20-25] as potential drug delivery systems was determined and compared with that of Zoptarelin doxorubicin (AN-152), a compound that reached phase III clinical trials. The codes of the GnRH–drug conjugates described here are shown in Figure 1 and Figure 2.

The GnRH derivatives were prepared by solid phase peptide synthesis (SPPS) according to Fmoc/*t*-Bu strategy (Supporting Information File 1). Three drug molecules, doxorubicin (Dox), daunorubicin (Dau) and methotrexate (Mtx), were employed in the preparation of drug conjugates. Dox has three potential conjugation sites; i) a primary OH group at C-14 on the aglycone part, which is suitable for ester bond formation, ii) an oxo group at C-13 is available for the generation of an oxime linkage and iii) the amino group on the daunosamine sugar moiety, which can be used for amide bond formation. The difference between Dox and Dau is the lack of the primary OH

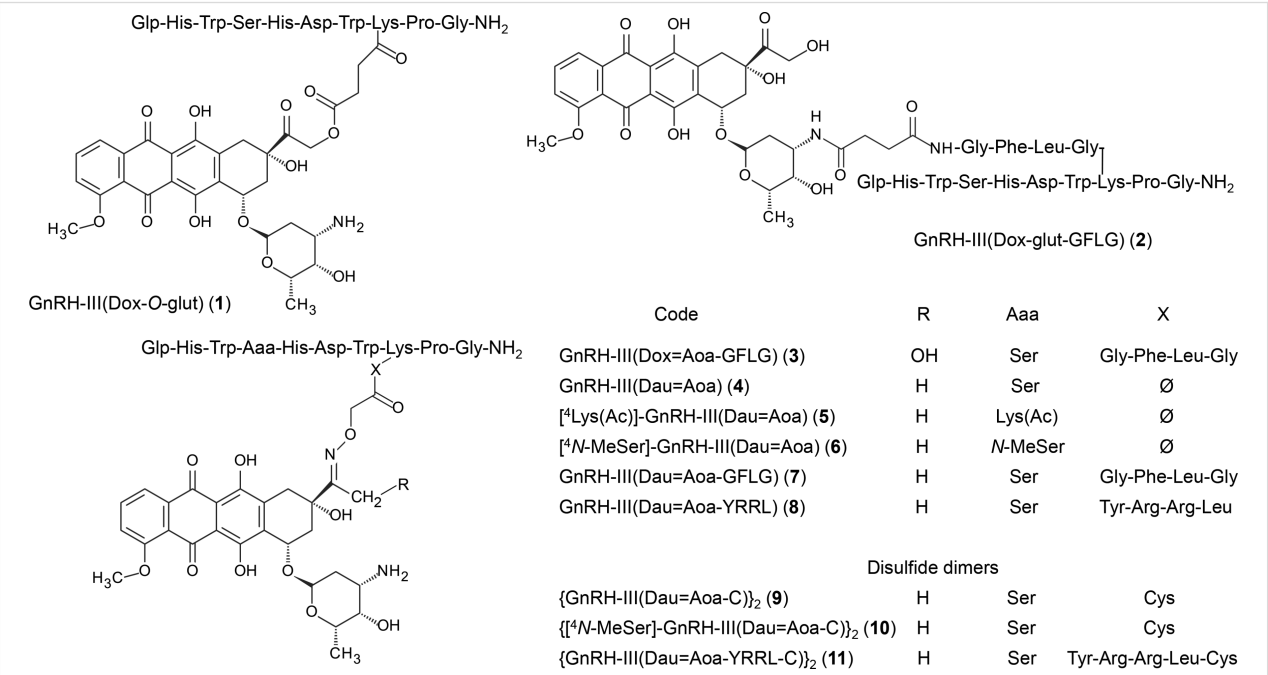

Code	R	Aaa	X
GnRH-III(Dox=Aoa-GFLG) (**3**)	OH	Ser	Gly-Phe-Leu-Gly
GnRH-III(Dau=Aoa) (**4**)	H	Ser	Ø
[^{4}Lys(Ac)]-GnRH-III(Dau=Aoa) (**5**)	H	Lys(Ac)	Ø
[^{4}*N*-MeSer]-GnRH-III(Dau=Aoa) (**6**)	H	*N*-MeSer	Ø
GnRH-III(Dau=Aoa-GFLG) (**7**)	H	Ser	Gly-Phe-Leu-Gly
GnRH-III(Dau=Aoa-YRRL) (**8**)	H	Ser	Tyr-Arg-Arg-Leu
Disulfide dimers			
{GnRH-III(Dau=Aoa-C)}$_2$ (**9**)	H	Ser	Cys
{[^{4}*N*-MeSer]-GnRH-III(Dau=Aoa-C)}$_2$ (**10**)	H	Ser	Cys
{GnRH-III(Dau=Aoa-YRRL-C)}$_2$ (**11**)	H	Ser	Tyr-Arg-Arg-Leu-Cys

Figure 1: Chemical structures of the GnRH-drug conjugates synthesized and investigated in the present work. Abbreviations: Aoa: aminooxyacetyl; Dox: doxorubicin; Dau: daunorubicin; Mtx: methotrexate; Glp: pyroglutamic acid; gult: glutaric acid.

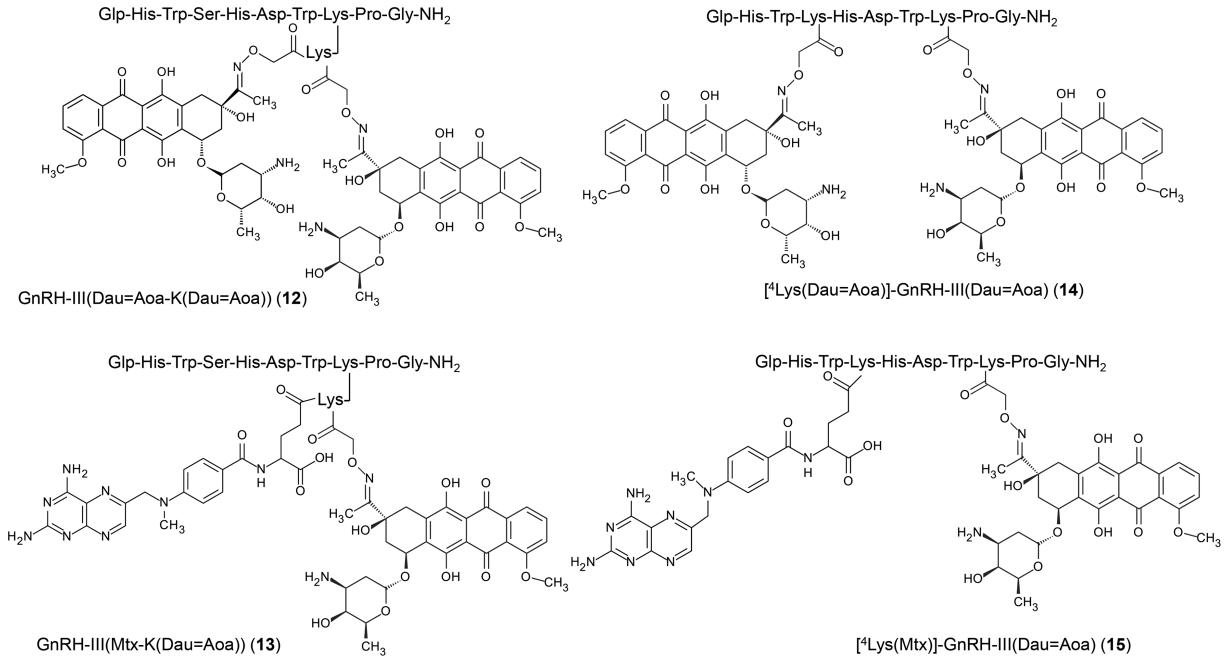

Figure 2: Chemical structures of the bifunctional GnRH-drug conjugates synthesized and investigated in the present work. Abbreviations: Aoa: aminooxyacetyl; Dox: doxorubicin; Dau: daunorubicin; Mtx: methotrexate; Glp: pyroglutamic acid.

group in the case of the latter one. Therefore, Dau cannot be attached to peptide carriers via an ester bond. Mtx contains a glutamic acid whose carboxyl groups are suitable for the attachment to peptides through amide bond (this can be carried out on a solid support, prior to the cleavage of the peptide from the resin). In the conjugates used as reference compounds, Dox was coupled to the Lys in position 8 of GnRH-III through glutaric acid linked via an ester bond (*O*-glut) (**1**) (similarly to AN-152) or an amide bond through the sugar moiety (glut) (**2**) in solution. Furthermore, an oxime linkage was formed between Dox and an aminooxyacetyl moiety connected to the enzymatically cleavable tetrapeptide spacer GFLG (**3**). These conjugates were prepared with the aim of comparing the influence of the homing peptide and of the type of the linkage on the toxic effect. Dau was coupled to the GnRH-III derivatives via oxime linkage in all cases. The oxime ligation was carried out under slightly acidic (pH 5) conditions [26] and the drug was attached directly either to GnRH-III (**4**) or to its derivatives in which Ser in position 4 was replaced by Lys(Ac) (**5**) or *N*-MeSer (**6**), modifications that increased the enzymatic stability of the conjugates [20]. Furthermore, Dau was attached to GnRH-III through two different Cathepsin B enzymatic cleavable spacers GFLG (**7**) and YRRL (**8**). These conjugates were used to compare the influence of sequence modification, the presence or absence of a spacer as well as the type of spacers on toxicity. Disulfide dimers were also developed based on conjugates **4**, **6** and **8,** resulting in compounds **9**, **10** and **11**. Four conjugates with two identical (Dau) or different (Dau and Mtx) drug molecules were also prepared. When the native GnRH-III was used, an additional Lys was incorporated to the side chain of Lys in position 8. A Dau was attached to its ε-amino group and the second Dau (**12**) or the Mtx (**13**) was connected to the α-amino group. In conjugate **14,** the two Dau molecules were linked to two lysines in positions 4 and 8, while in conjugate **15** Dau was replaced by Mtx on the ^{4}Lys. Using these compounds, the effect of the type and number of drug molecules could be compared. The isomers of Mtx conjugates (either α- or γ-carboxyl linked) were not separated, because our previous studies showed no significant differences in the biological activity of Mtx isomers in conjugated form [24].

Fmoc-protected Dox was reacted with glutaric anhydride in DMF. The prepared Fmoc-Dox-14-*O*-hemiglutarate was used for conjugation using PyBOP in the presence of NMM, followed by the removal of Fmoc group with 10% piperidine in DMF providing the conjugates AN-152 and **1**. It is worth mentioning that an O–N acyl shift (from the aglycone OH group to the daunosamine NH_2 group ca. in 10–20%) was observed during the synthesis of conjugates containing an ester bond. This could be detected by the MS fragmentation of the conju-

gate between the aglycon part and sugar moiety resulted in fragments in which the peptide was attached either the aglycon OH group or the amino group of sugar moiety [23]. When unprotected Dox was used for the reaction with glutaric anhydride, the amino group was modified with glutaric acid followed by its attachment to the ε-amino group of ^{8}Lys in GnRH-III. The conjugation was carried out in the presence of PyBOP/HOBt coupling agents resulting in conjugate **2**. For the preparation of the oxime linkage, a Boc protected aminooxyacetic acid was attached to the Lys side chain on solid phase prior to the cleavage of the peptide derivatives from the resin. The oxime bond formation was carried out in 0.2 M NaOAc solution at pH 5 for 12 hours. In contrast to the synthesis of the conjugates with ester or amide bond, the oxime bond formation was almost quantitatively. In the case of the conjugates with two different drug molecules or Lys(Ac) in position 4, orthogonal protecting schemes were applied during the SPPS. For the preparation of the disulfide dimers, an additional Cys was attached to the ε-amino group of ^{8}Lys of the GnRH-III derivatives. First, Dau was linked to the aminooxyacetyl moiety, followed by the oxidation in 10 mM Tris buffer, pH 8/DMSO (1:1, v/v) solution.

The purity of the prepared conjugates presented in the original manuscripts or in their Supplementary Information was over 95% in all cases and there were no free drug molecules among the impurities. The summary of the characteristic data of the conjugates are presented in Supporting Information File 1 (Table S1).

In vitro cytostasis

The in vitro cytostatic effect of GnRH-III–drug conjugates was determined on MCF-7 human breast and HT-29 human colon adenocarcinoma cells by 3-(4,5-dimethylthiazol-2-yl)-2,5-diphenyltetrazolium bromide (MTT) assay as it was described in the published articles [14,15,20-25]. All investigated bioconjugates exerted in vitro cytostatic effect with IC_{50} values in low μM range except the one (**2**) with amide bond between the drug and carrier molecule. The data are summarised below in Table 1. The data indicated, that conjugate **1** in which Dox linked via an ester bond to the homing peptide showed the highest antitumor activity on both cell lines. The conjugates with one Dau linked through oxime linkage showed similar potency on both types of cell. Small improvement of cytostatic effect could be detected when enzyme labile spacer was incorporated between the drug and GnRH peptide (conjugates **7**, **8**) compared with the basic conjugate (**4**). The enhancement of activity was also detected in case of dimers (**9**–**10**) compared to the monomers (**4**, **6**, **8**). The highest improvement in cytostatic effect was observed when Ser in position 4 of GnRH-III was replaced by Lys(Ac) (**5**), especially on HT-29 cells. However, the incorporation of *N*-MeSer (**6**) in this position lowered the efficacy. The conjugates with two drug molecules (either identical (**12**, **14**) or different (**13**, **15**)) belonged to the most efficient conjugates but no further significant improvement was detected to the conjugate **5** with one Dau.

Measurements on human endothelial cells (HUVEC)

The effect of chemotherapeutic drugs (doxorubicin, daunorubicin, methotrexate)

The effect of drugs used as chemotherapeutic agents was evaluated at seven different concentrations (10^{-12}–10^{-6} mol/L) on human endothelial cells. Doxorubicin and daunorubicin significantly increased the impedance level (DS: 0.063 and 0.037 for doxorubicin and 0.047 and 0.055 for daunorubicin, respectively) at the two highest concentration levels (10^{-6} and 10^{-7} mol/L) on short-term treatment (Supporting Information File 2, Table S1). However, on long-term (0–72 hours) relation, a significant decrease was measured at 10^{-6} mol/L concentration for doxorubicin (DS: −0.086) and at 10^{-6} and 10^{-7} mol/L concentration for daunorubicin (DS: −0.019 and −0.007, respectively), indicating an eventual cytotoxic effect. Methotrexate showed effects on a much smaller scale – slight but significant decrease in impedance in the middle concentration range (10^{-8} and 10^{-9} mol/L) in long-term (DS −0.022 and −0.017, respectively, Figure 3a and Supporting Information File 2, Table S1a). Considering that in this experiment the major effects were found at the higher concentrations of drugs, in the following experiments with drug–peptide conjugates only the three highest concentrations (10^{-8}, 10^{-7} and 10^{-6} mol/L) were investigated.

The effect of GnRH conjugates containing doxorubicin

In this study, three GnRH-III–Dox conjugates [GnRH-III(Dox-*O*-glut) (**1**), GnRH-III(Dox-glut-GFLG) (**2**), GnRH-III(Dox=Aoa-GFLG) (**3**)] were investigated in addition to AN-152, a doxorubicin-containing GnRH-I conjugate. In a short-term study, only conjugate **2** in which Dox is attached through an amide bond to the homing peptide showed a significant positive effect at 10^{-6} mol/L concentration (DS 0.058); nevertheless, the ester bond-linked conjugates AN-152 and **1** also proved to elicit a non-significant increase of the impedance measured (Supporting Information File 2, Table S2a). On long-term, at concentrations of 10^{-7} and 10^{-6} mol/L, besides doxorubicin (DS −0.019 and −0.046, respectively), AN-152 (DS −0.029 and −0.051, respectively), GnRH-III(Dox-*O*-glut) (DS −0.028 and −0.054, respectively) and GnRH-III(Dox-glut-GFLG) (DS −0.017 and −0.042) also showed a significant cytotoxic effect, while GnRH-III(Dox=Aoa-GFLG) had marginal effect (DS −0.009) only at the highest concentration level (10^{-6} mol/L) (Figure 3b and 3c; Supporting Information File 2, Table S2a).

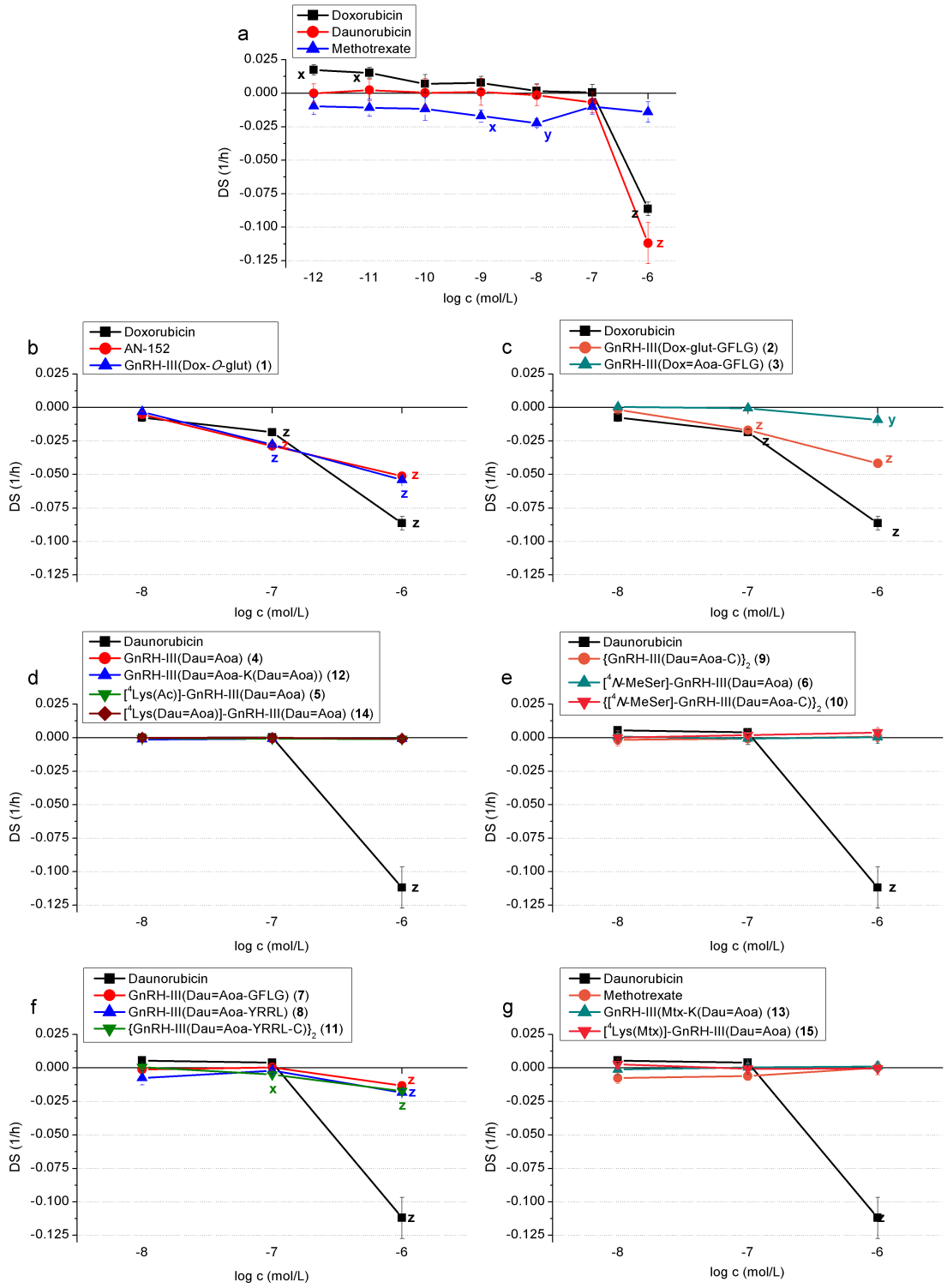

Figure 3: Long-term cytotoxic effects – impedimetrically registered negative effect on cell proliferation/viability – of chemotherapeutic drugs (doxorubicin, daunorubicin, methotrexate) and their GnRH-III conjugates on HUVEC cells. (a) Chemotherapeutic drugs (doxorubicin, daunorubicin, methotrexate); (b) GnRH conjugates containing doxorubicin without spacer sequence; (c) with spacer sequence GFLG; (d) oxime bond-linked, mono- and bifunctional daunorubicin-GnRH-III conjugates without spacer and modified in position 4 with Lys; (e) {GnRH-III(Dau=Aoa-C)}$_2$ dimer and conjugates modified in position 4 with *N*-MeSer; (f) GFLG or YRRL spacer containing monomer and dimer conjugates (g) GnRH-III conjugates containing methotrexate and daunorubicin.

The effect of oxime bond-linked daunorubicin–GnRH-III conjugates

Ten GnRH-III conjugates containing daunorubicin were investigated in this study. Seven of these compounds (GnRH-III(Dau=Aoa) (**4**), [^{4}Lys(Ac)]-GnRH-III(Dau=Aoa) (**5**), [^{4}*N*-MeSer]-GnRH-III (**6**), {GnRH-III(Dau=Aoa-C)}$_2$ (**9**), {[^{4}*N*-MeSer]-GnRH-III(Dau=Aoa-C)}$_2$ (**10**), GnRH-III(Dau=Aoa)-K(Dau=Aoa)) (**12**) and [^{4}Lys(Dau=Aoa)]-GnRH-III(Dau=Aoa) (**14**) completely lost the cytotoxic effect that was detected in the case of daunorubicin at high concentration levels, eliciting no effect at all. Even in short-term, only conjugate **10** increased significantly the measured impedance level (DS 0.017 in 10^{-6} mol/L), which is supposed to be a result of spreading of cells on the measuring electrode (Supporting Information File 2, Tables S3a and S4a). The three conjugates with spacer sequence GnRH-III(Dau=Aoa-GFLG) (**7**) (DS −0.013 in 10^{-6} mol/L), GnRH-III(Dau=Aoa-YRRL) (**8**) (DS −0.018 in 10^{-6} mol/L) and the dimeric {GnRH-III(Dau=Aoa-YRRL-C)}$_2$ (**11**) (DS −0.005 in 10^{-7} mol/L and −0.017 in 10^{-6} mol/L) retained the significant cytotoxic effect of daunorubicin, although this effect was somewhat diminished. (Figure 3d–f,; Supporting Information File 2, Tables S3a and S4a).

The effect of GnRH-III conjugates containing methotrexate and daunorubicin

Two conjugates containing methotrexate and daunorubicin were examined (GnRH-III(Mtx-K(Dau=Aoa)) (**13**) and [^{4}Lys(Mtx)]-GnRH-III(Dau=Aoa) (**15**)). On the short-term, conjugate **13** increased the measured impedance level significantly at the highest concentration (10^{-6} mol/L, DS 0.013) (Supporting Information File 2, Table S5a), while in the long-term study no significant effect was detected. Conjugate **15** showed no significant cytotoxic effect on either short- or long-term (Figure 3g; Supporting Information File 2, Table S5a).

Measurements on human cardiomyocytes (HCM)

The effect of chemotherapeutic drugs (doxorubicin, daunorubicin, methotrexate)

Compared to their effect on endothelial cells, doxorubicin and daunorubicin showed quite a similar effect on cardiomyocytes. On short-term, both drugs increased the measured impedance level at the highest (10^{-6} mol/L) concentration (DS 0.019 and 0.031, respectively) (Supporting Information File 2, Table S1b), while on long-term they exhibited significant cytotoxic effect at the two highest concentration levels (10^{-7} and 10^{-6} mol/L) (DS −0.006 and −0.016 for doxorubicin, and −0.007 and −0.019 for daunorubicin, respectively) (Figure 4a). In case of methotrexate, however, no significant effect was measured (Figure 4a and Supporting Information File 2, Table S1b). As in the case of endothelial cells, in the following experiments, only the three highest concentrations (10^{-8}, 10^{-7} and 10^{-6} mol/L) were evaluated. The investigated conjugates were the same as the ones used in the experiments with endothelial cells.

The effect of doxorubicin-containing GnRH conjugates

Two of the four investigated compounds, conjugate **1** (DS 0.012 in 10^{-6} mol/L) and **2** (DS 0.009 in 10^{-8} mol/L and 0.008 in 10^{-6} mol/L) exhibited a positive effect, similar to that of doxorubicin on short-term (the latter even at low concentration) (Supporting Information File 2, Table S2b). On long term, all of them had significant cytotoxic effect, conjugate **1** at all measured (10^{-8}, 10^{-7} and 10^{-6} mol/L) concentrations (DS −0.002, −0.00811 and −0.025, respectively), AN-152 (DS −0.008 and −0.023, respectively) and conjugate **2** (DS −0.004 and −0.019, respectively) at 10^{-7} and 10^{-6} mol/L concentrations, while the cytotoxicity of conjugate **3** was expressed only at the highest (10^{-6} mol/L) concentration and with a reduced strength of efficiency (DS −0.007). (Figure 4b and 4c; Supporting Information File 2, Table S2b).

The effect of oxime bond-linked daunorubicin–GnRH-III conjugates

In short-term, only conjugate **9** increased the measured impedance level significantly at the highest (10^{-6} mol/L) concentration (DS 0.003) (Supporting Information File 2, Table S3b and S4b). On long-term, six conjugates (**4, 6, 7, 9, 12** and **14)** completely lost their cytotoxic effect. Conjugates **5, 8** and **11** had significant cytotoxic effect at a 10^{-6} mol/L concentration (DS −0.003, −0.004 and −0.004, respectively), while conjugate **10** at concentrations of 10^{-7} mol/L and 10^{-6} mol/L, too (DS −0.003 and −0.005, respectively). However, these cytotoxic effects were much weaker than that of daunorubicin (Figure 4d–f; Supporting Information File 2, Table S3b and Table S4b).

The effect of GnRH-III conjugates containing methotrexate and daunorubicin

In contrast to daunorubicin but similarly to methotrexate, none of the two investigated mixed drug–GnRH-III conjugates (**13** and **15**) exerted any significant cytotoxic effect on cardiomyocytes (Figure 4g; Supporting Information File 2, Table S5b).

Discussion

The cardiovascular adverse effects of two chemotherapeutic agents, doxorubicin and daunorubicin, are well documented in the literature, while those of methotrexate are incidental or rare at most [18,19]. The results of our study are in agreement with the published ones: doxorubicin and daunorubicin had an in vitro cytotoxic effect both on cardiomyocytes and endothelial cells, while methotrexate had no cytotoxic effect on cardiomyocytes; furthermore, its cytotoxic effect was detectable only in

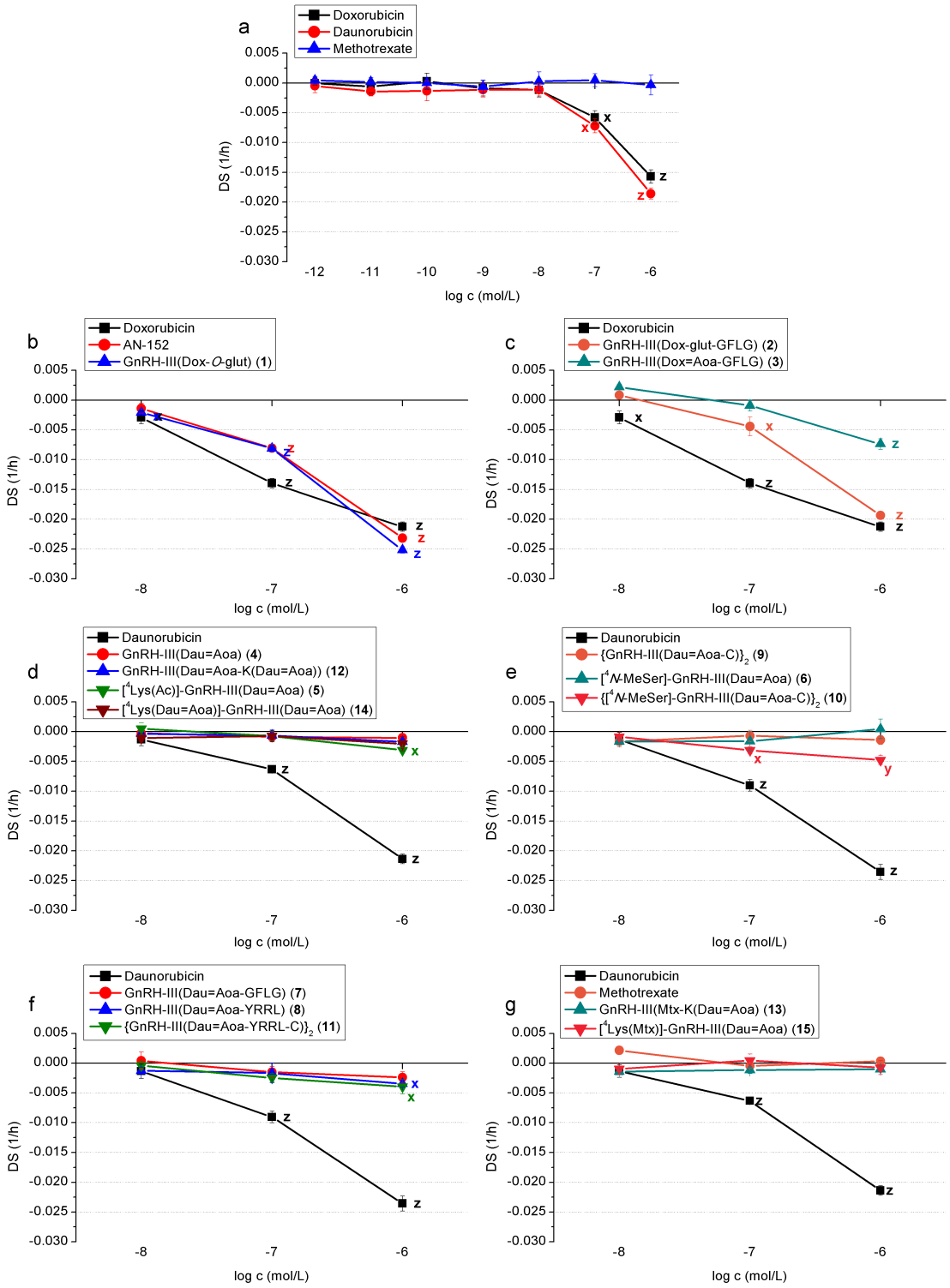

Figure 4: Long-term cytotoxic effects – impedimetrically registered negative effect on cell proliferation and viability – of chemotherapeutic drugs (doxorubicin, daunorubicin, methotrexate) and their GnRH-III conjugates on HCM cells. (a) Chemotherapeutic drugs (doxorubicin, daunorubicin, methotrexate); (b) GnRH conjugates containing doxorubicin without spacer sequence; (c) with spacer sequence GFLG; (d) oxime bond-linked, mono- and bifunctional daunorubicin-GnRH-III conjugates without spacer and modified in position 4 with Lys; (e) {GnRH-III(Dau=Aoa-C)}$_2$ dimer and conjugates modified in position 4 with *N*-MeSer; (f) GFLG or YRRL spacer containing monomer and dimer conjugates; (g) GnRH-III conjugates containing methotrexate and daunorubicin.

short-term on endothelial cells, while the long-term negative effects disappeared. (Figure 3a and Figure 4a; Supporting Information File 2, Table S1a and b).

AN-152 is a GnRH-I conjugate containing doxorubicin, which has been described to have a strong antitumor effect on a large number of human cancers and reached phase III clinical trials; however, it has recently been discontinued [12]. This drug conjugate was used as a reference compound in our comparative study on the cardiotoxicity of GnRH-III conjugates. In these experiments, AN-152 exerted a cytotoxic effect (in 10^{-6} mol/L and 10^{-7} mol/L concentration) on cardiomyocytes, like that of free doxorubicin, but to a moderate extent. The same cytotoxic effect was observed on endothelial cells, as well; thus, despite its good antitumor effect, AN-152 does not represent a conjugate with the ideal safety profile. (Figure 3b and Figure 4b; Supporting Information File 2, Table S2a and b).

The GnRH-III analogue of AN-152, GnRH-III(Dox-*O*-glut) (**1**) showed comparable antitumor effect with that of AN-152 [14]. Results of our study indicate that conjugate **1** had similar cytotoxic effect as doxorubicin and AN-152 on endothelial cells at the two highest concentrations (10^{-7} and 10^{-6} mol/L). In contrast, these conjugates showed significantly lower toxicity at 10^{-7} mol/L, but a slightly higher toxicity at the highest concentration level (10^{-6} mol/L) on cardiomyocytes in a long-term experiment. It is worth mentioning that none of the compounds showed toxicity on any cell types in a short-term experiment. (Figure 3b and Figure 4b; Supporting Information File 2, Table 2a and b).

The two Dox–GnRH-III conjugates containing a GFLG spacer sequence (GnRH-III(Dox-glut-GFLG) (**2**), GnRH-III(Dox=Aoa-GFLG) (**3**)) retained the cytotoxic effect of doxorubicin both on HMC cardiomyocytes and HUVEC endothelial cells in the long-term study. The oxime bond-linked Dox conjugate (**3**) showed significantly lower toxicity on both cell types, while conjugate **2** had a similar concentration-dependent toxicity to that of the ester bond-linked conjugates on endothelial cells. The toxicity of the latter conjugate was lower on cardiomyocytes; it was significant at a concentration of 10^{-7} mol/L and moderate at 10^{-6} mol/L. (Figure 3c and Figure 4c; Supporting Information File 2, Table 2a and b). Interestingly, when Dox (conjugate **3**) was replaced by Dau (**7**) the toxicity on HUVEC cells was almost identical, while on HMC cells a lower effect was observed at the highest concentration level. The replacement of GFLG spacer to YRRL slightly but not significantly increased the toxicity of the conjugates, result that might be explained by the higher instability of YRRL spacer in cell culture medium. The lack of an enzymatically cleavable spacer resulted in conjugate **4** without toxic effects on any cardiac cell types. Because the oxime bond-linked Dau conjugates with or without spacers showed a similar antitumor effect on cancer cells, conjugate **4** could be the safest compound for cancer treatment. The conjugate **5** in which Ser in position 4 of GnRH-III was replaced by Lys(Ac) had a moderately increased toxicity on HMC cells at the highest concentration but not on HUVEC cells compared to **4**. In contrast, the incorporation of *N*-MeSer resulted in conjugate **6** that did not show toxicity on any cardiac cell types through the whole concentration range measured. These trends correlate with the antitumor activity of the conjugates. It was also found that the dimerization of Dau containing conjugates (**9**–**11**) did not lead to a significant change in toxicity on any cardiac cell types, except conjugate {[^{4}*N*-MeSer]-GnRH-III(Dau=Aoa-C)}$_2$ (**10**) that showed higher cytotoxicity on cardiomyocytes. It is worth mentioning that the dimerization increased the enzymatic stability of the conjugates without losing their antitumor effect. Because conjugate **9** with significant antitumor effect did not show cytotoxicity either on HMC or on HUVEC cells, it might be a promising and safe candidate for targeted therapy.

None of the conjugates (**12**–**15**) containing two drug molecules, independent on their type (Dau, Mtx) or attachment site, showed cytotoxicity on any of the tested cell types. The two Dau containing conjugates (**12**, **14**) showed a higher antitumor effect on MCF-7 human breast, HT-29 human colon and LNCaP human prostate cancer cells in vitro than that of conjugate **4**, but not of conjugate **5**. Conjugates **13** and **15** containing one Mtx and one Dau were more effective only on HT-29 cells in comparison with conjugate **4**. Considering the lack of toxicity of these conjugates with two drug molecules, they might be good candidates for tumor drug targeting for the treatment of GnRH receptor-positive cancers.

In respect of potential clinical applications of the tested conjugates in the future, a table was prepared (Table 1) which helps to compare cytotoxic efficacy (IC_{50}) of the 15 GnRH-based antitumor conjugates in 3 reference tumor cell lines representing the most frequent malignancies (breast cancer – MCF-7, colorectal adenocarcinoma – HT-29 and acute monocytic leukemia – MonoMac6). In parallel, the cardiotoxic effects of the 15 conjugates are also demonstrated in the most important two targets of cardiac tissue (myocytes and endothelium). Data presented in Table 1 provide a good basis for structure–activity relationship analysis of the reported results. Comparison of IC_{50} values of conjugates possessing no cardiotoxicity (no cytotoxic effect both in HCM and HUVEC) shows that effectiveness of GnRH-based drug delivery is depending on the histological classification of the target tumor. Majority of the tested compounds (**4, 6, 12, 15**) possess the best IC_{50}-s in the acute monocytic leukemia model (MonoMac6), while in some

Table 1: Comparative study of cytotoxic effects and cardiotoxicity elicited by GnRH-based antitumor compounds (**1**–**15**) and reference substances (AN-152, Dox, Dau, Mtx). IC_{50} values show antitumor cytotoxic characteristics of the conjugates in human breast cancer (MCF-7), human colorectal adenocarcinoma (HT-29) and human acute monocytic leukemia (MM6) derived cell lines as representative tumor cells. Human cardiac myocytes (HCM) and human umbilical vein endothelial cells (HUVEC) as the chief targets of cardiotoxic compounds were studied and compared with tumor targets.

	Conjugates	IC_{50} values (μM)					Cardiotoxicity	
		MCF-7	HT-29	Ref.	MonoMac6	Ref.	HCM	HUVEC
	AN-152	0.2 ± 0.1	1.9 ± 0.3	[23]	0.035 ± 0.01	[27]	+++	+++
1	GnRH-III(Dox-*O*-glut)	0.1 ± 0.1	2.4 ± 0.2	[23]	0.039 ± 0.01	[27]	+++	+++
2	GnRH-III(Dox-glut-GFLG)	>100	>100	[14]	0.089 ± 0.02	[27]	+++	+++
3	GnRH-III(Dox=Aoa-GFLG)	5.4 ± 1.9	46.1 ± 6.1	[15]	0.430 ± 0.04	[28]	++	++
4	GnRH-III(Dau=Aoa)	6.5 ± 1.8	27.8 ± 4.2	[20]	>>1	[27]	0	0
5	[^{4}Lys(Ac)]-GnRH-III(Dau=Aoa)	3.1 ± 1.7	7.4 ± 2.6	[20]	0.925 ± 0.07	[28]	+	0
6	[^{4}*N*-MeSer]-GnRH-III(Dau=Aoa)	10.6 ± 2.1	nd	[20]	>>1	[28]	0	0
7	GnRH-III(Dau=Aoa-GFLG)	3.9 ± 1.2	22.5 ± 1.7	[21]	0.894 ± 0.25	[27]	+	++
8	GnRH-III(Dau=Aoa-YRRL)	1.8 ± 0.5	28.6 ± 5.5	[21]	>>1	[28]	+	++
9	[GnRH-III(Dau=Aoa-C)]$_2$	4.1 ± 0.8	nd	[22]	1.688 ± 0.41	[27]	0	0
10	{[^{4}*N*-MeSer]-GnRH-III(Dau=Aoa-C)}$_2$	6.2 ± 1.5	nd	[22]	0.783 ± 0.09	[28]	+	0
11	{GnRH-III(Dau=Aoa-YRRL-C)}$_2$	nd	nd		0.420 ± 0.05	[28]	+	++
12	GnRH-III(Dau=Aoa-K(Dau=Aoa))	3.0 ± 0.4	5.6 ± 2.0	[25]	>>1	[28]	0	0
13	GnRH-III(Mtx-K(Dau=Aoa))	5.4 ± 0.7	5.6 ± 3.0	[24]	1.413 ± 0.39	[28]	0	0
14	[^{4}Lys(Dau=Aoa)]-GnRH-III(Dau=Aoa)	2.9 ± 0.9	6.8 ± 1.0	[25]	0.513 ± 0.04	[28]	+	0
15	[^{4}Lys(Mtx)]-GnRH-III(Dau=Aoa)	5.8 ± 1.1	3.6 ± 1.5	[24]	>>1	[28]	0	0
	doxorubicin (Dox)	0.1 ± 0.0	0.1 ± 0.0	[23]	0.007 ± 0.0001	[27]	+++	+++
	daunorubicin (Dau)	0.4 ± 0.1	0.3 ± 0.2	[23]	0.00008 ± 0.0001	[27]	+++	+++
	methotrexate (Mtx)	nd	1.4 ± 0.6	[25]	0.008 ± 0.0002	[28]	0	+

cases the breast cancer (**9**) or colorectal adenocarcinoma (**9, 13**) proved to be also sensible to the Dau containing conjugates. On the other hand there are even sad lessons of the comparative study, some mainly Dox containing conjugates (**1**–**3**) proved to have strong cardiotoxic effects; however, they had moderate cytotoxicity (IC_{50}) in the compared three tumorous cell lines.

Conclusion

In the present study, the cytotoxic effect of sixteen GnRH-based conjugates containing doxorubicin, daunorubicin and methotrexate was determined on human cardiomyocytes and endothelial cells using an impedimetric technique. Seven conjugates with no cytotoxic effect on either cell types were identified, with two more conjugates with significantly milder cytotoxic effect. Based on these results, the monomeric GnRH-III(Dau=Aoa), the two multifunctional conjugates, [^{4}Lys(Dau=Aoa)]-GnRH-III(Dau=Aoa) and GnRH-III(Dau=Aoa-K(Dau=Aoa)), the modified GnRH-III containing compound, ([^{4}*N*-MeSer]-GnRH-III(Dau), the dimeric {GnRH-III(Dau-C)}$_2$ and the two multifunctional conjugates containing two different chemotherapeutic drugs, GnRH-III(Mtx-K(Dau=Aoa)) and [^{4}Lys(Mtx)]-GnRH-III(Dau=Aoa) are considered ideal compounds for tumor specific drug delivery with increased safety profiles; and in the future, could be the candidates for the development of effective chemotherapeutics with no cardiotoxic side effects.

Experimental

For experimental procedures and structures of the GnRH-based conjugates investigated in the present study see Supporting Information File 1.

Supporting Information

Supporting Information File 1

Experimental part – synthesis.
[https://www.beilstein-journals.org/bjoc/content/supplementary/1860-5397-14-136-S1.pdf]

Supporting Information File 2

Supplementary tables – comparative data of short- and long-term effects of GnRH-drug conjugates on cardiomyocytes and endothelial cells.
[https://www.beilstein-journals.org/bjoc/content/supplementary/1860-5397-14-136-S2.pdf]

Acknowledgements

The authors express their gratitude for the support provided by the National Research, Development and Innovation Office (NKFIH K119552), Hungary. The structures of the conjugates were made by MarvinSketch provided by ChemAxon (Budapest, Hungary). The heart image in the graphical abstract is derived from the image "Heart anterior exterior view" by Patrick J. Lynch, illustrator, and C. Carl Jaffe, MD, cardiologist, an image published under a Creative Commons Attribution 2.5 license.

ORCID® iDs

Pál Soós - https://orcid.org/0000-0002-3708-483X
Gábor Mező - https://orcid.org/0000-0002-7618-7954
László Kőhidai - https://orcid.org/0000-0002-9002-0296

References

1. Urbanski, H. F. *Front. Endocrinol.* **2012,** *3,* 20. doi:10.3389/fendo.2012.00020
2. Grundker, C.; Gunthert, A. R.; Westphalen, S.; Emons, G. *Eur. J. Endocrinol.* **2002,** *146,* 1–14. doi:10.1530/eje.0.1460001
3. Demirci, A.; Alkış, N.; Dane, F.; Durnalı, A.; Yazıcı, O. K.; Rzayev, R.; Kaya, S.; Yazılıtaş, D.; İnanç, M.; Özçelik, M.; Akman, T.; Kaplan, M. A.; Günaydın, Y.; Ulaş, A.; Sönmez, O.; Tokluoğlu, S.; Gököz Doğu, G.; Bal, O.; Gümüş, M. *Asia-Pac. J. Clin. Oncol.* **2017,** *14,* e145–e151. doi:10.1111/ajco.12685
4. Limonta, P.; Montagnani Marelli, M.; Mai, S.; Motta, M.; Martini, L.; Moretti, R. M. *Endocr. Rev.* **2012,** *33,* 784–811. doi:10.1210/er.2012-1014
5. Sower, S. A.; Chiang, Y. C.; Lovas, S.; Conlon, J. M. *Endocrinology* **1993,** *132,* 1125–1131. doi:10.1210/en.132.3.1125
6. Herédi-Szabó, K.; Lubke, J.; Toth, G.; Murphy, R. F.; Lovas, S. *Peptides* **2005,** *26,* 419–422. doi:10.1016/j.peptides.2004.10.007
7. Mező, G.; Czajlik, A.; Manea, M.; Jakab, A.; Farkas, V.; Majer, Z.; Vass, E.; Bodor, A.; Kapuvári, B.; Boldizsár, M.; Vincze, B.; Csuka, O.; Kovács, M.; Przybylski, M.; Perczel, A.; Hudecz, F. *Peptides* **2007,** *28,* 806–820. doi:10.1016/j.peptides.2006.12.014
8. Mezö, I.; Lovas, S.; Pályi, I.; Vincze, B.; Kálnay, A.; Turi, G.; Vadász, Z.; Seprödi, J.; Idei, M.; Tóth, G.; Gulyás, E.; Ötvös, F.; Mák, M.; Horváth, J. E.; Teplán, I.; Murphy, R. F. *J. Med. Chem.* **1997,** *40,* 3353–3358. doi:10.1021/jm9700981
9. Kovács, M.; Vincze, B.; Horváth, J. E.; Seprődi, J. *Peptides* **2007,** *28,* 821–829. doi:10.1016/j.peptides.2007.01.003
10. Mező, G.; Manea, M. *Expert Opin. Drug Delivery* **2010,** *7,* 79–96. doi:10.1517/17425240903418410
11. Nagy, A.; Schally, A. V.; Armatis, P.; Szepeshazi, K.; Halmos, G.; Kovacs, M.; Zarandi, M.; Groot, K.; Miyazaki, M.; Jungwirth, A.; Horvath, J. *Proc. Natl. Acad. Sci. U. S. A.* **1996,** *93,* 7269–7273. doi:10.1073/pnas.93.14.7269
12. Zoptarelin doxorubicin - AdisInsight. http://adisinsight.springer.com/drugs/800009722 (accessed Jan 17, 2018).
13. Lajkó, E.; Szabó, I.; Andódy, K.; Pungor, A.; Mező, G.; Kőhidai, L. *J. Pept. Sci.* **2013,** *19,* 46–58. doi:10.1002/psc.2472
14. Mezo, G.; Manea, M.; Szabo, I.; Vincze, B.; Kovacs, M. *Curr. Med. Chem.* **2008,** *15,* 2366–2379. doi:10.2174/092986708785909157
15. Szabó, I.; Manea, M.; Orbán, E.; Csámpai, A.; Bősze, S.; Szabó, R.; Tejeda, M.; Gaál, D.; Kapuvári, B.; Przybylski, M.; Hudecz, F.; Mező, G. *Bioconjugate Chem.* **2009,** *20,* 656–665. doi:10.1021/bc800542u
16. Escherich, G.; Zimmermann, M.; Janka-Schaub, G. *Pediatr. Blood Cancer* **2013,** *60,* 254–257. doi:10.1002/pbc.24273
17. Sun, X.; Liu, J.; Wang, Y.; Bai, X.; Chen, Y.; Qian, J.; Zhu, H.; Liu, F.; Qiu, X.; Sun, S.; Ji, N.; Liu, Y. *Oncotarget* **2017,** *8,* 49156–49164. doi:10.18632/oncotarget.17101
18. Shi, Y.; Moon, M.; Dawood, S.; McManus, B.; Liu, P. P. **2011,** *36,* 296–305. doi:10.1007/s00059-011-3470-3
19. Zhang, J.; Cui, X.; Yan, Y.; Li, M.; Yang, Y.; Wang, J.; Zhang, J. *Am. J. Transl. Res.* **2016,** *8,* 2862–2875.
20. Manea, M.; Leurs, U.; Orbán, E.; Baranyai, Z.; Öhlschläger, P.; Marquardt, A.; Schulcz, A.; Tejeda, M.; Kapuvári, B.; Továri, J.; Mező, G. *Bioconjugate Chem.* **2011,** *22,* 1320–1329. doi:10.1021/bc100547p
21. Orbán, E.; Mező, G.; Schlage, P.; Csík, G.; Kulić, Z.; Ansorge, P.; Fellinger, E.; Möller, H. M.; Manea, M. *Amino Acids* **2011,** *41,* 469–483. doi:10.1007/s00726-010-0766-1
22. Schreier, V. N.; Mező, G.; Orbán, E.; Dürr, C.; Marquardt, A.; Manea, M. *Bioorg. Med. Chem. Lett.* **2013,** *23,* 2145–2150. doi:10.1016/j.bmcl.2013.01.114
23. Schlage, P.; Mező, G.; Orbán, E.; Bősze, S.; Manea, M. *J. Controlled Release* **2011,** *156,* 170–178. doi:10.1016/j.jconrel.2011.08.005
24. Leurs, U.; Lajkó, E.; Mező, G.; Orbán, E.; Öhlschläger, P.; Marquardt, A.; Kőhidai, L.; Manea, M. *Eur. J. Med. Chem.* **2012,** *52,* 173–183. doi:10.1016/j.ejmech.2012.03.016
25. Leurs, U.; Mező, G.; Orbán, E.; Öhlschläger, P.; Marquardt, A.; Manea, M. *Biopolymers* **2012,** *98,* 1–10. doi:10.1002/bip.21640
26. Shao, J.; Tam, J. P. *J. Am. Chem. Soc.* **1995,** *117,* 3893–3899. doi:10.1021/ja00119a001
27. Kőhidai, L.; Lajkó, E.; Polgár, L.; Manea, M.; Mező, G. GnRH based drug targeting: Cell adhesion and migration modulator effects of GnRH derivatives in tumor cells. In *Gonadotropin-Releasing Hormone (GnRH): Production, Structure, and Function;* Sills, E. S., Ed.; Nova Science Publishers: New York, USA, 2013; pp 251–272.
28. Lajkó, E. Investigation of basic cell physiological activities induced by bioactive molecules in mammalian and unicellular models. Ph.D. Thesis, Semmelweis University, Budapest, Hungary, 2013.

License and Terms

BEILSTEIN JOURNAL OF ORGANIC CHEMISTRY

Comparative cell biological study of in vitro antitumor and antimetastatic activity on melanoma cells of GnRH-III-containing conjugates modified with short-chain fatty acids

Eszter Lajkó[*1], Sarah Spring[1,2], Rózsa Hegedüs[3], Beáta Biri-Kovács[3,4], Sven Ingebrandt[2], Gábor Mező[3,4] and László Kőhidai[1]

Full Research Paper

Open Access

Address:
[1]Department Genetics, Cell- and Immunobiology, Semmelweis University, Nagyvárad tér 4., 1089 Budapest, Hungary, [2]Department of Informatics and Microsystem Technology, University of Applied Sciences Kaiserslautern, Amerikastraße 1, 66482 Zweibrücken, Germany, [3]Research Group of Peptide Chemistry, Hungarian Academy of Sciences, Eötvös Loránd University, Pázmány Péter sétány 1/A, 1117 Budapest, Hungary and [4]Eötvös Loránd University, Faculty of Science, Institute of Chemistry, Pázmány Péter sétány 1/A, 1117 Budapest, Hungary

Email:
Eszter Lajkó[*] - lajesz@gmail.com

* Corresponding author

Keywords:
drug-targeting conjugates; gonadotropin-releasing hormone-III; holographic microscopy; impedimetry; short-chain fatty acids

Beilstein J. Org. Chem. **2018,** *14,* 2495–2509.
doi:10.3762/bjoc.14.226

Received: 03 March 2018
Accepted: 30 August 2018
Published: 26 September 2018

This article is part of the Thematic Series "Peptide–drug conjugates".

Guest Editor: N. Sewald

Abstract

Background: Peptide hormone-based targeted tumor therapy is an approved strategy to selectively block the tumor growth and spreading. The gonadotropin-releasing hormone receptors (GnRH-R) overexpressed on different tumors (e.g., melanoma) could be utilized for drug-targeting by application of a GnRH analog as a carrier to deliver a covalently linked chemotherapeutic drug directly to the tumor cells. In this study our aim was (i) to analyze the effects of GnRH-drug conjugates on melanoma cell proliferation, adhesion and migration, (ii) to study the mechanisms of tumor cell responses, and (iii) to compare the activities of conjugates with the free drug.

Results: In the tested conjugates, daunorubicin (Dau) was coupled to ^{8}Lys of GnRH-III (GnRH-III(Dau=Aoa)) or its derivatives modified with ^{4}Lys acylated with short-chain fatty acids (acetyl group in [^{4}Lys(Ac)]-GnRH-III(Dau=Aoa) and butyryl group in [^{4}Lys(Bu)]-GnRH-III(Dau=Aoa)). The uptake of conjugates by A2058 melanoma model cells proved to be time dependent. Impedance-based proliferation measurements with xCELLigence SP system showed that all conjugates elicited irreversible tumor growth inhibitory effects mediated via a phosphoinositide 3-kinase-dependent signaling. GnRH-III(Dau=Aoa) and [^{4}Lys(Ac)]-GnRH-

III(Dau=Aoa) were shown to be blockers of the cell cycle in the G2/M phase, while [^{4}Lys(Bu)]-GnRH-III(Dau=Aoa) rather induced apoptosis. In short-term, the melanoma cell adhesion was significantly increased by all the tested conjugates. The modification of the GnRH-III in position 4 was accompanied by an increased cellular uptake, higher cytotoxic and cell adhesion inducer activity. By studying the cell movement of A2058 cells with a holographic microscope, it was found that the migratory behavior of melanoma cells was increased by [^{4}Lys(Ac)]-GnRH-III(Dau=Aoa), while the GnRH-III(Dau=Aoa) and [^{4}Lys(Bu)]-GnRH-III(Dau=Aoa) decreased this activity.

Conclusion: Internalization and cytotoxicity of the conjugates showed that GnRH-III peptides could guard Dau to melanoma cells and promote antitumor activity. [^{4}Lys(Bu)]-GnRH-III(Dau=Aoa) possessing the butyryl side chain acting as a "second drug" proved to be the best candidate for targeted tumor therapy due to its cytotoxicity and immobilizing effect on tumor cell spreading. The applicability of impedimetry and holographic phase imaging for characterizing cancer cell behavior and effects of targeted chemotherapeutics with small structural differences (e.g., length of the side chain in ^{4}Lys) was also clearly suggested.

Introduction

The application of more selective, targeted drugs has become increasingly important in the treatment of tumors, where the use of chemotherapeutics with low therapeutic index is restricted by the adverse events coming from the toxicity of these drugs to normal cells [1]. One of the most promising approaches to diminish this kind of cytotoxic effects on healthy tissues is the employment of drug delivery systems directed specifically to cancer cells. The chemotherapeutic drug targeting is often based on the receptors for certain peptide hormones that are preferentially expressed by cancer cells. The utilization of these receptors for cancer cell targeting allows for minimizing the toxic side effects and producing high drug concentration selectively at the tumor site. In general, drug delivery systems consist of a targeting moiety in order to recognize a receptor on tumor cells and a cytotoxic drug covalently linked directly or through a suitable linker [1,2].

The gonadotropin-releasing hormone receptor (GnRH-R) is one of the receptors overexpressed on a wide range of tumors, and has limited expression in normal peripheral tissues [3]. The GnRH itself is a decapeptide hormone, which is responsible for the regulation of gonadal steroidogenesis and gametogenesis by integrating the nervous and endocrine system in the pituitary gland [4]. Regarding the targeted chemotherapy, it is highly advantageous that several native GnRH analogs, including the two human isoforms (GnRH-I and GnRH-II), and their synthetic derivatives have been reported to exert an antiproliferative effect in different types of tumors related (e.g., breast, endometrial cancer [5]) and unrelated (e.g., melanoma, colon carcinoma [6,7]) to reproductive organs. Considering these aspects, the GnRH could serve as a targeting unit with the aim to increase the concentration of an attached cytotoxic drug at the tumor cells overexpressing GnRH-R, and to decrease the unnecessary exposure of normal cells lacking GnRH-R [8]. Once the drug-targeting conjugate binds to its tumor-specific receptor, the receptor–conjugate complex can internalize into the cells by receptor-mediated manner, where the attached drug should be released from the conjugate in order to exert its antineoplastic activity [1].

The first GnRH-drug hybrids were developed by Schally and co-workers [9]. One of their most efficient conjugates was the zoptarelin doxorubicin (formerly known as AEZS-108 or AN-152), in which the superagonist [D-^{6}Lys]-GnRH-I allows the tumor targeting of the traditional chemotherapeutical drug doxorubicin covalently linked via an ester bond [3,10]. However, while in the phase II trial, zoptarelin doxorubicin showed promising antitumor activity combined with the lower rate of adverse effects in recurrent endometrial cancers [11], in the phase III study, there was no meaningful difference between the patients treated with zoptarelin doxorubicin or doxorubicin with respect to efficacy of agents and incidence of adverse effects (e.g., cardiac disorders typical for anthracyclines) [12]. The adverse effects were supposed to be related to (i) doxorubicin released early from the conjugate because of the instability of the ester linkage and (ii) [D-^{6}Lys]-GnRH-I induced endocrine side effects [8]. Therefore, recent strategies for the targeted chemotherapy favor conjugation methods resulting in a better stability of a conjugate in systemic circulation as well as GnRH derivatives with high affinity for tumor's GnRH-R and negligible endocrine activity [13,14].

The GnRH-III (Glp-His-Trp-Ser-His-Asp-Trp-Lys-Pro-Gly-NH_2), a native variant of GnRH, could display strong antiproliferative effects in the breast, prostate, colon carcinoma cell lines, whereas induce 500–1000 times less LH-release than GnRH-I derivatives [14]. In our previous studies, the side chain of Lys^8 was used for attachment of daunorubicin (Dau) via a more stable oxime bond through an aminooxyacetyl (Aoa) linker to form different drug-containing conjugates [15,16]. Based on the

enzymatic stability and capability of different Dau–GnRH-III conjugates to providing appropriate intracellular drug release [15], the oxime bond was used for coupling Dau to GnRH-III or its derivatives in the later studies.

There are some factors that could fundamentally limit the effectiveness of the GnRH-III-based targeting: (i) the relatively rapid proteolytic degradation of the peptide part [17], (ii) the variable density of the GnRH-R on cancer cells [18], (iii) the slow receptor-mediated endocytosis of the receptor–conjugate complex and (iv) the desensitization of GnRH-R [4,18].

The ^{3}Trp-^{4}Ser bond is a most susceptible site to be cleaved by proteolytic enzymes (e.g., chymotrypsin, angiotensin-converting enzyme). The substitution of Ser^{4} by its *N*-methyl analog (N-Me-Ser), or acetyl-Lys (Lys(Ac)) could improve the proteolytic stability of conjugates [17]. The results of in vitro and in vivo assays demonstrated that the conjugate containing Lys(Ac) in position 4 and Dau in position 8 ([^{4}Lys(Ac)]-GnRH-III(Dau=Aoa)) had higher tumor growth inhibition activity than the unmodified GnRH-III-based one (GnRH-III(Dau=Aoa)) [17]. It is worth mentioning that the free Lys in this position also increased the in vitro cytostatic effect of the conjugate; however, its cellular uptake and enzyme stability were even lower than the parent conjugate had [17]. Therefore, it was not used in any further experiments. Based on these findings next generation of Dau–GnRH-III bioconjugates was developed in which Ser in position 4 was replaced with Lys acylated with short-chain fatty acids with 2–6 and 13 carbon atoms by Hegedüs et al. [19]. The replacement of ^{4}Ser by Lys with a chain of 2–6 carbon atoms resulted in an increased cytostatic effect, while the conjugate with myristic acid (13 carbon atoms) had a lower activity compared to the GnRH-III(Dau=Aoa). Among these conjugates, [^{4}Lys(Bu)]-GnRH-III(Dau=Aoa) containing butyric acid (Bu) acylated at the ^{4}Lys residue was proved to be the most potent one in all different assays (enzymatic stability, cellular uptake, and in vitro antitumor activity) on HT-29 colon carcinoma cell lines [19]. The different hydrophobicity of conjugates having a short, fatty acid side chain (2–6 carbon atoms) could be excluded as an explanation for their different enzymatic stability and cellular uptake because these conjugates were found to have similar octanol–water partition index and membrane permeability. Nevertheless, the higher hydrophobicity (lower solubility) of the conjugate with myristic acid seemed to correlate with its increased stability, cellular uptake and weaker antitumor activity [17,19]. The increased cytostatic activity of Dau–GnRH-III conjugates acylated by a short-chain fatty acid as a "second drug" can be due to the known potential of short-chain fatty acids – especially butyric acid – to induce apoptosis in various tumor cell lines (e.g., colon [20], breast cancer cells [21]). Based on a former receptor binding experiment, the conjugates with Lys(Ac) or Lys(Bu) have a more suitable structure for receptor binding, which is even more preferential in case of the butyryl side chain; however, the even longer side chain linked to ^{4}Lys could negatively affect the fitting of the conjugates to the N-terminal part of the GnRH-R. On the basis of these findings [^{4}Lys(Bu)]-GnRH-III(Dau=Aoa), was chosen for the further studies (e.g., in vivo experiments [22]) to evaluate the suitability of this conjugate for targeted chemotherapy.

Malignant melanoma, despite the improving chemotherapeutic and surgical strategies, remains the leading cause of skin cancer deaths. The strong ability to disseminate metastases and to develop resistance to chemotherapy results in poor prognosis especially in advanced cases [23]. The expression GnRH-R was demonstrated in a very high percentage of human melanoma specimens derived from primary tumors or metastases and cell lines [24]. Activation of these receptors by means of GnRH agonists was shown to significantly decrease the proliferation and the motility of melanoma cell lines and the tumor growth inhibitory effect of a drug-containing GnRH conjugate (AN-207) clearly indicated that GnRH-R receptors are suitable for targeted tumor therapy [24,26]. Besides the well-established antitumor activity of GnRH variants (e.g., goserelin), their negative effects on tumor cell migration and invasion have been also demonstrated in melanoma cell lines [25,26].

There are also evidences that the short-chain fatty acids, including sodium butyrate and valproic acid, could inhibit the proliferation of melanoma cells both in in vitro (e.g., A2058 [27], B16 cell lines [28]) and in vivo experiments [28,29] or could abrogate the anticancer drug resistance as they are co-administrated with other chemotherapeutics [29,30]. Nevertheless, there is some controversy about the effects of short-chain fatty acids on the metastatic ability of melanoma cells, since both pro-invasive [31] and anti-invasive [29,32] activities have been described.

Taken together the aforementioned findings and considering the key roles of impaired adhesion and migratory phenotype of tumor cells in metastatic dissemination, we assumed that the Dau–GnRH-III conjugates substituted with short-chain fatty acids containing Lys may have not only the cytotoxic activity but also modulatory effects on cell adhesion and migration of melanoma cells. In our present work the effects of 3 Dau-GnRH-III conjugates – those carrying ^{4}Lys with acetyl or butyryl side chain a "second drug" ([^{4}Lys(Ac)]-GnRH-III(Dau=Aoa), [^{4}Lys(Bu)]-GnRH-III(Dau=Aoa)) and the parent conjugate GnRH-III(Dau=Aoa) (Figure 1) – were investigated in respect of their cell biological activity and their applicability for targeted melanoma therapy. The significance of the above-

described modification in position 4 of GnRH-III was evaluated by characterization of the cellular uptake, the antiproliferative/cytotoxic activities, the cell adhesion and migration modulator effects of conjugates and their ability to induce apoptosis or cell cycle arrest in A2058 melanoma cell line.

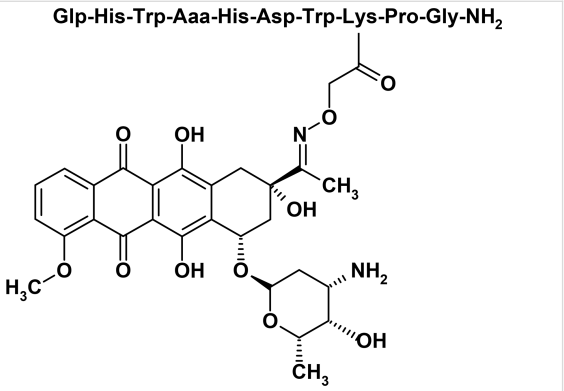

Compounds	Aaa
GnRH-III(Dau=Aoa)	Ser
[^{4}Lys(Ac)]-GnRH-III(Dau-Aoa)	Lys(Ac)
[^{4}Lys(Bu)]-GnRH-III(Dau-Aoa)	Lys(Bu)

Figure 1: Schematic structure of Dau-conjugated GnRH-III or its derivatives containing ^{4}Lys with acetyl or butyryl (Bu) side chain.

Results and Discussion

Synthesis of Dau–GnRH-III conjugates

The modified GnRH-III derivatives were prepared by solid phase peptide synthesis (SPPS) using Fmoc/*t*-Bu strategy with the orthogonal protecting scheme as described before [17,19] and presented in detail in Supporting Information File 1. In all cases, a Mtt (methyltrityl) protecting group was applied to block the side chain of Lys in position 8. For the development of acylated Lys in position 4, the side chain of it was protected either with Dde (1-(4,4-dimethyl-2,6-dioxocyclohex-1-ylidene)ethyl) or with ivDde ((1-(4,4-dimethyl-2,6-dioxocyclohex-1-ylidene)isovaleryl). The previous one can be removed easier with 2% hydrazine in DMF (2 × 15 min) while ivDde needs higher hydrazine concentration (4% in DMF) and longer treatment (12 × 5 min) for the complete removal of the protecting group. However, ivDde is more stable in circumstances (2% DBU, 2% piperidine in DMF) used for the Fmoc removal. To avoid the unwanted Dde removal during the synthesis ivDde was applied in this study. After acylation of the free amino group on the side chain of ^{4}Lys using either acetic or butyric anhydride, the Mtt protecting group was detached. Though the application of bis-Boc-aminooxyacetic acid to incorporate the Aoa moiety provided better results (10–15% better yield according to the previous studies) than Boc-Aoa-OH because the overreaction of the sterically unhindered nitrogen in the case of the later one, here the Boc-Aoa-OH was used. After these on resin modifications of the peptide chain, the peptide derivatives were removed with a mixture of 95% TFA, 2.5% TIS, and 2.5% water (v/v/v) for 2.5 h at room temperature (rt) and then precipitated with ice-cold diethyl ether followed by purification on RP-HPLC. Daunorubicin was attached to the purified peptides via oxime linkage that was formed under slightly acidic conditions (0.2 M NH_4OAc buffer at pH 5) at rt overnight. The reaction mixture was injected directly to RP-HPLC to separate the unreacted excess of Dau. Conjugates (Figure 1) were analyzed and identified by analytical HPLC-MS and ESIMS suggesting the right composition of the conjugates (Table 1 and Figures S1–S3 in Supporting Information File 2). The purity of the drug-containing conjugates was over 97% in all cases and untinged from free Dau, that can cause a significant influence on biological assays.

Cellular uptake of conjugates compared to Dau

An initial western blot study was done by using polyclonal anti-GnRH-R antibody (Proteintech Group, Rosemont, IL, USA) to detect the expression of GnRH-R in A2058 melanoma cells. Lysate of GnRH-R positive HT-29 colon carcinoma cells [33] was used as a positive control. Western blot analysis could reveal the presence of GnRH-R in A2058 cells; however, besides the band at approximately 37 kDa indicating the nascent full-length GnRH-R protein, there were bands in higher molecular weight in both samples (Figure S4 in Supporting Information File 2). The presence of extra bands could be explained by

Table 1: Analytical characteristics of Dau–GnRH-III conjugates

compounds	RP-HPLC (C-4) t_R[min][a]	RP-HPLC (C-18) t_R [min][b]	ESIMS MW_{calcd}/MW_{exp} [g/mol][c]
GnRH-III(Dau=Aoa)	21.37	21.37	1841.89/1841.85
[^{4}Lys(Ac)]-GnRH-III(Dau=Aoa)	21.83	21.52	1925.02/1924.14
[^{4}Lys(Bu)]-GnRH-III(Dau=Aoa)	22.42	22.05	1953.07/1952.97

[a]Column: Hichrom, Vydac 214TP5 C4 (300 Å, 5 µm, 250 × 4.6 mm) as a stationary phase. Linear gradient elution (0 min 0% B; 5 min 0% B; 40 min 90%). [b]Column: Macherey-Nagel, Nucleosil C18 (100 Å, 5 µm, 250 × 4.6 mm) as a stationary phase. Linear gradient elution (0 min 0% B; 5 min 0% B; 30 min 90%). [c]Bruker Daltonics Esquire 3000+ ion trap mass spectrometer. Dau: daunorubicin

the different glycosylated variant of GnRH-R [34]. It is worth mentioning that based on this results it is hard to quantify or compare the amount of GnRH-R protein in these cell types.

For investigation and comparison of the cellular uptake of the conjugates, A2058 cells were treated with the conjugates at 10^{-5} M concentration for 1, 4 and 6 h. The fluorescence intensity of intracellular Dau built in the conjugates and as the free drug was determined by flow cytometry (FACSCalibur; Becton Dickinson, San Jose, CA, USA). GeoMean (geometric mean channel) values normalized to the control are shown in Figure 2.

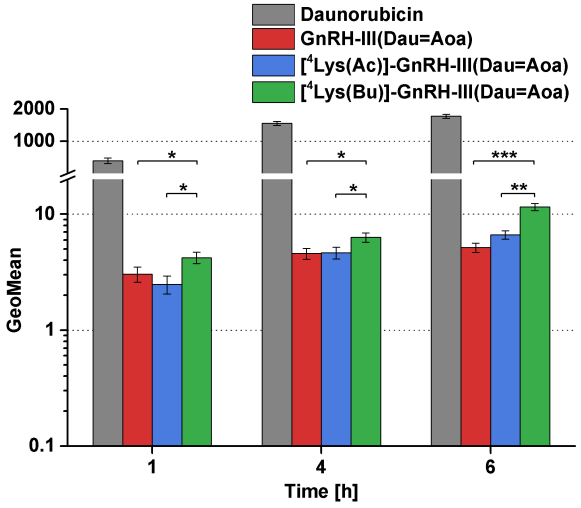

Figure 2: Cellular uptake of Dau–GnRH-III conjugates and free daunorubicin (Dau) by A2058 cells. Cellular uptake of the compounds was studied in 10^{-5} M concentration. GeoMean (geometric mean channel) value is a dimensionless value and refers to the relative fluorescence intensity. Data shown are mean of 2 parallels ± SD. The levels of significance are shown as follows: *: $p < 0.05$; **: $p < 0.01$, ***: $p < 0.001$.

The conjugates were internalized by A2058 cells in a time-dependent manner. In case of all conjugates, the cellular uptake could already be observed after 1 h of incubation. Comparing the conjugates, the butyrate containing conjugate ([^{4}Lys(Bu)]-GnRH-III(Dau=Aoa)) was taken up most effectively, while there was no difference between the intracellular fluorescence intensity of GnRH-III(Dau=Aoa) and [^{4}Lys(Ac)]-GnRH-III(Dau=Aoa). Dau served as a positive control in this experiment and showed a high level of intracellular fluorescence. Considering that Dau is a small molecule and can diffuse through the plasma membrane while the conjugates can enter the cells by receptor-mediated endocytosis with low capacity, this large-scale difference in the intracellular fluorescence intensity between the free Dau and the conjugates is not surprising. In addition, the free Dau has a ca. 10 times higher fluorescent intensity than the conjugates [35]. Comparing these results with the previous findings [19], [^{4}Lys(Bu)]-GnRH-III(Dau=Aoa) was shown to be the best-internalized conjugate and this ability proved to be independent of the tumor cells.

Antiproliferative/cytotoxic effect of conjugates

One of the major requirements for a drug-delivery conjugate is the ability to provide the antitumor activity of the attached drug inside the cells. The antiproliferative/cytotoxic effect of conjugates was investigated by an impedimetric technique, xCELLigence System (ACEA Biosciences, San Diego, CA, USA). The real-time measurement of the impedance change, which is in direct correlation with the number of adhered cells on an electrode surface, makes this impedimetric assay sensitive enough for cytotoxicity experiments [36]. In the event of a cytotoxic compound, the cells detach from the electrode surface and a drop in the impedance – given as Cell index values – could be observed.

According to the time-course study, the conjugates elicited their tumor-growth inhibitory effect only at high concentrations (10^{-5} to 10^{-4} M) and in long-term manner; 15–20 h after the treatment the Cell index values constantly decreased, which means that the cell viability was gradually lower as the time passed. Dau had a more immediate effect (0–5 h) in 10^{-6} to 10^{-4} M range (Figure S5 in Supporting Information File 2). IC_{50} values – a concentration that decreases the cell viability by 50% – were calculated from Cell index values obtained at 48 h and 72 h for each concentration and used for comparing the effects of conjugates. It is clearly seen that the presence of acylated Lys could increase almost 10-fold the antitumor activity ($p < 0.001$) of parent conjugate (GnRH-III(Dau=Aoa)). In case of the acylated ^{4}Lys-containing conjugates, [^{4}Lys(Bu)]-GnRH-III(Dau=Aoa) had a slightly but not significantly higher cytotoxic activity than that of [^{4}Lys(Ac)]-GnRH-III(Dau=Aoa) after 48 h or 72 h of incubation (Table 2).

A similar enhanced antitumor activity was also detected for conjugates modified with acylated ^{4}Lys in the HT-29 human colon [19], LNCaP [17] and DU145 [37] human prostate cancer cell lines compared to the conjugate containing native GnRH-III sequence. Despite the increased activity of conjugates substituted with acylated ^{4}Lys, they displayed their dose-dependent cytotoxic activity at higher concentrations comparing to the free Dau. This difference could be explained by the internalization ability of the compounds. The action of conjugates requires their receptor-mediated internalization and the lysosomal degradation, while Dau could diffuse through the plasma membrane and exerts its antitumor activity by intercalating directly to DNA. Furthermore, it was previously demonstrated that the smallest Dau-containing fragment (H-Lys(Dau=)-OH)) formed

Table 2: Determination of the long-term cytotoxic effect of GnRH-III-based conjugates and daunorubicin (Dau).

compounds	48 h IC_{50} (μM)	72 h IC_{50} (μM)
daunorubicin	0.19 ± 0.017	0.053 ± 0.009
GnRH-III(Dau=Aoa)	42.6 ± 6.54	14.8 ± 1.47
[^{4}Lys(Ac)]-GnRH-III(Dau=Aoa)	6.10 ± 0.59	4.94 ± 0.45
[^{4}Lys(Bu)]-GnRH-III(Dau=Aoa)	5.89 ± 0.91	4.19 ± 0.31

IC_{50} values were calculated by fitting a sigmoidal dose-response curve with RTCA 2.0 software. Data shown represent the mean ± SD of three parallel measurements.

via lysosomal degradation of this type of conjugates had a lower binding affinity to DNA, than the free drug [35]. The two-fold higher intracellular fluorescence intensity of Dau was accompanied by almost two-fold higher cytotoxic activity compared to the conjugates. By comparing the effects of the parent conjugate and the acylated ^{4}Lys-containing ones, there was no clear correlation between their cellular uptake and long-term cytotoxicity. To interpret the significance of the modification with acylated Lys it would be useful to confront the effects of the acetyl-Lys-containing conjugates with the non-acylated Lys-containing one ([^{4}Lys]-GnRH-III(Dau=Aoa)). However, the substitution with ^{4}Lys was formerly shown to lead increased cytostatic activity on different cancer cell lines (e.g., MCF-7, HT-29), this conjugate was less stable against different digestive enzymes and was taken up less effectively compared to GnRH-III(Dau=Aoa) [17]. Therefore, ([^{4}Lys]-GnRH-III(Dau=Aoa) was not involved in our present study.

The effect of the short-term treatment (6 h) with the conjugates and Dau was also determined. The viability of A2058 cells treated with the 10^{-6} and 10^{-5} M compounds was detected by alamarBlue®-assay after washing out the substances from the cells and a further 48 h of culturing. The results of the short-term growth inhibitory effect are presented in Figure 3.

Compared to the free drug, all conjugates elicited lower growth inhibitory effects. The conjugate containing a butyryl side chain ([^{4}Lys(Bu)]-GnRH-III(Dau=Aoa)) decreased slightly, but significantly the cell viability already at a concentration of 10^{-6} M, while it had a strong antiproliferative/cytotoxic effect at 10^{-5} M. [^{4}Lys(Ac)]-GnRH-III(Dau=Aoa) and GnRH-III(Dau=Aoa) displayed a similar growth inhibitory effect, respectively, but only at 10^{-5} M concentration, and they proved to be significantly less effective than [^{4}Lys(Bu)]-GnRH-III(Dau=Aoa).

However, the tumor growth inhibitory effect of the long-term treatment manifested after 17–24 h, the short-term exposure (6 h) could still cause a significant antitumor effect, suggesting that the conjugates could irreversibly reduce the melanoma cell

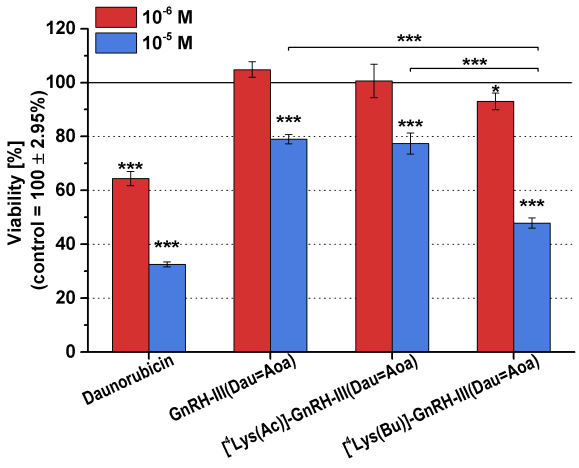

Figure 3: Short-term growth inhibitory effects of the conjugates and daunorubicin (Dau) on A2058 cells. The model cells were incubated with the compounds at 10^{-6} and 10^{-5} M concentrations for 6 h. The 'Viability' is expressed as a percentage of the control. Data shown in the figure represent mathematical averages of six parallels and ± S.D. values. The level of significance is shown as follows: *: $p < 0.05$; ***: $p < 0.001$.

viability. In contrast to the long-term treatments, the order of the internalization rate and the antitumor activity of the compounds was the same: Dau >> [^{4}Lys(Bu)]-GnRH-III(Dau=Aoa) > [^{4}Lys(Ac)]-GnRH-III(Dau=Aoa) ~ GnRH-III(Dau=Aoa). While there were no significant differences between [^{4}Lys(Ac)]-GnRH-III(Dau=Aoa) and [^{4}Lys(Bu)]-GnRH-III(Dau=Aoa) in terms of long-term (48 h) toxicity, the conjugate with butyryl side chain proved to be more effective after 6 h-long exposure. It seems that the short-term effects of conjugates could be due to their different internalization kinetics, or different mechanism of their action (e.g., induction of apoptosis or inhibition of cell cycle) rather than in case of the long-term activities. This could mean that once the acylated conjugates are internalized into the cell and completely degraded in the lysosome they could behave not so differently with each other in a long-term manner.

It is important to emphasize that all of the conjugates were stable in human serum for at least 24 h [17,19,35]. Therefore, in

case of the in vitro conditions (the serum content of the medium was 10%), it could be excluded that the different stability of conjugates and the premature release of Dau would cause the difference in their time-dependent antitumor activities. It was previously shown that all Dau–GnRH-III conjugates were degraded already after short-term incubation (2–8 h) with lysosomal homogenate, leading to the formation of various peptide fragments and Dau-containing metabolites such as H-Lys(Dau=Aoa)-OH [17,19,35]. LC–MS spectra recorded during the lysosomal degradation studies could also indicate the cleavage of an amide bond between the side chain of ^{4}Lys and the fatty acids [19]. This result suggests that besides the Dau-metabolites the fatty acids could also be released and – as second drugs – could contribute to the tumor growth inhibitory action of conjugates. It is assumed that the higher short-term cytotoxic activity of [^{4}Lys(Bu)]-GnRH-III(Dau=Aoa) could be attributed to the presence of butyrate, which has been demonstrated to inhibit the proliferation as well as to induce apoptosis and cell cycle arrest in different cell lines (e.g., colon carcinoma, melanoma, T-cell lymphoma) as a histone deacetylase inhibitor and/or via activation of orphan G-protein-coupled receptor GPR43 [20,27,38]. In short-term, the butyryl side chain of the intact conjugate may exert its tumor suppressor effect via acting on cell surface receptor (e.g., GPR43) [20] or after the conjugate being internalized, the released butyrate may induce apoptosis via caspase-3 [39]. It is possible that the Dau-metabolites formed inside the cells need longer time to exert their more prominent antitumor effect, which could explain why the long-term cytotoxic effect was almost the same for the two acylated conjugates.

It has been reported that doxorubicin (an analog of Dau) had a synergistic effect with histone deacetylase inhibitors (e.g., prodrug of butyric acid) in several malignant cell lines [38]. This finding could also be a possible explanation for the increased cytotoxic effect of the conjugates containing acylated Lys compared to the parent one.

Involvement of phosphatidylinositol 3-kinase in the antitumor effects of conjugates

Binding of GnRH or its conjugates to the GnRH-R receptor on tumor cells could stimulate different signaling elements (e.g., phosphatidylinositol 3-kinase – PI3K, mitogen-activated protein kinases) and effector proteins, which could play a significant role in the antitumor activity of a drug-containing conjugate [40].

The association of PI3K activation with the antitumor activity of the conjugates was determined by pretreating the cells with PI3K inhibitors (wortmannin – W and LY294002 – LY). The antitumor effect of the conjugates and Dau on the cells pretreated with PI3K inhibitors or with DMSO (solvent of the inhibitors) was assessed by an alamarBlue-assay after 48 h of incubation. The results of the PI3K-assay were given by calculating the inhibition index as the ratio of the viability of the pretreated and control (DMSO-treated) cell populations being incubated with medium or conjugates (10^{-5} M). The smaller inhibition index is than 100%, the lower antitumor activity compounds elicited on the cells pretreated with PI3K inhibitors than the control cells.

According to the inhibition indices shown in Table 3, none of the inhibitors had any influence on the antitumor activity of Dau and GnRH-III(Dau=Aoa). On the contrary, the antitumor effect of conjugates modified in position 4 was sensitive to the inhibitors. The effect of [^{4}Lys(Bu)]-GnRH-III(Dau=Aoa) could be slightly reduced by both inhibitors (W: 91.4%, LY: 80.0%), while in case of [^{4}Lys(Ac)]-GnRH-III(Dau=Aoa), only the pretreatment with W resulted in this kind of inhibition (89.3%) (Table 3). These results indicated that the conjugates containing acylated Lys in position 4 exerted their cytotoxic effect, at least in part, via a PI3K-dependent mechanism, while the PI3K seemed to be not involved in the cytotoxicity of the parent conjugate (GnRH-III(Dau=Aoa)). These results are in good agreement with previous studies about the involvement of PI3K

Table 3: The effect of the inhibition of phosphatidylinositol 3-kinase on the antitumor activity of conjugates and daunorubicin (Dau).

compounds	inhibition index[a] [%]	
	wortmannin	LY294002
daunorubicin	121.0 ± 8.1	100.7 ± 4.0
GnRH-III(Dau=Aoa)	102.6 ± 10.1	102.0 ± 3.9
[^{4}Lys(Ac)]-GnRH-III(Dau=Aoa)	89.3 ± 5.4*	94.3 ± 4.3
[^{4}Lys(Bu)]-GnRH-III(Dau=Aoa)	91.4 ± 2.0*	80.0 ± 9.1*

[a]The antitumor activity of the cells pretreated with wortmannin or LY294002 was characterized by inhibition index = (G_{nh} × C_c)/(C_{inh} × G_c) × 100%. Cells pretreated with DMSO were incubated with control medium (C_c) or a compound (G_c); cells pretreated with PI3K blockers were assayed for the control medium (C_{inh}) or a compound (G_{inh}). Data shown in the table were calculated from the averages of 6 parallels.
The level of significance is shown as follows: *: $p < 0.05$.

signaling pathway in the pro-apoptotic effects of GnRH analogs on prostate [41] and ovarian [42] cancer cells as well as in the chemotaxis of leukemic cells [43] induced by GnRH-III derivatives.

Apoptotic and cell cycle blocking effects of conjugates

In order to understand the mechanism of the antitumor effect of conjugates and consequently explain the difference in their activity, we determined whether these conjugates could induce apoptosis and/or cell cycle arrest in melanoma cells.

The pro-apoptotic effects of conjugates and Dau at 10^{-5} M concentration was studied after 24 h incubation by flow cytometry using FITC-annexin V (Sony Biotechnology, Weybridge, UK) and a novel image cytometer (NucleoCounter® NC-250™, ChemoMetec A/S, Lillerød, Denmark) using Vitabright-48™ (ChemoMetec A/S, Lillerød, Denmark), a cell permeable dye that reacts with thiol groups to form a fluorescent product. An inverse correlation has been shown between the concentration of thiols and progression of apoptosis; the level of thiols, and hence the fluorescence intensity of this dye decrease in response to induction of apoptosis [44].

Based on the percentages of apoptotic cells shown in Table 4, there was a good match between the values provided by these two different methods. As expected, the maximum apoptotic effect was detected in the Dau-treated group. Among the conjugates, only [^{4}Lys(Bu)]-GnRH-III(Dau=Aoa) had a slight, but significant apoptotic activity compared to the control. In the case of both assays, GnRH-III(Dau=Aoa) and [^{4}Lys(Ac)]-GnRH-III(Dau=Aoa) failed to exert any significant apoptotic effect in melanoma cells (Table 4).

Since the conjugates had no or minor apoptotic effect, the cell cycle kinetics of the cells treated with GnRH-III-based conjugates was also investigated to reveal the mechanism of growth inhibition of these conjugates. The distribution of the control and treated cells in the different cell cycle phases was analyzed by measurements of relative DNA contents of individual cells by flow cytometry after propidium iodide (Sigma-Aldrich, St. Louis, MO, USA) staining. The effects of conjugates and Dau on cell cycle phase distribution of A2058 cells are shown in Figure 4. The apoptotic inducer activity of Dau was also manifested in the pattern of cell cycle phases; the percentage of sub-G1 phase representing apoptotic cells (cell fragments) was increased after cells were treated with 10^{-5} M Dau up to 14.1% compared with 3.4% of the control. In parallel, a decrease in the proportions of cells in G1/G0 and G2/M phase and an increase in the percentage of S phase cells were also observed. Treatment with [^{4}Lys(Bu)]-GnRH-III(Dau=Aoa) also resulted in the accumulation of cells in the sub-G1 phase to 10.2%, accompanied by a decrease in the percentage of cells in G1/G0 phase. Whereas, [^{4}Lys(Ac)]-GnRH-III(Dau=Aoa) had a very similar effect on cell cycle progression as GnRH-III(Dau=Aoa). Cells treated with these conjugates showed higher G2/M populations (70.8% and 65.3%, respectively) and concomitant lower G1/G0 populations (10.9% and 12.6%, respectively) compared with the control (G2/M: 34.3% and G1/G0: 47.6%).

Overall, these results indicated that (i) the accumulation of the apoptotic population of melanoma cells might be partly responsible for the [^{4}Lys(Bu)]-GnRH-III(Dau=Aoa)-induced inhibition of cell growth, while [^{4}Lys(Ac)]-GnRH-III(Dau=Aoa) and GnRH-III(Dau=Aoa) could mediate their effect on melanoma cell proliferation via blocking cell cycle progression in G2/M phase. In a previous study, Pályi and his co-workers demonstrated that a conjugate containing GnRH analog + copolymer could also cause the accumulation of endometrial cancer cells in the G2/M phase [45]. In contrast to their [45] and our findings, different GnRH analogs were shown to inhibit the transition of G1 to S phase [46,47]. These studies also suggested that the greater tumor growth inhibitory effect of peptide conjugates than the free GnRH peptide could be explained by their differ-

Table 4: Apoptosis inducer effects of the conjugates and daunorubicin (Dau) in melanoma cells.

compounds	the ratio of apoptotic cells [%]	
	annexin V	Vitabright-48™
control	10.6 ± 0.51	8.7 ± 0.72
daunorubicin	33.6 ± 5.51***	30.9 ± 0.68***
GnRH-III(Dau=Aoa)	16.2 ± 3.28	10.6 ± 0.91
[^{4}Lys(Ac)]-GnRH-III(Dau=Aoa)	13.4 ± 0.54	13.5 ± 0.91
[^{4}Lys(Bu)]-GnRH-III(Dau=Aoa)	17.1 ± 1.83*	15.3 ± 0.89*

The model cell was incubated with the compounds at 10^{-5} M concentration for 24 h. The 'ratio of apoptotic cells' is expressed as a percentage of viable cells measured by flow cytometry or NucleoCounter® NC-250™. Data shown represent mathematical averages of two parallels and ± S.D. values. The level of significance is given as follows: *: $p < 0.07$; ***: $p < 0.001$.

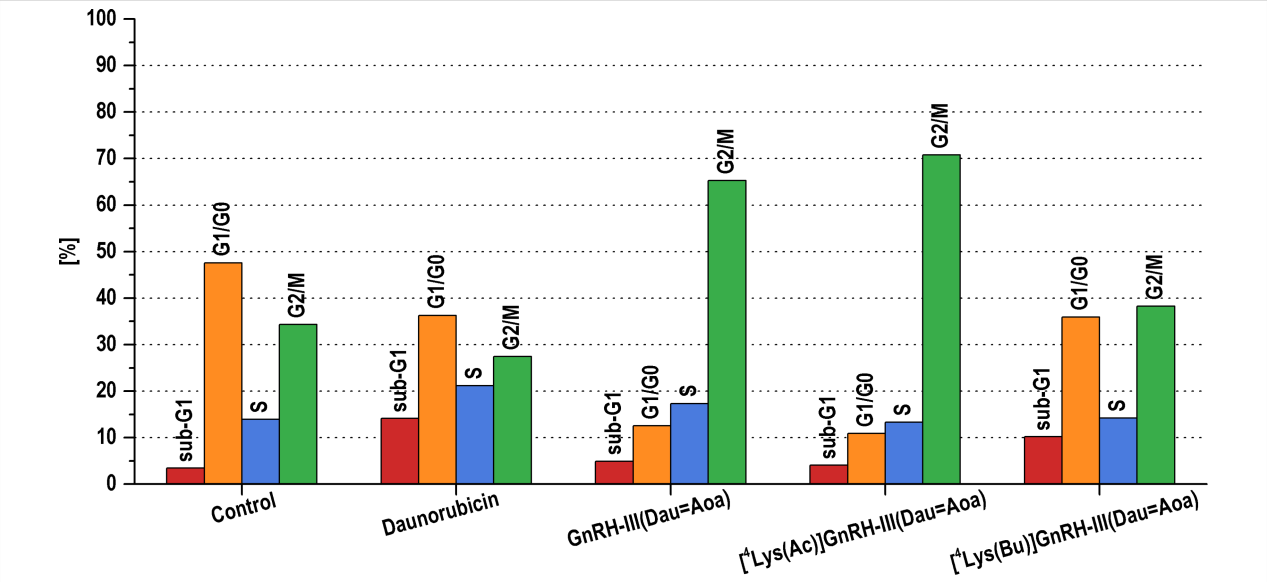

Figure 4: Effects of conjugates and daunorubicin (Dau) on cell cycle progression of A2058 melanoma cells. The model cell was incubated with the compounds at 10^{-5} M concentration for 24 h. Results are expressed as a percentage of cells in the sub-G1 area and the major phases (G1/G0, S and G2/M) of the cell cycle. Data shown in the figure represent mathematical averages of two parallel measurements.

ent effects on cell cycle phase distribution [45,47]. Based on the findings about the different mechanism of [^{4}Lys(Bu)]-GnRH-III(Dau=Aoa) than the other conjugates, it is assumed that its apoptotic effect could attribute to the presence of butyryl side chain, known for its ability to activate apoptosis [20,39].

Cell adhesion modulator effect of the conjugates

The dissemination of tumor cells is an important aspect of the tumor progression and could significantly affect the success of the targeted tumor therapy, as well. The first crucial steps in metastasis cascade are the impaired adhesion contacts and in parallel the increased motility of tumor cells. These two events substantially provide for tumor cells to detach from the primary tumor and migrate to the surrounding tissue [48,49]. Besides the tumor-selective antiproliferative/cytotoxic activity of the conjugates, they could be also desired to have an ability to interfere with the dissemination of cancer cells by modulating their adhesion and migration. In order to evaluate the conjugates as antimetastatic therapeutics, their effects on melanoma cell adhesion were investigated by the impedance-based xCELLigence System. The cell adhesion modulator effects of compounds were characterized by Delta Cell index values. These values were calculated for the rapid adhesion phase of A2058 – for the 3 hour long time interval after the cell seeding and treatment – and displayed in Figure 5.

Dau itself was able to induce the adhesion of A2058 cells at low concentrations (10^{-8} to 10^{-7} M), whereas a decrease was detected at 10^{-5} M, which could be explained by its immediate cytotoxic effect described above. In case of the adhesion measurements, GnRH-III(Dau=Aoa) and [^{4}Lys(Ac)]-GnRH-III(Dau=Aoa) had very similar adhesion inducer effects at 10^{-6} to 10^{-5} M concentrations. The adhesion of A2058 cells was also increased by [^{4}Lys(Bu)]-GnRH-III(Dau=Aoa), but at lower concentrations (10^{-8} to 10^{-6} M, Figure 5).

One of the first events of tumor progression is a decrease in anchorage dependency of tumor cells, which lead to their detachment and acquisition of migratory activity. One of the possible strategies to limit the local invasion of malignant cells is to increase their adhesion and consequently restrict their motility within the primary lesion [48]. Based on the detected adhesion inducer activity of Dau–GnRH-III conjugates, they might be effective in the prevention of tumor cell dissemination.

Holographic microscopic measurements were also performed to visualize the morphological changes induced by the conjugates and Dau. This novel technique provided several morphological parameters (e.g., surface area, optical thickness, eccentricity etc.) that allowed understanding of the results of impedance-based adhesion measurement. Holographic images were taken before and after the 3-hour treatment of A2058 cells with the compounds. The change in the morphological parameters shown in Table S1 in Supporting Information File 2 was calculated from a fold change during 3 h long treatment and this value was normalized to that of the control cells. The adhesion inducer effects of Dau and GnRH-III(Dau=Aoa) detected by the impedimetric assay were reflected in the morphometry analysis. Both compounds could increase the surface area of adhered

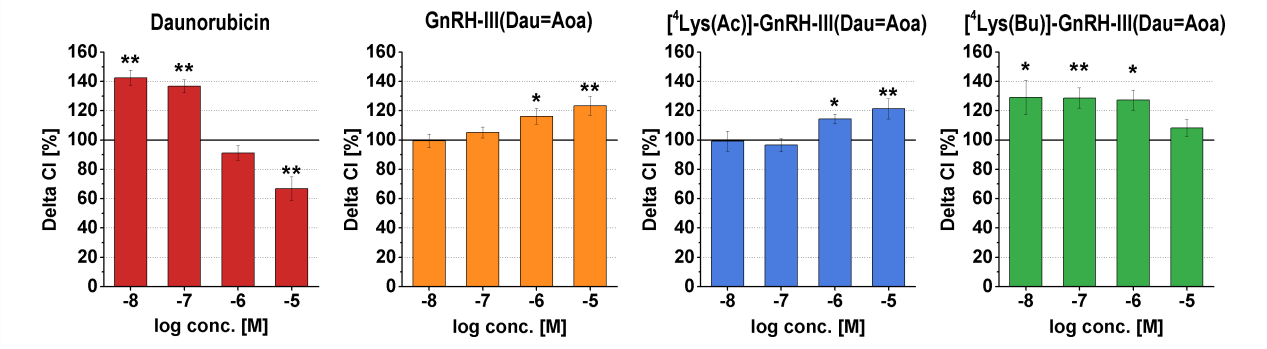

Figure 5: Effects of the conjugates and daunorubicin (Dau) on melanoma cell adhesion. The Delta CI (Delta Cell index) normalized to the control (control = 100%) refers to the difference of the Cell index value at the point in time of cell inoculation and the Cell index value at 3 h later. Data shown in the figures represent mathematical averages of three parallels and ± SD values. The levels of significance are shown as follows: *: $p < 0.05$; **: $p < 0.01$.

melanoma cells (124.1% ± 4.64, $p < 0.001$ and 115.7% ± 4.67, $p < 0.05$), while the optical thickness was reduced but only in case of the GnRH-III(Dau=Aoa) treated cells (85.6 ± 1.45, $p < 0.001$). Although [^{4}Lys(Ac)]-GnRH-III(Dau=Aoa) proved to be an adhesion inducer, but it had a negative or no effect on these morphological indices (surface area: 84.2 ± 3.32 – 92.5 ± 3.5; thickness: 95.7 ± 1.94 – 103.1 ± 2.21). Opposite tendencies were shown for [^{4}Lys(Bu)]-GnRH-III(Dau=Aoa), it could increase slightly, but significantly the surface area (114.0 ± 5.64, $p < 0.05$) and in parallel reduce the optical thickness (85.7 ± 1.85, $p < 0.01$) at 10^{-6} M concentration.

This apparent lack of consistence between the results of impedimetry and the basic morphometric parameters provided by holographic microscopy can be attributed to some method- and cell-related factors. The change in impedance (Cell index) during cell adhesion depends on (i) the cell–cell junctions, (ii) the seal resistance related to the cleft height between the cell and the electrode surface as well as (iii) the membrane capacitance correlated well with the amount of attached membrane area. The stronger adhesion could be due to a decrease in the cleft height, without any change in the surface area of the attached cells [50]. This can be a possible explanation for the neutral effect of [^{4}Lys(Ac)]-GnRH-III(Dau=Aoa) on the optical thickness and surface area at 10^{-6} to 10^{-5} M concentrations. The cellular shape could also influence the impedimetric results. The complex morphological parameters (e.g., eccentricity, irregularity and hull convexity) describing the shape or the circumference of the cells proved to be sensitive to the effects of the conjugates. The eccentricity and/or irregularity were elevated by GnRH-III(Dau=Aoa) (eccentricity: 107.4% ± 1.87, $p < 0.05$; irregularity: 110.9% ± 2.43, $p < 0.05$) and [^{4}Lys(Bu)]-GnRH-III(Dau=Aoa) (irregularity: 117.8% ± 2.99, $p < 0.01$). Some holographic microscope-related factors could also influence the interpretation of the results. For example, the background noise could limit the vertical and lateral resolution of the instrument and consequently, the very thin parts of cells or cell spreading cannot be sensed perfectly [51].

Effect of the conjugates on melanoma cell movement

Besides the altered tumor cell adhesion, there is growing evidence implicating tumor cell motility in early tumor invasion, and therapeutic targeting the migratory behavior of tumor cells within the primary tumor could limit local invasion [48]. To check the hypothesis that GnRH-based conjugates could inhibit the melanoma cell movement, their chemotactic (inducing vectorial migration) and chemokinetic (modulating locomotion) activities were investigated.

Firstly the chemotaxis of A2058 cells towards the conjugates was measured by a NeuroProbe® chemotaxis chamber. Both GnRH-III(Dau=Aoa) and [^{4}Lys(Bu)]-GnRH-III(Dau=Aoa) proved to have weak, but significant chemorepellence in 10^{-5} M concentration (Figure 6), while the conjugate with ^{4}Lys(Ac) elicited a rather neutral effect in the tested concentration range (10^{-8} to 10^{-5} M, Figure 6).

Considering the short-term treatments (0–3 h) in case of the measurements of cell movement and adhesion, the effects of conjugates on melanoma cell adhesion and movement are supposed to be mediated via GnRH-R activated signaling rather than via intracellular mechanisms induced after the internalization of conjugates. Although the conjugates showed an opposite activity on melanoma adhesion (increasing effects) and chemotaxis (decreasing or neutral effects), based on our previous studies about the receptor binding affinity of conjugates [19] and the chemotactic and adhesion modulator effect of native GnRH isoforms [19] it is assumed that the tested conjugates act as agonists on GnRH-R, but depending on the cellular function the resultant effects are different. It has been already

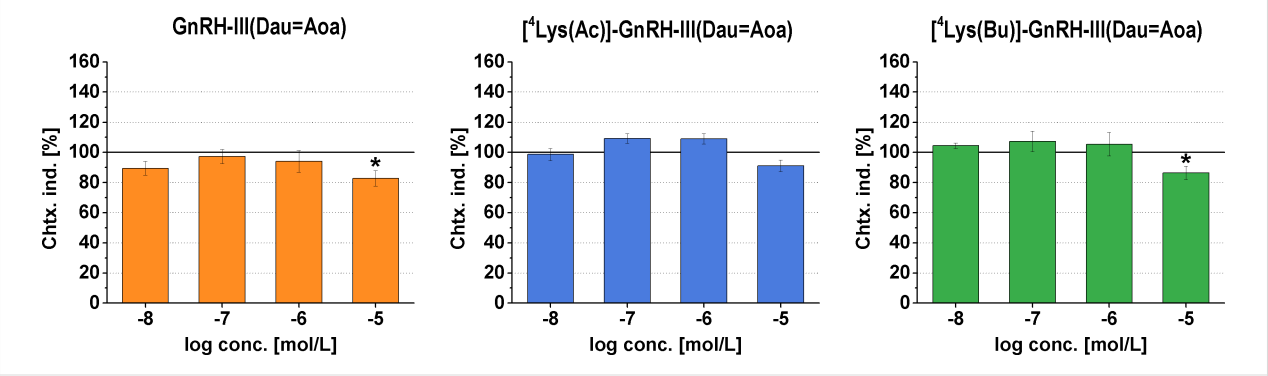

Figure 6: Chemotactic effects of Dau–GnRH-III conjugates on A2058 cell line. The 'Chemotaxis index' (Chtx. ind.) is expressed as a percentage of the control. Dau: daunorubicin. Data shown in the figures represent averages calculated for 8 parallels ± SD values. The level of significance is shown as *: $p < 0.05$.

reported for several tumor cell types, that depending on the cellular milieu or function, the GnRH analogs could elicit different – even opposite – actions [6,40]. For example, Aguilar-Rojas and his co-workers reported a similar combination of actions (invasion inhibitory and adhesion increasing effects) of a GnRH agonist in a breast cancer cell line [52]. It is also important to note that the effects on cell migration/chemotaxis and cell attachment are not independent cellular functions from each other. The cell-surface attachments basically influence the cell movement; the increased adhesiveness could result in a reduced cellular movement because of difficulty in realizing adhesion contacts to the substrate [53]. Our present results about the chemorepellent character of the conjugates appeared to be well-correlated to their effect on cell adhesion and cellular morphology of A2058 cells.

Next, the chemokinetic activities (inducing random cell movement or locomotion) of conjugates were investigated by monitoring the locomotion of A2058 cells with holographic microscopy under the condition that the conjugates (10^{-7} to 10^{-5} M) were added directly to the cells in a uniform concentration. For the characterization of cellular movement, three parameters – migration (shortest distance), motility (actual path) and motility speed (ratio of actual path and time) were quantified by tracking single cells in time-lapse videos recorded by a HoloMonitor™ M4 microscope (Phase Holographic Imaging AB, Lund, Schweden).

Based on the results, the GnRH-III(Dau=Aoa) and the ^{4}Lys(Bu)-containing derivative conjugates displayed rather negative effects on the melanoma cell locomotion (Figure 7). By comparing the results of GnRH-III(Dau=Aoa) to the control this conjugate decreased the migration of A2058 cells in a concentration-dependent manner (Figure 7a), while a slight increase in the motility and the motility speed could be detected but only at 10^{-6} M concentration (Figure 7b and c). The highest concentration of [^{4}Lys(Bu)]-GnRH-III(Dau=Aoa) decreased the migration, the motility and the motility speed of A2058 cells compared to that of the control cells (Figure 7g–i). However, the motility was slightly increased by 10^{-7} M [^{4}Lys(Bu)]-GnRH-III(Dau=Aoa), the migration was similar to the control group (Figure 7g,h). These results could indicate that GnRH-III(Dau=Aoa) and [^{4}Lys(Bu)]-GnRH-III(Dau=Aoa) would rather keep the cells in place. On the contrary, [^{4}Lys(Ac)]-GnRH-III(Dau=Aoa) could increase all of the parameters at 10^{-7} M concentration (Figure 7d–f), which means the cells travel further in a more winding path with a higher velocity than the control cells. The migration inducer effect of 10^{-6} M [^{4}Lys(Ac)]-GnRH-III(Dau=Aoa) indicated a more directed movement of cells (Figure 7d).

In some cases (e.g., [^{4}Lys(Ac)]-GnRH-III(Dau=Aoa)) concentration-dependent dual effects were observed. This kind of concentration dependence of GnRH effects is not unique in the literature. A similar diverse migratory response was found to GnRH-I actions in case of ovarian cell lines. This kind of biphasic effect could be explained by the presence of different GnRH receptors or depending on the concentration of a GnRH derivative/conjugate it could stimulate a different signaling pathway via a GnRH-R [40]. The opposite chemokinetic effects of the conjugates containing ^{4}Lys(Ac) (stimulatory) or ^{4}Lys(Bu) (inhibitory) could be explained by the ligand-induced selective signaling theory. According to this theory, different GnRH-R agonists may selectively stabilize different receptor conformation and consequently, different signaling pathways may be activated [6,40].

There was a good correlation between the chemorepellent and locomotion decreasing activity of GnRH-III(Dau) and the conjugate with ^{4}Lys(Bu), whereas the locomotion enhancer effect of [^{4}Lys(Ac)]-GnRH-III(Dau=Aoa) was accompanied with a neutral effect or a slight positive trend in the chemo-

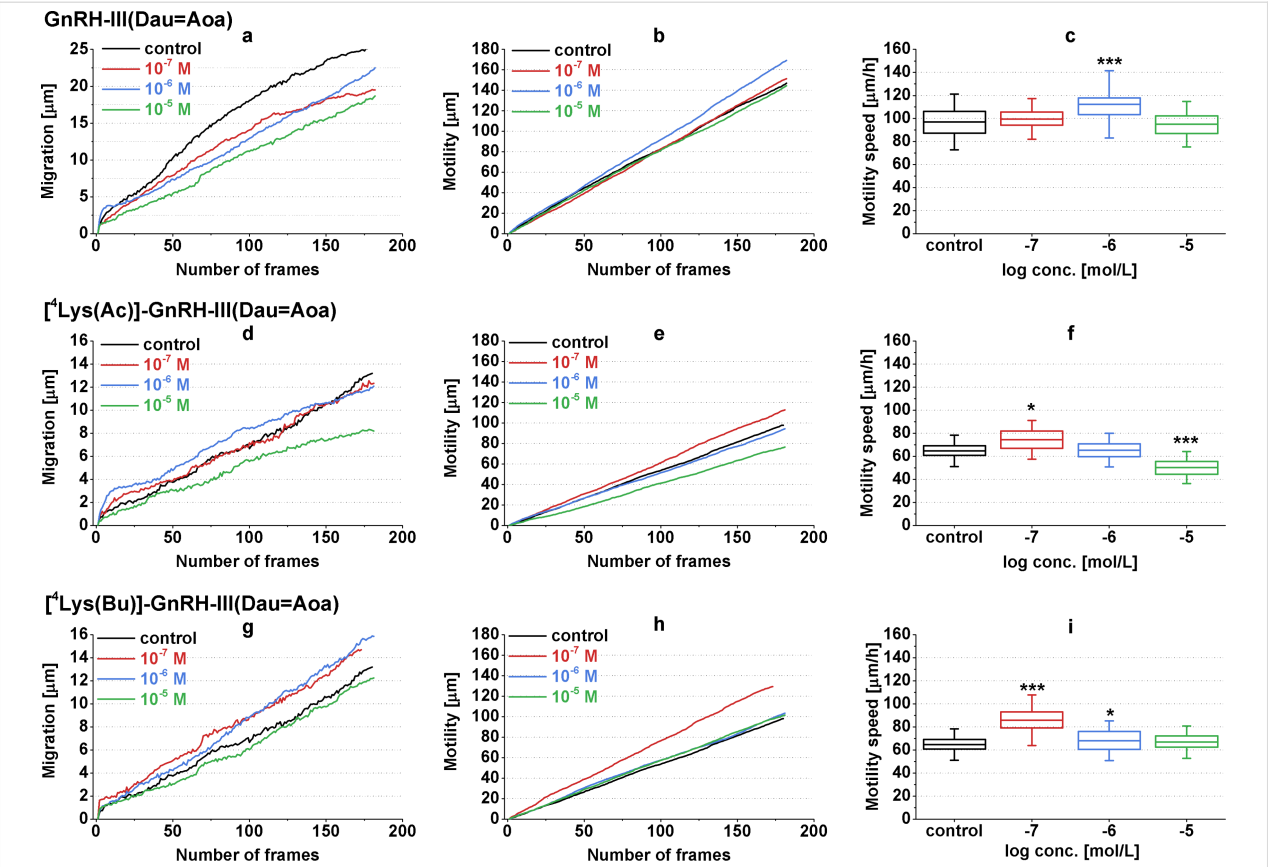

Figure 7: Effects of GnRH-III(Dau=Aoa) (a–c), [^{4}Lys(Ac)]-GnRH-III(Dau=Aoa) (d–f) and [^{4}Lys(Bu)]-GnRH-III(Dau=Aoa) (g–i) on the locomotion of A2058 cell line. The migration (a, d, g), motility (b, e, h) and motility speed (c, f, i) were investigated by HoloMonitor^{TM} M4 holographic microscopy. Dau: daunorubicin. Data shown in the figures represent averages calculated for 50 cell/group in 180 consecutive frames. The levels of significance are shown as follows *: $p < 0.05$; ***: $p < 0.001$.

tactic responsiveness of A2058 cells. Our present results are in harmony with studies demonstrating the migration inhibitory effect of GnRH agonists on melanoma [25] and prostate cancer cell lines [54,55]. These studies also suggested that modulation of cell adhesion or actin cytoskeleton remodelling (morphological changes) by GnRH analogs could determine their effects either on vectorial or random cell movements. In spite of the fact that many morphological parameters were examined, our results proved to be modest to demonstrate an unambiguous association between the morphological changes and cell migratory responses of A2058 melanoma cells induced by the conjugates but raised the need to investigate the molecular background of these cell physiological effects. The above-mentioned studies about the antimetastatic activity of different GnRH analogs anticipate that Dau-containing conjugates might influence the (i) expression of cell adhesion molecules (e.g., α3 integrin [25], non-integrin laminin receptor [56]) and (ii) regulate the actin polymerization by interacting with small GTPases (e.g., Rac1, CdC24 [54]) or (iii) interfere with the expression/activity of matrix-degrading enzymes (e.g., MMP-2 [25], urokinase-type plasminogen activator [55]).

Taken together our findings of cell movement and adhesion studies, GnRH-III(Dau=Aoa) and the conjugate containing ^{4}Lys(Bu) could have the ability to immobilize the cells at the primary tumor, diminish their spreading and consequently the chance of metastasis development.

Conclusion

In the present study, GnRH-III or its analog substituted with a short-chain fatty acid containing Lys in position 4 was applied as a targeting unit to deliver Dau to melanoma cells. By reading their complex cell physiological activities these conjugates, in which Dau was linked via an oxime bond to ^{8}Lys of GnRH-III derivatives, their suitability was demonstrated for targeted melanoma therapy. After the conjugates being internalized by time-dependent manner, they proved to exert an irreversible tumor growth inhibitory effect leading to the conclusion that GnRH-III and its analogs were able to deliver Dau to A2058 human melanoma cells and provide its antineoplastic activity. The presence of short-chain fatty acid containing Lys in position 4 was shown to be accompanied by an increased cellular uptake and a higher long-term cytotoxic activity mediated

via a PI3K-dependent signaling (Figure 8). Our findings also suggested that the underlying mechanisms of their antitumor effects, as well as their adhesion modulator and chemotactic/chemokinetic activities depends on the length of the side chain in ^{4}Lys. It was clearly shown that [^{4}Lys(Bu)]-GnRH-III(Dau=Aoa) possessing a longer, butyryl side chain could reduce the cell viability through its pro-apoptotic effect and the migratory/chemotactic behavior of melanoma cells, as well. Whereas, [^{4}Lys(Ac)]-GnRH-III(Dau=Aoa) was appeared to elicit its antitumor effect by arresting the cell cycle in G2/M phase and enhanced the migratory responses of melanoma cells. Our findings indicate the possibility that the locomotory reaction of melanoma cells induced by [^{4}Lys(Bu)]-GnRH-III(Dau=Aoa) and GnRH-III(Dau=Aoa) could be associated with the cell adhesion and morphological changes induced by these conjugates.

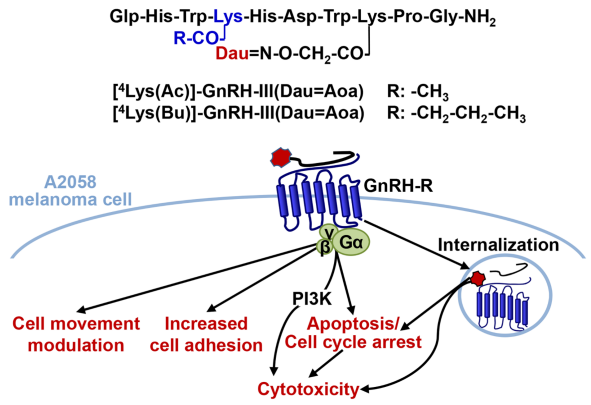

Figure 8: Schematic representation of the proposed mechanisms of the effects of GnRH-III conjugates containing acylated ^{4}Lys in A2058 melanoma cell line. Dau: daunorubicin.

The present results of measurements on cell adhesion and movement, together with data from the literature [6], suggest that these cell physiological responses could represent a novel therapeutic target of GnRH-III-based conjugates (Figure 8). In addition, we have provided further evidence that the impedimetry and holographic phase imaging are useful and suitable techniques for the characterization of cancer cell behavior and for the evaluation of effects of drug targeting conjugates with small structural differences (e.g., length of the side chain in ^{4}Lys).

Based on the overall cell biological effects of [^{4}Lys(Bu)]-GnRH-III(Dau=Aoa), the presence of butyrate-containing Lys could provide benefits over the conjugates possessing Lys(Ac) or Ser in position 4. Our results, together with previous data, would suggest the idea that the butyrate could work as a "second drug" in the conjugate. On the basis of the combined cytotoxic, adhesion inducer and cell movement inhibitory effect, [^{4}Lys(Bu)]-GnRH-III(Dau=Aoa) proved to be the best candidate in our study for application in the targeted melanoma therapy as a multifunctional antitumor and antimetastatic drug delivery system.

Supporting Information

Supporting Information File 1

Experimental.
[https://www.beilstein-journals.org/bjoc/content/supplementary/1860-5397-14-226-S1.pdf]

Supporting Information File 2

Analytical parameters and cell biological effects of Dau–GnRH-III conjugates.
[https://www.beilstein-journals.org/bjoc/content/supplementary/1860-5397-14-226-S2.pdf]

Acknowledgements

Authors express their gratitude to Auro-Science Consulting Kft as well as G and G Instruments Kft for their expert technical assistance. This project was supported by the National Research, Development and Innovation Office (NKFIH K119552 and NVKP_16-1-2016-0036).

ORCID® iDs

Eszter Lajkó - https://orcid.org/0000-0002-4796-4646
Beáta Biri-Kovács - https://orcid.org/0000-0001-5803-9969
Sven Ingebrandt - https://orcid.org/0000-0002-0405-2727
Gábor Mező - https://orcid.org/0000-0002-7618-7954
László Kőhidai - https://orcid.org/0000-0002-9002-0296

References

1. Jaracz, S.; Chen, J.; Kuznetsova, L. V.; Ojima, I. *Bioorg. Med. Chem.* **2005,** *13,* 5043–5054. doi:10.1016/j.bmc.2005.04.084
2. Bohme, D.; Beck-Sickinger, A. G. *J. Pept. Sci.* **2015,** *21,* 186–200. doi:10.1002/psc.2753
3. Nagy, A.; Schally, A. V.; Armatis, P.; Szepeshazi, K.; Halmos, G.; Kovacs, M.; Zarandi, M.; Groot, K.; Miyazaki, M.; Jungwirth, A.; Horvath, J. *Proc. Natl. Acad. Sci. U. S. A.* **1996,** *93,* 7269–7273. doi:10.1073/pnas.93.14.7269
4. Millar, R. P.; Lu, Z.-L.; Pawson, A. J.; Flanagan, C. A.; Morgan, K.; Maudsley, S. R. *Endocr. Rev.* **2004,** *25,* 235–275. doi:10.1210/er.2003-0002
5. Grundker, C.; Gunthert, A. R.; Westphalen, S.; Emons, G. *Eur. J. Endocrinol.* **2002,** *146,* 1–14.
6. Aguilar-Rojas, A.; Huerta-Reyes, M. *Oncol. Rep.* **2009,** *22,* 981–990. doi:10.3892/or_00000525
7. Limonta, P.; Montagnani Marelli, M.; Mai, S.; Motta, M.; Martini, L.; Moretti, R. M. *Endocr. Rev.* **2012,** *33,* 784–811. doi:10.1210/er.2012-1014

8. Nagy, A.; Schally, A. V. *Curr. Pharm. Des.* **2005,** *11,* 1167–1180. doi:10.2174/1381612053507594
9. Bajusz, S.; Janaky, T.; Csernus, V. J.; Bokser, L.; Fekete, M.; Srkalovic, G.; Redding, T. W.; Schally, A. V. *Proc. Natl. Acad. Sci. U. S. A.* **1989,** *86,* 6313–6317. doi:10.1073/pnas.86.16.6313
10. Engel, J. B.; Tinneberg, H.-R.; Rick, F. G.; Berkes, E.; Schally, A. V. *Curr. Drug Targets* **2016,** *17,* 488–494. doi:10.2174/1389450117051603031547 17
11. Emons, G.; Gorchev, G.; Harter, P.; Wimberger, P.; Stähle, A.; Hanker, L.; Hilpert, F.; Beckmann, M. W.; Dall, P.; Gründker, C.; Sindermann, H.; Sehouli, J. *Int. J. Gynecol. Cancer* **2014,** *24,* 260–265. doi:10.1097/igc.0000000000000044
12. http://adisinsight.springer.com/drugs/800009722 (accessed July 22, 2018).
13. Mező, G.; Manea, M. *Expert Opin. Drug Delivery* **2010,** *7,* 79–96. doi:10.1517/17425240903418410
14. Manea, M.; Mezo, G. *Protein Pept. Lett.* **2013,** *20,* 439–449. doi:10.2174/0929866511320040008
15. Mezo, G.; Manea, M.; Szabo, I.; Vincze, B.; Kovacs, M. *Curr. Med. Chem.* **2008,** *15,* 2366–2379. doi:10.2174/092986708785909157
16. Szabó, I.; Manea, M.; Orbán, E.; Csámpai, A.; Bősze, S.; Szabó, R.; Tejeda, M.; Gaál, D.; Kapuvári, B.; Przybylski, M.; Hudecz, F.; Mező, G. *Bioconjugate Chem.* **2009,** *20,* 656–665. doi:10.1021/bc800542u
17. Manea, M.; Leurs, U.; Orbán, E.; Baranyai, Z.; Öhlschlager, P.; Marquardt, A.; Schulcz, Á.; Tejeda, M.; Kapuvári, B.; Tóvári, J.; Mező, G. *Bioconjugate Chem.* **2011,** *22,* 1320–1329. doi:10.1021/bc100547p
18. Leurs, U.; Mező, G.; Orbán, E.; Öhlschlager, P.; Marquardt, A.; Manea, M. *Biopolymers* **2012,** *98,* 1–10. doi:10.1002/bip.21640
19. Hegedüs, R.; Manea, M.; Orbán, E.; Szabó, I.; Kiss, É.; Sipos, É.; Halmos, G.; Mező, G. *Eur. J. Med. Chem.* **2012,** *56,* 155–165. doi:10.1016/j.ejmech.2012.08.014
20. Tang, Y.; Chen, Y.; Jiang, H.; Robbins, G. T.; Nie, D. *Int. J. Cancer* **2011,** *128,* 847–856. doi:10.1002/ijc.25638
21. Thirunavukkarasan, M.; Wang, C.; Rao, A.; Hind, T.; Teo, Y. R.; Siddiquee, A. A.-M.; Goghari, M. A. I.; Kumar, A. P.; Herr, D. R. *PLoS One* **2017,** *12,* e0186334. doi:10.1371/journal.pone.0186334
22. Kapuvári, B.; Hegedüs, R.; Schulcz, Á.; Manea, M.; Tóvári, J.; Gacs, A.; Vincze, B.; Mező, G. *Invest. New Drugs* **2016,** *34,* 416–423. doi:10.1007/s10637-016-0354-7
23. Luke, J. J.; Flaherty, K. T.; Ribas, A.; Long, G. V. *Nat. Rev. Clin. Oncol.* **2017,** *14,* 463–482. doi:10.1038/nrclinonc.2017.43
24. Keller, G.; Schally, A. V.; Gaiser, T.; Nagy, A.; Baker, B.; Westphal, G.; Halmos, G.; Engel, J. B. *Cancer Res.* **2005,** *65,* 5857–5863. doi:10.1158/0008-5472.can-04-3816
25. Moretti, R. M.; Montagnani Marelli, M.; Mai, S.; Limonta, P. *Int. J. Oncol.* **2008,** *33,* 405–413. doi:10.3892/ijo_00000022
26. Moretti, R. M.; Montagnani Marelli, M.; Van Groeninghen, J. C.; Limonta, P. *J. Clin. Endocrinol. Metab.* **2002,** *87,* 3791–3797. doi:10.1210/jcem.87.8.8755
27. Wolny, D.; Chodurek, E.; Dzierzewicz, Z. *Acta Pol. Pharm.* **2014,** *71,* 1056–1059.
28. Xiong, F.; Mou, Y. Z.; Xiang, X. Y. *Int. J. Clin. Exp. Med.* **2015,** *8,* 4170–4174.
29. López-Cobo, S.; Pieper, N.; Campos-Silva, C.; García-Cuesta, E. M.; Reyburn, H. T.; Paschen, A.; Valés-Gómez, M. *Immunology* **2018,** *7,* e1392426. doi:10.1080/2162402x.2017.1392426
30. Roos, W. P.; Jöst, E.; Belohlavek, C.; Nagel, G.; Fritz, G.; Kaina, B. *Cancer Res.* **2011,** *71,* 4150–4160. doi:10.1158/0008-5472.can-10-3498
31. Díaz-Núñez, M.; Díez-Torre, A.; De Wever, O.; Andrade, R.; Arluzea, J.; Silió, M.; Aréchaga, J. *BMC Cancer* **2016,** *16,* 667. doi:10.1186/s12885-016-2693-3
32. Kuwajima, A.; Iwashita, J.; Murata, J.; Abe, T. *Anticancer Res.* **2007,** *27,* 4163–4169.
33. Mező, G.; Czajlik, A.; Manea, M.; Jakab, A.; Farkas, V.; Majer, Z.; Vass, E.; Bodor, A.; Kapuvári, B.; Boldizsár, M.; Vincze, B.; Csuka, O.; Kovács, M.; Przybylski, M.; Perczel, A.; Hudecz, F. *Peptides* **2007,** *28,* 806–820. doi:10.1016/j.peptides.2006.12.014
34. Terashima, R.; Laoharatchatathanin, T.; Kurusu, S.; Kawaminami, M. *J. Reprod. Dev.* **2016,** *62,* 495–499. doi:10.1262/jrd.2016-035
35. Orbán, E.; Mező, G.; Schlage, P.; Csík, G.; Kulic, Ž.; Ansorge, P.; Fellinger, E.; Möller, H. M.; Manea, M. *Amino Acids* **2011,** *41,* 469–483. doi:10.1007/s00726-010-0766-1
36. Urcan, E.; Haertel, U.; Styllou, M.; Hickel, R.; Scherthan, H.; Reichl, F. X. *Dent. Mater.* **2010,** *26,* 51–58. doi:10.1016/j.dental.2009.08.007
37. Montagnani Marelli, M.; Manea, M.; Moretti, R. M.; Marzagalli, M.; Limonta, P. *Int. J. Oncol.* **2015,** *46,* 243–253. doi:10.3892/ijo.2014.2730
38. Moyal, L.; Goldfeiz, N.; Gorovitz, B.; Rephaeli, A.; Tal, E.; Tarasenko, N.; Nudelman, A.; Ziv, Y.; Hodak, E. *Invest. New Drugs* **2018,** *36,* 1–9. doi:10.1007/s10637-017-0500-x
39. Ramos, M. G.; Rabelo, F. L. A.; Duarte, T.; Gazzinelli, R. T.; Alvarez-Leite, J. I. *Braz. J. Med. Biol. Res.* **2002,** *35,* 161–173. doi:10.1590/S0100-879X2002000200004
40. Cheung, L. W. T.; Wong, A. S. T. *FEBS J.* **2008,** *275,* 5479–5495. doi:10.1111/j.1742-4658.2008.06677.x
41. Kraus, S.; Levy, G.; Hanoch, T.; Naor, Z.; Seger, R. *Cancer Res.* **2004,** *64,* 5736–5744. doi:10.1158/0008-5472.can-04-1156
42. Zhang, N.; Qiu, J.; Zheng, T.; Zhang, X.; Hua, K.; Zhang, Y. *Oncol. Rep.* **2018,** *39,* 1034–1042. doi:10.3892/or.2017.6159
43. Lajkó, E.; Szabó, I.; Andódy, K.; Pungor, A.; Mező, G.; Kőhidai, L. *J. Pept. Sci.* **2013,** *19,* 46–58. doi:10.1002/psc.2472
44. Skindersoe, M. E.; Rohde, M.; Kjaerulff, S. *Cytometry, Part A* **2012,** *81,* 430–436. doi:10.1002/cyto.a.22032
45. Pályi, I.; Vincze, B.; Lovas, S.; Mező, I.; Pató, J.; Kálnay, A.; Turi, G.; Gaál, D.; Mihalik, R.; Péter, I.; Teplán, I.; Murphy, R. F. *Proc. Natl. Acad. Sci. U. S. A.* **1999,** *96,* 2361–2366. doi:10.1073/pnas.96.5.2361
46. Kim, J. W.; Lee, Y. S.; Kim, B. K.; Park, D. C.; Lee, J. M.; Kim, I. K.; Namkoong, S. E. *Gynecol. Oncol.* **1999,** *73,* 368–371. doi:10.1006/gyno.1999.5398
47. Ravenna, L.; Salvatori, L.; Morrone, S.; Lubrano, C.; Cardillo, M. R.; Sciarra, F.; Frati, L.; Di Silverio, F.; Petrangeli, E. *J. Androl.* **2000,** *21,* 549–557.
48. Palmer, T. D.; Ashby, W. J.; Lewis, J. D.; Zijlstra, A. *Adv. Drug Delivery Rev.* **2011,** *63,* 568–581. doi:10.1016/j.addr.2011.04.008
49. van Zijl, F.; Krupitza, G.; Mikulits, W. *Mutat. Res.* **2011,** *728,* 23–34. doi:10.1016/j.mrrev.2011.05.002
50. Wegener, J.; Keese, C. R.; Giaever, I. *Exp. Cell Res.* **2000,** *259,* 158–166. doi:10.1006/excr.2000.4919
51. Peter, B.; Nador, J.; Juhasz, K.; Dobos, A.; Korosi, L.; Székács, I.; Patko, D.; Horvath, R. *J. Biomed. Opt.* **2015,** *20,* 067002. doi:10.1117/1.jbo.20.6.067002

52. Aguilar-Rojas, A.; Huerta-Reyes, M.; Maya-Núñez, G.; Arechavaleta-Velásco, F.; Conn, P. M.; Ulloa-Aguirre, A.; Valdés, J. *BMC Cancer* **2012,** *12,* 550. doi:10.1186/1471-2407-12-550
53. Palecek, S. P.; Loftus, J. C.; Ginsberg, M. H.; Lauffenburger, D. A.; Horwitz, A. F. *Nature* **1997,** *385,* 537–540. doi:10.1038/385537a0
54. Enomoto, M.; Utsumi, M.; Park, M. K. *Endocrinology* **2006,** *147,* 530–542. doi:10.1210/en.2005-0460
55. Dondi, D.; Festuccia, C.; Piccolella, M.; Bologna, M.; Motta, M. *Oncol. Rep.* **2006,** *15,* 393–400. doi:10.3892/or.15.2.393
56. Chen, A.; Ganor, Y.; Rahimipour, S.; Ben-Aroya, N.; Koch, Y.; Levite, M. *Nat. Med.* **2002,** *8,* 1421–1426. doi:10.1038/nm801

BEILSTEIN JOURNAL OF ORGANIC CHEMISTRY

Novel solid-phase strategy for the synthesis of ligand-targeted fluorescent-labelled chelating peptide conjugates as a theranostic tool for cancer

Sagnik Sengupta[1], Mena Asha Krishnan[2], Premansh Dudhe[1], Ramesh B. Reddy[1], Bishnubasu Giri[1], Sudeshna Chattopadhyay[2,3] and Venkatesh Chelvam[*1,2,§]

Full Research Paper

Open Access

Address:
[1]Discipline of Chemistry, Indian Institute of Technology Indore, Khandwa Road, Simrol, Indore 453 552, India, [2]Discipline of Biosciences and Biomedical Engineering, Indian Institute of Technology Indore, Khandwa Road, Simrol, Indore 453 552, India and [3]Discipline of Physics and Discipline of Metallurgy Engineering & Material Sciences, Indian Institute of Technology Indore, Khandwa Road, Simrol, Indore 453 552, India

Email:
Venkatesh Chelvam[*] - cvenkat@iiti.ac.in

* Corresponding author
§ Phone: +91-731-2438789

Keywords:
chelating linker; confocal studies; continuous synthetic process; fluorescent tag; Fmoc-Lys-(Tfa)-OH; prostate cancer and ovarian cancer; solid-phase peptide synthesis

Beilstein J. Org. Chem. **2018,** *14,* 2665–2679.
doi:10.3762/bjoc.14.244

Received: 27 June 2018
Accepted: 28 September 2018
Published: 18 October 2018

This article is part of the Thematic Series "Peptide–drug conjugates"

Associate Editor: N. Sewald

Abstract

In this article, we have successfully designed and demonstrated a novel continuous process for assembling targeting ligands, peptidic spacers, fluorescent tags and a chelating core for the attachment of cytotoxic molecules, radiotracers, nanomaterials in a standard Fmoc solid-phase peptide synthesis in high yield and purity. The differentially protected Fmoc-Lys-(Tfa)-OH plays a vital role in attaching fluorescent tags while growing the peptide chain in an uninterrupted manner. The methodology is versatile for solid-phase resins that are sensitive to mild and strong acidic conditions when acid-sensitive side chain amino protecting groups such as Trt (chlorotrityl), Mtt (4-methyltrityl), Mmt (4-methoxytrityl) are employed to synthesise the ligand targeted fluorescent tagged bioconjugates. Using this methodology, DUPA rhodamine B conjugate (DUPA = 2-[3-(1,3-dicarboxypropyl)ureido]-pentanedioic acid), targeting prostate specific membrane antigen (PSMA) expressed on prostate, breast, bladder and brain cancers and pteroate rhodamine B, targeting folate receptor positive cancers such as ovarian, lung, endometrium as well as inflammatory diseases have been synthesized. In vitro studies using LNCaP (PSMA +ve), PC-3 (PSMA −ve, FR −ve) and CHO-β (FR +ve) cell lines and their respective competition experiments demonstrate the specificity of the newly synthesized bioconstructs for future application in fluorescent guided intra-operative imaging.

Introduction

The understanding of cell processes is indispensable to devise new strategies for diagnosis and treatment of cancer and inflammatory diseases through targeted drug delivery techniques [1]. The complex molecular processes in a cell are discerned by tagging fluorescent probes or radioactive tracers to a targeting ligand that will undergo internalization after binding to cell surface proteins overexpressed in diseased conditions. The internalized tracers along with the targeting ligand act as a tracking molecule to understand the destination of delivered cargos or biologics. For bioimaging of cancer and inflammatory diseases through specific biomarkers [2], several methods including single positron emission computed tomography (SPECT), positron emission tomography (PET) and magnetic resonance imaging (MRI) are exploited and each modality has its own strengths and weaknesses [3]. However, imaging studies using fluorescent probes [4] or radioactive isotopes [5,6] offers real-time, non-invasive, high-resolution images, during the examination of pathological diseased state.

Prostate specific membrane antigen (PSMA) [7-9] and the folate receptor [10-13] are well characterized and most attractive cancer biomarkers present in primary and metastatic stages of prostate and ovarian cancers, respectively. PSMA belongs to a family of type II membrane bound glycoprotein overexpressed on the cell surface of prostate, brain, bladder and breast cancers. Whereas folate receptors are attached to the cell membrane by a glycophosphatidylinositol anchor and overexpressed on several cancers as well as activated macrophages during inflammation. Moreover, folate receptors were also discovered to be overexpressed on activated macrophages [14] but not on resting macrophages [15]. Many inflammatory diseases such as rheumatoid arthritis, inflammatory osteoarthritis, ischemia reperfusion injury, atherosclerosis, psoriasis, vasculitis, lupus, diabetes, glomerulonephritis, sarcoidosis, Crohn's and Sjogren's disease are caused by activated macrophages [16]. Recently EC17, (λ_{ex} = 465–490 nm and λ_{em} = 520–530 nm) a conjugate of folic acid and fluorescein isothiocyanate has been used for intraoperative surgery of ovarian cancer [17], lung adenocarcinoma [18-20], and breast cancer [21]. Therefore, targeting these biomarkers brings forth new insight to know the cause and treatment for such ailments. These biomarkers belong to a family of cell surface transmembrane proteins [22] over-expressed mainly in diseased tissues and exploited in delivering chemical tools for early diagnosis of malignancy [23] and inflammatory diseases. They are also utilized for targeted drug delivery [24,25] of therapeutics to avoid any off-site toxicity to normal and healthy cells. Unfortunately, strategies to construct diagnostic and therapeutic chemical tools consisting of a polypeptidic spacer, a homing ligand for biomarkers, a fluorescent tag and a chelating moiety for tethering cargo in a continuous process using solid-phase peptide synthesis is poorly developed. Traditional solid-phase peptide synthesis methods for preparation of bioconstructs employ orthogonally protected functional moieties present in commercial resins such as Universal Nova tag or hyperacid labile resins such as Rink acid [26], 4-hydroxymethylphenoxybutyryl (HMPB), chlorotrityl [27], SASRIN [28] and Sieber amide [29]. Even though such resins are very useful, they suffer from several disadvantages. For example, i) they are cost ineffective, ii) possess low resin loading, iii) incompatible in medium to strongly acidic [30] or basic conditions employed for deprotection of coupled amino acids and iv) undergo premature cleavage of polypeptide chain from solid support resulting in moderate yield during deprotection of acid sensitive side chain protecting moieties to introduce fluorescent tags.

In addition to the above drawbacks, conventional methods for the synthesis of targeted fluorescent tagged bioconjugates [31] are a mixed approach of both solid and solution phase synthesis [32]. These involve several intermediary purification steps to separate side products and unreacted fluorescent components. Moreover, there are reports wherein receptor-targeted multimodal tools have been synthesized solely by employing solution phase chemistry [33-35]. These multistep synthetic protocol results in the escalation of the cost of intra-operative imaging tools that would otherwise be produced by our methodology with a single purification step. Even though Universal Nova tag resin [36] (Figure 1a) has resolved this problem to

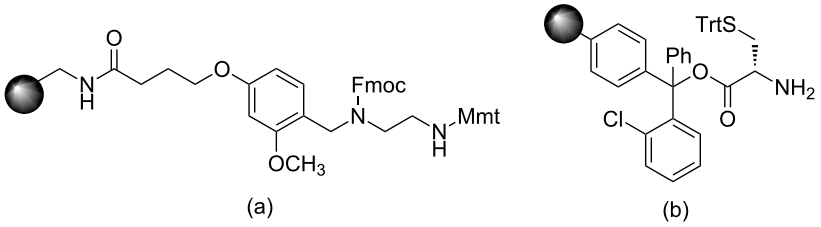

Figure 1: (a) Structure of universal nova tag resin, (b) structure of H-L-Cys(Trt)-2-ClTrt resin.

some extent, it suffers from a problem of employing acidic condition to deprotect side chain 4-methoxytrityl (Mmt) amino protecting group before attachment of fluorescent tag with the peptidic spacer. This results in premature cleavage of the peptide chain and loss of chemical yield during the bioconjugate synthesis. Further, attaching a radiotracer chelating core containing acid sensitive functional groups and the amino acid cysteine is also cumbersome and challenging. Recently, Low et al. reported synthesis of various targeted conjugates in which fluorescent tag [37] has been attached in a solution phase reaction. Also, they have reported the synthesis of ligand-conjugated peptides containing a radiotracer segment [38] without fluorescent tag using Wang resin that is cleaved in strongly acidic conditions.

Contrary to the aforementioned drawbacks, the present manuscript elicits a novel synthetic strategy for building new bioconstructs with several components in a continuous process without isolation of any of the intermediates. The various components that are assembled include the cell surface protein recognition ligand, a peptide spacer for enhanced solubility and binding affinity, a fluorescent tag for tissue staining and a chelating core to tether therapeutic cargos. This goal is smoothly achieved in high chemical yield and purity by strategically introducing differentially protected dibasic amino acids such as lysine whose α- and ε-amino groups are protected as base labile Fmoc and trifluoroacetyl (Tfa) protecting groups, respectively. The whole concept is successfully illustrated using commonly available and less expensive cysteine-labelled 2-chlorotrityl resin (Figure 1b). The methodology is general and can be significantly useful for acid-sensitive resins that contain acid-labile orthogonal amino acids with 4-methoxytrityl (Mmt) and 4-methyltrityl (Mtt) protecting groups.

Results and Discussion

PSMA has a very high affinity [39] for a small molecule homing ligand called DUPA or 2-[3-(1,3-dicarboxypropyl)-ureido]pentanedioic acid with an inhibition constant K_i of 8 nM. Folate protein binds to folic acid and their derivatives [40] such as pteroate ligand [41] with high degree of specificity ($K_d \approx 10$ nM) to deliver attached cargos to the interior of cells. These targeting ligands, DUPA and pteroate, have been exploited in the design and synthesis of our new ligand targeted tracer conjugates **13** and **17** (Figure 2) to target $PSMA^+$ and FR^+ diseased conditions.

Analysis of the crystal structure [42] of PSMA reveals that small molecule ligands such as DUPA would reach the PSMA active site through a gradually narrowing tunnel of amino acids of 20 Å length. Moreover, the inner surface of the PSMA tunnel possesses two hydrophobic pockets suitable for hydrophobic interactions with the amino acids present in the peptide spacer [38]. Therefore, it is pertinent to design a PSMA targeted conjugate that can pass through the tunnel smoothly and reach the active site as well as fit in hydrophobic pockets via hydrophobic interactions. Additionally, the carbonyl oxygen of the urea moiety of DUPA directly coordinates with two zinc atoms present in the active site of PSMA. The γ′-carboxylic acid of the DUPA ligand does not play a significant role in the interaction with the PSMA active site and hence exploited as a handle for the construction of peptidic spacer of bioconjugate **13**.

While designing the required peptide spacer [38] of **13** (Figure 2) for the tunnel, an eight-carbon amino acid such as 8-aminocaprylic acid has been covalently attached to the γ′-carboxylic acid of the DUPA ligand. This ensures the adequate distance between targeting ligand and peptidic spacer so that the specific binding to the protein is not compromised. The additional distance and hydrophobic pockets present in the 20 Å channel is crossed over by introduction of two phenylalanine (Phe) amino acids in the spacer. The polypeptide chain is also attached to another molecule of 8-aminocaprylic acid to ensure that the molecular position of the fluorescent tag and chelating core would lie outside the surface of the protein tunnel. Moreover, differentially protected α- and ε-amino groups of the amino acid lysine (Lys), Fmoc-Lys-(Tfa)-OH, is also introduced in the peptide chain. The main purpose of this exercise is to connect the chelating core through carboxylic acid of lysine and attachment of fluorescent probe via ε-amino group present in the lysine amino acid. Increased hydrophobicity due to the introduction of long chain amino acids, aromatic amino acids in the targeted ligand peptide conjugate **13** would decrease the solubility. This is compensated by introduction of dibasic amino acid like diaminopropionic acid (Dap), acidic amino acids like aspartic acid (Asp) and polar cysteine amino acid (Cys) that makes up the chelating core.

In the case of FR targeted fluorescent conjugate **17**, the targeting ligand, folic acid, is modified by removal of the L-glutamic acid residue to give the pteroic acid moiety (Figure 2). The binding affinity of the modified folate is relatively weaker than folic acid [41]. The targeting ligand, pteroic acid, is covalently coupled to 8-aminocaprylic acid to separate the active binding site of folate protein from the interference of fluorescent cargo attached to lysine and the chelating core as described for **13**.

Thus our newly designed bioconstructs **13** and **17** have the following four components, (i) a cell surface protein recognition ligand, (ii) a peptidic spacer which enhances the binding affinity of the PSMA-targeting conjugate **13**; it minimizes the repulsive interaction between the bulky dye molecule and the

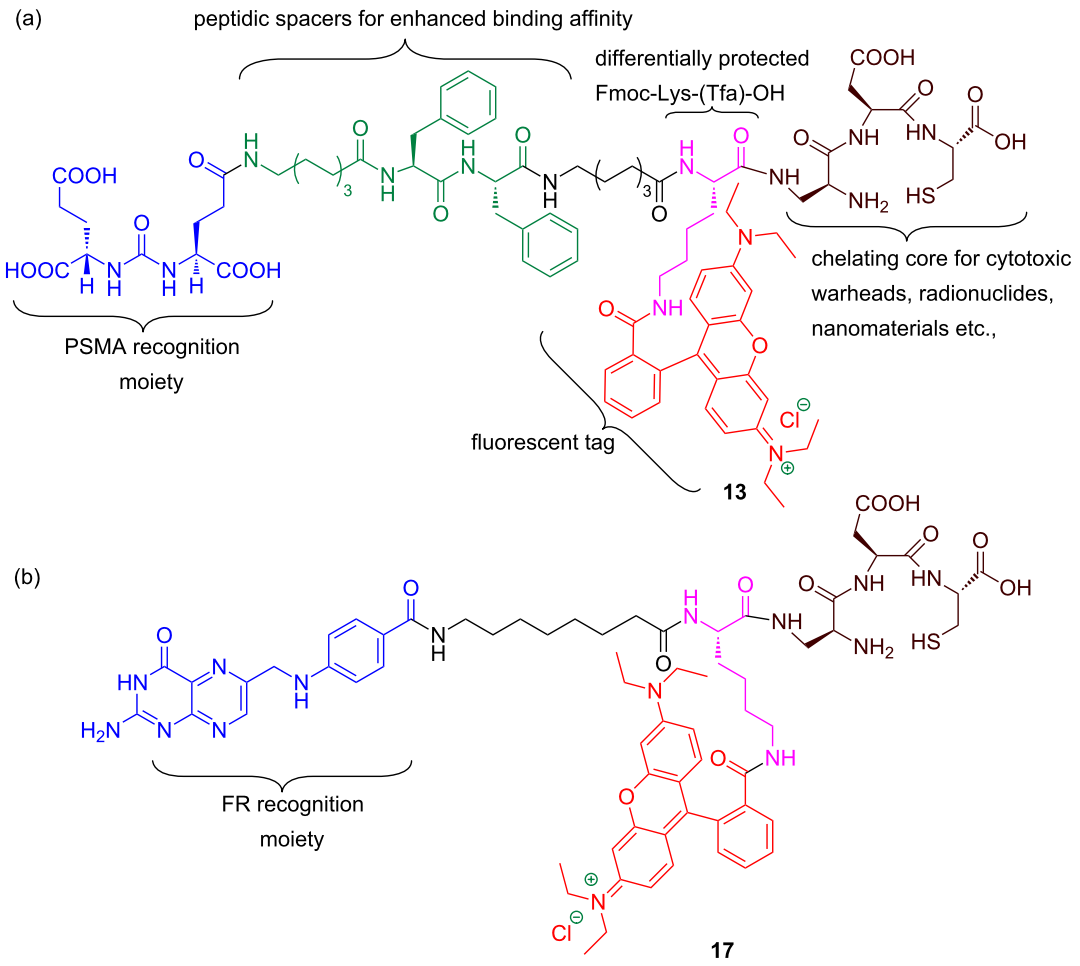

Figure 2: (a) PSMA targeted DUPA rhodamine B chelating conjugate **13**. (b) Folate receptor targeted pteroate rhodamine B chelating conjugate **17**.

targeted folate protein active site in the case of folate receptor targeting bioconstruct **17**, (iii) a fluorescent tag to track the cellular destination of bioconjugates and visualization aid for tissue staining, (iv) a chelating core as a multipurpose handle for loading drug cargos, radionuclides, or nanomaterials.

The tris(*tert*-butoxy) protected DUPA precursor **4** required for the preparation of conjugate **13** was prepared as per reported procedure [38] (Scheme 1).

Starting from commercially available cysteine capped chlorotrityl resin, H-L-Cys(Trt)-2-ClTrt **5**, we begin the synthesis of bioconjugate **13** as shown in Scheme 2. Using standard Fmoc solid-phase peptide synthesis methodology, amino acids such as Fmoc-Asp(O*t*-Bu)-OH, Boc-Dap(Fmoc)-OH were coupled in sequence to cysteine amino acid attached to chlorotrityl resin via dipeptide intermediate **6** to give the tripeptide intermediate **7**. The tripeptide **7** was then attached to strategic lysine amino acid, Fmoc-Lys-(Pg)-OH, whose ε-amino group is protected as either an Mtt (4-methyltrityl) or an Mmt (4-methoxytrityl) protecting group (Pg) to give tetrapeptides **8a** or **8b**. The tetrapeptides **8a** or **8b** were tethered sequentially to 8-aminocaprylic acid, two phenyalanine residues, another 8-aminocaprylic acid and finally to DUPA precursor **4**, to provide polypeptide chains **9a** or **9b** (Scheme 2).

The ε-amino protecting groups present in the polypeptide chains **9a** (Pg = Mtt) and **9b** (Pg = Mmt) are generally cleaved under acidic conditions. Therefore, it becomes pertinent to analyze the stability of the chlorotrityl resin and ε-amino protecting groups in the polypeptide chains **9a** and **9b** to achieve our multiple objectives in a continuous synthetic process without the isolation of any of the intermediates.

The peptide chain cleavage conditions for chlorotrityl resin are well established and the ε-amino trityl protecting groups of Fmoc-Lys-(Mtt or Mmt)-OH of the side chain are usually acid-labile with an order of stability: Trt (chlorotrityl) > Mtt

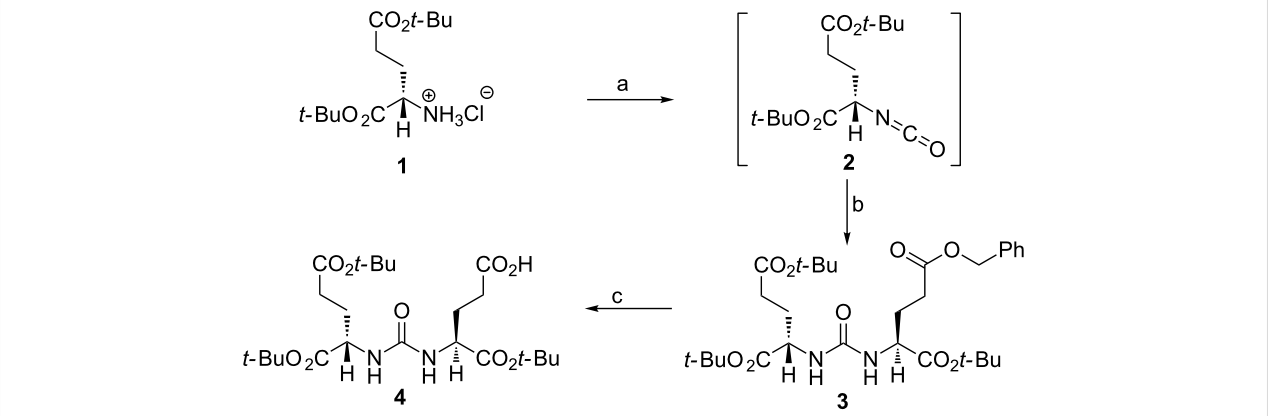

Scheme 1: Synthesis of PSMA tris(*tert*-butoxy) protected DUPA ligand **4**. Reagents and conditions: (a) Triphosgene, triethylamine, dichloromethane (DCM), −50 °C to rt; (b) L-glutamic acid γ-benzyl-α-*tert*-butylester hydrochloride, triethylamine, DCM, rt, overnight; (c) H_2, Pd/C, CH_2Cl_2, 24 h, rt.

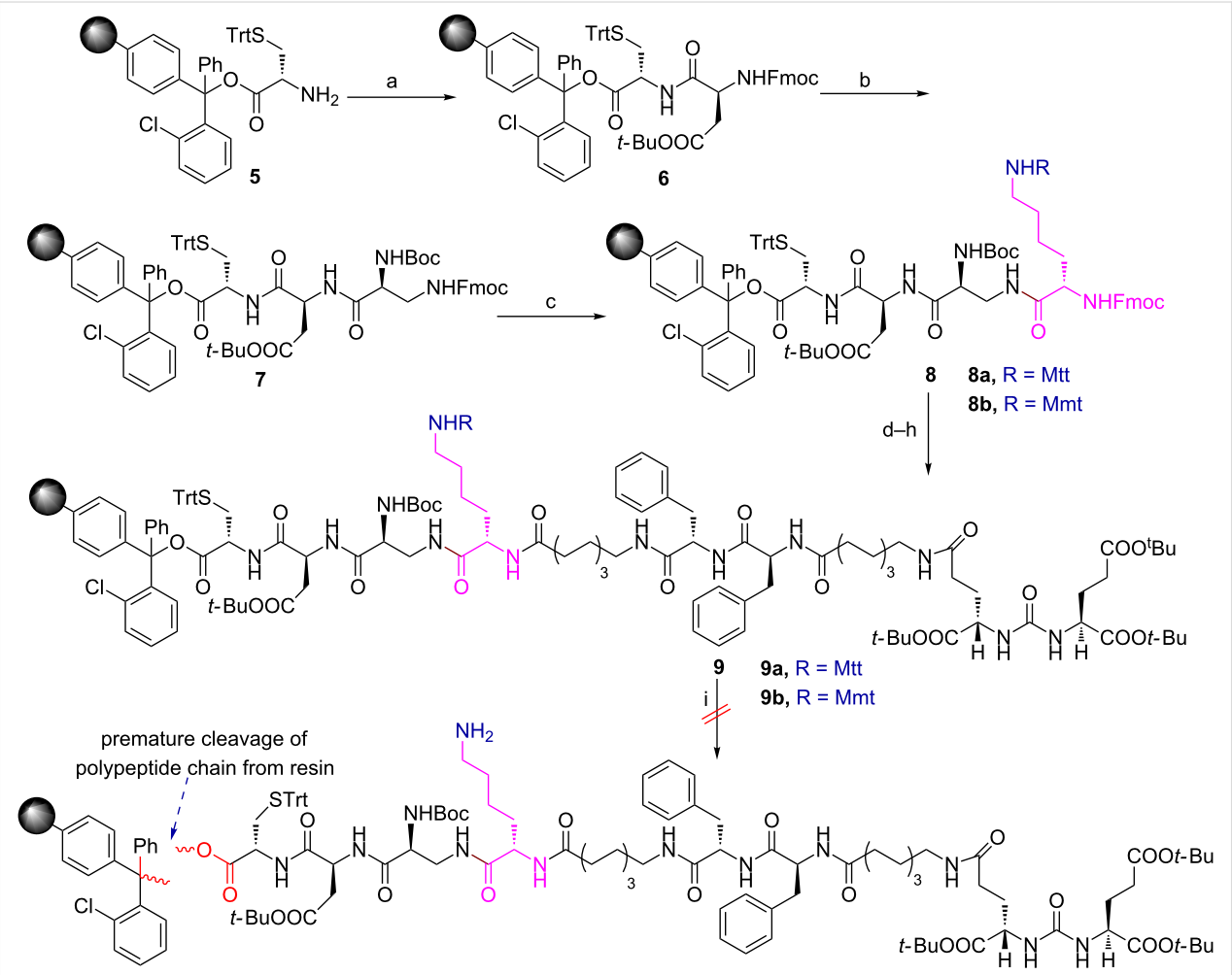

Scheme 2: Attempted synthesis of PSMA targeted DUPA rhodamine B chelating conjugate **13** using Fmoc-Lys(Mtt/Mmt)-OH. Reagents and conditions: (a) Fmoc-Asp(O*t*-Bu)-OH, PyBOP, DIPEA, DMF, 6 h; (b) (1) 20% piperidine in DMF, rt, 30 min; (2) Boc-Dap(Fmoc)-OH, PyBOP, DIPEA, DMF, 6 h; (c) (1) 20% piperidine in DMF, rt, 30 min; (2) Fmoc-Lys(Mtt/Mmt)-OH, PyBOP, DIPEA, DMF, 6 h; (d) (1) 20% piperidine in DMF, rt, 30 min; (2) Fmoc-8-aminocaprylic acid, PyBOP, DIPEA, DMF, 6 h; (e) (1) 20% piperidine in DMF, rt, 30 min; (2) Fmoc-Phe-OH, PyBOP, DIPEA, DMF, 6 h; (f) (1) 20% piperidine in DMF, rt, 30 min; (2) Fmoc-Phe-OH, PyBOP, DIPEA, DMF, 6 h; (g) (1) 20% piperidine in DMF, rt, 30 min; (2) Fmoc-8-aminocaprylic acid, PyBOP, DIPEA, DMF, 6 h; (h) (1) 20% piperidine in DMF, rt, 30 min; (2) DUPA(O*t*-Bu)$_3$-OH **4**, PyBOP, DIPEA, DMF, 6 h; (i) acetic acid/ trifluoroethanol/DCM (1:2:7), rt, 1 h or HOBt (1 M) in DCM/TFE (1:1), 1 h.

(4-methyltrityl) > Mmt (4-methoxytrityl). In our initial attempt, we opined that the Mtt- (4-methyltrityl-) protected ε-amino group of Fmoc-Lys-(Mtt)-OH should undergo selective cleavage under mildly acidic conditions without cleavage of polypeptide chain **9a** from the resin. Selective deprotection of the Mtt protecting group was achieved when **9a** was treated with either 1% TFA in dichloromethane or a mixture of acetic acid/trifluoroethanol/DCM in 1:2:7 ratio for 1 h at room temperature [43]. Unfortunately, the polypeptide chain **9a** cleaved off too from the resin beads (Scheme 2). Therefore, it became difficult to identify and marginally separate the acidic conditions required for selective cleavage of the Mtt protecting group in the side chain of **9a** from chlorotrityl resin.

Because of this reason we questioned the introduction of better electron-releasing groups such as 4-methoxytrityl (Mmt) instead of Mtt in the strategic amino acid, as in the case of Fmoc-Lys-(Mmt)-OH. This would increase the margin of difference and lower the acid strength required for the exclusive cleavage of the Mmt protecting group in the side chain of the **9b** from the chlorotrityl resin. With this view, **9b** containing Fmoc-Lys-(Mmt)-OH is subjected to cleavage under milder acidic conditions using 1 M HOBt (hydroxybenzotriazole) in trifluoroethanol/dichloromethane (1:1). However, these conditions did not provide the required solution and failed to differentiate the acidic strength needed for exclusive cleavage of the Mmt protecting group in the side chain of **9b** from the chlorotrityl resin resulting in the detachment of the polypeptide chain **9b** (Scheme 2). Therefore, we turned our attention to replace the acid labile trityl protecting groups with a base labile protecting group such as trifluoroacetyl (Tfa) as in the case of Fmoc-Lys-(Tfa)-OH amino acid.

With the hope that introduction of a base-labile protecting group in lysine could provide the required solution, we began the synthesis of polypeptide chain **10** with Fmoc-Lys-(Tfa)-OH derivative (Scheme 3). This idea for the synthesis of polypeptide chain **10** has been adapted from an earlier work reported by Moroder et al. in which trifluoroacetyl (Tfa) moiety was deprotected during a peptide synthesis [44] using 1 M aqueous piperidine at ice cold temperature. The polypeptide chain **10** was thus subjected to 1 M aqueous piperidine at 0 °C to deprotect the ε-amino trifluoroacetyl moiety. The literature reported conditions, however, failed to deprotect the Tfa group from polypeptide chain **10**. We have tested few reaction conditions and after optimization, we have successfully deprotected ε-amino Tfa protecting group from the side chain using 2 M aq piperidine at room temperature for 6–12 h (the completion of the reaction being monitored through the Kaiser's test) to give polypeptide chain **11** with free ε-amino group. It is also interesting to note that the reaction is smooth, clean without resulting in rupture of the polypeptide chain **10** from chlorotrityl resin. The protecting groups of other amino acids present in **11** remain intact during this process. After the successful cleavage of the Tfa protecting group to give **11**, the free ε-amino group was covalently bonded to a fluorescent tag such as rhodamine B using standard peptide coupling chemistry to afford rhodamine B conjugated polypeptide chain **12**. Amino acid protecting groups such as Boc, *tert*-butyl and Trt of diaminopropionic acid, aspartic acid and cysteine thiol moieties, respectively, in **12** were cleaved traceless using a cocktail of trifluoroacetic acid, triisopropylsilane, ethanedithiol in water. The final PSMA targeted rhodamine B peptide conjugate **13** was thus obtained from chlorotrityl resin as shown in Scheme 3 in high yield and purity. By using this new procedure, we have successfully demonstrated for the first-time a selective cleavage of the base sensitive ε-amino protecting group (Tfa) in the side chain of the growing polypeptide chain. The methodology could be extended to incorporate any basic natural or unnatural amino acids in a peptide chain in which the α-amino group is protected as Fmoc and the side chain amino group, in any position (β, γ, δ) along the carbon side chain, is protected as a trifluoroacetyl moiety. The methodology is thus successfully utilized to install fluorescent tags that are sensitive to strong inorganic bases. Moreover, the methodology is applicable to resins that are sensitive to mild and strong acidic conditions and peptide chains that contain side chain protecting groups such as Trt (chlorotrityl), Mtt (4-methyltrityl), Mmt (4-methoxytrityl) for the synthesis of targeted fluorescent bioconjugates.

The methodology was further extended to synthesize FR targeted fluorescent chelating conjugate **17** as shown in Scheme 4. Using standard Fmoc SPPS methodology, Fmoc amino acids such as Fmoc-Asp(O*t*-Bu)-OH, Boc-Dap(Fmoc)-OH were coupled in sequence to STrt protected cysteine amino acid attached to a chlorotrityl resin to give dipeptide **6** and tripeptide **7** intermediates**.** The tripeptide **7** was then attached to Fmoc-Lys-(Tfa)-OH to give tetrapeptide **8c**. The tetrapeptide **8c** was coupled to Fmoc-8-aminocaprylic acid followed by the introduction of folate protein targeting ligand in the form of N^{10}-(trifluoroacetyl)pteroic acid to give polypeptide **14**. It's noteworthy to mention that the ligand targeted chelating polypeptide **14** contains two different trifluoroacetyl moieties which protect the secondary amine of pteroate core as well as primary amine of ε-amino lysine residue. The N^{10}-(trifluoroacetyl) or secondary amine protecting group of pteroic acid is selectively cleaved using 1% $NH_2NH_2{\cdot}H_2O$ in DMF without affecting the trifluoroacetyl protecting group of lysine residue. This is unequivocally confirmed by performing the Kaiser test on polypeptide chain **15** which does not turn dark blue after the cleavage of the N^{10}-(trifluoroacetyl) group from the pteroate entity (Scheme 4). The secondary amine of the pteroate core

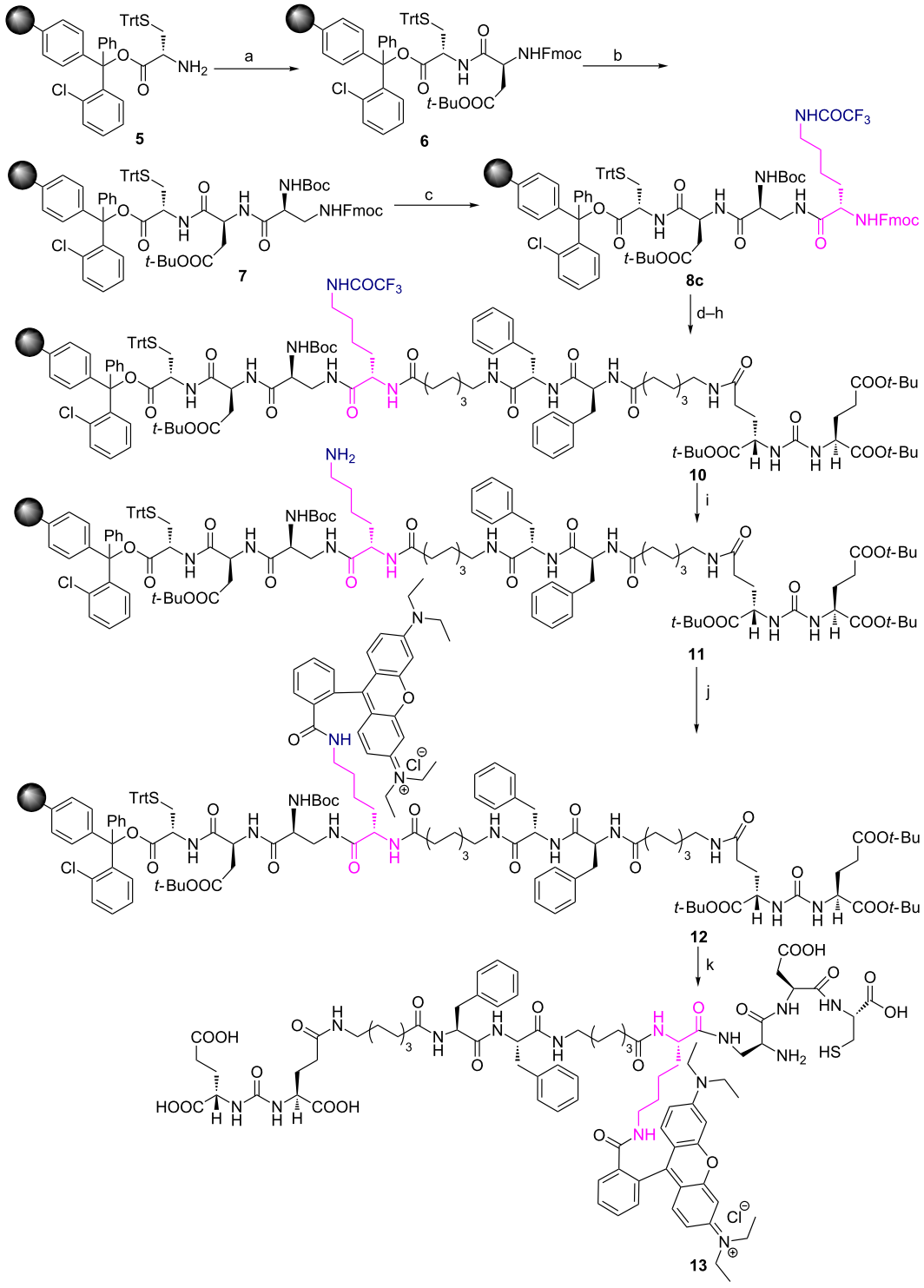

Scheme 3: Synthesis of PSMA targeting DUPA rhodamine B chelating conjugate **13**. Reagents and conditions: (a) Fmoc-Asp(O*t*-Bu)-OH, PyBOP, DIPEA, DMF, 6 h; (b) (1) 20% piperidine in DMF, rt, 30 min; (2) Boc-Dap(Fmoc)-OH, PyBOP, DIPEA, DMF, 6 h; (c) (1) 20% piperidine in DMF, rt, 30 min; (2) Fmoc-Lys(Tfa)-OH, PyBOP, DIPEA, DMF, 6 h; (d) (1) 20% piperidine in DMF, rt, 30 min; (2) Fmoc-8-aminocaprylic acid, PyBOP, DIPEA, DMF, 6 h; (e) (1) 20% piperidine in DMF, rt, 30 min; (2) Fmoc-Phe-OH, PyBOP, DIPEA, DMF, 6 h; (f) (1) 20% piperidine in DMF, rt, 30 min; (2) Fmoc-Phe-OH, PyBOP, DIPEA, DMF, 6 h; (g) (1) 20% piperidine in DMF, rt, 30 min; (2) Fmoc-8-aminocaprylic acid, PyBOP, DIPEA, DMF, 6 h; (h) (1) 20% piperidine in DMF, rt, 30 min; (2) DUPA(O*t*-Bu)$_3$-OH, PyBOP, DIPEA, DMF, 6 h; (i) 2 M piperidine in water, rt, 6–12 h; (j) rhodamine B, PyBOP, DIPEA, DMF, 6 h; (k) (1) TFA/TIS/EDT/H_2O (9.25:0.25:0.25:0.25, 1 × 5 mL, 30 min; 2 × 5 mL, 5 min); (2) evaporate TFA; (3) precipitate in ice cold diethyl ether.

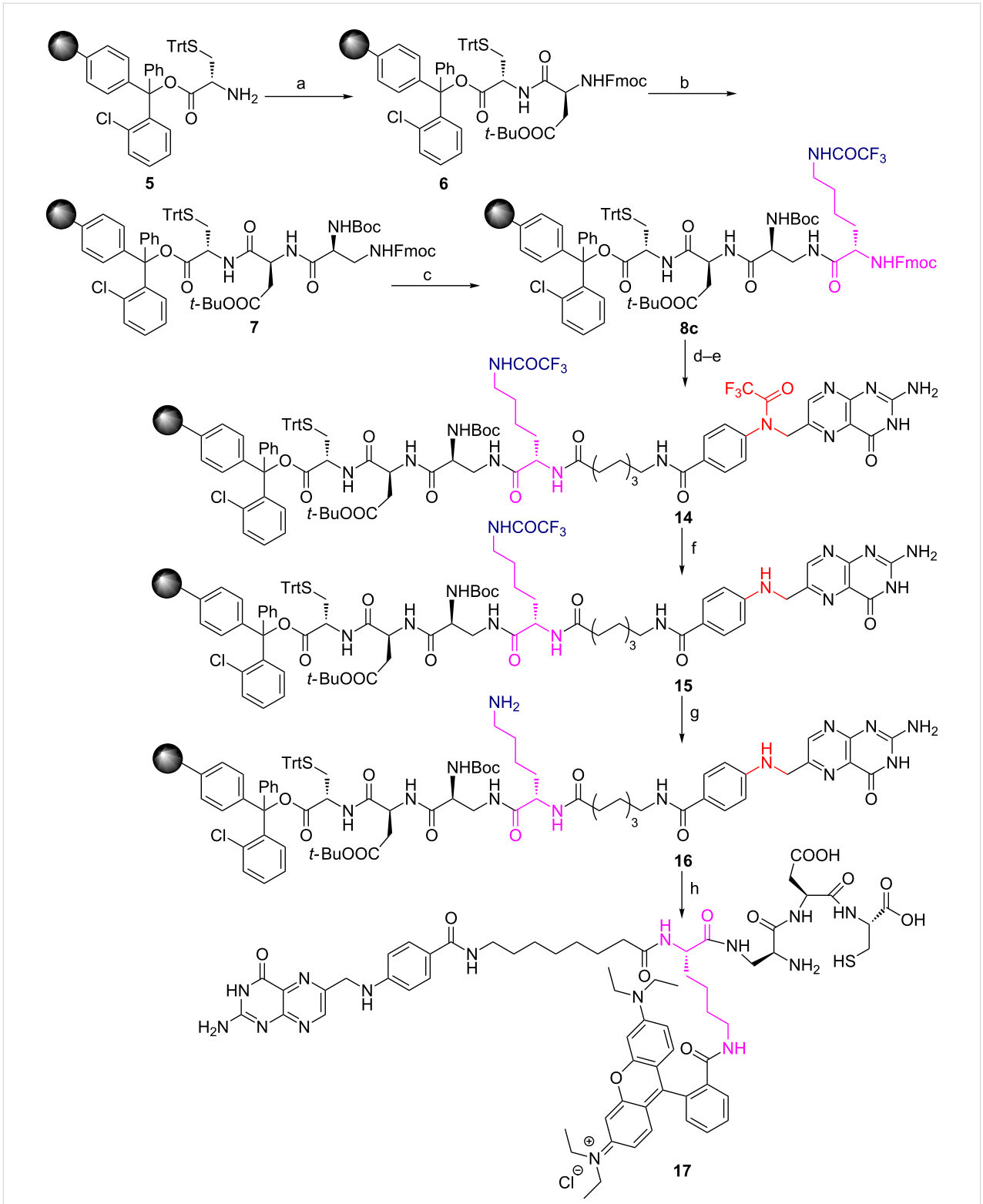

Scheme 4: Synthesis of folate receptor targeting pteroate rhodamine B chelating conjugate **17**. Reagents and conditions: (a) Fmoc-Asp(O*t*-Bu)-OH, PyBOP, DIPEA, DMF, 6 h; (b) (1) 20% piperidine in DMF, rt, 30 min; (2) Boc-Dap(Fmoc)-OH, PyBOP, DIPEA, DMF, 6 h; (c) (1) 20% piperidine in DMF, rt, 30 min; (2) Fmoc-Lys(Tfa)-OH, PyBOP, DIPEA, DMF, 6 h; (d) (1) 20% piperidine in DMF, rt, 30 min; (2) Fmoc-8-aminocaprylic acid, PyBOP, DIPEA, DMF, 6 h; (e) (1) 20% piperidine in DMF, rt, 30 min; (2) N^{10}-(trifluoroacetyl)pteroic acid, PyBop, HOBt·H_2O, DIPEA, DMSO, DMF, 6 h; (f) 1% NH_2NH_2·H_2O, DMF (3 × 2 mL) 10 min each; (g) 2 M piperidine in water, rt, 6–12 h; (h) (1) rhodamine B, PyBOP, DIPEA, DMF, 6 h; (2) TFA/TIS/EDT/H_2O (9.25:0.25:0.25:0.25, 1 × 5 mL, 30 min; 2 × 5 mL, 5 min); (3) evaporate TFA; (4) precipitate in ice cold diethyl ether.

generated in **15** after the cleavage of the N^{10}-(trifluoroacetyl) group does not give positive Kaiser test (see Experimental section).

Using 2 M aqueous piperidine we successfully cleaved the Tfa protecting group from the side chain of **15** to give a polypeptide chain **16** that is still intact with the resin. The successful cleavage of the Tfa group from the lysine side chain is confirmed by performing the Kaiser test on resin beads containing polypeptide chain **16** which turned dark blue. The free ε-amino group thus liberated was covalently attached to the fluorescent tag such as tetraethylrhodamine B by standard peptide bond formation chemistry. Protecting groups such as Boc, *tert*-butyl and Trt present in diaminopropionic acid, aspartic acid and cysteine thiol aminoacids, respectively, were cleaved using a cocktail of trifluoroacetic acid, triisopropyl silane, ethanedithiol in water to give folate receptor targeted chelating rhodamine B conjugate **17** in high yield and purity (Scheme 4).

Because bioconjugates **13** and **17** have the amino acid cysteine in the peptide chain, which is an essential requirement for construction of the chelating core, other protected ε-amino lysine derivatives [45,46] such as *N*-Fmoc-Lys(Alloc)-OH have not been employed in our synthetic strategy. Usually, the allyl protecting group in *N*-Fmoc-Lys(Alloc)-OH is deprotected using $Pd(PPh_3)_4$ catalyst. However, the sulfur atom present in the cysteine moiety of the chelating core is known to poison palladium catalysts resulting in complete failure of the deprotection of the ε-amino allyl protecting moiety. Moreover, palladium is a heavy metal and traceless removal of it from the resulting bioconjugates **13** and **17** is near to impossible. Since the prepared bioconjugates **13** and **17** are to be utilized for imaging of human cancer cell lines, presence of any heavy metals in the synthetic strategy would cause unwanted toxicity and inaccuracy in the biological study. The SH group present in the bioconjugate handle or chelating core of compound **13** and **17** can be utilized for the attachment of drugs [47], nanomaterial and radionuclide for therapeutic purposes. This added advantage makes the bioconjugates a potential theranostic tool for cancer.

The newly synthesized bioconjugates **13** and **17**, that can selectively target $PSMA^+$ and FR^+ cancers, were further evaluated by performing in vitro studies using laser scanning confocal microscopy on $PSMA^+$ LNCaP cells, FR^+ epithelial CHO-β cells and $PSMA^-$, FR^- PC-3 cells (Figure 3). The negative cell line was used to prove the protein specificity of newly synthesized ligand targeted bioconjugates **13** and **17**. In Figure 3 the confocal microscopic images depict the delivery of conjugates to cells via receptor-mediated endocytosis negating any possibility of non-specific uptake. The specificity of bioconjugates is indispensable to prevent collateral damage and toxicity to healthy cells when the chelating core is tethered to deliver radionuclides or cytotoxic drugs. The confocal microscopic images in Figure 3, panel (ii) shows the uptake of chelating DUPA rhodamine B conjugate in LNCaP cells at 100 nM concentration, panel (vi) shows the uptake of chelating pteroate rhodamine B conjugate in CHO-β cells at 150 nM concentration. The specificity of the ligand conjugates was further established by studying the uptake of bioconjugates **13** and **17** in malignant cells which express neither PSMA nor folate receptors [panels (iv) and (viii)]. The absence of any rhodamine B bioconjugates **13** and **17** uptake in the cytoplasm of negative cell line, PC-3 cells, show that the bioconjugates are very specific which is an important criterion in targeted drug delivery systems for avoiding off-site toxicity. In vitro specificity of bioconjugates, **13** and **17** were further examined by prior incubation of LNCaP cells and CHO-β cells with 100-fold excess of 2-PMPA and folic acid to block PSMA and folate receptors, respectively. Receptor blocked LNCaP and CHO-β cells display minimal uptake of bioconjugates **13** and **17** [panels (x) and (xii)], confirming the specificity of the synthesized bioconjugates. Thus, we have developed a novel strategy to synthesize targeted fluorescent tagged bioconjugates by introducing differentially protected α- and ε-amino groups of lysine amino acid derivative, Fmoc-Lys-(Tfa)-OH. Thus, our primary goal of introducing all the four components in **13** and **17** viz., targeting ligand, peptidic spacer, fluorescent tag as well as chelating core in a continuous synthesis process in cost effective manner, was achieved in high yield, purity and free of any heavy metal usually employed in other synthesis that is detrimental for biological studies.

Conclusion

In conclusion, we have developed a new synthetic strategy for assembling targeting ligand, peptidic spacer, a fluorescent tag and chelating core in a continuous process without isolation of intermediates during the bioconjugate synthesis. The synthesis is carried out from a relatively non-expensive and commercially available H-Cys(trt)-(2-Cltrt) resin. The mode of linking the fluorophore to the growing peptide chain using a lysine derivative such as Fmoc-Lys(Tfa)-OH containing differentially protected amino groups that are labile only under basic conditions was found to be crucial in synthesizing the conjugates. With this synthetic protocol we have synthesized chelating DUPA rhodamine B and pteroate rhodamine B conjugates for targeting malignant cells as well as inflammatory cells expressing PSMA and folate receptors. The in vitro uptake study has been performed using laser scanning confocal microscopy and the bioconjugates are found to be delivered specifically to cells expressing corresponding cell surface proteins. The small molecule targeted imaging probes prepared in this study are de-

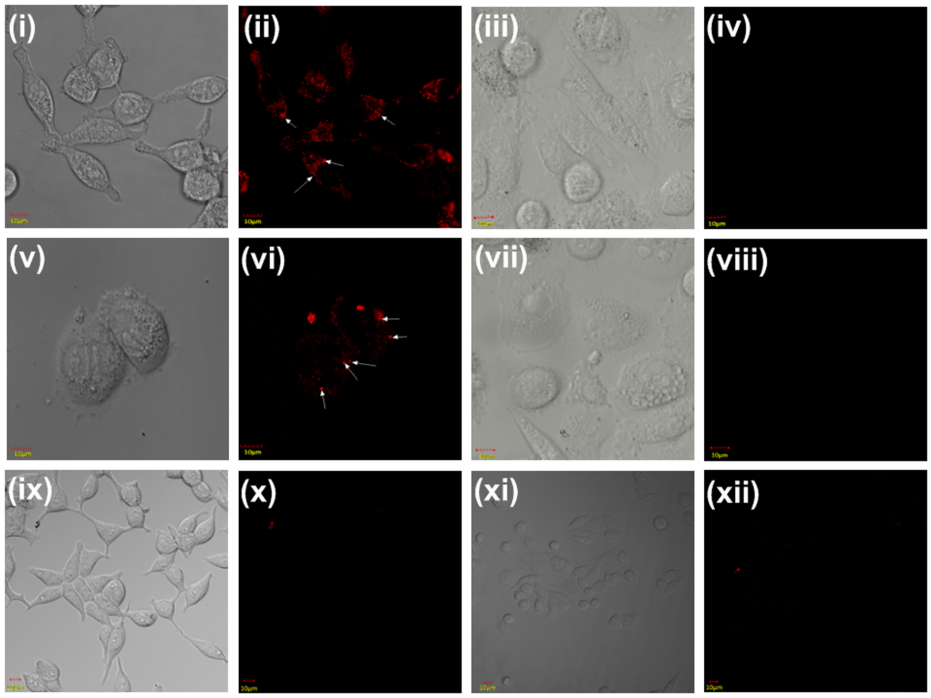

Figure 3: (i) and (ix) DIC image of LNCaP cells ($PSMA^+$); (ii) binding and internalization of DUPA-rhodamine B conjugate **13** to LNCaP cells by confocal microscopy at 100 nM concentration [endosomes are marked with white arrows]; (iii) and (vii) DIC image of PC-3 cells ($PSMA^-$ and FR^-); (iv) specificity of DUPA-rhodamine-B conjugate **13** in $PSMA^-$ cell line such as PC-3 cells; (v) and (xi) DIC image of cells CHO-β cells (FR^+); (vi) binding and internalization of pteroate-rhodamine B conjugate **17** in CHO-β cells by confocal microscopy at 150 nM concentration [endosomes are marked with white arrows]; (viii) specificity of pteroate-rhodamine B conjugate **17** in FR^- cell line such as PC-3 cells (DIC = differential interference contrast); (x) binding and internalization of DUPA-rhodamine B conjugate **13** to LNCaP cells in the presence of 100-fold excess 2-PMPA; (xii) binding and internalization of pteroate-rhodamine B conjugate **17** to CHO-β cells in the presence of 100-fold excess folic acid.

signed for diagnosis and deep tissue imaging of cancers and inflammatory diseases. Near infrared fluorophores containing a free or activated carboxylic group (e.g., IRDye 800CW NHS ester) can also be conjugated with the peptidic spacer using this methodology through amide coupling reaction. Moreover, the bioconjugates can be employed as potential theranostic tools by attaching macromolecules, cytotoxic warheads, radioactive tracers, nanomaterials etc., via the chelating core.

Experimental

Materials and methods

H-Cys-2-ClTrt resin, Fmoc amino acids and amide coupling agents, reagents and solvents used in solid-phase peptide synthesis (SPPS) as well as in chemical synthesis were purchased from Iris Biotech GmbH, Sigma-Aldrich, Merck and Spectrochem. Dry solvents were prepared by using drying agents and following usual methods. Peptide syntheses were carried out in sintered glass peptide vessels (Chemglass) by standard peptide coupling procedures. ^1H and ^{13}C NMR data were recorded using a Bruker AV 400 MHz NMR spectrometer with TMS (tetramethylsilane) as internal reference. Mass spectra were recorded on a Brukermicro TOF-Q II spectrometer in positive mode and negative mode electrospray ionization methods. Reactions were monitored by TLC using MERCK 60 F_{254} precoated silica gel plates and the products were visualized under UV light. The purity of ligand targeted rhodamine B peptide conjugates was confirmed by a Dionex HPLC-Ultimate 3000 instrument and peptide conjugates were purified through Büchi reveleris prep instrument using RP-PFP column (XSelect CSH Prep Fluorophenyl 5 µm OBD).

Synthesis of targeting ligand

Procedure for synthesis (*S*)-5-benzyl 1-*tert*-butyl 2-(3-((*S*)-1,5-di-*tert*-butoxy-1,5-dioxopentan-2-yl)ureido)pentanedioate (3): Triphosgene (0.050 g, 0.169 mmol) was dissolved in 3 mL dry DCM and the solution was stirred at −50 °C under an inert atmosphere (Scheme 1). Bis(*tert*-butyl)-L-glutamate·HCl (**1**, 0.150 g, 0.507 mmol) dissolved in 2 mL of dry DCM was added to triphosgene solution at −50 °C and triethylamine (0.5657 mL, 4.056 mmol) was added dropwise to the reaction mixture. The reaction mixture was stirred for 1.5 h at −50 °C and stirred for another 1.5 h at room temperature for the generation of isocyanate intermediate **2**. Thereafter, a solution of L-glutamic-γ-benzyl-α-*tert*-butyl·HCl (0.159 g, 0.507 mmol) and triethylamine (0.14 mL, 1.014 mmol) in DCM was added to the reaction mixture and the progress of the reaction was moni-

tored through TLC using an ethyl acetate and hexane (1:3) mixture as eluent. The reaction mixture was further stirred overnight at room temperature. After the completion of reaction, the reaction mixture was concentrated under reduced pressure, diluted with ethyl acetate, washed with water and brine. The organic layer was dried over anhydrous Na_2SO_4, filtered and the solvent was evaporated under reduced pressure to afford crude reaction mixture which was purified by column chromatography over 100–200 mesh silica gel using 25% ethyl acetate and hexane as eluent. The purified benzyl tris(*tert*-butoxy) protected DUPA precursor **3**.

(*S*)-5-Benzyl 1-*tert*-butyl 2-(3-((*S*)-1,5-di-*tert*-butoxy-1,5-dioxopentan-2-yl)ureido)pentanedioate (3): Yellowish gummy liquid (yield = 85%, 249 mg), R_f = 0.29 (EtOAc/hexane = 1:3); ^{1}H NMR (400 MHz, $CDCl_3$) δ 7.33 (m, 5H), 5.10–5.04 (m, 4H), 4.38–4.28 (m, 2H), 2.51–2.37 (m, 2H), 2.32–2.23 (m, 2H), 2.20–2.12 (m, 1H), 2.09–2.00 (m, 1H), 1.96–1.81 (m, 2H), 1.44 (s, 9H), 1.43 (s, 9H), 1.41 (s, 9H); ^{13}C NMR (100 MHz, $CDCl_3$) δ 172.9, 172.5, 172.0, 171.9, 156.8, 135.8, 128.5, 128.2, 82.1, 82.0, 80.5, 66.4, 53.1, 53.0, 31.5, 30.3, 28.4, 28.3, 28.1, 28.0; HRMS (ESI) *m*/*z*: $[M + Na]^+$ calcd for $C_{30}H_{46}N_2O_9$, 601.3096; found, 601.3092.

Procedure for debenzylation of benzyl tris(*tert*-butoxy)-protected DUPA precursor 3 to give (*S*)-5-(*tert*-butoxy)-4-(3-((*S*)-1,5-di-*tert*-butoxy-1,5-dioxopentan-2-yl)ureido)-5-oxopentanoic acid (4): To a solution of benzyl tris(*tert*-butoxy) protected DUPA precursor **3** (0.250 g, 0.434 mmol) in dichloromethane (10 mL), 10 mol % Pd/C (40 mg) was added. The reaction mixture was hydrogenated under an atmosphere of H_2 gas (1 atm) for 24 h at room temperature. After completion of the reaction, Pd/C was filtered off through a celite bed and washed with DCM (3 × 5 mL). The solvent was evaporated under reduced pressure and the crude product was purified through column chromatography (hexane/ethyl acetate = 50:50) to afford the tris(*tert*-butoxy)-protected DUPA precursor **4** which was further used for peptide coupling reaction in the solid-phase peptide synthesis.

(*S*)-5-(*tert*-Butoxy)-4-(3-((*S*)-1,5-di-*tert*-butoxy-1,5-dioxopentan-2-yl)ureido)-5-oxopentanoic acid (4): Colourless viscous liquid solidified on standing (yield = 80%, 169 mg), R_f = 0.48 (EtOAc/hexane = 1:1); ^{1}H NMR (400 MHz, $CDCl_3$) δ 5.01 (d, *J* = 7.76 Hz, 2H), 4.32 (ddd, *J* = 5.0, 5.26, 7.76 Hz, 2H), 2.37–2.21 (m, 4H), 2.10–2.01 (m, 2H), 1.89–1.80 (m, 2H), 1.45 (s, 9H), 1.42 (s, 18H); ^{13}C NMR (100 MHz, $CDCl_3$) δ 176.1, 173.1, 172.5, 171.9, 157.8, 82.5, 82.1, 80.6, 53.3, 53.0, 31.5, 30.3, 28.4, 28.1, 28.0, 27.9, 27.8; HRMS (ESI) *m*/*z*: $[M + Na]^+$ calcd for $C_{23}H_{40}N_2O_9$, 511.2626; found, 511.2640.

General procedure for solid-phase synthesis

Resin swelling

All the resins used in solid-phase peptide synthesis were swelled initially with 5 mL of DCM for 30 minutes by bubbling nitrogen and after draining DCM, the resin is swelled once again with 5 mL DMF thrice for 15 minutes each.

General procedure for the Kaiser test

Few resin beads were taken in a test-tube and 2 drops of each of ninhydrin, phenol and 0.1% potassium cyanide solution were added to the test-tube and heated for 2 minutes at 110 °C in a sand bath. The presence of free amine groups was confirmed by the appearance of dark blue colored resin beads in the test tube. The test was performed after coupling of each amino acid by the aforementioned procedure.

General procedure for NHFmoc deprotection

The Fmoc-amino group in the growing peptide chain was deprotected in each step using 20% piperidine in DMF (10 mL) by bubbling nitrogen for 10 minutes through the swelled resin beads. The procedure was repeated thrice (1 × 4 mL; 2 × 3 mL) to ensure complete deprotection of Fmoc protecting group.

General procedure for peptide cleavage from resin beads

A mixture of 9.25 mL trifluoroacetic acid (TFA), 0.25 mL triisopropylsilane (TIPS), 0.25 mL EDT and 0.25 mL H_2O was prepared and 5 mL of this cocktail solution was added to resin beads and nitrogen was bubbled through the solution for 30 minutes. The same procedure was repeated twice using 2.5 mL of cocktail solution. The collected mother liquor from cleavage was evaporated under reduced pressure and the concentrated viscous liquid was precipitated in ice cold diethyl ether. The precipitated product was dried under nitrogen atmosphere and utilized for further studies.

General procedure for solid-phase peptide synthesis

Synthesis of PSMA targeted DUPA rhodamine B conjugate 13, DUPA-NH-$(CH_2)_7$CO-Phe-Phe-NH-$(CH_2)_7$CO-Lys(rhodamineB)-Dap-Asp-Cys: H-Cys-2-ClTrt resin (0.050 g, 0.031 mmol) was initially swelled in DCM (5 mL) followed by DMF (5 mL). *N*-Fmoc-Asp(O*t*-Bu)-OH (0.032 g, 0.078 mmol), PyBOP (0.040 g, 0.078 mmol) and DIPEA (0.135 mL, 0.78 mmol) in 0.5 mL DMF was added to the peptide vessel containing resin beads and the coupling reaction was continued for 6 h. The resin beads were washed with DMF (3 × 5 mL) followed by the washing with isopropanol (3 × 3 mL). Completion of the peptide coupling reaction was confirmed by performing the Kaiser test (KT). Then a solution of 20% piperidine in DMF (1 × 4 mL; 2 × 3 mL) was added to

the peptide vessel to cleave NHFmoc protecting group. Resin beads were washed with DMF (3 × 3 mL) followed by isopropanol (3 × 3 mL) and the formation of free amine was confirmed by the Kaiser test. After the swelling of resin in DMF, Boc-DAP(Fmoc)-OH (0.033 g, 0.078 mmol), PyBOP (0.040 g, 0.078 mmol) and DIPEA (0.135 mL, 0.78 mmol) in 0.5 mL DMF was added to the resin beads and the same steps were followed as described above. A series of amino acids including of Fmoc-Lys(Tfa)-OH (0.036 g, 0.078 mmol), Fmoc-8-aminocaprylic acid (0.030 g, 0.078 mmol), Fmoc-Phe-OH (0.030 g, 0.078 mmol), Phe-OH (0.030 g, 0.078 mmol) followed by Fmoc-8-aminocaprylic acid (0.030 g, 0.078 mmol) were coupled to the growing peptide chain as described earlier. After deprotection of Fmoc groups, tris(*tert*-butyl) protected DUPA (0.023 g, 0.047 mmol), PyBOP (0.040 g, 0.078 mmol) and DIPEA (0.135 mL, 0.78 mmol) in 0.5 mL DMF was added to the resin beads and swelled for 6 h. The completion of reaction was confirmed by the Kaiser test. At last the trifluoroacetyl-protected amino group of lysine was cleaved by treatment with 2 M aqueous piperidine for 6–12 h at room temperature and the complete deprotection of Tfa group was confirmed by the Kaiser test. Rhodamine B (0.023 g, 0.047), PyBOP (0.040 g, 0.078 mmol) and DIPEA (0.135 mL, 0.78 mmol) in 0.5 mL DMF was added to the peptide vessel and swelled for 6 h at room temperature. The completion of rhodamine B coupling reaction was confirmed by the Kaiser test. Finally, the resin was cleaved using a cocktail solution as described earlier in the Experimental section. The crude fluorescent peptide conjugate was concentrated under reduced pressure to evaporate TFA and ice-cold ether was added to precipitate the DUPA rhodamine B conjugate **13** as bright red solid. The crude product **13** was purified through a Büchi reveleris prep instrument using RP-PFP preparative column (XSelect CSH Prep Fluorophenyl 5 µm OBD, 5 µm, 19 mm × 150 mm) at λ = 280 or 555 nm (detailed procedure was mentioned in the preparative HPLC chromatography method). Acetonitrile was removed under reduced pressure, and pure fractions were freeze-dried to yield DUPA rhodamine B conjugate **13** as red solid. The yield of **13** was 76% (41 mg) and the purity of the conjugate **13** is further confirmed by reverse phase analytical high-pressure liquid chromatography (RP-HPLC) t_R = 9.8 min. The molecular mass is determined by LCMS. HRMS (+ESI) calcd for $[M - Cl]^+$ $(C_{89}H_{121}N_{14}O_{21}S)^+$: 1753.8546; found, 1753.8557.

General procedure for solid-phase peptide synthesis of pteroate rhodamine B conjugate 17, pteroate-NH-$(CH_2)_7$CO-Lys(rhodamine B)-DAP-Asp-Cys: H-Cys(Trt)-2-ClTrt resin (0.050 g, 0.031 mmol) was swelled first using DCM (5 mL) followed by DMF (5 mL) according to the aforementioned procedure. Fmoc-Asp(O*t*-Bu)-OH (0.032g, 0.078 mmol), PyBOP (0.040 g, 0.078 mmol) and DIPEA (0.135 mL, 0.78 mmol) in 0.3 mL DMF was added to peptide vessel with resin beads and bubbled using nitrogen gas for 6 h. The resin beads were washed with DMF (3 × 5 mL) followed by the washing with isopropanol (3 × 3 mL). The completion of reaction was confirmed by performing the Kaiser test. After the completion of coupling, a solution of 20% piperidine in DMF (1 × 4 mL; 2 × 3 mL) was added to the peptide vessel to cleave the NHFmoc protecting group according to the procedure mentioned in experimental section. Resin beads were washed with DMF (3 × 3 mL) and isopropanol (3 × 3mL) and the formation of free amine was confirmed by the Kaiser test. After swelling the resin again in DMF, Boc-Dap(Fmoc)-OH (0.033 g, 0.078 mmol), PyBOP (0.040 g, 0.078 mmol) and DIPEA (0.135 mL, 0.78 mmol) in 0.5 mL DMF was added to the resin and same steps were followed as described above. Amino acids Fmoc-Lys(Tfa)-OH (0.036 g, 0.078 mmol), Fmoc-8-aminocaprylic acid (0.030g, 0.078 mmol) were coupled sequentially to the peptide chain following similar procedure. Finally after the cleavage of NHFmoc group from the peptide chain using 20% piperidine in DMF (1 × 4 mL; 2 × 3 mL), N^{10}-(trifluoroacetyl)pteroic acid (0.046 g, 0.019 mmol), PyBOP (0.040 g, 0.078 mmol) and DIPEA (0.135 mL, 0.78 mmol) in 0.3 mL DMSO was added to the resin beads in peptide vessel and bubbled for 6 h. The peptide vessel was wrapped with aluminum foil to protect from light. The completion of reaction was ensured by the Kaiser test after washing the resin beads with DMF (3 × 5 mL) and isopropanol (3 × 5 mL). An aliquot of 1% hydrazine in DMF (3 × 2 mL) was added to the resin beads to deprotect N^{10}-(trifluoroacetyl) protecting group by bubbling through resin beads for 10 min each. The resin beads were washed with DMF (3 × 3 mL) followed by isopropanol (3 × 3 mL). The secondary amine group generated in the pteroate core does not give a positive Kaiser test. The lysine trifluoroacetyl protected amino group was now deprotected by 6–12 h treatment with 2 M aqueous piperidine at room temperature and the completion of deprotection was confirmed by the Kaiser test. Rhodamine B (0.023 g, 0.047 mmol), PyBOP (0.040 g, 0.078 mmol) and DIPEA (0.135 mL, 0.78 mmol) in 0.5 mL DMF was added to the resin beads in the peptide vessel and the coupling was continued for 6 h at room temperature. The completion of the reaction was confirmed by the Kaiser test. The resin beads were dried for 30 minutes under nitrogen atmosphere. The pteroate rhodamine B conjugate **17** was obtained as a red precipitate after cleavage from the resin beads. The crude product **17** was purified through a Büchi reveleris prep instrument using RP-PFP (pentafluorophenyl) preparative column (5 µm, 19 mm × 150 mm) at λ = 280 or 555 nm (detailed procedure was mentioned in the preparative HPLC chromatography method). Acetonitrile was removed under reduced pressure, and pure fractions were freeze-dried to yield

pteroate Rhodamine B conjugate **17** as red solid. The yield of the product **17** was 70% (33 mg) and the purity of the conjugate **17** is further confirmed by reverse phase analytical high-pressure liquid chromatography, (RP-HPLC) t_R = 3.09 min. The molecular mass is determined by LCMS and HRMS (+ESI) calcd for $[M - Cl]^+$ $(C_{66}H_{84}N_{15}O_{12}S)^+$: 1310.6139; found, 1310.6352.

Analytical HPLC method

The purity of bioconjugates **13** and **17** were analyzed using a Dionex HPLC-Ultimate 3000 system. Typically a solution of either **13** or **17** (20 µL, 1.0 mg/1.0 mL) dissolved in a mixture of CH_3CN/H_2O (1:1) was injected via the autosampler and eluted using a Dionex Acclaim® 120 C_{18}, 5 µm, 4.6 mm × 250 mm analytical column at a flow rate of 1 mL/min (mobile phase, A = 0.1% trifluoro acetic acid/H_2O and B = acetonitrile). An isocratic flow of 40% B (v/v) was used during the run for 0 to 4 min and gradually a linear gradient of B upto 100% B (v/v) was applied over a period of 40 min. The chromatogram was recorded using Ultimate 3000 RS Variable Wavelength detector at 225–280 nm.

Preparative HPLC method

The purification of bioconjugates **13** and **17** was performed using a Büchi Reveleris Prep HPLC System. Crude bioconjugates **13** or **17** were dissolved in a mixture of CH_3CN/H_2O (1:1, 1 mL) and injected into the sample injector for elution using a RP-PFP (Reverse Phase PentafluoroPhenyl) preparative column (XSelect CSH Prep Fluorophenyl 5 µm OBD, 19 mm × 150 mm). A flow rate of 10 mL/min (mobile phase, A = 0.1% trifluoro acetic acid/H_2O and B = acetonitrile) is maintained throughout the run and the mobile phase gradient was changed from 1% B (v/v) to 50% B (v/v) over a period of 40 min. The mobile phase gradient was further changed to 80% B (v/v) in the next 15 min and the chromatogram was recorded at λ = 280 or 555 nm. Pure fractions of **13** or **17** were collected using an automatic fraction collector, acetonitrile was evaporated under reduced pressure and freeze dried to obtain pure conjugates **13** or **17**.

Culture of human cancer and epithelial cell lines: LNCaP and CHO-β cells were obtained as gift from Prof. Philip S. Low, Purdue University, West Lafayette, USA whereas the PC-3 cell line was purchased from NCCS, Pune, India. LNCaP cells were grown as a monolayer using 1640 RPMI medium containing 10% heat-inactivated fetal bovine serum and 1% penicillin streptomycin and CHO-β cells in folate-deficient RPMI 1640 containing 10% heat-inactivated foetal bovine serum and supplemented with 1% penicillin streptomycin. Both the cell lines were grown in a 5% CO_2:95% air-humidified atmosphere at 37 °C.

Procedure for uptake study of peptide conjugates 13 and 17 using laser scanning confocal microscope in human cancer cell lines LNCaP, PC-3 and epithelial cell line CHO-β: LNCaP cells (15,000 cells/well in 1 mL), CHO-β (10,000 cells/well in 1 mL) and PC-3 (10,000 cells/well) were seeded into German borosilicate confocal dishes and allowed cells to form monolayers over 24 h. Spent medium was replaced with fresh medium containing DUPA-rhodamine B, **13** (100 nM) and pteroate-rhodamine B, **17** (150 nM) in LNCaP and CHO-β cells, respectively and the cells were incubated with the compound for 1 h at 37 °C. For competition experiments, a 100-fold excess concentration of binding ligand, 2-PMPA for LNCap cells and folic acid for CHO-β cells were incubated for 1 h at 37 °C prior to incubation with bioconjugate **13** (100 nM) and **17** (150 nM), respectively. After rinsing with fresh medium (3 × 1.0 mL) to remove unbound conjugates, confocal images were acquired using a laser scanning confocal microscopy (FV 1000, Olympus) by excitation at 559 nm (yellow diode laser) and emission at 618 nm.

Author's Contributions

Sagnik Sengupta (SS) chemically synthesized and characterized the targeting ligands and bioconjugate **13**, Bishnubasu Giri synthesized and characterized the bioconjugate **17**, Mena Asha Krishnan (MAK) performed biological studies of bioconjugates **13** and **17** using confocal microscopy on various cell lines, SS, MAK, Premansh Dudhe and Ramesh B Reddy wrote the initial draft of the manuscript and involved in updating the latest references with proper format. Sudeshna Chattopadhyay and Venkatesh Chelvam ideated the research, executed the project for biological and nanomaterial delivery applications along with drafting and revising the final manuscript critically for important intellectual content.

Supporting Information

Supporting Information File 1

NMR and HRMS spectra of compounds **3**, **4** and analytical HPLC spectra of purified (λ at 254 nm and 225 nm) as well as crude (λ at 225 nm), electrospray ionization mass spectra and high-resolution mass spectra for bioconjugates **13** and **17**.

[https://www.beilstein-journals.org/bjoc/content/supplementary/1860-5397-14-244-S1.pdf]

Acknowledgements

The authors are thankful to the Ministry of Human Resource Development (MHRD), Government of India and Indian Institute of Technology (IIT) Indore, India for research funding and student's research fellowships. We also thank Sophisticated

Instrumentation Centre (SIC), IIT Indore for facilitating the use of their instruments required for purification and characterization of our synthesized biomolecules. We are also thankful to Prof. Philip S. Low, Purdue University, USA for providing LNCaP, and CHO-β cell lines as gift for performing biological studies.

References

1. Srinivasarao, M.; Low, P. S. *Chem. Rev.* **2017,** *117,* 12133–12164. doi:10.1021/acs.chemrev.7b00013
2. Bernsen, M. R.; Kooiman, K.; Segbers, M.; van Leeuwen, F. W. B.; de Jong, M. *Eur. J. Nucl. Med. Mol. Imaging* **2015,** *42,* 579–596. doi:10.1007/s00259-014-2980-7
3. Yankeelov, T. E.; Abramson, R. G.; Quarles, C. C. *Nat. Rev. Clin. Oncol.* **2014,** *11,* 670–680. doi:10.1038/nrclinonc.2014.134
4. Gao, M.; Yu, F.; Lv, C.; Choo, J.; Chen, L. *Chem. Soc. Rev.* **2017,** *46,* 2237–2271. doi:10.1039/C6CS00908E
5. Cutler, C. S.; Hennkens, H. M.; Sisay, N.; Hucklier-Markai, S.; Jurisson, S. S. *Chem. Rev.* **2013,** *113,* 858–883. doi:10.1021/cr3003104
6. Mather, S. *Bioconjugate Chem.* **2009,** *20,* 631–643. doi:10.1021/bc800401x
7. Chang, S. S. *Rev. Urol.* **2004,** *6* (Suppl. 10), S13–S18.
8. Barrio, M.; Fendler, W. P.; Czernin, J.; Herrmann, K. *Expert Rev. Mol. Diagn.* **2016,** *16,* 1177–1188. doi:10.1080/14737159.2016.1243057
9. Ristau, B. T.; O'Keefe, D. S.; Bacich, D. J. *Urol. Oncol.: Semin. Orig. Invest.* **2014,** *32,* 272–279. doi:10.1016/j.urolonc.2013.09.003
10. Kalli, K. R.; Oberg, A. L.; Keeney, G. L.; Christianson, T. J. H.; Low, P. S.; Knutson, K. L.; Hartmann, L. C. *Gynecol. Oncol.* **2008,** *108,* 619–626. doi:10.1016/j.ygyno.2007.11.020
11. Lutz, R. J. *Transl. Cancer Res.* **2015,** *4,* 118–126. doi:10.3978/j.issn.2218-676X.2015.01.04
12. Sega, E. I.; Low, P. S. *Cancer Metastasis Rev.* **2008,** *27,* 655–664. doi:10.1007/s10555-008-9155-6
13. Low, P. S.; Kularatne, S. A. *Curr. Opin. Chem. Biol.* **2009,** *13,* 256–262. doi:10.1016/j.cbpa.2009.03.022
14. Lu, Y.; Stinnette, T. W.; Westrick, E.; Klein, P. J.; Gehrke, M. A.; Cross, V. A.; Vlahov, I. R.; Low, P. S.; Leamon, C. P. *Arthritis Res. Ther.* **2011,** *13,* R56. doi:10.1186/ar3304
15. Jager, N. A.; Teteloshvili, N.; Zeebregts, C. J.; Westra, J.; Bijl, M. *Autoimmun. Rev.* **2012,** *11,* 621–626. doi:10.1016/j.autrev.2011.11.002
16. Low, P. S.; Henne, W. A.; Doorneweerd, D. D. *Acc. Chem. Res.* **2008,** *41,* 120–129. doi:10.1021/ar7000815
17. van Dam, G. M.; Themelis, G.; Crane, L. M. A.; Harlaar, N. J.; Pleijhuis, R. G.; Kelder, W.; Sarantopoulos, A.; de Jong, J. S.; Arts, H. J. G.; van der Zee, A. G. J.; Bart, J.; Low, P. S.; Ntziachristos, V. *Nat. Med.* **2011,** *17,* 1315–1319. doi:10.1038/nm.2472
18. Keating, J. J.; Okusanya, O. T.; De Jesus, E.; Judy, R.; Jiang, J.; Deshpande, C.; Nie, S.; Low, P.; Singhal, S. *Mol. Imaging Biol.* **2016,** *18,* 209–218. doi:10.1007/s11307-015-0878-9
19. Kennedy, G. T.; Okusanya, O. T.; Keating, J. J.; Heitjan, D. F.; Deshpande, C.; Litzky, L. A.; Albelda, S. M.; Drebin, J. A.; Nie, S.; Low, P. S.; Singhal, S. *Ann. Surg.* **2015,** *262,* 602–609. doi:10.1097/SLA.0000000000001452
20. Okusanya, O. T.; DeJesus, E. M.; Jiang, J. X.; Judy, R. P.; Venegas, O. G.; Deshpande, C. G.; Heitjan, D. F.; Nie, S.; Low, P. S.; Singhal, S. J. *Thorac. Cardiovasc. Surg.* **2015,** *150,* 28–35. doi:10.1016/j.jtcvs.2015.05.014
21. Tummers, Q. R. J. G.; Hoogstins, C. E. S.; Gaarenstroom, K. N.; de Kroon, C. D.; van Poelgeest, M. I. E.; Vuyk, J.; Bosse, T.; Smit, V. T. H. B. M.; van de Velde, C. J. H.; Cohen, A. F.; Low, P. S.; Burggraaf, J.; Vahrmeijer, A. L. *Oncotarget* **2016,** *7,* 32144–32155. doi:10.18632/oncotarget.8282
22. Kelemen, L. E. *Int. J. Cancer* **2006,** *119,* 243–250. doi:10.1002/ijc.21712
23. Bouchelouche, K.; Choyke, P. L.; Capala, J. *Discov. Med.* **2010,** *9,* 55–61.
24. Jin, W.; Qin, B.; Chen, Z.; Liu, H.; Barve, A.; Cheng, K. *Int. J. Pharm.* **2016,** *513,* 138–147. doi:10.1016/j.ijpharm.2016.08.048
25. Zhao, X.; Li, H.; Lee, R. J. *Expert Opin. Drug Delivery* **2008,** *5,* 309–319. doi:10.1517/17425247.5.3.309
26. Rink, H. *Tetrahedron Lett.* **1987,** *28,* 3787–3790. doi:10.1016/S0040-4039(00)96384-6
27. Bollhagen, R.; Schmiedberger, M.; Barlos, K.; Grell, E. *J. Chem. Soc., Chem. Commun.* **1994,** 2559–2560. doi:10.1039/c39940002559
28. Mergler, M.; Nyfeler, R.; Tanner, R.; Gosteli, J.; Grogg, P. *Tetrahedron Lett.* **1988,** *29,* 4009–4012. doi:10.1016/S0040-4039(00)80406-2
29. Sieber, P. *Tetrahedron Lett.* **1987,** *28,* 2107–2110. doi:10.1016/S0040-4039(00)96055-6
30. Aletras, A.; Barlos, K.; Gatos, D.; Koutsogianni, S.; Mamos, P. *Int. J. Pept. Protein Res.* **1995,** *45,* 488–496. doi:10.1111/j.1399-3011.1995.tb01065.x
31. Zhao, N.; Williams, T. M.; Zhou, Z.; Fronczek, F. R.; Sibrian-Vazquez, M.; Jois, S. D.; Vicente, M. G. H. *Bioconjugate Chem.* **2017,** *28,* 1566–1579. doi:10.1021/acs.bioconjchem.7b00211
32. Kuil, J.; Buckle, T.; Yuan, H.; van den Berg, N. S.; Oishi, S.; Fujii, N.; Josephson, L.; van Leeuwen, F. W. B. *Bioconjugate Chem.* **2011,** *22,* 859–864. doi:10.1021/bc2000947
33. Napp, J.; Stammes, M. A.; Claussen, J.; Prevoo, H. A. J. M.; Sier, C. F. M.; Hoeben, F. J. M.; Robillard, M. S.; Vahrmeijer, A. L.; Devling, T.; Chan, A. B.; de Geus-Oei, L.-F.; Frauke, A. *Int. J. Cancer* **2018,** *142,* 2118–2129. doi:10.1002/ijc.31236
34. Viehweger, K.; Barbaro, L.; García, K. P.; Joshi, T.; Geipel, G.; Steinbach, J.; Stephan, H.; Spiccia, L.; Graham, B. *Bioconjugate Chem.* **2014,** *25,* 1011–1022. doi:10.1021/bc5001388
35. Xing, T.; Yang, X.; Wang, F.; Lai, B.; Yan, L. *J. Mater. Chem.* **2012,** *22,* 22290–22300. doi:10.1039/c2jm35627a
36. Kularatne, S. A.; Wang, K.; Santhapuram, H.-K. R.; Low, P. S. *Mol. Pharmaceutics* **2009,** *6,* 780–789. doi:10.1021/mp900069d
37. Kelderhouse, L. E.; Chelvam, V.; Wayua, C.; Mahalingam, S.; Poh, S.; Kularatne, S. A.; Low, P. S. *Bioconjugate Chem.* **2013,** *24,* 1075–1080. doi:10.1021/bc400131a
38. Kularatne, S. A.; Zhou, Z.; Yang, J.; Post, C. B.; Low, P. S. *Mol. Pharmaceutics* **2009,** *6,* 790–800. doi:10.1021/mp9000712
39. Kozikowski, A. P.; Zhang, J.; Nan, F.; Petukhov, P. A.; Grajkowska, E.; Wroblewski, J. T.; Yamamoto, T.; Bzdega, T.; Wroblewska, B.; Neale, J. H. *J. Med. Chem.* **2004,** *47,* 1729–1738. doi:10.1021/jm0306226
40. Ross, T. L.; Honer, M.; Müller, C.; Groehn, V.; Schibli, R.; Ametamey, S. M. *J. Nucl. Med.* **2010,** *51,* 1756–1762. doi:10.2967/jnumed.110.079756

41. Leamon, C. P.; You, F.; Santhapuram, H. K.; Fan, M.; Vlahov, I. R. *Pharm. Res.* **2009,** *26,* 1315–1323. doi:10.1007/s11095-009-9840-3
42. Mesters, J. R.; Barinka, C.; Li, W.; Tsukamoto, T.; Majer, P.; Slusher, B. S.; Konvalinka, J.; Hilgenfeld, R. *EMBO J.* **2006,** *25,* 1375–1384. doi:10.1038/sj.emboj.7600969
43. Li, D.; Elbert, D. L. *J. Pept. Res.* **2002,** *60,* 300–303. doi:10.1034/j.1399-3011.2002.21018.x
44. Moroder, L.; Filippi, B.; Borin, G.; Marchiori, F. *Biopolymers* **1975,** *14,* 2061–2074. doi:10.1002/bip.1975.360141007
45. Pazos, E.; Vázquez, O.; Mascareñas, J. L.; Vázquez, M. E. *Chem. Soc. Rev.* **2009,** *38,* 3348–3359. doi:10.1039/b908546g
46. Benešová, M.; Schäfer, M.; Bauder-Wüst, U.; Afshar-Oromieh, A.; Kratochwil, C.; Mier, W.; Haberkorn, U.; Kopka, K.; Eder, M. *J. Nucl. Med.* **2015,** *56,* 914–920. doi:10.2967/jnumed.114.147413
47. Kularatne, S. A.; Chelvam, V.; Santhapuram, H.-K. R.; Wang, K.; Vaitilingam, B.; Henne, W. A.; Low, P. S. *J. Med. Chem.* **2010,** *53,* 7767–7777. doi:10.1021/jm100729b

License and Terms

BEILSTEIN JOURNAL OF ORGANIC CHEMISTRY

Synthesis of a tubugi-1-toxin conjugate by a modulizable disulfide linker system with a neuropeptide Y analogue showing selectivity for hY1R-overexpressing tumor cells

Rainer Kufka[‡1], Robert Rennert[‡1,2], Goran N. Kaluđerović[1], Lutz Weber[2], Wolfgang Richter[3] and Ludger A. Wessjohann[*1,§]

Full Research Paper

Open Access

Address:
[1]Department of Bioorganic Chemistry, Leibniz Institute of Plant Biochemistry, Weinberg 3, D-06120 Halle (Saale), Germany, [2]OntoChem GmbH, Blücherstr. 24, D-06120 Halle (Saale), Germany and [3]TUBE Pharmaceuticals GmbH, Leberstr. 20, A-1110 Vienna, Austria

Email:
Ludger A. Wessjohann[*] - wessjohann@ipb-halle.de

* Corresponding author ‡ Equal contributors
§ Fax: +49 345 5582 1309; Tel: +49 345 5582 1301

Keywords:
drug targeting; neuropeptide Y; PDC; peptide–drug conjugate; targeted tumor therapy; tubugi; tubulysin A; Ugi reaction

Beilstein J. Org. Chem. **2019,** *15,* 96–105.
doi:10.3762/bjoc.15.11

Received: 11 May 2018
Accepted: 21 November 2018
Published: 10 January 2019

This article is part of the Thematic Series "Peptide–drug conjugates".

Guest Editor: N. Sewald

Abstract

Tubugi-1 is a small cytotoxic peptide with picomolar cytotoxicity. To improve its cancer cell targeting, it was conjugated using a universal, modular disulfide derivative. This allowed conjugation to a neuropeptide-Y (NPY)-inspired peptide [K^4(C-βA-),F^7,L^{17},P^{34}]-hNPY, acting as NPY Y1 receptor (hY1R)-targeting peptide, to form a tubugi-1–SS–NPY disulfide-linked conjugate. The cytotoxic impacts of the novel tubugi-1–NPY peptide–toxin conjugate, as well as of free tubugi-1, and tubugi-1 bearing the thiol spacer (liberated from tubugi-1–NPY conjugate), and native tubulysin A as reference were investigated by in vitro cell viability and proliferation screenings. The tumor cell lines HT-29, Colo320 (both colon cancer), PC-3 (prostate cancer), and in conjunction with RT-qPCR analyses of the hY1R expression, the cell lines SK-N-MC (Ewing`s sarcoma), MDA-MB-468, MDA-MB-231 (both breast cancer) and 184B5 (normal breast; chemically transformed) were investigated. As hoped, the toxicity of tubugi-1 was masked, with IC_{50} values decreased by ca. 1,000-fold compared to the free toxin. Due to intracellular linker cleavage, the cytotoxic potency of the liberated tubugi-1 that, however, still bears the thiol spacer (tubugi-1-SH) was restored and up to 10-fold higher compared to the entire peptide–toxin conjugate. The conjugate shows toxic selectivity to tumor cell lines overexpressing the hY1R receptor subtype like, e.g., the hard to treat triple-negative breast cancer MDA-MB-468 cells.

Introduction

Until recently, the medication of tumor diseases was primarily based on more or less unspecific chemotherapeutics and the corresponding combination therapies [1-5]. However, severe impairments of normal, non-transformed tissues caused by widespread off-target effects have limited the therapeutic benefits of many classical chemotherapeutics [6]. Within the last two decades, progress in basic research on the biochemical, molecular biological and medicinal aspects of a broad range of tumor diseases, as well as progress in drug development technologies provided the basis for a fundamental paradigm shift in cancer treatment, away from non-selective cytotoxic chemotherapeutics towards specifically tumor-targeting therapeutics [7,8]. Such targeted therapeutics are able to address transformed cells selectively by recognition of disease-associated membrane structures, e.g., dysregulated membrane proteins, or by modulation of metabolic or regulatory characteristics that are specific or at least differential for tumor cells. Members of one prominent novel class of targeted anticancer drugs that has been developed over the last years are antibody–drug conjugates (ADCs) [9-11]. Due to their high antibody-mediated target specificity, ADCs are designed for selective treatments of tumor cells with very potent, mostly cytotoxic drug molecules while avoiding or at least limiting the off-target toxicity that would be characteristic for the stand-alone cytotoxic drugs. Currently, four therapeutic ADCs are approved, e.g., with brentuximab vedotin and trastuzumab emtansine as the first ones on the market. However, many other ADC development projects are in clinical trials [12,13].

More recently, peptide–drug conjugates (PDCs) have been recommended as targeted therapeutics [14,15]. While sharing the ADCs' therapeutic concept of targeted and highly selective drug addressing to the diseased cells, PDCs are smaller in size – which may improve tissue and cell permeability, allows a more flexible and cost-efficient production, and in many cases small peptides are less antigenic [16].

Generally, a useful PDC must exhibit at least four major skills that are all required for the selective and potent treatment of, for instance, cancer cells: (1) a sufficient in vivo half-life, ideally hours to days, to reach the diseased cells with a high portion of intact PDC; (2) a selective conjugate binding to a specific target molecule, e.g., a cell-surface receptor, that is characteristic for the diseased cells; (3) a fast and efficient but target-dependent binding, or better internalization, of the PDC into targeted cells; and (4) the efficient cleavage of the linker structure and, thereby, efficient liberation of the drug molecule from the conjugate at or within the diseased cell, resulting in an efficient intracellular drug dose, ideally killing the tumor cells.

PDCs have been demonstrated to achieve efficient and target-specific delivery of conjugated payloads, primarily highly potent toxins or chelated radiotracers, to tumor cells. In that context, the peptide moiety of the PDC is responsible for the selective targeting of the conjugate towards a specific molecular structure that has been identified to be characteristic for a diseased state of cells and tissues. Particularly G protein-coupled receptors (GPCRs) that are endogenously activated by agonistic peptide or protein ligands can be suitable target structures. Many peptide or protein ligand receptors have been associated with various diseases, e.g., cancer malignancies [17]. Amongst the GPCRs, the neuropeptide Y (NPY) receptor family comprises four closely related receptor subtypes in human (hY1R, hY2R, hY4R, and hY5R) that have been discussed in the context of several diseases [18-20]. Representing a multi-receptor/multi-ligand system, the four receptor subtypes are activated in a subtype-specific manner by three endogenous peptide ligands, namely neuropeptide Y (NPY), peptide YY (PYY), and pancreatic polypeptide (PP) [21,22]. Notably, the hY1R subtype has been discussed as promising drug target in recent years, particularly with respect to tumor diseases. Reubi and co-workers detected its pathological overexpression in ≈85% of the studied breast tumor samples and virtually all of the infiltrated lymph nodes, whereas the surrounding healthy breast tissue was found to express negligible amounts of hY1R but predominantly the closely related Y_2 receptor subtype (hY2R) [23]. Hence, a switch from hY2R to hY1R expression during pathogenic breast-cell transformation was hypothesized. Furthermore, many breast cancers of all major breast cancer types, i.e., hormone receptor positives, HER2/neu positives, as well as triple-negatives, seem to overexpress hY1R (results not published, R. Rennert, Ontochem). Beyond breast cancers, hY1R overexpression was also detected in other cancer conditions, particularly in Ewing's sarcoma, synovial sarcoma and leiomyosarcoma [24], but also renal cell carcinoma and nephroblastoma [25], neuroblastic tumors, paraganglioma, pheochromocytoma and adrenal cortical tumors [26], ovarian sex cord-stromal tumors and ovarian adenocarcinoma [27,28]. Besides its prevalent overexpression in tumor tissues, the NPY Y1 receptor has been identified as fast and efficiently internalizing GPCR in those cells upon agonist binding [29,30].

The NPY Y1 receptor subtype for these reasons is a very promising molecular target to be addressed by selective peptide–drug conjugates (PDCs), notably for cancer treatment or diagnosis. However, the peptide moiety of such hY1R-targeting PDCs cannot be native NPY as it is receptor-subtype unspecific. Therefore, highly hY1R-selective artificial analogues thereof are required. Consequently, a modified pig NPY analogue – namely [F^7,P^{34}]-pNPY, which is comparable to the human NPY

analogue [F^7,L^{17},P^{34}]-hNPY – has been identified and claimed to be especially selective for the NPY Y1 receptor subtype in comparison to the other, very closely related NPY receptor subtypes hY2R, hY4R and hY5R [31]. Recently, Ahrens et al., in cooperation with OntoChem GmbH amongst others, tested [F^7,P^{34}]-pNPY as well as a peptide–tubulysin A conjugate [K^4(C(TubA)-βA-),F^7,P^{34}]-pNPY – representing a comparable PDC – compared to wildtype pNPY for their binding affinities at the NPY Y1 receptor subtype. While [F^7,P^{34}]-pNPY (IC_{50} = 1.3 nM) showed a comparable binding affinity as pNPY (IC_{50} = 1.8 nM), the Y1 receptor binding of the peptide–tubulysin A conjugate [K^4(C(TubA)-βA-),F^7,P^{34}]-pNPY (IC_{50} = 47.6 nM) was detected to be slightly reduced. However, when testing the functional receptor activation – using an second messenger (IP) accumulation assay, Ahrens and co-workers found all three peptides and PDC, respectively, in the same EC_{50} range (1.7 to 2.6 nM) at the NPY Y1 receptor. Interestingly, at the NPY Y2 receptor subtype the EC_{50} value of the subtype-unspecific wildtype pNPY was found in the same range, but the EC_{50} values of [F^7,P^{34}]-pNPY and [K^4(C(TubA)-βA-),F^7,P^{34}]-pNPY were detected with higher than 100 nM, i.e., around two magnitudes higher than at the Y1 receptor subtype. Furthermore the authors illustrated the Y1 receptor subtype-specific endocytotic internalization of the aforementioned peptides [32]. These findings indicate the highly affine receptor binding, effective NPY Y1 receptor activation, Y1 receptor-mediated PDC internalization, as well as the payload liberation, of this type of peptide–toxin conjugate. Due to the structural identity of the used peptide moieties, we suppose a similar Y1 receptor binding and activation behavior for the tubugi-1 bearing PDC described herein, albeit not tested separately.

Meanwhile, based on this hY1R-prefering peptide [F^7,P^{34}]-pNPY, several approaches of peptide conjugates have been published with diagnostic indications [33,34]. In 2010, the Beck-Sickinger group demonstrated the suitability of hY1R-targeting for the diagnosis of NPY1R-overexpressing breast cancers in a patients pilot study (n = 5) by using a PET tracer based on the hY1R-specific NPY analogue [F^7,P^{34}]-pNPY [35]. This study demonstrated that it is not to be expected that NPY-based diagnostic or therapeutic PDCs will pass the blood-brain barrier and therefore could induce undesired adverse effects at the major native sites of NPY Y1 receptor occurrence and activity. Both Zwanziger et al. and Hofmann et al. later synthesized N-terminally truncated NPY analogues, namely NPY(28–36) analogues, with the intention to develop hY1R-selective agonists and conjugates of reduced size [36,37]. However, in most cases they lost more or less the hY1R binding, or selectivity, or receptor-activation efficacy, and had low metabolic stability. Besides diagnostic approaches, several therapeutic NPY-derived PDCs have been reported. Langer and co-workers conjugated daunorubicin and doxorubicin as cytotoxic drugs to native NPY by using various linker chemistries. However, due to missing hY1R-selectivity and relatively weak antitumor efficacy these conjugates were found unsuitable as PDCs [38]. More recently, further approaches of hY1R-addressing PDCs for therapeutic applications have been published, whereby the peptide moiety always is based on [F^7,P^{34}]-pNPY [32,39,40]. However, so far none of these [F^7,P^{34}]-pNPY-based conjugates proved a convincing in vivo efficacy. To further improve the general setting of peptide–drug conjugates, major efforts have been made to enhance target affinity and specificity as well as metabolic stability of the peptide moiety, and to identify novel PDC payloads permitting superior PDC efficacies.

Even with a good targeting peptide at hand, many other constrains apply to achieve a good conjugate drug: (1) the toxin (warhead, payload) must be highly active, as normal activity (medium to high nM IC_{50} like in taxanes or epothilones) [41-43] often is insufficient considering common receptor densities; (2) the linker must be designed to either not negatively affect activity of the payload, or even better to preclude activity in non-activated transport form which after recognition at the target site is cleaved to release an active form. It should be be sufficiently stable in plasma to survive delivery, and ideally should improve solubility and cell entry. After all, only very few toxins are known that are suitable for PDCs, and the design and synthesis of suitable linkers is a task of crucial importance and synthetic challenge that still is underestimated by many entering the field.

The most promising PDC payloads, often also referred to as ‘warheads’, are toxins of limited molecular size but with outstanding potency in the picomolar or lower concentration range. Consequently, the few candidates often have a very narrow or even non existing therapeutic window as stand-alone drug. Recently, our group was the first to publish total synthetic strategies towards tubulysins and the so-called tubugis, the latter as more suitable 2nd generation derivatives (Figure 1) [44-46]. Tubulysins were originally discovered and isolated from myxobacteria [47,48], with picomolar in vitro activities [45,46,49-54], that are caused by a destabilization and degradation of the microtubuli network undermining its function in mitosis of eukaryotic cells. Hence, these toxins primarily affect fast dividing cells, for instance all active cancer cells. Tubugis as derivatives of natural tubulysins have an almost identical antitumor activity, but are readily available and, most importantly, are chemically more inert and less degradable than native tubulysins.

The aim of this work was to prepare a novel branched NPY Y1-receptor-selective peptide–toxin conjugate version

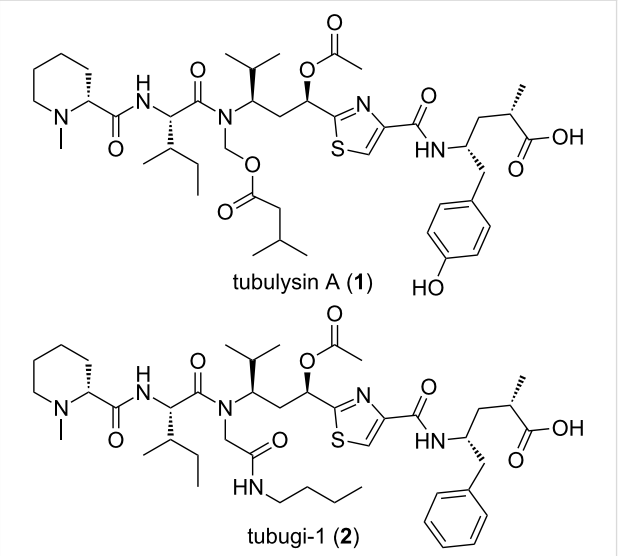

Figure 1: Tubulysin A (**1**) and tubugi-1 (**2**).

with a tubugi toxin. Therefore, the NPY analogue [K^4(C-βA-),F^7,L^{17},P^{34}]-hNPY was conjugated with tubugi-1 (**2**) as therapeutic payload, using a linker that promises a more general use than just for the present case. The study furthermore comprises the investigation of the PDCs' in vitro efficacies on the viability and proliferation of colon and prostate as well as several breast cancer and Ewing`s sarcoma cell lines. Thereby the correlation with the hY1R expression levels of the latter three cell lines was determined as proof for targeted delivery.

Results and Discussion

Synthesis of tubugi-1 building blocks

We established the Ugi reaction as a powerful tool for peptide synthesis and ligation, including the first syntheses of tubulysine derivatives by us and later also others [44,53,55,56]. In a single step, the Ugi reaction permits the introduction of different functionalities which may be followed with additional modifications on the side chain (e.g., via ring-closing metathesis or Click reaction) [53].

For tubugi conjugates we learned that alkyl amide bonds and several types of linkers are unsuitable, as they rendered the peptide inactive (results not shown). However, disulfide-bonded linkers retained activity, presumably by cleavage in the reductive milieu of cancer cells, if connected via a short ester or amide linkage at the C-terminus.

The retrosynthetic analysis (Scheme 1) shows that, in addition to tubugi-1 itself, only the readily accessible building block **4** is required to construct the activated compound tubugi-1-SSPy (**3**) as a universal precursor for peptide–toxin conjugate syntheses [57]. The pyridyl disulfide is a leaving group which can be substituted by all nucleophilic thiolates (bound to various target peptides) by directed disulfide exchange. Compound **4** is accessible by reaction of the commercially available substances cysteamine (**5**) and 2,2'-dithiodipyridine (**6**).

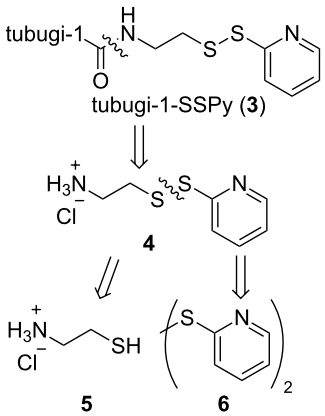

Scheme 1: Retrosynthetic analysis of the modular attachment linker tubugi-1-SSPy (**3**).

In practice, the synthesis of tubugi-1-SSPy from the published methyl ester precursor **7** is more efficient via the non-acetylated tubugi-1, because in this case it is not necessary to isolate tubugi-1 (**2**) itself (Scheme 2). Therefore, methyl ester **7** is hydrolyzed at all ester bonds, and the resulting acid is acetylated at the tubuvaline hydroxy group to give tubugi-1 (**2**). Without isolation this is directly converted using building block **4** and HBTU and DIPEA as reagents to give tubugi-1-SSPy (**3**, Scheme 2). Purification by column chromatography finally yields the target compound tubugi-1-SSPy (**3**), which constitutes the payload with a rather universally pre-activated linker.

The disulfide linkage was chosen for the tubugi-1 coupling to the peptide moiety due to own promising preliminary work. Several linker chemistries were tested with tubulysin-like peptides – amongst them amide and ester linkers, hydrazone linker, VC linker etc. – the disulfide linker described herein, however, showed the best performance regarding synthetic practicability in conjunction with tubugi-1 and a peptide moiety, as well as the best results liberating the toxin from the conjugate.

Synthesis of hY1R-targeting PDC using tubugi-1 (**2**)

The peptide–toxin conjugate bearing the payload tubugi-1, [K^4(C(tubugi-1)-βA),F^7,L^{17},P^{34}]-hNPY (**8**), was synthesized by reacting the tubugi-1-SSPy (**3**) with the free thiol function of a β-alanine–cysteine dipeptide (βAC) linked to the side chain of Lys^4 of the targeting peptide. For this purpose, 1 mol equiv of

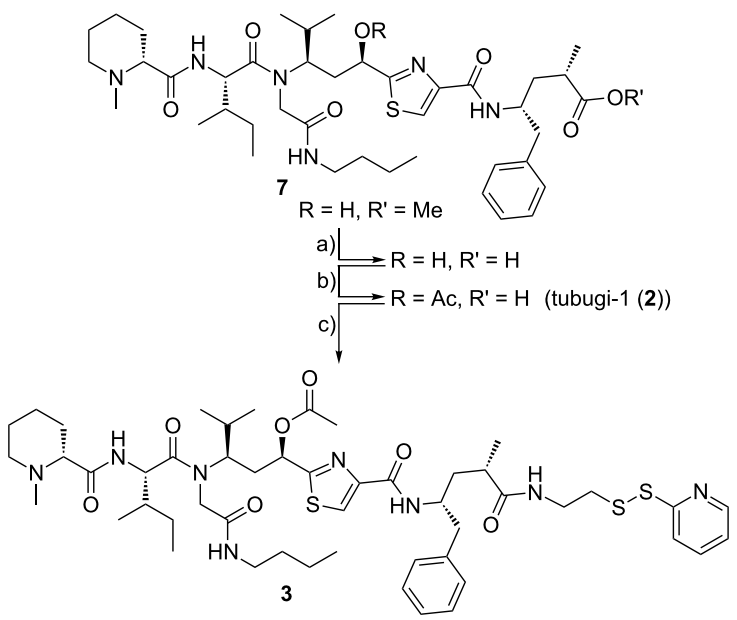

Scheme 2: Synthesis of tubugi-1-SSPy (**3**): a) LiOH·H_2O, THF/H_2O, 0 °C → rt; b) Ac_2O, py; c) **4**, HBTU, DMF, DIPEA, MeOH, under N_2 atmosphere, 42% (3 steps).

the tubugi-1-SSPy building block **3** and one molar equivalent of the targeting peptide, [K^4(C-βA-),F^7,L^{17},P^{34}]-hNPY, were reacted for 60 min in an air- and moisture-free atmosphere (Scheme 3). The desired tubugi-1–NPY conjugate **8** with cleavable disulfide bridge was isolated by RP-HPLC and the purity of the substance was determined by analytical HPLC. The conjugate **8** was characterized by ESI–FTICR–MS measurements (see Supporting Information File 1). All signals for $[M + nH]^{n+}$ with n = 4–8 could be identified.

After NPY Y_1 receptor-mediated, endocytotic accumulation of the respective peptide–toxin conjugate **8** in the targeted tumor cells, the cytotoxic tubugi-1 should be released by cleavage of the disulfide bridge in the highly reducing environment of the endo-lysosomal compartments. From the synthetic point of view, this compound is accessible, as shown by reduction of tubugi-1-SSPy (**3**) with DTT (Scheme 4). Comparable reactivity is expected within the endo-lysosomal compartments after NPY Y_1 receptor-mediated internalization of the peptide–toxin conjugate into the target cells via clathrin-dependent endocytosis. In the following, in vitro studies were conducted to verify if this expectation is met, and to study the biological consequences thereof with respect to the antitumor impact of the peptide–toxin conjugate **8**.

Effect on cell viability and proliferation

Due to their very high toxic potency, tubulysins as well as their synthetic tubugi analogues can also exhibit toxic effects on healthy cells. Therefore, considerable adverse effects can occur in vivo in case of untargeted applications. For that reason, feasible therapeutic windows of this class of toxins are only realistic if the toxins are applied as 'detoxified' prodrugs, e.g., in the form of peptide–toxin conjugates, whereby the effect of tubulysin or tubugi, respectively, is strongly hampered in its cytotoxic activity, and the peptide moiety ensures the target-specific toxin delivery toward the diseased cells, while omitting (most) healthy cells.

To assess the impact of the chemical modifications due to the linker-assisted peptide–toxin conjugation and toxin liberation on the tubugi-1 toxin's, in vitro antitumor efficiency of free tubugi-1 (**2**), tubugi-1–NPY-derived conjugate **8**, as well as its reduced linker product **9** were initially tested against HT-29, PC-3 and Colo320 tumor cells. Contrarily to, for instance, SK-N-MC cells shown in Figure 2, the three aforementioned cell lines are not known for high NPY receptor expression levels. Throughout the three cell lines, PC-3 expresses the highest level of NPY Y1 receptor [58], but by magnitudes lower than SK-N-MC for instance. This might also explain the gap of the toxic potencies (factor ≈1.000) of **2** and **8**, respectively, as shown in Table 1. Furthermore, the PC-3 cells were indeed detected to be the most sensitive cell line compared to HT-29 and Colo320, since PC-3 probably expresses a higher NPY Y1 receptor level and internalizes, consequently, more peptide–toxin conjugate.

The antiproliferative activities of the investigated compounds and conjugates are summarized in Table 1. Natural tubulysin A

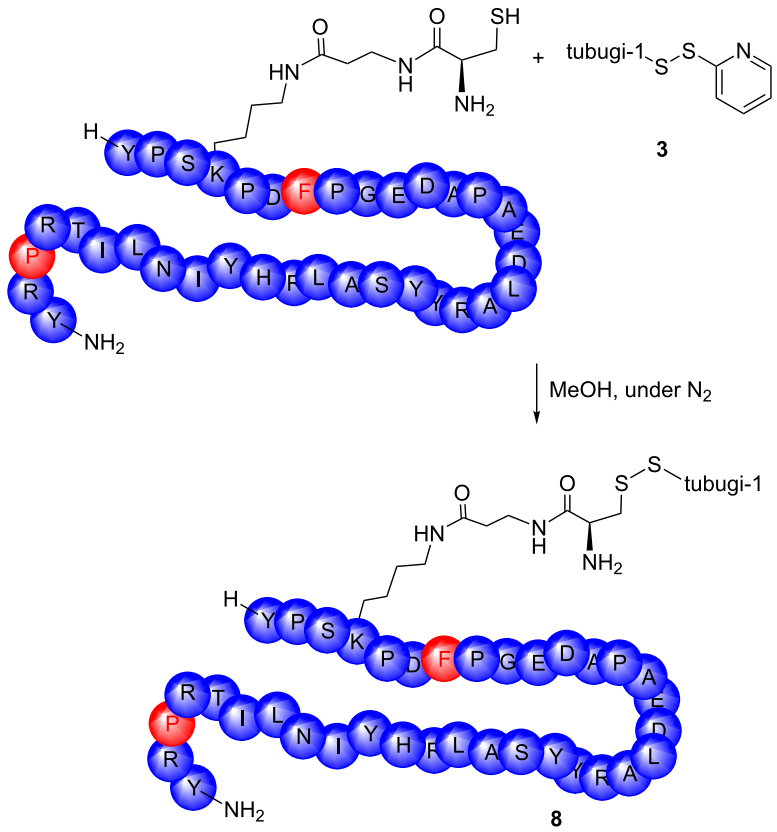

Scheme 3: Synthesis of the tubugi-1–NPY conjugate [K^4(C(tubugi-1)-βA-),F^7,L^{17},P^{34}]-hNPY (**8**).

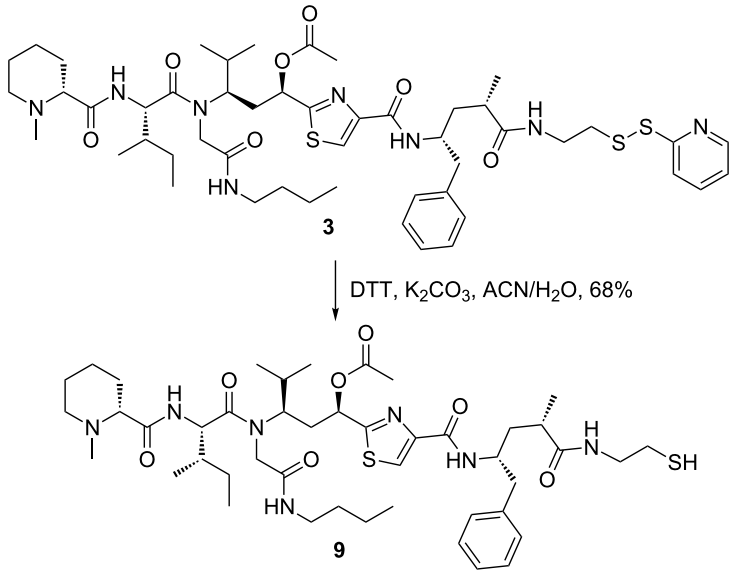

Scheme 4: Toxin liberation by disulfide linker cleavage from the activated toxin conjugate under reductive conditions using DTT.

(**1**), used for comparison, and the synthetic analogue tubugi-1 (**2**) expressed similar cytotoxic activities against the selected cancer cell lines in medium pM concentrations. Both compounds, **1** and **2**, are able to penetrate the cells' membrane by unspecific, receptor-independent pathways, not discriminating between normal and transformed cells. For that reason it is very

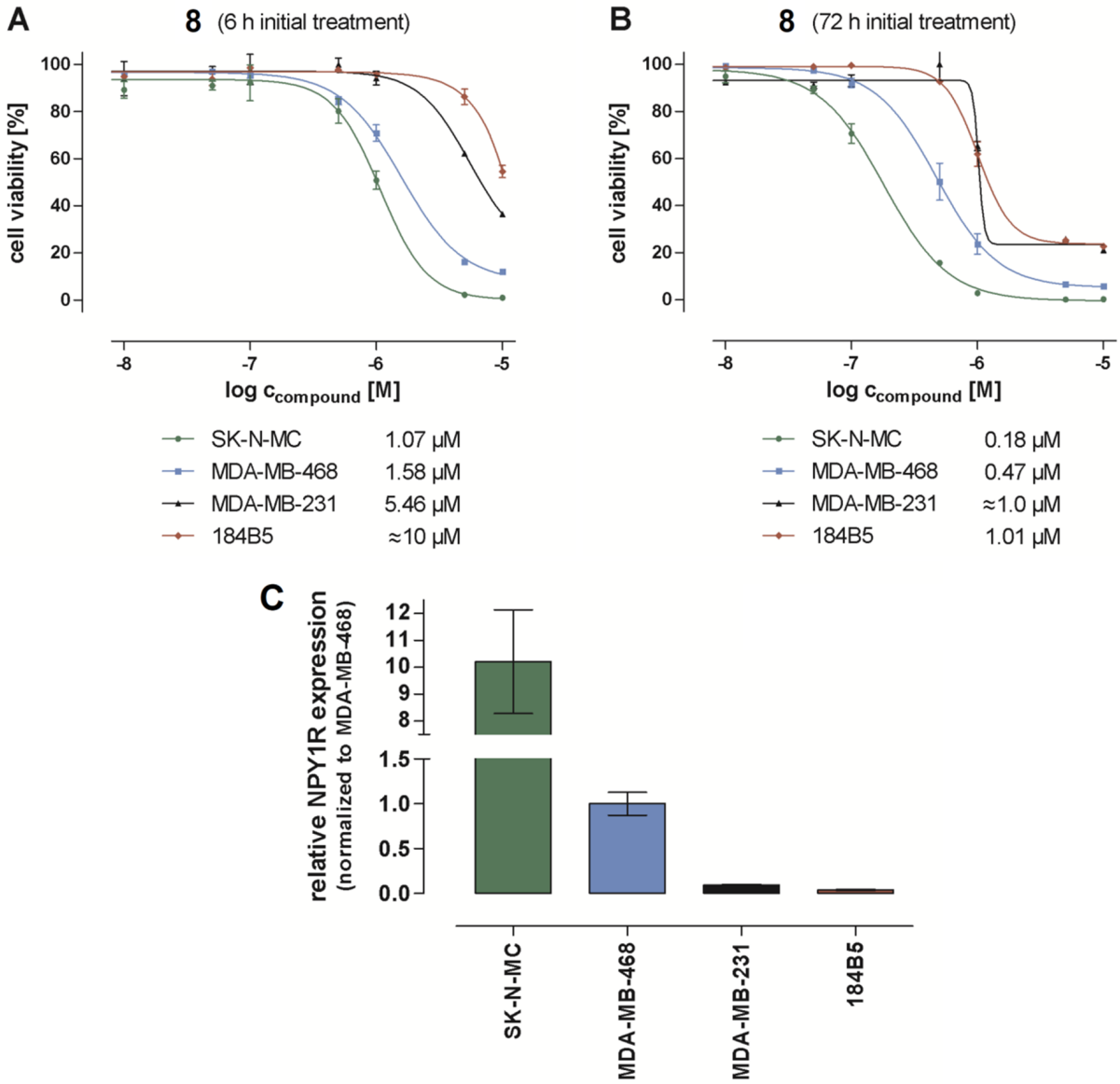

Figure 2: Reduction of viability and proliferation of SK-N-MC, MDA-MB-468, MDA-MB-231 cancer cell lines, and normal mammary gland epithelium cell line 184B5 treated with NPY Y1 receptor-targeting peptide–toxin conjugate **8**: (A) pulse setting (initial 6 h treatment followed by 66 h growth in PDC-free standard medium); (B) 72 h treatment; (C) NPY Y1 receptor expression of the SK-N-MC, MDA-MB-468, MDA-MB-231 and 184B5 cell lines determined by using RT-qPCR quantification; the NPY1R expression levels are normalized to NPY1R expression level in MDA-MB-468 cells (set to 1.0).

difficult to adjust a practicable therapeutic window for these toxins. All the more, it is important to mask the high toxicity of tubulysin A and tubugi-1 until the toxins are delivered to the cells targeted. Indeed, in its conjugated form, represented by **8**, attached to the peptide moiety designed to target the NPY Y1 receptor, the toxicity of tubugi-1 was found to be masked, with IC_{50} values increased ≈1,000-fold compared to the free toxin. The restoration of the tubugi-1 toxicity presupposes the intracellular cleavage of the disulfide linker within the reducing environment of the endo-lysosomal compartments of the addressed tumor cells, what should be simulated by testing tubugi-1-SH (**9**). As shown in Table 1, the cytotoxic potency of the tubugi-1-SH was – in case of HT-29 and PC-3 – by factors ≈5 to 8 higher compared to the entire peptide–toxin conjugate **8**. The only slight increase of cytotoxic activity of compound **9** compared to the complete conjugate **8** in Colo320 cells is most likely caused

Table 1: IC_{50} values [nM] of the reference and linker-modified toxin against HT-29, PC-3 and Colo320 cell lines.

compound		IC_{50} [nM]		
		HT-29	PC-3	Colo320
1	tubulysin A	0.21 ± 0.05	0.32 ± 0.06	0.38 ± 0.01
2	tubugi-1	0.14 ± 0.02	0.23 ± 0.05	0.46 ± 0.05
8	tubugi-1–SS–NPY	452 ± 60	205 ± 49	706 ± 185
9	tubugi-1-SH	60 ± 6	41 ± 8	556 ± 77

by a generally weak responsiveness of Colo320 cells towards tubugi-1-SH and the entire conjugate tubugi-1–SS–NPY. When compared with HT-29 and PC-3 cells, the IC50 value of tubugi-1-SH is by factor 10 higher in Colo320. Since the membrane passage of tubugi-1-SH is not depending on a NPY receptor, there have to be other explanations for the reduced cytotoxic impact of tubugi-1 and corresponding derivatives in Colo320, rather than the NPY Y1 receptor expression level.

A significant aspect of the present concept of a hY1R-targeting peptide–toxin conjugate is the fact that intact tubugi-1–NPY conjugate **8** permits in the systemic situation before reaching the target cells much lower toxicity than the cytotoxic compound tubugi-1 alone, thus opening a feasible therapeutic window for the class of tubugi toxins. In that context, a loss of tubugi-1 activity is expectable due to its chemical modification caused by the linker-based conjugation, and after linker cleavage the intracellular activities of **8**, i.e., the activities of the linker cleavage product **9**, are within an acceptable range, and are comparable or higher than that of some commercially used anticancer compounds (e.g., cisplatin and doxorubicin). Further in vitro cell proliferation and viability assays were conducted to investigate the impact of various durations of incubation of **8**, and for the correlation of its potency with the hY1R expression levels of the cells.

For that reason, a collection of tumor cell lines was used that represents a wide range of cellular hY1R expression levels, i.e., highly hY1R-overexpressing Ewing`s sarcoma SK-N-MC cells, the triple-negative breast cancer cell lines MDA-MB-468 and MDA-MB-321 which are moderately and weakly expressing, respectively, as well as the 184B5 cell line, representing a normal, but chemically immortalized mammary gland epithelium with very weak hY1R expression. These cell lines were incubated with PDC **8** in two treatment regimens. One regime considered a pulsed setting, i.e., initial treatment with the drug for 6 h, washing and subsequently culturing without the PDC to reach 72 h (Figure 2A). In the second regime, the cells were treated for the whole 72 h period with the PDC (Figure 2B). As to be expected, the 72 h treatment is more effective than the 6 h pulse treatment. Notably, in vitro antitumor activities of **8** were found to correlate very good with the hY1R expression levels, as detected by gene expression analyses using RT-qPCR (Figure 2C). Both the cytotoxic activity and the hY1R expression level rank in the order SK-N-MC > MDA-MB-468 > MDA-MB-231 > 184B5, what proofs the hY1R-specific and -selective nature of the mode of antitumor action of the designed PDC **8**. Importantly, the activity of **8** against the selected normal breast cell line 184B5 is in the same order of magnitude as for the hY1R-deficient tumor cell line (MDA-MB-231), both tested at even higher concentration of the PDC than for the Y1 cell lines. This points out good selectivity not only between tumor cell lines with the different hY1R expression levels but also good discrimination against normal (non-cancerous) cells.

Conclusion

The highly active cytotoxin tubugi-1 was successfully conjugated to a truncated and modified neuropeptide-Y mimetic to form a new peptide–toxin conjugate (PDC **8**) with a reductively cleavable disulfide linker. The tubugi-1–NPY conjugate has a strongly masked antitumor activity against HT-29, PC-3 and Colo320 cells in comparison to the active compound alone, but the activity is restored to a sufficient extent upon linker cleavage (tubugi-1–SS–NPY → tubugi-1-SH). Most importantly, the cytotoxic potential of tubugi-1–SS–NPY correlates very well with the hY1R expression levels of a panel of tumor cell lines. For instance, the hY1R-overexpressing Ewing`s sarcoma cell line SK-N-MC was much more affected by the PDC than the normal (but chemically transformed) cell line 184B5 with weak hY1R expression. However, further efforts should be made to improve activity after internalization of the PDC.

Overall, the investigations carried out up to this point provide a biological validation of the developed conjugate. The principally modular conjugation protocol for tubugis bears promise for further cancer targeting conjugates.

Supporting Information

Supporting Information File 1

Complete experimental procedures and characterization data.
[https://www.beilstein-journals.org/bjoc/content/supplementary/1860-5397-15-11-S1.pdf]

Acknowledgements

The authors acknowledge support from the State of Saxony-Anhalt (MK-LSA, Projekt “Lipopeptide”). We thank Dr. Jürgen Schmidt and Ms. Anja Ehrlich for HRMS and HPLC support, respectively.

ORCID® iDs

Goran N. Kaluđerović - https://orcid.org/0000-0001-5168-1000
Lutz Weber - https://orcid.org/0000-0002-0101-4346
Wolfgang Richter - https://orcid.org/0000-0002-8719-1131
Ludger A. Wessjohann - https://orcid.org/0000-0003-2060-8235

References

1. Saung, M. T.; Zheng, L. *Clin. Ther.* **2017,** *39,* 2125–2134. doi:10.1016/j.clinthera.2017.08.015
2. Bilen, M. A.; Carlisle, J. W.; Sonpavde, G. *Expert Opin. Invest. Drugs* **2018,** *27,* 163–170. doi:10.1080/13543784.2018.1427731
3. Kaluđerović, G. N.; Paschke, R. *Curr. Med. Chem.* **2011,** *18,* 4738–4752. doi:10.2174/092986711797535308
4. Vancurova, I.; Uddin, M. M.; Zou, Y.; Vancura, A. *Trends Pharmacol. Sci.* **2018,** *39,* 295–306. doi:10.1016/j.tips.2017.11.008
5. Chang, L.; Guo, R. *Oncotarget* **2017,** *8,* 49515–49533. doi:10.18632/oncotarget.17259
6. Gómez-Ruiz, S.; Maksimović-Ivanić, D.; Mijatović, S.; Kaluđerović, G. N. *Bioinorg. Chem. Appl.* **2012,** No. 140284. doi:10.1155/2012/140284
7. Loktev, A.; Haberkorn, U.; Mier, W. *Curr. Med. Chem.* **2017,** *24,* 2141–2155. doi:10.2174/0929867324666170316120304
8. Joubert, N.; Denevault-Sabourin, C.; Bryden, F.; Viaud-Massuard, M.-C. *Eur. J. Med. Chem.* **2017,** *142,* 393–415. doi:10.1016/j.ejmech.2017.08.049
9. Chalouni, C.; Doll, S. *J. Exp. Clin. Cancer Res.* **2018,** *37,* 20. doi:10.1186/s13046-017-0667-1
10. Luginbuehl, V.; Meier, N.; Kovar, K.; Rohrer, J. *Biotechnol. Adv.* **2018,** *36,* 613–623. doi:10.1016/j.biotechadv.2018.02.005
11. Mercatelli, D.; Bortolotti, M.; Bazzocchi, A.; Bolognesi, A.; Polito, L. *Biomedicines* **2018,** *6,* 19. doi:10.3390/biomedicines6010019
12. Bakhtiar, R. *Biotechnol. Lett.* **2016,** *38,* 1655–1664. doi:10.1007/s10529-016-2160-x
13. Diamantis, N.; Banerji, U. *Br. J. Cancer* **2016,** *114,* 362–367. doi:10.1038/bjc.2015.435
14. Wang, Y.; Cheetham, A. G.; Angacian, G.; Su, H.; Xie, L.; Cui, H. *Adv. Drug Delivery Rev.* **2017,** *110–111,* 112–126. doi:10.1016/j.addr.2016.06.015
15. Ahrens, V. M.; Bellmann-Sickert, K.; Beck-Sickinger, A. G. *Future Med. Chem.* **2012,** *4,* 1567–1586. doi:10.4155/fmc.12.76
16. Gilad, Y.; Firer, M.; Gellerman, G. *Biomedicines* **2016,** *4,* 11. doi:10.3390/biomedicines4020011
17. Dorsam, R. T.; Gutkind, J. S. *Nat. Rev. Cancer* **2007,** *7,* 79–94. doi:10.1038/nrc2069
18. Sun, W.-w.; Zhu, P.; Shi, Y.-c.; Zhang, C.-l.; Huang, X.-f.; Liang, S.-y.; Song, Z.-y.; Lin, S. *Diabetes Vasc. Dis. Res.* **2017,** *14,* 277–284. doi:10.1177/1479164117704380
19. Tilan, J.; Kitlinska, J. *Neuropeptides* **2016,** *55,* 55–66. doi:10.1016/j.npep.2015.10.005
20. Mittapalli, G. K.; Roberts, E. *Bioorg. Med. Chem. Lett.* **2014,** *24,* 430–441. doi:10.1016/j.bmcl.2013.11.061
21. Michel, M. C.; Beck-Sickinger, A.; Cox, H.; Doods, H. N.; Herzog, H.; Larhammar, D.; Quirion, R.; Schwartz, T.; Westfall, T. *Pharmacol. Rev.* **1998,** *50,* 143–150.
22. Cabrele, C.; Beck-Sickinger, A. G. *J. Pept. Sci.* **2000,** *6,* 97–122. doi:10.1002/(sici)1099-1387(200003)6:3<97::aid-psc236>3.0.co;2-e
23. Reubi, J. C.; Gugger, M.; Waser, B.; Schaer, J. C. *Cancer Res.* **2001,** *61,* 4636–4641.
24. Körner, M.; Waser, B.; Reubi, J. C. *Clin. Cancer Res.* **2008,** *14,* 5043–5049. doi:10.1158/1078-0432.ccr-07-4551
25. Körner, M.; Waser, B.; Reubi, J. C. *Int. J. Cancer* **2005,** *115,* 734–741. doi:10.1002/ijc.20948
26. Körner, M.; Waser, B.; Reubi, J. C. *Clin. Cancer Res.* **2004,** *10,* 8426–8433. doi:10.1158/1078-0432.ccr-04-0821
27. Körner, M.; Waser, B.; Reubi, J. C. *Lab. Invest.* **2004,** *84,* 71–80. doi:10.1038/labinvest.3700009
28. Körner, M.; Reubi, J. C. *Peptides* **2007,** *28,* 419–425. doi:10.1016/j.peptides.2006.08.037
29. Gicquiaux, H.; Lecat, S.; Gaire, M.; Dieterlen, A.; Mély, Y.; Takeda, K.; Bucher, B.; Galzi, J.-L. *J. Biol. Chem.* **2002,** *277,* 6645–6655. doi:10.1074/jbc.m107224200
30. Ouedraogo, M.; Lecat, S.; Rochdi, M. D.; Hachet-Haas, M.; Matthes, H.; Gicquiaux, H.; Verrier, S.; Gaire, M.; Glasser, N.; Mély, Y.; Takeda, K.; Bouvier, M.; Galzi, J.-L.; Bucher, B. *Traffic* **2008,** *9,* 305–324. doi:10.1111/j.1600-0854.2007.00691.x
31. Söll, R. M.; Dinger, M. C.; Lundell, I.; Larhammer, D.; Beck-Sickinger, A. G. *Eur. J. Biochem.* **2001,** *268,* 2828–2837. doi:10.1046/j.1432-1327.2001.02161.x
32. Ahrens, V. M.; Kostelnik, K. B.; Rennert, R.; Böhme, D.; Kalkhof, S.; Kosel, D.; Weber, L.; von Bergen, M.; Beck-Sickinger, A. G. *J. Controlled Release* **2015,** *209,* 170–178. doi:10.1016/j.jconrel.2015.04.037
33. Zwanziger, D.; Khan, I. U.; Neundorf, I.; Sieger, S.; Lehmann, L.; Friebe, M.; Dinkelborg, L.; Beck-Sickinger, A. G. *Bioconjugate Chem.* **2008,** *19,* 1430–1438. doi:10.1021/bc7004297
34. Hofmann, S.; Maschauer, S.; Kuwert, T.; Beck-Sickinger, A. G.; Prante, O. *Mol. Pharmaceutics* **2015,** *12,* 1121–1130. doi:10.1021/mp500601z
35. Khan, I. U.; Zwanziger, D.; Böhme, I.; Javed, M.; Naseer, H.; Hyder, S. W.; Beck-Sickinger, A. G. *Angew. Chem., Int. Ed.* **2010,** *49,* 1155–1158. doi:10.1002/anie.200905008
36. Hofmann, S.; Frank, R.; Hey-Hawkins, E.; Beck-Sickinger, A. G.; Schmidt, P. *Neuropeptides* **2013,** *47,* 59–66. doi:10.1016/j.npep.2012.12.001
37. Zwanziger, D.; Böhme, I.; Lindner, D.; Beck-Sickinger, A. G. *J. Pept. Sci.* **2009,** *15,* 856–866. doi:10.1002/psc.1188
38. Langer, M.; Kratz, F.; Rothen-Rutishauser, B.; Wunderli-Allenspach, H.; Beck-Sickinger, A. G. *J. Med. Chem.* **2001,** *44,* 1341–1348. doi:10.1021/jm001065f

39. Ahrens, V. M.; Frank, R.; Stadlbauer, S.; Beck-Sickinger, A. G.; Hey-Hawkins, E. *J. Med. Chem.* **2011,** *54,* 2368–2377. doi:10.1021/jm101514m
40. Böhme, D.; Krieghoff, J.; Beck-Sickinger, A. G. *J. Med. Chem.* **2016,** *59,* 3409–3417. doi:10.1021/acs.jmedchem.6b00043
41. Cao, Y.-N.; Zheng, L.-L.; Wang, D.; Liang, X.-X.; Gao, F.; Zhou, X.-L. *Eur. J. Med. Chem.* **2018,** *143,* 806–828. doi:10.1016/j.ejmech.2017.11.062
42. Rogalska, A.; Bukowska, B.; Marczak, A. *Toxicol. In Vitro* **2018,** *47,* 48–62. doi:10.1016/j.tiv.2017.11.001
43. Liebmann, J. E.; Cook, J. A.; Lipschultz, C.; Teague, D.; Fisher, J.; Mitchell, J. B. *Br. J. Cancer* **1993,** *68,* 1104–1109. doi:10.1038/bjc.1993.488
44. Pando, O.; Stark, S.; Denkert, A.; Porzel, A.; Preusentanz, R.; Wessjohann, L. A. *J. Am. Chem. Soc.* **2011,** *133,* 7692–7695. doi:10.1021/ja2022027
45. Pando, O.; Dörner, S.; Preusentanz, R.; Denkert, A.; Porzel, A.; Richter, W.; Wessjohann, L. *Org. Lett.* **2009,** *11,* 5567–5569. doi:10.1021/ol902320w
46. Dömling, A.; Beck, B.; Eichelberger, U.; Sakamuri, S.; Menon, S.; Chen, Q.-Z.; Lu, Y.; Wessjohann, L. A. *Angew. Chem., Int. Ed.* **2006,** *45,* 7235–7239. doi:10.1002/anie.200601259
47. Steinmetz, H.; Glaser, N.; Herdtweck, E.; Sasse, F.; Reichenbach, H.; Höfle, G. *Angew. Chem., Int. Ed.* **2004,** *43,* 4888–4892. doi:10.1002/anie.200460147
48. Sasse, F.; Steinmetz, H.; Heil, J.; Höfle, G.; Reichenbach, H. *J. Antibiot.* **2000,** *53,* 879–885. doi:10.7164/antibiotics.53.879
49. Kazmaier, U.; Hebach, C. *Synlett* **2003,** 1591–1594. doi:10.1055/s-2003-40987
50. Shibue, T.; Hirai, T.; Okamoto, I.; Morita, N.; Masu, H.; Azumaya, I.; Tamura, O. *Chem. – Eur. J.* **2010,** *16,* 11678–11688. doi:10.1002/chem.201000963
51. Burkhart, J. L.; Müller, R.; Kazmaier, U. *Eur. J. Org. Chem.* **2011,** 3050–3059. doi:10.1002/ejoc.201100155
52. Friestad, G. K.; Banerjee, K.; Marié, J.-C.; Mali, U.; Yao, L. *J. Antibiot.* **2016,** *69,* 294–298. doi:10.1038/ja.2016.7
53. Hoffmann, J.; Gorges, J.; Junk, L.; Kazmaier, U. *Org. Biomol. Chem.* **2015,** *13,* 6010–6020. doi:10.1039/c5ob00587f
54. Kaur, G.; Hollingshead, M.; Holbeck, S.; Schauer-Vukašinović, V.; Camalier, R. F.; Dömling, A.; Agarwal, S. *Biochem. J.* **2006,** *396,* 235–242. doi:10.1042/bj20051735
55. Puentes, A. R.; Morejón, M. C.; Rivera, D. G.; Wessjohann, L. A. *Org. Lett.* **2017,** *19,* 4022–4025. doi:10.1021/acs.orglett.7b01761
56. Wessjohann, L. A.; Morejón, M. C.; Ojeda, G. M.; Rhoden, C. R. B.; Rivera, D. G. *J. Org. Chem.* **2016,** *81,* 6535–6545. doi:10.1021/acs.joc.6b01150
57. Daly, T. A.; Almeida, P. F.; Regen, S. L. *J. Am. Chem. Soc.* **2012,** *134,* 17245–17252. doi:10.1021/ja3074825
58. Stull, R. A.; Tavassoli, R.; Kennedy, S.; Osborn, S.; Harte, R.; Lu, Y.; Napier, C.; Abo, A.; Chin, D. J. *BMC Genomics* **2005,** *6,* No. 55. doi:10.1186/1471-2164-6-55